



HAL
open science

Chiral symmetry breaking: asymmetry and origin of chiral molecules relevant in prebiotic evolution

Iuliia Myrgorodska

► **To cite this version:**

Iuliia Myrgorodska. Chiral symmetry breaking: asymmetry and origin of chiral molecules relevant in prebiotic evolution. Other. COMUE Université Côte d'Azur (2015 - 2019), 2016. English. NNT: 2016AZUR4057 . tel-01438842

HAL Id: tel-01438842

<https://theses.hal.science/tel-01438842v1>

Submitted on 18 Jan 2017

HAL is a multi-disciplinary open access archive for the deposit and dissemination of scientific research documents, whether they are published or not. The documents may come from teaching and research institutions in France or abroad, or from public or private research centers.

L'archive ouverte pluridisciplinaire **HAL**, est destinée au dépôt et à la diffusion de documents scientifiques de niveau recherche, publiés ou non, émanant des établissements d'enseignement et de recherche français ou étrangers, des laboratoires publics ou privés.

UNIVERSITE DE NICE SOPHIA ANTIPOLIS - UFR Sciences
Ecole Doctorale Sciences Fondamentales et Appliquées

THESE

pour obtenir le titre de

Docteur en Sciences

de L'UNIVERSITE de Nice Sophia Antipolis

Discipline : Chimie

Présentée est soutenue par

Iuliia MYRGORODSKA

RUPTURE DE SYMÉTRIE CHIRALE :
ASYMÉTRIE ET ORIGINE DES MOLÉCULES CHIRALES IMPLIQUÉES
DANS L'ÉVOLUTION PRÉBIOTIQUE

CHIRAL SYMMETRY BREAKING:
ASYMMETRY AND ORIGIN OF CHIRAL MOLECULES RELEVANT IN
PREBIOTIC EVOLUTION

Soutenue le 16 Septembre 2016 devant un jury composé de :

Pr. Hervé COTTIN	Université Paris-Est Créteil	Rapporteur
Dr. Guillermo M. MUNOZ CARO	Centro de Astrobiología Instituto Nacional de Técnica Aeroespacial	Rapporteur
Dr. Jeanne CRASSOUS	Université de Rennes 1	Examineur
Dr. Thomas BUHSE	Universidad Autónoma del Estado de Morelos	Membre externe
Dr. Cornelia MEINERT	Université Nice Sophia Antipolis	Membre externe
Dr. Laurent NAHON	Synchrotron SOLEIL	Co-directeur de thèse
Pr. Uwe MEIERHENRICH	Université Nice Sophia Antipolis	Directeur de thèse



ACKNOWLEDGMENTS

Foremost, I would like to express my sincere gratitude to my thesis supervisor Prof. Uwe MEIERHENRICH for the continuous support and guidance through my PhD. It was a great pleasure for me to work in his team and to learn how to do research. I am equally grateful to my thesis co-adviser Dr. Laurent NAHON, for his assistance during the radiation experiments and expertise that he brought into this project, as I learned a lot from his supervision. The valuable experience I obtained from them is now summarized in my thesis manuscript.

Besides my thesis advisors, I would like to thank the rest of my thesis committee Prof. Hervé COTTIN, Dr. Guillermo M. MUNOZ CARO and Dr. Jeanne CRASSOUS, for accepting to judge the work conducted over the last three years. I am especially thankful to Dr. Thomas BUHSE who came all the way from Mexico and who will assist at my PhD defense as an external member.

Another person from my thesis committee whom I would like to thank is Dr. Cornelia MEINERT. As we worked closely together I appreciate her vast knowledge of chromatography as much as her practical skills. I would like to thank her for introducing me into the field of analytical chemistry.

I would like to acknowledge the rest of our international team: Dr. Louis le Sergent d'HENDECOURT and Dr. Pierre de MARCELLUS for simulating the evolution of interstellar ice, Dr. Søren V. HOFFMANN and Dr. Nykola C. JONES for close collaboration on CD and anisotropy spectroscopy, Dr. Zita MARTINS for the extraction of a Murchison meteorite sample, my summer intern Thomas JAVELLE for some help with analysis.

Moreover, I would like to thank the French Minister of Science and Education for my PhD funding.

Special thanks go to the EON foundation for financing my research visit to Earth Life Science Institute, Tokyo, Japan, and especially to Dr. Jim CLEAVES for supporting my proposal and hosting me in his team. Few names of our Japanese colleagues should be mentioned here: Dr. Matsuo KOICHI, Dr. Kensei KOBAYASHI and Dr. Masahiro KATOH, as all of them actively participated in advancement of the proposed research project.

Eventually, I am very grateful to Dr. Jean-Jacques FILIPPI for the numerous practical advices and his aid in GC maintenance. I would like to thank my dear friends Luisa and Miryana for being such a great support and encouragement. Another person in my life who I would like to thank is Sasha. His sense of humor brought me a lot of good moments in the last year of my PhD.

Lastly, I would like to thank my family for all their love and encouragement, and my parents who raised me with a love of science and supported me in all my pursuits.



Sommaire

ACKNOWLEDGMENTS	iii
LIST OF ABBREVIATIONS	ix
RESUME (FR)	xi
RESUME (EN)	xv
INTRODUCTION (FR)	1
INTRODUCTION (EN)	3
CHAPTER I: Bibliographic overview	5
Article 1. Molecular Chirality in Meteorites and Interstellar Ices, and the Chirality Experiment on Board the ESA Cometary Rosetta Mission	5
Abstract	5
1. Introduction	6
1. Enantiomeric enhancement in meteoritic samples.....	7
1.1. The stereochemistry of organic molecules in meteorites.....	7
1.2. Enantiomeric enhancement in meteorites: Up to 18% <i>ee</i> in L-isovaline	8
2. Chirality investigations in simulated comets	10
2.1. Organic Molecules in Simulated Cometary Ices	10
2.2. Enantiomeric enhancements in simulated cometary ices.....	12
3. Stereochemical mechanism of enantiomeric enrichments	12
3.1. Enantiomeric enhancement induced by asymmetric photochemistry	13
3.2. Enantiomeric enhancement induced upon crystallization, phase transition, and Viedma ripening	14
3.3. Enantiomeric enhancement induced by weak nuclear interaction ...	15
3.4. Amplification of enantiomeric enhancement by autocatalytic processes	16
4. The chirality module on board the Rosetta lander Philae	17
5. Summary and outlook.....	18
References	19
Article 2. Light on Chirality: Absolute Asymmetric Formation of Chiral Molecules Relevant in Prebiotic Evolution	27
Abstract	27
1. Introduction	28
1. Chiroptical response and absolute asymmetric formation of amino acids	29
1.1. Circular Dichroism spectroscopy.....	30

1.2.	Anisotropy spectroscopy	32
1.3.	Absolute asymmetric photolysis	34
2.	Aldehydes as prebiotic precursor molecules	36
2.1.	Aldehydes as amino acid precursors	37
2.2.	Aldehydes as nucleic acid precursors	38
3.	Other chiral species relevant for prebiotic enantiomeric discrimination	39
3.1.	The evolution and detection of chiral amines	39
3.2.	The evolution and detection of chiral hydroxycarboxylic acids	41
4.	Outlook	42
	References	43
CHAPTER II: Analytical methods		51
	Article 3. Quantitative enantioseparation of amino acids by comprehensivetwo-dimensional gas chromatography applied to non- terrestrialsamples	51
	Abstract	51
1.	Introduction	52
2.	Experiments	53
2.1.	Chemicals, reagents, and tools	53
2.2.	Derivatization	53
2.3.	GC × GC–TOFMS	54
3.	Result and discussion	54
3.1.	Mass spectra of the derivatives	54
3.2.	Method validation	57
3.3.	Enantioseparation	58
3.4.	Method application	59
4.	Conclusions	61
	References	63
	Supporting information	66
1.	Method validation	66
2.	Extraction of amino acids from the Murchsion meteorite	68
3.	Interpretation of mass spectra	69
4.	GC×GC chromatograms of a standard solution of amino acids	73
CHAPTER III: Prebiotic chemistry of interstellar ice analogues		77
	Article 4. Aldehydes and sugars from evolved precometary iceanalogs: Importance of ices in astrochemical andprebiotic evolution	77
	Abstract	77
	Significance statement	78
1.	Introduction	78
2.	Results	79
3.	Astrophysical discussion	83
4.	Implications for prebiotic chemistry	85
5.	Conclusions	86
	Material and Methods	87

References	88
Supporting information	93
Extraction, Derivatization, and GC×GC Analysis.....	93
References	94
Article 5. Ribose and related sugars from ultraviolet irradiation of interstellar ice analogs	97
Abstract	97
References	107
Supplementary materials	108
Materials and Methods	108
1. Preparation of the interstellar pre-cometary ice analogue	108
2. Analysis of the interstellar pre-cometary ice analogue	109
3. Analyte quantification	110
4. Identification of organic molecules in the interstellar pre-cometary ice analogue.....	111
4.1. Identification of monosaccharides in the interstellar pre-cometary ice analogue	111
4.2. Identification of sugar alcohols in the interstellar pre-cometary ice analogue	112
4.3. Identification of saccharinic, hydroxycarboxylic, and dicarboxylic acids in the interstellar pre-cometary ice analogue.....	113
CHAPTER IV: Photo Electron Circular Dichroism	121
Article 6. Determination of accurate electron chiral asymmetries in fenchone and camphor in the VUV range: sensitivity to isomerism and enantiomeric purity.....	121
Abstract	121
1. Introduction	122
2. Experimental methods	123
3. Results and discussions	125
3.1. Camphor data.....	125
3.2. Fenchone data.....	129
3.3. Camphor/fenchone comparison: sensitivity to isomerism	132
4. Conclusions and future prospects	135
References.....	138
Supplementary information	142
References	146
CONCLUSIONS (FR).....	147
CONCLUSIONS (EN).....	151
CONCLUSIONS (EN).....	151
INDEX.....	155



LIST OF ABBREVIATIONS

67P/C-G	– comet 67P/Churyumov-Gerasimenko
$[\alpha]_D^{24}$	– optical rotation of a sample measured at 24 °C and wavelength λ for the sodium D line
β	– asymmetry parameter
σ	– standard deviation (CHAPTER II, III) cross section (CHAPTER IV)
ε	– extinction coefficient
ξ	– extent of reaction
μ	– electric dipole momentum
A	– absorption (CHAPTER I)/peak area (CHAPTER II)
AIB	– amino isobutyric acid
AIS	– anisotropy spectroscopy
ALMA	– Atacama large millimeter array
B	– magnetic field vector
b_1	– dichroic parameter
BL	– baseline
BSTFA	– <i>N,O</i> -Bis(trimethylsilyl)trifluoroacetamide
CD	– circular dichroism
CM2	– Mighei-like meteorites, number indicates group according to the degree of aqueous alteration
CMS- $X\alpha$	– continuum multiple scattering $X\alpha$, a model of photoionization that approximates the interaction between an electron and an ion core by one-electron muffin-tin potential.
COSAC	– Cometary Sampling and Composition
CPL (LPC)	– circularly polarized light (lumière polarisée circulairement)
CR2	– Renazzo-like meteorites, number indicates group according to the degree of aqueous alteration
D	– dispersion
DAP	– 2,3-diaminopropanoic acid
E	– electric field vector
ee	– enantiomeric excess
ECHFBE	– <i>N(O,S)</i> -ethoxy-carbonylheptafluorobutyl ester
EI	– electron impact
ESA	– European Space Agency
FEL	– free electron laser
FWHM	– full width at half maximum
g	– anisotropy factor
GNA	– glycerol nucleic acids
\hat{H}	– Hamiltonian operator
HHG	– high harmonic generation
HMT	– hexamethylenetetramine
HOMO	– highest occupied molecular orbital
HV	– high tension voltage

x LIST OF ABBREVIATIONS

i ² PEPICO	– double imaging photoelectron/photoion coincidences
IDP	– interplanetary dust particle
IOM	– insoluble organic matter
IS	– internal standard
<i>k</i>	– rate constant
KE	– kinetic energy
LCP	– left circular polarization
LMH	– large molecular heimat
LOD	– limit of detection
LOQ	– limit of quantification
<i>m</i>	– magnetic dipole momentum
<i>m/z</i>	– mass-to-charge ratio
MCA	– monocarboxylic acid
MD	– magnetochiral dichroism
NIST	– National Institute of Standards and Technology
OPA/NAC	– mixture of <i>O</i> -phthaldialdehyde and <i>N</i> -acetyl-L-cysteine
ORD	– optical rotation dispersion
PAD	– photoelectron angular distribution
PECD	– photoelectron circular dichroism
PEM	– photoelastic modulator
PES	– photoelectron spectra
PFBHA	– <i>O</i> -(pentafluorobenzyl)hydroxylamine
PFBO	– <i>O</i> -pentafluorobenzyl oxime
PMT	– photo-multiplier tube
PNA	– peptide nucleic acid
ppb	– parts per billion (1 ppb = 10 ⁻³ ppm)
ppm	– parts per million (10000 ppm = 1%)
<i>R</i>	– rotational strength
<i>R</i> ²	– coefficient of determination
<i>rac</i>	– racemic
RCP	– right circular polarization
REMPI	– resonance enhanced multi-photon ionization
<i>RRF</i>	– relative response factor
<i>S</i>	– slope of the calibration curve
<i>S</i> ₁ , <i>S</i> ₂ , <i>S</i> ₃	– Stokes parameters of light
<i>S/N</i>	– signal to noise ratio
SOM	– soluble organic matter
SR	– synchrotron radiation
SRCD	– synchrotron radiation circular dichroism
TDDFT	– time-dependent density functional theory
TMS	– trimethylsilyl
TNA	– threose nucleic acid
TOFMS	– time of flight mass spectrometer
TR-PECD	– time-resolved photoelectron circular dichroism
VMI	– velocity map imaging
VUV	– vacuum ultraviolet

RESUME (FR)

L'absence de symétrie aussi appelée asymétrie est très présente dans la nature. On la voit sous différentes formes comme la violation de parité dans les interactions faibles, l'asymétrie biologiques chez les crabes violonistes ou la sélection d'énantiomères spécifiques dans la constitution des biomolécules. Cette dernière porte le nom d'homochiralité de la vie : les acides aminés et les acides nucléiques, les molécules chirales qui constituent les briques élémentaires des protéines et du matériel génétique, n'existent dans le monde vivant que sous une seule forme énantiomérique.

Depuis la découverte de la chiralité moléculaire par Pasteur il y a plus de 150 ans, l'origine de l'homochiralité de la vie reste un mystère non résolu et troublant, qui remonte probablement à l'origine de la vie elle-même. Cette énigme a récemment été recensée dans *Nature* comme étant l'une des cinq plus grandes énigmes non résolues par la science.

Aujourd'hui il existe deux façons d'aborder le problème de l'origine de l'asymétrie moléculaire impliquant des scénarios soit déterministes soit aléatoires. Ces derniers étant basés sur la résolution spontanée des énantiomères, et sont donc impossible à tester. En revanche, les théories déterministes peuvent être confrontées à l'expérience afin notamment de valider la reproductibilité de leur influence chirale.

Parmi les scénarios déterministes, figurent ceux basés sur des processus asymétriques induits par la lumière, mettant en jeu l'interaction de la lumière polarisée circulairement (LPC) ayant des propriétés de reconnaissance chirale. En effet, des sources astronomiques de LPC ont effectivement été identifiées, notamment dans des régions de formations d'étoiles lourdes. De plus des acides aminés d'origine extraterrestre ont été découverts dans des météorites carbonées avec des excès énantiomériques compatibles avec l'origine extraterrestre de l'asymétrie moléculaire.

Le présent manuscrit est une synthèse bibliographique et expérimentale mettant en évidence les interactions de la LPC avec des molécules chirales dans le cadre de l'origine de l'homochiralité de la vie. Ces travaux ont pour but de mieux comprendre les propriétés chiroptiques de molécules chirales ainsi que de déterminer les espèces chirales susceptibles d'être présentes dans la glace cométaire.

Le manuscrit comporte quatre parties. Dans un premier temps je présente une étude bibliographique. Puis, sont décrites les méthodes analytiques utilisées dans le cadre de ma thèse. Ensuite, j'aborde le thème de la détection de molécules prébiotiques des analogues de glace interstellaire. Enfin je propose une étude sur les aspects analytiques du dichroïsme circulaire de photoélectrons.

L'étude bibliographique introduit la problématique de la thèse et donne un bref aperçu des travaux déjà effectués dans ce domaine. Un scénario photochimique pour l'origine de l'homochiralité est proposé dans ce chapitre. Dans le premier article, les molécules d'origine extraterrestre déjà détectées avec un excès énantiomérique ont été groupées dans un tableau accompagné d'une discussion sur la pertinence des résultats déjà publiés. Parmi eux, les acides aminés α -méthylés

(e.g. isovaline) présentent la plus grande asymétrie, qui peut aller jusqu'à 18% d'excès énantiomérique. Après une discussion sur la détection des molécules météoritiques, les molécules prébiotiques formées dans la glace interstellaire artificielle sont décrites. Également le modèle de Greenberg de la formation de la glace interstellaire est présenté suivi d'une illustration explicative. Comme les molécules chirales, telles que les acides aminés, peuvent être formées par simulation de glace cométaire, l'article décrit les expériences d'induction d'asymétrie dans ce type de précurseurs. Ensuite la brisure de symétrie est étudiée comme produit i) des forces chirales, ii) de la violation de parité, et iii) de transitions de phases. Les avantages et les inconvénients de chaque théorie sont soulignés dans ce chapitre. Selon ces hypothèses, l'obtention d'un composé énantiopur impose que la brisure de symétrie initiale soit toujours suivie par l'amplification de cet excès énantiomérique, dont le principe est décrit dans cette partie. Finalement toutes les informations présentées sont mises en perspectives dans le contexte de la mission Rosetta, la première mission spatiale conçue pour les analyses in-situ d'un noyau cométaire.

Le deuxième article de cette étude bibliographique s'intéresse principalement aux propriétés chiroptiques des molécules chirales et aux méthodes spectroscopiques qui permettent de les étudier. Tout d'abord le concept de fausse et de vraie chiralité est introduit. Il s'en suit une discussion sur les forces chirales parmi lesquelles la LPC, le champ magnétique colinéaire avec le vecteur de propagation d'un faisceau lumineux, et les électrons polarisés en spin. Comme la LPC est très présente dans l'espace et qu'elle est le seul objet capable d'induire un enrichissement énantiomérique significatif, les autres processus d'induction chirale sont omis dans la discussion qui suit. L'article explique en détail le principe de la spectroscopie de dichroïsme circulaire (CD) ainsi que la conception des instruments correspondants. Les spectres de CD d'acides aminés publiés précédemment ont été réunis dans ce chapitre, où ils ont été placés dans le contexte de la photolyse asymétrique. Pourtant l'information déduite de ces spectres n'est pas suffisante pour prédire un excès énantiomérique induit par la LPC à une longueur d'onde donnée. Ceci requiert en effet le passage de la spectroscopie de dichroïsme circulaire à la spectroscopie d'anisotropie qui nous permet d'obtenir des mesures quantitatives. Le spectre d'anisotropie est obtenu en divisant le coefficient d'extinction différentiel enregistré pendant les mesures de CD par le coefficient d'extinction moyen enregistré au cours des mesures d'absorption. Plusieurs spectres d'anisotropie d'acides aminés sont présentés dans cette étude bibliographique. Les valeurs d'enrichissement énantiomérique obtenues ont été ensuite corrélées aux expériences de photolyse asymétrique précédemment effectuées. Les propriétés chiroptiques des molécules chirales prébiotiques autres que les acides aminés sont aussi décrites de façon approfondie.

Le chapitre intitulé "Méthodes analytiques" présente un travail sur une procédure analytique perfectionnée pour la résolution et la quantification des énantiomères d'acides aminés par chromatographie en phase gazeuse multidimensionnelle. Le protocole consiste en une étape de dérivation, par laquelle des acides aminés ont été transformés en *N*(O,S)-éthoxycarbonylheptafluorobutyl ester. Cette étape a été optimisée pour la résolution d'acides aminés non protéique-

dans la matrice d'échantillons complexes d'origine extraterrestre. La procédure s'est avérée être très sensible et présente un large domaine de linéarité avec des limites de détection de l'ordre 0.005-3 pmol pour des mesures quantitatives. La procédure mise au point a été testée sur un échantillon de la météorite Murchison, pour lesquels les chromatogrammes obtenus montrent une excellente résolution, avec un minimum de co-élution. Finalement, nous avons conclu que la chromatographie en phase gazeuse bidimensionnelle est une technique très appropriée pour l'analyse d'échantillons présents en faible quantité et contenant des molécules potentiellement prébiotiques, comme dans des analogues de glace cométaire et météoritique.

Le chapitre sur la chimie prébiotique des analogues de glace interstellaire est composé de deux articles. L'intérêt scientifique pour les analogues de glaces vient du fait qu'ils pourraient être sans doute être considérés comme une simulation de la matière cométaire qui serait ensuite tombée sur les planètes telluriques primitives, enrichissant celles-ci avec des composés organiques complexes. Le premier article de la troisième partie de ce manuscrit porte sur la détection d'une nouvelle famille de molécules d'intérêt prébiotique dans la glace cométaire simulée en laboratoire. L'utilisation de la chromatographie en phase gazeuse multidimensionnelle couplée à la spectrométrie de masse à temps de vol, a permis la détection de 10 aldéhydes, y compris le glycolaldéhyde et glyceraldéhydes - deux espèces considérées comme les intermédiaires clés de la chimie prébiotique intervenant dans les premières étapes de la synthèse de ribonucléotides. La présence d'ammoniac dans des glaces produites avec un mélange d'eau et de méthanol apparaît comme essentielle pour la formation et/ou la détection de ces aldéhydes dans le résidu organique réfractaire à température ambiante, bien que ces produits soient exempts d'azote. Enfin l'importance de la détection des aldéhydes et des sucres dans des environnements extraterrestres est soulignée. Les molécules présentes dans la phase gazeuse de nuages moléculaires chauds ainsi que dans les comètes et les météorites primitives ont été le plus probablement apportées sur Terre lors du grand bombardement d'il y a 4,2 milliards d'années.

La suite de ce travail de recherche de nouvelles espèces moléculaires est présentée dans le deuxième article du chapitre "La chimie prébiotique des analogues de glace interstellaire". Cette fois-ci le ribose, une des briques élémentaires de l'ARN, a été détectée dans des résidus organiques d'analogues de glaces interstellaires initialement composées de H₂O, CH₃OH et NH₃. Hormis le ribose, un grand nombre d'aldopentoses a été détecté également dans un même résidu. Ces résultats suggèrent que la synthèse de nombreuses molécules de sucre, y compris le ribose, puisse être produite suite à des processus photochimiques et thermiques sur des glaces cométaires lors des derniers stades de l'évolution de la nébuleuse solaire. La détection du ribose fournit des indications sur les processus chimiques qui pourraient conduire à la formation de molécules d'intérêt biologique dans des environnements planétaires.

La dernière partie de ce manuscrit est centrée sur le dichroïsme circulaire de photoélectrons (PECD), un effet chiroptique en phase gaz étudié ici sur des molécules chirales modèles: le camphre et la fenchone. Le PECD se manifeste par une intense asymétrie avant / arrière dans la distribution angulaire des photoélectrons

produits par photoionisation induite par une LPC sur des énantiomères orientés de façon aléatoire. En tant que sonde sensible à la dynamique de photoionisation ainsi qu'au potentiel moléculaire chiral, le PECD a attiré beaucoup d'intérêt, suite au développement récent d'expériences menées non plus avec du rayonnement synchrotron mais avec des lasers. Dans cette partie du manuscrit des nouvelles valeurs de mesures d'asymétries très précises sont reportées pour le camphre et la fenchone qui sont des isomères. Les valeurs ont été obtenues par l'utilisation de la LPC quasi-parfaite du rayonnement synchrotron combinée avec un spectromètre de double imagerie de photoélectrons/photoion détectés en coïncidence (i^2 PEPICO). Ces données ont en outre été normalisées par rapport à l'énantiopureté absolue de l'échantillon telle que mesurée par une technique de chromatographie en phase gazeuse bidimensionnelle. Ils peuvent donc être utilisés comme données de référence pour de nouvelles expériences PECD, ainsi que pour les modèles théoriques. Au cours de cette étude, le potentiel analytique du PECD a également été évalué. Il a été conclu que la technique PECD-PICO permet la corrélation des mesures de PECD avec les masses d'ions parents spécifiques, ce qui ouvre des perspectives intéressantes quant à son application pour l'analyse énantiomériques de mélanges complexes.

RESUME (EN)

The absence of symmetry also known as asymmetry is often found in nature. It can manifest itself in different forms such as a parity violation in weak interactions, as a biological asymmetry in fiddler crabs or as a selection of specific enantiomeric form for construction of biomolecules. The latest refers to the phenomenon known as homochirality: amino acids and nucleic acids, chiral molecules that form elementary building blocks of proteins and genetic material, exist in the biosphere only in one enantiomeric form.

Since the Pasteur's discovery of chirality more than 150 years ago, the origin of homochirality remains to be an unresolved mystery, which is probably linked to the origin of life-itself. This puzzle was named by the journal *Nature* as one of the five biggest unresolved puzzles in modern science.

Today there exist two ways to address the question of the origin of molecular homochirality. It implies either deterministic or chance scenario. The latest is based on the spontaneous resolution of enantiomers by phase transition, and in consequence, it cannot be tested. On the other hand, deterministic theories can be subjected to experimental confirmation, since if there was, in fact, a chiral influence that imposed its chirality this should in principle be reproducible.

Among the deterministic scenarios, one may find those based on the asymmetric processes induced by light. They involve interactions with circularly polarized light (CPL) which is capable of chiral recognition. Such type of light has been previously identified in several astronomical sources. Mainly it can be found in heavy star forming regions. Moreover, amino acids of extraterrestrial origin have been detected in carbonaceous meteorites with enantiomeric excesses indicating the possible origin of molecular asymmetry to be extraterrestrial.

The presented manuscript is a synthesis of bibliographic research and experimental studies that focus on the interaction of CPL with chiral molecules which are put in the context of the origin of homochirality of life. This work is aiming to advance our understanding of chiroptical properties of chiral molecules as well as to determine chiral species susceptible to be present in cometary ice.

The manuscript consists of four chapters. At first the bibliographic overview is presented. Then, it describes analytical method implied in the current studies. Afterwards, the prebiotic chemistry of interstellar ice analogues with corresponding experiments is discussed in details. Finally, analytical properties of photoelectron circular dichroism are presented in the last chapter.

The bibliographic overview introduces the problematic of the thesis and gives a brief survey of the research that has been already conducted in this domain. The photochemical scenario for the origin of homochirality is highlighted in this chapter. In the first article, the molecules of extraterrestrial origin, previously detected with enantiomeric excess, have been grouped into a table followed by a discussion on the relevance of previously published results. Among them, α -methylated amino acids (e.g. isovaline) show the highest degree of asymmetry which can be as high as 18% of enantiomeric excess. Shortly after discussion on meteoritic molecules, the prebiotic molecules formed in the simulated interstellar ice were described. Additionally, the Greenberg model of the formation of inter-

stellar ice is presented following by explanatory illustration. Since chiral molecules such as amino acids can be formed during simulations of cometray ice, the experiences with asymmetry induction in this type of precursors have been presented as well. Afterwards, the symmetry breaking has been studied as a product of: i) chiral forces, ii) parity violation, and iii) phase transition. Flows and advantages of each theory have been highlighted in this chapter. According to the presented hypothesis, to reach the absolute enantioselectivity any symmetry breaking should be followed by amplification of enantiomeric excess the principle of which is described in this manuscript. Finally, all the presented information was put in the context of the Rosetta mission, the first space mission constructed for the systematic in-situ analysis of a cometary nucleus.

The second article of bibliographic overview is focused on the chiroptical properties of chiral molecules and spectroscopic methods to study them. First of all, the concept of false and true chirality was introduced, followed by the discussion on chiral forces, among which are CPL, magnetic field collinear with a propagating electromagnetic vector, and spin polarized electrons. As CPL is abundant in space and it is probably the only chiral driving force capable of inducing significant enantiomeric enrichment, other symmetry breaking processes were omitted in the following discussion. The article explains in details the principle of circular dichroism spectroscopy as well as it describes the corresponding equipment. Previously published CD spectra of amino acids have been presented in this chapter, where they were discussed in the context of asymmetric photochemistry. Nevertheless, information deduced from CD spectra is insufficient to predict enantiomeric enhancement induced by CPL at a given wavelength. Therefore, we pass from CD spectroscopy to anisotropy spectroscopy in the following discussion. The anisotropy spectra are obtained by dividing differential extinction coefficient recorded during CD measurements by the extinction coefficient recorded during adsorption measurements. Several anisotropy spectra of amino acids were presented in this bibliographic overview. The values of enantiomeric enrichment were then linked to the experiences on asymmetric photolysis. The chiroptical properties of chiral prebiotic molecules other than amino acids have been mentioned as well.

The chapter "Analytical methods" presents an improved analytical procedure for the resolution and quantification of amino acid enantiomers by multidimensional gas chromatography. The procedure contains a derivatization step, by which amino acids were transformed into *N*(*O,S*)-ethoxycarbonylheptafluorobutyl esters. It was optimized for the resolution of non-proteinogenic amino acids in the matrix of complex non-terrestrial samples. The procedure has proven to be highly sensitive and shows a wide linearity range with 0.005–3 pmol detection limits for quantitative determinations. The developed procedure was tested on a sample of the Murchison meteorite, for which obtained chromatograms show excellent peak resolution with minimal co-elution. Finally, it was concluded that comprehensive two dimensional chromatography is a highly suitable technique for the analysis of samples with very limited quantities and containing potentially prebiotic molecules, such as interstellar ice analogs and meteorites.

The following chapter "Prebiotic chemistry of interstellar ice analogues" is composed of two articles. The scientific interest in the cometary ice analogues

comes from the fact that they can be considered as an approximation of precometary materials that will later fall on primitive telluric planets. The first article of this chapter is devoted to the discovery of a new family of prebiotic molecules in simulated interstellar ice. Multidimensional gas chromatography coupled to time-of-flight mass spectrometry, allowed the detection of 10 aldehydes, including the sugar-related glycolaldehyde and glyceraldehyde—two species considered as key prebiotic intermediates in the first steps toward the synthesis of ribonucleotides. Moreover glyceraldehyde is a chiral unit that stereodictates the prebiotic synthesis of activated pyrimidine nucleotides, and therefore might be the key to the homochirality of genetic material. The presence of ammonia in water and methanol ice mixtures appears essential for the formation and/or recovery of these aldehydes, although these products are free of nitrogen. Finally, the importance of aldehydes and sugars detection has been stated. Molecules present in the gas phase of hot molecular clouds, as well as in comets and in primitive meteorites have been most probably brought to Earth with a heavy bombardment that occurred 4.2 billion years ago.

The follow-up study of new prebiotic species in cometary ice is presented in the second article of this chapter. This time ribose – the molecular sub-unit of RNA – has been detected in the organic residue of interstellar ice analogs initially composed of H₂O, CH₃OH, and NH₃. Apart from ribose, other aldopentoses have been as well detected in the same residue. These results suggest that the generation of numerous sugar molecules, including the ribose, may be possible from the photochemical and thermal treatment of cosmic ices in the late stages of the solar nebula. The detection of ribose provides plausible insights into the chemical processes that could lead to the formation of biologically relevant molecules in suitable planetary environments.

The last part of the manuscript is devoted to photoelectron circular dichroism (PECD), a chiroptical orbital-specific effect in the gas phase studied here on the showcases chiral molecules fenchone and camphor. Photoelectron circular dichroism (PECD) manifests itself as an intense forward/backward asymmetry in the angular distribution of photoelectrons produced by photoionization with circularly polarized light (CPL) of randomly-oriented enantiomers. As a sensitive probe of both photoionization dynamics and of the chiral molecular potential, PECD attracted much interest recently with the recent development of laser-based PECD experiments. In this part of the manuscript new and accurate values of the corresponding asymmetries of chiral camphor and fenchone were presented. These values were obtained by use of quasi-perfect CPL VUV synchrotron radiation and using a double imaging photoelectron/photoion coincidence (*i*²PEPICO) spectrometer. The data have additionally been normalized to the absolute enantiopurity of the samples measured by two dimensional gas chromatography. They can, therefore, be used as reference data for new PECD experiments, as well as for theoretical models. In the course of this study, we could also evaluate the analytical potential of PECD in terms of relative enantiomeric excess determination. It was concluded that the PECD-PICO technique allows correlating PECD measurements to specific parent ion masses, which open interest in perspectives in terms of its application to the ee analysis of complex mixture



INTRODUCTION (FR)

“Everything existing in the universe is the fruit of chance and necessity.”

Democritus

“The most beautiful experience we can have is the mysterious. It is the fundamental emotion which stands at the cradle of true art and true science. Whosoever does not know it and can no longer wonder, no longer marvel, is as good as dead, and his eyes are dimmed.”

A. Einstein

Dès le début de son existence l'humanité s'estposé la question sur ses origines et sur l'origine de la vie elle-même. Les recherches de réponse continuant à ces jours nous amènent vers de nombreuses mystifications et théories purement théologiques. Les philosophes de l'antiquité comme Démocrite et Aristote croyaient à l'apparition d'un être vivant sans descendant, de nulle part et indépendamment de la matière inanimée. Il faudra attendre le XVIIe siècle pour tester cette hypothèse et encore deux siècles pour la rejeter complètement. Ensuite, la révolution scientifique s'est produite par la découverte de structure d'ADN mais également par le déchiffrement de la structure de polypeptides. Ces deux découvertes ont démontré que tous les êtres vivants se constituent des mêmes briques moléculaires : d'acides aminés et d'acides nucléiques.

Auparavant une autre découverte importante a été réalisée par un chimiste français. En 1847, Louis Pasteur sépare les deux formes du cristaux de tartrate et note que les solutions correspondantes font dévier la lumière polarisée soit vers la gauche, soit vers la droite. Il en déduit que les cristaux étudiés présentent deux structures géométriques différentes, dextrogyre ou lévogyre, et que la dissymétrie de la forme cristalline correspond à une dissymétrie interne de la molécule. C'était la première apparition de la notion de chiralité moléculaire, qui a abouti à la naissance du domaine de stéréochimie.

Aujourd'hui, on dit que la molécule est chirale si elle n'est pas superposable avec son image dans un miroir, autrement dit si elle ne présente aucune symétrie intrinsèque. Ces deux formes non superposables constituent un couple d'énantiomères. Souvent les molécules ayant un centre stéréogène, comme un atome de carbone lié à quatre radicaux différents, ont des propriétés chirales. Parmi eux, les constituants des protéines - les acides aminés avec un centre stéréogène en position α et aussi les composantes des acides nucléiques - ribose et désoxyribose avec ces 4 carbones asymétriques. Les études de suivi ont démontré que les acides aminés et glucides naturels n'existent que sous une de leurs formes énantiomériques. La synthèse de ces molécules à partir de méthane, ammoniac, hydrogène et a été effectuée dans une fameuse expérience de Miller-Urey. Pourtant les briques moléculaires obtenues se trouvent toujours réparties en part

2 INTRODUCTION

égale entre la forme dextrogyre et lévogyre, c'est-à-dire un mélange racémique optiquement inactif. La stéréosélectivité trouvée au sien de tous les organismes vivants est un phénomène qu'on appelle aujourd'hui l'homochiralité biomoléculaire.

La question de l'origine de l'asymétrie des molécules biologiques est considérée comme étant étroitement associée au problème de l'origine de la vie elle-même. Une hypothèse séduisante pour expliquer l'origine de l'homochiralité de la vie fait appel à une irradiation intensive de précurseurs des biomolécules par une source de lumière interstellaire polarisée circulairement. La polarisation circulaire d'un rayonnement électromagnétique est une polarisation où la norme du vecteur du champ électrique ne change pas, alors que son orientation change selon un mouvement de rotation. Ce type de lumière peut exister sous deux formes opposées, polarisée dans le sens horaire ou antihoraire, et présente donc un système chiral. La photolyse de mélange racémique par une source de lumière polarisée a été utilisée pour produire un excès énantiomérique dans quelques acides aminés. Or, récemment, une forte polarisation circulaire de la lumière infrarouge a été découverte dans la nébuleuse d'Orion. Par ailleurs, la météorite de Murchison présente un surplus d'acides aminés lévogyres. L'homochiralité de la vie pourrait donc être née dans l'espace. Cependant, ce scénario suppose une photochimie asymétrique importante des molécules pour l'obtention d'un enrichissement énantiomérique significatif.

Le degré d'excès induit dépend des propriétés physico-chimiques de la matière, ces dernières peuvent être étudiées par spectroscopie de dichroïsme circulaire et par spectroscopie d'anisotropie. Ces deux techniques sont complémentaires et permettent de prédire un enrichissement énantiomérique pour l'avancement de réaction connue et longueur d'onde choisie.

Ce manuscrit inclut quelques axes de recherche qui ont été menés afin de mieux comprendre le phénomène de la photolyse asymétrique et la possible évolution chimique de molécules organiques dans l'espace. Pour examiner l'hypothèse de l'origine extraterrestre de l'homochiralité, les excès énantiomériques ont été plus précisément déterminés sur des matériaux provenant de météorites, les seuls objets d'origine interstellaire facilement accessibles sur terre. La méthode d'analyse par la chromatographie en phase gazeuse a été testée sur l'extrait de météorite de Murchison et aussi sur des glaces interstellaires simulées au laboratoire. De plus, la cote analytique de dichroïsme circulaire photoélectronique a été étudiée en utilisant un système de double imagerie photoélectron/photoion coïncidence (i^2 PEPICO) spectromètre.

INTRODUCTION (EN)

“Everything existing in the universe is the fruit of chance and necessity.”

Democritus

“The most beautiful experience we can have is the mysterious. It is the fundamental emotion which stands at the cradle of true art and true science. Whosoever does not know it and can no longer wonder, no longer marvel, is as good as dead, and his eyes are dimmed.”

B. Einstein

From the very beginning of its existence humanity was wondering about its origins and the origins of life itself. The searches for an answer continuing till nowadays brought us numerous mystifications and purely theological theories. The ancient philosophers like Democritus and Aristotle believed that living organisms did not have any predecessors, appeared from nowhere and evolved independently from non-living matter. One would have to wait until the XVII century to test this hypothesis and two more centuries to refute it completely. The scientific revolution started shortly afterwards with the discovery of DNA structure and decipherment of the molecular composition of polypeptides. Those two discoveries demonstrated that all living organisms were made of the same set of molecular building blocks: amino acids and nucleic acids.

Even before that another important discovery was made by a French chemist. In 1847, Louis Pasteur separated two forms of tartrate crystals and he noticed that corresponding solutions rotate the plane of polarization either in left or in the right direction. He deduced from it that crystals under the question represent two geometrically different structures, dextrorotatory and levorotatory and that dissymmetry of crystalline structure corresponds to internal dissymmetry of the molecule. This was the first notion of molecular chirality that resulted in the development of the field of stereochemistry.

Today, we say that a molecule is chiral if it is not superimposable with its image in the plane mirror, or in other words if it does not have any intrinsic symmetry. Those two non superimposable images form a pair of enantiomers. Often molecules with the stereogenic center, i.e. a carbon atom linked to four different substituents, have chiral properties. Among them building blocks of proteins – amino acids with stereogenic center at α position, as well as building blocks of nucleic acids – ribose and deoxyribose with 4 asymmetric carbons. The follow-up studies demonstrated that natural amino acids and sugars exist only in one of two possible enantiomeric forms. The synthesis of those molecules starting from methane, ammoniac, hydrogen and water has been achieved in famous experiment of Miller-Urey. Nevertheless, obtained molecular building blocks were always found as an equal mixture of two enantiomeric forms, also known as an optically inactive

4 INTRODUCTION

racemic mixture. The stereoselectivity observed among the all living organisms a phenomenon known nowadays as biomolecular homochirality.

The question of the origin of the asymmetry of biomolecules is considered closely associated to the problem of the origin of life itself. An attractive hypothesis to explain the origin of life homochirality implies intensive irradiation of precursors of biomolecules by a circularly polarized interstellar light source. Circular polarization of electromagnetic radiation is a polarization where the norm of the vector of electric field does not change while its orientation changes and describes a circle as time progresses. Such light exists in two opposite forms clockwise and anti-clockwise, and thus, represents another form of the chiral system. The photolysis of a racemic mixture by circularly polarized light was used to induce enantiomeric excess in several amino acids. Moreover, recently, strong circular polarization was discovered at the Orion Nebula. Furthermore, an excess of left-handed amino acid was detected in the Murchison meteorite. All the above-mentioned discoveries indicated that the homochirality of life may have originated in space. In the meanwhile, the proposed scenario assumes an important asymmetric photochemical destruction of chiral molecules to obtain significant enantiomeric enrichment.

The degree of the induced excess depends on the physico-chemical properties of the matter under the question. They can be studied by circular dichroism spectroscopy and by anisotropy spectroscopy. These two techniques are complementary as they help to predict enantiomeric excess for given extent of reaction and a chosen wavelength.

This manuscript includes several research axes that were carried out to achieve a better understanding of asymmetric photolysis and a possible chemical evolution of organic molecules in space. To examine the hypothesis of the extraterrestrial origin of homochirality, enantiomeric excesses were precisely determined in the meteoritic organic matter, as those samples are the only extraterrestrial samples easily accessible on earth. The analytical method of enantioselective analysis by gas chromatography was tested on the extracts of Murchison meteorite as well as on the interstellar ice analogues. Moreover, the analytical side of photoelectron circular dichroism was investigated by using a double imaging photoelectron/photoion coincidence (i^2 PEPICO) spectrometer.

CHAPTER I: Bibliographic overview

Article 1. Molecular Chirality in Meteorites and Interstellar Ices, and the Chirality Experiment on Board the ESA Cometary Rosetta Mission

Iuliia Myrgorodska, Cornelia Meinert, Zita Martins, Louis Le Sergeant d'Hendecourt, and Uwe J. Meierhenrich

Abstract

Life, as it is known to us, uses exclusively L-amino acid and D-sugar enantiomers for the molecular architecture of proteins and nucleic acids. This Mini-review explores current models of the original symmetry-breaking influence that led to the exogenic delivery to Earth of prebiotic molecules with a slight enantiomeric excess. We provide a short overview of enantiomeric enhancements detected in bodies of extraterrestrial origin, such as meteorites, and interstellar ices simulated in the laboratory. Data are interpreted from different points of view, namely, photochirogenesis, parity violation in the weak nuclear interaction, and enantioenrichment through phase transitions. Photochemically induced enantiomeric imbalances are discussed more specifically in the topical context of the “chirality module” on board the cometary Rosetta spacecraft of the ESA. This device will perform the first enantioselective in situ analyses of samples taken from a cometary nucleus.

Key words: chirality, circularly polarized light, mirror-symmetry breaking, origin of life, Rosetta mission

Published article: *Angewandte Chemie International Edition* (2015) 53: 1402 – 1412.

1. Introduction

The ESA Rosetta mission [1], successfully launched in March 2004, has now completed its 10 year journey to comet 67P/Churyumov-Gerasimenko (67P/C-G). Contrary to its predecessor missions Giotto and Vega to comet 1P/Halley, [2] Deep-Space 1 to comet 19P/Borrelly [3], Stardust to comet 81P/Wild 2 [4], and Deep Impact to comet 9P/Tempel 1 [5], Rosetta is the first space mission designed and constructed to follow a cometary nucleus through perihelion passage and to deposit a landing unit on the cometary nucleus. The Philae lander detached from the Rosetta spacecraft on November 12, 2014 and soft-landed on the surface of the cometary nucleus, the morphology and chemical composition of which is largely unknown. Philae contains the “Cometary Sampling and Composition” (COSAC) instrument, which is equipped with a chirality module for the in situ identification, separation, and quantification of organic molecules, including enantiomers, expected to be present in cometary ices. The planned analyses will provide essential information on the formation of the solar system and possibly on the origin of molecular asymmetry in biological systems [6].

Nature’s selectivity in the discrimination between left and right enantiomers has fascinated scientists since Louis Pasteur’s first investigations on chiral molecules. The origin of this distinctive and essential feature of homochirality, however, remains elusive. A multitude of hypotheses and speculations have been put forward during the last few decades. One possible scenario involves the photochirogenesis of small enantiomeric excesses (*ee*) in extraterrestrial matter, followed by the exogenous delivery of organic molecules to Earth and the amplification of the generated asymmetry to a near homochiral state. Three distinct approaches are commonly in use for the validation of this hypothesis: 1) meteorite analysis to provide information on enantiomeric enhancements of extraterrestrial origin, 2) laboratory simulations of interstellar ices to advance our understanding of asymmetric photochemical mechanisms involved in the generation of an enantiomeric excess, and 3) the ultimate step, in situ analysis of pristine cometary matter by the COSAC instrument of the Rosetta mission. Data obtained by research in these fields is expected to provide valuable insight into the origins of biomolecular homochirality.

This Minireview links the experimental simulation of interstellar ices with information obtained from the stereochemical elucidation of extraterrestrial organic matter. It will serve as a basis for the interpretation of upcoming data from the Rosetta lander and for understanding the enantiomeric enhancements detected in extraterrestrial samples and in cometary ices in particular. We give an overview of current studies on the homochirality of life as a result of the asymmetric evolution of cosmic matter and highlight existing scientific hypotheses on the source of the chiral bias in biomolecules.

1. Enantiomeric enhancement in meteoritic samples

Meteorites, in particular carbonaceous chondrites, are some of the oldest and most primitive solid materials. They display unique physical and chemical records of the formation of the solar system approximately 4.56 billion years ago, long before homochiral life originated on Earth. The enantiomeric enhancements observed in some meteoritic organic compounds are to date the only reference for molecular asymmetry that is not influenced by the terrestrial biosphere. Therefore, understanding of the origin of this phenomenon is crucial for solving the puzzle of biomolecular homochirality.

1.1. The stereochemistry of organic molecules in meteorites

It became apparent through the epochal experiments of Harold C. Urey and Stanley L. Miller that specific biological building blocks can be formed from a primitive reducing gas mixture of water, methane, and ammonia [7]. However, our vision of the atmosphere on early Earth has evolved since 1953, and it is now believed to have consisted mostly of carbon dioxide, nitrogen, and water. Under such conditions prebiotic molecules are produced only in trace amounts [8]. As an alternative source of prebiotic molecules, outer-space chemistry has been suggested [9]. In space, chemical reactions can take place both in the gas phase and on ice and mineral grain surfaces during the accretion phase of protoplanetary bodies. Many of the reaction products are thus incorporated into asteroids, interplanetary dust particles (IDPs), cometary ices, and other interplanetary objects. The structure of this diverse range of organic molecules depends on the environment in which they have formed.

Meteorites are asteroid remnants that survived impact on the surface of the Earth. Primitive meteorites, such as carbonaceous chondrites, are important reservoirs of a wide variety of organic compounds. Their material can be broadly described in terms of solubility in aqueous and organic solvent systems. Insoluble and soluble components make up 70 and 30% of the total carbon content, respectively. Insoluble organic matter (IOM) has a complex kerogen-like macromolecular network. Regardless of its high abundance, little is known about the molecular composition of IOM. Spectroscopic [10] and decomposition [11] studies suggest a general structure composed of aromatic-ring clusters bridged by aliphatic chains containing S, N, and O atoms, with peripheral branching and functional groups. However, this refractory material is not soluble in water, and its influence on prebiotic chemistry is disputable.

The complex distribution of soluble organic matter has been studied extensively in carbonaceous meteorites, including the Murchison and Murray meteorites. These studies revealed a series of alkyl-substituted bicyclic and tricyclic aromatic compounds [13], aliphatic compounds ranging from C₁ to C₇, including both saturated and unsaturated hydrocarbons [14], more than 80 amino acids (Fig. 1.1), including diamino acids [15], *N*-alkylated amino acids [16] and iminodiacids [17], small amounts of aldehydes and ketones up to C₅ [18], a wide spectrum of carboxylic acids and hydroxycarboxylic acids [19], several nucleobases [20], and sugar acids [21]. A comprehensive overview of the organic

composition of carbonaceous chondrites is provided by theme-specific review articles [22].

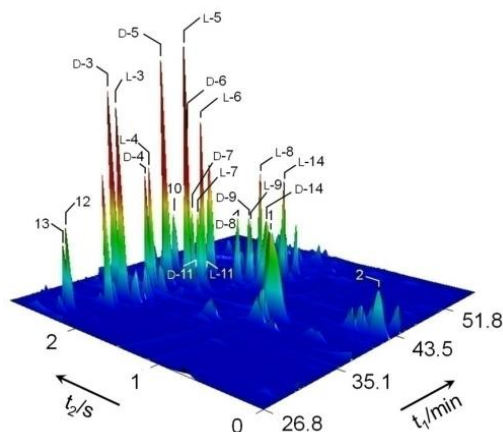


Figure 1.1. Section of a two-dimensional enantioselective gas chromatogram showing amino acids detected in the Murchison meteorite. Many of the detected amino acids are chiral. 1: glycine; 2: β -alanine; 3: alanine; 4: isovaline; 5: α -aminobutyric acid; 6: valine; 7: α -methylvaline; 8: isoleucine; 9: *allo*-isoleucine; 10: proline; 11: *tert*-leucine; 12: *N*-ethylglycine; 13: *N*-methylalanine; 14: leucine. Single-ion monitoring (SIM) at 102, 116, 130, 144, and 158 amu; chromatographic conditions are provided in Ref. [12].

From the diverse array of meteoritic organic molecules, amino acids, hydroxycarboxylic acids, monocarboxylic acids, and amines have been investigated in terms of their stereochemical composition. The chirality of meteoritic amino acids is discussed in detail in Section 2.2. Amino acids exhibit the widest range of reported *ee* values: from 60% *D-ee* for *allo*-isoleucine [23] to 18% *L-ee* for isovaline [24]. The *ee* value varies significantly for different amino acids, as well as for the same amino acid in different meteorite samples, even within the same chondrite [25]. Surprisingly, meteoritic aliphatic amines and carboxylic acids that might share a common chemical origin with amino acids were recently detected as racemates [26]. Studies of enantiomeric distribution within hydroxycarboxylic acids gave another unexpected result: Lactic acid turned out to be the only hydroxy acid species to display an excess of one enantiomer [27]. The lack of consistency in the observed enantiomeric distribution may speak against a universal explanation of their origin. Such explanations take into account the possible role of ultraviolet circularly polarized light (UV-CPL) [28], deracemization during aqueous alterations, and possible asymmetric effects of inorganic matrices within the meteorite [30], or, alternatively, the complex interplay between compound-specific physicochemical properties, synthetic pathways, and/or so-far unknown symmetry-breaking effects [25].

1.2. Enantiomeric enhancement in meteorites: Up to 18% *ee* in *L*-isovaline

After the first discovery by Engel and Nagy [31], enantiomeric enrichment in meteoritic amino acids attracted much attention in the scientific communi-

ty. In an extract of the Murchison meteorite, an *ee* value of 30% in the L enantiomer was found for alanine, which is assumed to be one of the first molecular building blocks. Even though it was later concluded that the presented *ee* value was not entirely indigenous [32], this study deserves special mention as pioneering research on extraterrestrial enantiomeric enrichment.

Subsequent studies focused on α -dialkylated amino acids as species with rare occurrence in the biosphere and a low rate of racemization. In contrast to proteinogenic amino acids, which can lose and reacquire their α -hydrogen atom through the attainment of equilibrium during aqueous alteration, α -dialkylated amino acids are believed to preserve pristine *ee* values. An investigation on the terrestrially rare C₅–C₇ amino acids in the Murchison meteorite demonstrated nonzero *ee* values in favor of the L configuration for α -amino- α,β -dimethylpentanoic acid, isovaline, norvaline, and α -methylnorvaline [24, 25, 33], whereas β -aminobutyric acid was found to be racemic [34]. Table 1.1 presents an overview of reported *ee* values of amino acids in carbonaceous meteorites.

Table 1.1. Detected enantiomeric excesses of amino acids in carbonaceous meteorites.

Amino acid	L- <i>ee</i> (%)	Meteorite
Isovaline	-1.0 to +18.5[24]	EET, LEW, LON, MN, MY, OR, QUE
Norvaline	-0.7 to +3.7[24b]	EET, LON, MN, OR, QUE
α -Methylnorvaline	2.8, 1.4[33]	MN, MY
Valine	-0.4 to +43.6[24b,34]	EET, LEW, LON, MN, MY, OR, QUE
α -Methylvaline	2.8, 1.0 [33]	MN, MY
α -Methylnorleucine	4.4, 1.8[33]	MN, MY
Isoleucine	3.6 – 50[23]	EET, GRA LAP, ME, MIL, PCA, QUE
<i>allo</i> -Isoleucine	-60 to -2.2 [23]	EET, GRA LAP, ME, MIL, PCA, QUE
α -Amino- α -methylheptanoic acid	7.0[25]	MN
α -Amino- α,β -dimethylpentanoic acid	1.4 – 5.2[25]	MN, MY
<i>allo</i> - α -Amino- α,β -dimethylpentanoic acid	2.2 – 10.4[25]	MN, MY
α -Methylglutamic acid	2 – 3[23]	MN

EET, EET 92042; GRA, GRA 95229; LAP, LAP 02342; LEW, LEW 90500; LON, LON 94102; MN, Murchison; MY, Murray; OR, Orgueil; ME, MET 00426; MIL, MIL 07525; PCA, PCA 91082; QUE, QUE 99177.

Isovaline, the most abundant of the α -dialkylated chiral amino acids, shows one of the highest reported *ee* values (see Table 1.1 and Fig. 1.2) [24]. Pizzarello et al. [24a] interpreted the high enrichment of isovaline in the L form as a

result of its distinct synthetic pathway. It is generally thought that amino acids in meteorites are formed through Strecker cyanohydrins synthesis from aldehydes and ketones. In this case, the enantiomeric enhancement of isovaline was proposed to be derived from its aldehyde precursor. Later, Glavin and Dworkin [24b] demonstrated a direct relationship between the degree of aqueous alteration and the amplification of meteoritic L-isovaline. Although the indigenosity of the *ee* values of α -dialkylated amino acids leaves no doubt, the question of the origin of this enantiomeric enrichment remains open.

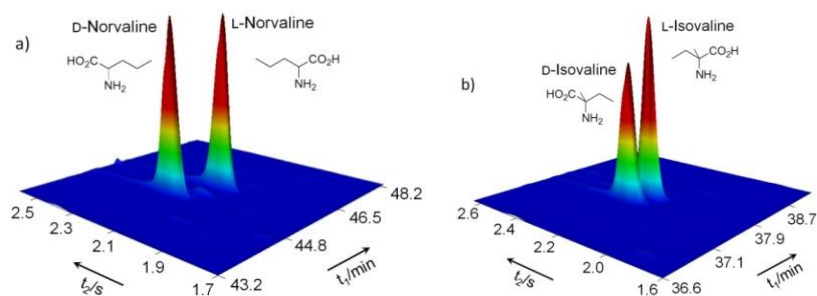


Figure 1.2. Sections of a two-dimensional enantioselective GC x GC-TOFMS gas chromatogram showing a) racemic D- and L-norvaline enantiomers ($(-0.04 \pm 0.39) \% ee$) and b) enantiomerically enriched D- and L-isovaline enantiomers ($(4.61 \pm 0.83) \% ee$) identified in a sample of the Murchison meteorite. SIM at 144 amu; for analytical conditions, see Ref. [12].

2. Chirality investigations in simulated comets

Taking into consideration the evolutionary relationship between meteorites and IDPs with their icy mantles [35], one would expect to find similar molecular and chiral signatures (e.g. amino acids and their *ee* values) within comets. So far, however, only small volatile molecules have been detected with confidence in cometary atmospheres. The failure to detect such signatures can be explained by the insufficient sensitivity of telescopes for the analysis of refractory compounds or the absence of liquid water essential for prebiotic chemical processing [36]. The achiral amino acid glycine was identified in a sample of the comet Wild 2 [37]. For better insight into the molecular and stereochemical composition of pristine cometary matter and thus an understanding of the original symmetry-breaking influence, laboratory interstellar-simulation experiments and the in situ analysis of cometary ices are necessary.

2.1. Organic Molecules in Simulated Cometary Ices

Knowledge on cometary ices has been obtained by remote observations of comets and by the identification of volatile and refractory components adsorbed on interstellar dust. The results have led to the development of experimental methods that enable the production of both refractory materials and frozen volatiles with chemical, structural, and morphological characteristics that are assumed to reproduce those observed and/or expected in comets [38]. According to the comet core-mantle grain model developed by Greenberg [39], small molecules

condense from the gas phase on the cold surface of interstellar dust grains, thereby forming an icy mantle. During the deposition, the grain and mantle are subjected to energy in the form of UV photons and cosmic-ray particles. This processing is assumed to result in the formation of free radicals and creates a highly conducive environment for the transformation of ice-trapped radicals and molecules into prebiotically relevant organic compounds, such as amino acids, nucleobases, and sugars [40] (Fig. 1.3). Further aggregation of interstellar dust particles results in the formation of larger bodies, such as comets.

Such processes are generally simulated in the laboratory by the deposition of a gaseous mixture of key interstellar species under high vacuum on a cold surface and irradiation with UV light or charged particles. The organic residue formed in such experiments provides valuable information on the possible composition of the cometary nucleus: information that is inaccessible by remote observations.

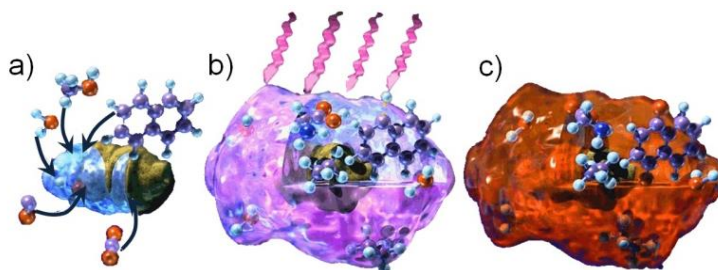


Figure 1.3. Development phases of interstellar dust particles: a) Silicate grains accrete ice layers from volatile molecules present in the surrounding gas phase (H_2O , CO_2 , CO , CH_3OH , and NH_3). b) During the growth process, the icy mantle is irradiated with UV photons, which create radicals and initiate photochemical reactions. c) The radical-induced reactions produce a complex network of organic molecules, including amino acids. Adapted from reference [28a].

A remarkable diversity of organic compounds has been synthesized within interstellar-ice analogues by both UV and charged-particle irradiation [41]. Bernstein et al. [42] detected glycine, alanine, and serine as products after acid hydrolysis of a residue originating from a 20:2:1:1 $\text{H}_2\text{O}/\text{CH}_3\text{OH}/\text{NH}_3/\text{CH}_3\text{CN}$ gas mixture. Independently, Muñoz Caro et al. [43] identified 16 amino acids in the hydrolyzed and derivatized organic residue obtained by UV irradiation of $\text{H}_2\text{O}/\text{CH}_3\text{OH}/\text{NH}_3/\text{CO}/\text{CO}_2$ (2:1:1:1:1). Muñoz Caro et al. used ^{13}C -labeled precursors to exclude contamination as a possible source of organic molecules. Further experiments of Meinert et al. [44] provided an up-to-date list of 26 amino acids, including proteinogenic and nonproteinogenic amino acids, diamino acids, and *N*-(2-aminoethyl)glycine. All amino acids were detected as racemates, as no chiral influence was introduced into the system. The analysis of a nonhydrolyzed residue by Briggs et al. [45] resulted in the detection of only glycine, the simplest amino acid (see also Ref. [46]). It was therefore proposed that the products of the photochemical reactions are incorporated into some macromolecular structure, and then released upon acid hydrolysis. Apart from amino acids, different mixtures of simulated interstellar ices produced purine and pyrimidine compounds, urea, and polyols, along with other prebiotic molecular structures [47].

The majority of the detected compounds were identified in meteorites as well. Thus, a logical question arises: “Do pristine cometary chiral molecules, like the further-altered meteoritic molecules, exhibit any enantiomeric preference?” To answer this question, we introduce in Sections 3.2 and 4.1 a set of experiments in which prebiotic chiral molecules and/or their precursors have been subjected to truly chiral entities, such as CPL.

2.2. Enantiomeric enhancements in simulated cometary ices

The interaction of matter with UV-CPL has been proposed as one of the possible sources of biomolecular asymmetry (see Section 4). This notion implies a scenario in which the first symmetry-breaking event occurred when the giant molecular cloud from which our solar system formed was exposed to asymmetric CPL of a given helicity [48]. This hypothesis was tested by systematically simulating interstellar ices by irradiation with right- and left-handed UV-CPL.

The first attempts to perform absolute asymmetric synthesis from an ice mixture of H₂O, CH₃OH, and NH₃ by irradiation with CPL at a wavelength of $\lambda = 167$ nm resulted in a small *ee* value of 1%, which lay within the limits of detection of the instruments and methods [49]. Further improvement of the experimental procedure by changing the CPL wavelength to $\lambda = 187$ nm and using multi-dimensional gas chromatography for advanced analysis yielded in *ee_L* values of up to -1.34% [50]. In recent investigations by Modica et al. [51], statistically relevant *ee* values were induced in five enantiomeric pairs of amino acids, with a maximum value of -2.54% *ee_L* for 2-aminobutyric acid. The sign of the induced *ee* values depends on the helicity as well as the energy of the CPL and was identical for all five amino acids at $\lambda = 121$ nm for each given helicity. Similar *ee* values to those induced photochemically in laboratory ices can be expected for cometary amino acids.

These studies, however, do not provide information on the mechanism for the asymmetric formation of amino acids. It remains difficult to distinguish between the two relevant mechanisms of absolute asymmetric photosynthesis and absolute asymmetric photolysis.

3. Stereochemical mechanism of enantiomeric enrichments

Many theories exist to explain the original instance of enantiomeric enrichment. These theories can be broadly classified according to Jacques Monod’s famous phrase into “chance and necessity” or alternately “probabilistic versus deterministic” [52]. The “chance” school hypothesizes that homochirality arose from a random symmetry-breaking event and assumes an equal probability of generating a world with an opposite handedness. The supporters of the “necessity” model assume a selection process between enantiomers and a unique definitive solution to the origin of biological asymmetry. In this section, we group the main theories for the generation of an enantiomeric excess according to the nature of the chiral influence involved.

3.1. Enantiomeric enhancement induced by asymmetric photochemistry

Among photochemical effects, only circularly polarized light and a static magnetic field collinear with a light beam are truly chiral systems and thus can potentially produce an enantiomeric enhancement within initially racemic mixtures [53]. Both of these mechanisms were proposed to be responsible for the symmetry breaking in biomolecules [48, 54].

With CPL, the electric-field vector E and the magnetic field vector B remain constant in magnitude but proceed in the form of left or right helices around the axis of the direction of propagation. Therefore, CPL can distinguish between two enantiomers owing to the difference in absorption of left-handed and right-handed CPL, an effect that is wavelength-dependent and known as circular dichroism (CD). This chiroptical property leads to the preferential destruction of one of the enantiomers, as demonstrated in numerous experiments [55]. A detailed mechanistic understanding of the photochemical nature of the mirror-symmetry-breaking event upon CPL irradiation is provided in the literature [28, 56] and illustrated in Fig. 1.4.

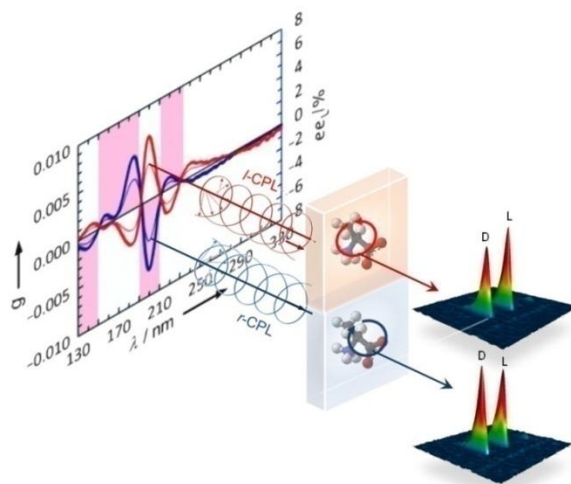


Figure 1.4. Photolytic induction of enantiomeric enrichment in racemic alanine. Interaction with CPL of sufficient energy imparts a slight bias for the less photoabsorbent enantiomer as the more photoabsorbent enantiomer undergoes faster photolysis. The degree and sign of the induced asymmetry depend on the helicity of the CPL, the energy of the driving electromagnetic radiation, the photolysis rate, and the ratio between the differential extinction ($\Delta\epsilon$) and the extinction coefficient (ϵ) of the enantiomers. This ratio is also known as anisotropy, $g = \Delta\epsilon/\epsilon$, which itself depends on the wavelength of the incident CPL. Anisotropy spectra include crucial information about enantioselective photolysis. These data enable the selection of a CPL wavelength for induction of greater enantiomeric enrichment, prediction of the sign of the induced enantiomeric enrichment, and the calculation of expected ee values.

It is hypothesized that extraterrestrial organic material, prior to its delivery to Earth by IDPs, meteorites, and/or comets, has been exposed to interstellar UV-CPL and thus become enriched in one of the enantiomeric forms; its sym-

metry has been broken. Autocatalytic processes could have amplified small ee values to produce a state close to homochirality. The detection of circularly polarized electromagnetic radiation in the infrared wavelength domain from several star-forming regions [48d, 57] provided additional support for this proposed scenario. Calculations show that ultraviolet CPL capable of inducing enantiomeric enhancement is also present [58] but cannot be observed owing to the high degree of dust obscuration of UV light in such environments.

An oriented beam of unpolarized light passing through a static magnetic field is another example of a truly chiral influence. Similarly to the CPL model, enantiomers absorb the radiation traveling parallel or antiparallel to the applied magnetic field to different extents. This effect is referred to as magnetochiral dichroism (MD). It was demonstrated to induce very small ee values (10^{-5} %) in specific chiral ferromagnetic molecules [59]. The ubiquity of magnetic fields and unpolarized light in the cosmos led Barron [54] to propose this effect as a candidate for the abiotic generation of an enantiomeric excess. However, given the fact that MD depends upon very high magnetic fields of up to 15 T and results in such small asymmetry, it is now thought by adherents of this assumption that meteoritic enantiomeric enhancement has been caused either by UV-CPL generated from a directed magnetic field (Faraday effect) or by direct asymmetrical magneto-optical effects distinct from Faraday rotation [60].

Both chiral influences cause enantiomeric enhancement in either the L or the D form, depending on the local nebular region, but not when averaged over the entire cosmos. Given the data from astronomical observations [48d, 57] and the most recent experiments [49, 50, 55] we can conclude that the origin of biomolecular asymmetry is probably a consequence of photochemical effects based on CPL.

3.2. Enantiomeric enhancement induced upon crystallization, phase transition, and Viedma ripening

Chiral-symmetry breaking upon spontaneous crystallization has long been known for sodium chlorate solution [61]. Achiral sodium and chlorate ions are known to crystallize as two separate chiral solid phases in the form of a racemic mixture [62], but under specific stirring conditions, the sodium chlorate can precipitate randomly as a single chiral phase. Later, this phenomenon was determined to be a result of secondary nucleation enhanced by agitation under far-from-equilibrium conditions [63].

In 2005, a new mechanism of symmetry breaking was demonstrated for sodium chlorate. A single chiral solid state was formed under “near-equilibrium” conditions, under which no new crystals nucleate. This phenomenon is known as “Viedma ripening” [64]. Extension of this approach to proteinogenic amino acids under prebiotically plausible conditions resulted in a solid-phase enantiomeric enrichment of up to 99% for aspartic acid [64b]. L-Aspartic acid was thus proposed to be an ancestor of left-handed molecules [65]. The choice of aspartic acid was by no means a coincidence, as it is one of two proteinogenic amino acids that meets all necessary requirements for “Viedma ripening”, that is, 1) the formation of conglomerate crystals and 2) fast racemization of the enantiomers in solution.

These restrictions leave little room for chiral-symmetry breaking in the other 17 chiral proteinogenic amino acids, and especially in meteoritic α -dialkylated analogues, which are resistant against racemization. The sublimation protocol recently introduced by Viedma et al. [66] reveals both the conversion of a racemic compound into a racemic conglomerate and subsequent enantioenrichment; it might open new horizons for the enantiomeric purification of previously overlooked amino acids.

Regardless of the significance of chiral-symmetry breaking upon crystallization, current data provide a rather poor explanation for the observed meteoritic *ee* values, and the model has low astrophysical relevance, as chiral molecules in outer space are believed to be incorporated in a macromolecular matrix [25] rather than existing in a solution under constant stirring or grinding. Further investigation of chiral resolution through sublimation and other astrophysically admissible processes may provide new insight on this topic [67].

3.3. Enantiomeric enhancement induced by weak nuclear interaction

All universal interactions were considered to be entirely symmetrical before the discovery in 1956 of the parity violation in the weak force [68]. Parity violation means that the true mirror image of an object or experiment is energetically not equivalent to the original [69]. It was demonstrated that in the β -decay, mediated by the weak force, radioactive ^{60}Co nuclei emit exclusively left-polarized electrons, which therefore violate parity [70]. As a consequence, we expect a small energy difference between two enantiomers [71]. This energy gap has not yet been measured, but it was calculated to have an order of 10^{-12} – 10^{-15} Jmol $^{-1}$ [72] with a magnitude and sign that depend on the particular conformer of the studied compound. Owing to this dependence, there is no general answer to the question of which enantiomer is generally favored. Quack [73] pointed out that even if parity violation causes a left or right preference on the molecular level, this preference is not necessarily linked to the evolution of biomolecular homochirality.

Another indirect way that weak nuclear forces could cause enantiomeric enhancement is chirality transfer from spin-polarized electrons to chiral molecules. The enantiomers of a chiral molecule become ionized at different rates upon irradiation with β -electrons, thus resulting in enantioselective degradation. This effect known as “electronic circular dichroism” was first measured for the optical isomers D- and L-camphor, which did not weaken the passing spin-polarized electrons equally [74]. It was applied to induce optical activity in leucine [75], tryptophan [76], and alanine [77]; however, the kinetic energy of the investigated spin-polarized electrons was by orders of magnitude too high for efficient enantiomer-discriminating absorption.

In early 1962, Ulbricht and Vester [78] proposed to use bremsstrahlung radiation produced by decelerated spin-polarized electrons to produce enantioselective interactions within organic matter. Each individual step in the Vester–Ulbricht mechanism has received experimental confirmation. First encouraging results were obtained by Garay [79], who detected small differences in the ultravi-

olet absorption spectra of D- and L-tyrosine after exposure for 18 months to $^{90}\text{SrCl}_2$ β -rays and bremsstrahlen. Subsequent experiments produced either very small [80] or no [81] asymmetrical effects and were considered inconclusive and contradictory [82]. However, they do not preclude the contribution of the Vester–Ulbricht scenario to enantiomeric enrichment in interstellar evolution, during which numerous β -radiators have been present [28].

3.4. Amplification of enantiomeric enhancement by autocatalytic processes

A tiny enantiomeric excess produced by one of the above-mentioned mechanisms can be increased by means of autocatalytic processes to homochirality. Models for the amplification of an enantiomeric imbalance were divided by Blackmond [83] into those governed by kinetics in far-from-equilibrium processes and those based on thermodynamics and equilibrium phase behavior.

The first theoretical model of spontaneous asymmetric amplification was proposed by Frank in 1953 [84]. In this model, a large enantiomeric excess can be generated in a chemical reaction in which one enantiomer catalyzes its own formation while inhibiting the formation of the other enantiomer. Soai et al. [85] provided the first experimental proof for this model when they reported the formation of 5-pyridyl alcohol with up to 90% *ee* from the same alcohol with a small initial *ee* value upon treatment with diisopropylzinc and pyrimidine-5-carboxaldehyde. This reaction clearly does not occur under prebiotic conditions, but it is an important example of the absolute asymmetric synthesis of enantiomerically enriched products. The Soai reaction was later shown to be extremely sensitive to initial *ee* values as small as those produced upon CPL irradiation [86]. Its kinetic model has been studied in detail by the groups of Blackmond [87] and Buhse [88].

Another example of the Frank model is the amplification of an initial enantiomeric disproportion through physical processes, such as evaporation, crystallization, or sublimation under “far-from-equilibrium” conditions. This strategy has proven to be effective for threonine [89], aspartic acid, and glutamic acid [90], as well as for valine [91].

The autocatalysis based on equilibrium phase behavior is fully reflected in crystallization under “near-equilibrium” conditions as described by Viedma [64b, 92]. Moreover, Klusmann et al. [93] established that the coupling of solid–liquid phase behavior and amino acid catalysis results in an efficient thermodynamically controlled mechanism for asymmetric amplification.

In attempts to link the opposite chirality of nucleotides and amino acids, it was proposed that a small imbalance in the D/L ratio of amino acids might have played a crucial role in the generation and/or amplification of *ee* values in nucleotide precursors. Studies carried out by Mathew et al. [94] showed that proline could influence a reaction by increasing the rate of the formation of one of the two possible optical isomers of the product. Further investigations by the same research group revealed that amino acids with a small initial enantiomeric excess can drive the formation of enantiomerically enriched nucleotide precursors, thus paving the way to homochiral RNA [95].

4. The chirality module on board the Rosetta lander Philae

For the advancement of our scientific knowledge about the origin and evolution of extraterrestrial molecules and particularly about the origin of the observed asymmetry in meteoritic matter, the underlying mechanisms of the formation of these molecules have to be understood. This challenge is being taken up, at least partially, by the Rosetta mission.

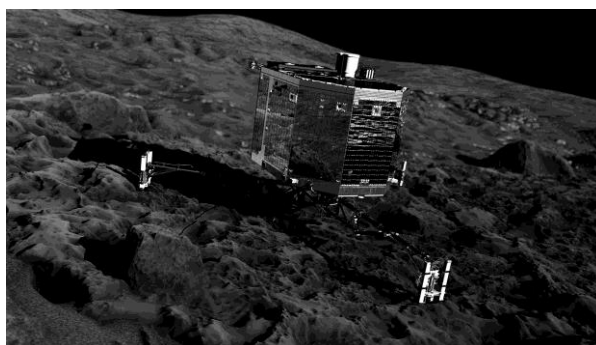


Figure 1.5. Computer graphic of the Rosetta lander Philae on the surface of the nucleus of comet 67P/Churyumov-Gerasimenko. Philae is equipped with an enantioselective GC–MS instrument with three chiral stationary phases. Image credit: ESA.

Approved in 1993 as the “Planetary Cornerstone Mission” of the ESA and launched in 2004, the Rosetta spacecraft has finally reached its target comet 67P/C-G. The Rosetta [1] spacecraft is composed of two principal elements: the lander Philae and the orbiter Rosetta. Each of them is equipped with 10 instruments specifically designed to accomplish the mission objectives. In November 2014, the Philae lander detached from the Rosetta spacecraft to perform the first scientific in situ investigation of a cometary nucleus (Fig. 1.5).

A drilling system (SD-2) will obtain samples from a depth of up to 23 cm and distribute them to the other instruments for the investigation of their chemical composition, density, near-surface strength, porosity, texture, ice phase, and thermal properties. Among these instruments, the “Cometary Sampling and Composition” (COSAC) [96] experiment is of high importance for stereochemical investigations. The COSAC instrument is equipped with a multicolumn gas chromatograph (GC) and a time-of-flight mass spectrometer (TOFMS), and is connected to an electronic system that allows remote operation of the suite. The GC system includes a set of eight parallel capillary columns and two types of pyrolysis ovens. The chromatographic columns vary in their stationary phase, film thickness, diameter, and length; three of them can resolve chiral organic molecules. COSAC is the first instrument sent to space for the investigation of chirality [97].

On the basis of remote observations [36], previous flyby missions [2–5], and interstellar ice simulations [42, 43, 45, 49–51], the cometary nucleus has been imagined as a “dirty snowball” owing to its high content of dust, organic material, and ice. Analysis of the stereochemical and molecular composition of this “dirty

snowball” is the objective of the COSAC experiment. Before a cometary sample is subjected to chromatographic separation, it will be derivatized with *N,N*-dimethylformamide dimethyl acetal [98] to transform refractory molecules through methylation into volatile species. After separation on the GC column, these molecules enter the TOFMS, where they become ionized and produce characteristic spectral signals allowing structural elucidation.

The main interest in the COSAC instrument regards the separation and quantification of chiral organic molecules [99]. The list of Rosetta-relevant chiral molecules includes hydrocarbons, amines, alcohols, diols, carboxylic acids, and amino acids [97–100]. The investigators responsible for the COSAC chiral module assume that there is a reasonable chance of finding partial enantiomeric enrichment in chiral molecules as result of the exposure of the cometary ices to extraterrestrial chiral fields [28]. An identical or similar excess of L-configured molecules to those observed in meteorites would support the assumption that chiral organic molecules were indeed delivered to early Earth during the late heavy-bombardment phase by comets and/or other small interplanetary bodies whose organic content may be of interstellar/presolar origin, from the molecular cloud from which our solar system formed. Even though the physicochemical mechanisms for the generation of an enantiomeric excess are not yet fully understood, the results of the COSAC experiment will bring us one step closer to solving the puzzle of how homochiral life could have originated on Earth.

5. Summary and outlook

The main astrobiologically relevant hypotheses to explain the origin of biomolecular asymmetry assume the induction of a small enantiomeric excess by either photochemical effects, parity violation, or phase changes and its amplification by autocatalytic processes on Earth. The key step, chiral-symmetry breaking, has been puzzling scientists for over 50 years. In view of the results of ice-simulation experiments and analyses of meteoritic samples, UV-CPL can be considered as one favorable candidate for the original asymmetrical influence. Nevertheless, alternative sources of chiral imbalance must not be overlooked. The long-awaited results from Rosetta’s chirality module will hopefully provide crucial insight into the stereochemistry of prebiotic molecules within interstellar objects. The detection of prebiotic chiral molecules in comets will be an important step towards understanding the emergence and development of homochiral life.

References

- [1] U. J. Meierhenrich, *Comets and their Origin—The Tool to Decipher a Comet*, Wiley-VCH, Weinheim, **2015**.
- [2] a) H. Keller, C. Arpigny, C. Barbieri, R. Bonnet, S. Cazes, M. Coradini, C. Cosmovici, W. Delamere, W. Huebner, D. Hughes, et al., *Nature* **1986**, *321*, 320 – 326; b) R. Sagdeev, F. Szabo, G. Avanesov, P. Cruvellier, L. Szabo, K. Szegő, A. Abergel, A. Balazs, I. Barinov, J. Bertaux, et al., *Nature* **1986**, *321*, 262 – 266.
- [3] L. Soderblom, T. Becker, G. Bennett, D. Boice, D. Britt, R. Brown, B. Buratti, C. Isbell, B. Giese, T. Hare, et al., *Science* **2002**, *296*, 1087 – 1091.
- [4] D. Brownlee, P. Tsou, J. Aléon, C. M. D. Alexander, T. Araki, S. Bajt, G. A. Baratta, R. Bastien, P. Bland, P. Bleuet, et al., *Science* **2006**, *314*, 1711 – 1716.
- [5] M. F. A'Hearn, M. Belton, W. Delamere, J. Kissel, K. Klaasen, L. McFadden, K. Meech, H. Melosh, P. Schultz, J. Sunshine, et al., *Science* **2005**, *310*, 258 – 264.
- [6] E. Gibney, *Nature* **2014**, *505*, 269 – 270.
- [7] a) S. L. Miller, *Science* **1953**, *117*, 528 – 529; b) T. M. McCollom, *Annu. Rev. Earth Planet. Sci.* **2013**, *41*, 207 – 229.
- [8] a) G. Schlesinger, S. Miller, *J. Mol. Evol.* **1983**, *19*, 383 – 390; b) K. Kobayashi, T. Ogawa, H. Tonishi, T. Kaneko, Y. Takano, J.-I. Takahashi, T. Saito, Y. Muramatsu, S. Yoshida, Y. Utsumi, *Electron. Comm. Jpn.* **2008**, *91*, 15 – 21.
- [9] C. Chyba, C. Sagan, *Nature* **1992**, *355*, 125 – 132.
- [10] a) J. R. Cronin, S. Pizzarello, J. S. Frye, *Geochim. Cosmochim. Acta* **1987**, *51*, 299 – 303; b) T. J. Wdowiak, G. C. Flickinger, J. R. Cronin, *Astrophys. J.* **1988**, *328*, L75 – 79.
- [11] a) R. L. Levy, M. A. Grayson, C. J. Wolf, *Geochim. Cosmochim. Acta* **1973**, *37*, 467 – 483; b) R. Hayatsu, R. E. Winans, R. G. Scott, R. L. McBeth, P. M. Leon, M. H. Studier, *Science* **1980**, *207*, 1202 – 1204.
- [12] C. Meinert, U. J. Meierhenrich, *ChemPlusChem* **2014**, *79*, 781 – 785.
- [13] a) K. L. Pering, C. Ponnampereuma, *Science* **1971**, *173*, 237 – 239; b) B. P. Basile, B. S. Middleditch, J. Oró, *Org. Geochem.* **1984**, *5*, 211 – 216.
- [14] a) K. Kvenvolden, J. Lawless, K. Pering, E. Peterson, J. Flores, C. Ponnampereuma, I. R. Kaplan, C. Moore, *Nature* **1970**, *228*, 923 – 926; b) J. R. Cronin, S. Pizzarello, *Geochim. Cosmochim. Acta* **1990**, *54*, 2859 – 2868.
- [15] U. J. Meierhenrich, G. M. Muñoz Caro, J. H. Bredehöft, E. K. Jessberger, W. H.-P. Thiemann, *Proc. Natl. Acad. Sci. USA* **2004**, *101*, 9182 – 9186.
- [16] a) A. Shimoyama, C. Ponnampereuma, K. Yanai, *Nature* **1979**, *282*, 394 – 396; b) J. R. Cronin, S. Pizzarello, G. U. Yuen, *Geochim. Cosmochim. Acta* **1985**, *49*, 2259 – 2265; c) J. R. Cronin, S. Pizzarello, *Geochim. Cosmochim. Acta* **1986**, *50*, 2419 – 2427; d) G.W. Cooper, J. R. Cronin, *Geochim. Cosmochim. Acta* **1995**, *59*, 1003 – 1015.
- [17] N. R. Lerner, G.W. Cooper, *Geochim. Cosmochim. Acta* **2005**, *69*, 2901 – 2906.
- [18] G. A. Jungclauss, G. U. Yuen, C. B. Moore, J. G. Lawless, *Meteoritics* **1976**, *11*, 231 – 237.

- [19] a) J. G. Lawless, B. Zeitman, W. E. Pereira, R. E. Summons, A. M. Duffield, *Nature* **1974**, 251, 40 – 42; b) E. T. Peltzer, J. L. Bada, *Nature* **1978**, 272, 443 – 444; c) J. G. Lawless, G. U. Yuen, *Nature* **1979**, 282, 396 – 398; d) G. Yuen, N. Blair, D. J. DesMarias, S. Chang, *Nature* **1984**, 307, 252 – 254; e) J. R. Cronin, S. Pizzarello, S. Epstein, R. V. Krishnamurthy, *Geochim. Cosmochim. Acta* **1993**, 57, 4745 – 4752.
- [20] a) P. G. Stoks, A.W. Schwartz, *Nature* **1979**, 282, 709 – 710; b) Z. Martins, O. Botta, M. L. Fogel, M. A. Sephton, D. P. Glavin, J. S. Watson, J. P. Dworkin, A.W. Schwartz, P. Ehrenfreund, *Earth Planet. Sci. Lett.* **2008**, 270, 130 – 136.
- [21] G. Cooper, N. Kimmich, W. Belisle, J. Sarinana, K. Brabham, L. Garrel, *Nature* **2001**, 414, 879 – 883.
- [22] a) O. Botta, J. L. Bada, *Surveys in Geophysics* **2002**, 23, 411 – 467; b) M. A. Sephton, *Nat. Prod. Rep.* **2002**, 19, 292 – 311; c) Z. Martins, M. A. Sephton in *Amino Acids, Peptides and Proteins in Organic Chemistry* (Ed.: A. B. Hughes), Wiley, Weinheim, **2009**, p. 2 – 42.
- [23] a) S. Pizzarello, D. L. Schrader, A. A. Monroe, D. S. Lauretta, *Proc. Natl. Acad. Sci. USA* **2012**, 109, 11949 – 11954; b) J. E. Elsila, D. P. Glavin, J. P. Dworkin, Z. Martins, J. L. Bada, *Proc. Natl. Acad. Sci. USA* **2012**, 109, E3288.
- [24] a) S. Pizzarello, M. Zolensky, K. A. Turk, *Geochim. Cosmochim. Acta* **2003**, 67, 1589 – 1595; b) D. P. Glavin, J. P. Dworkin, *Proc. Natl. Acad. Sci. USA* **2009**, 106, 5487 – 5492.
- [25] S. Pizzarello, T. L. Groy, *Geochim. Cosmochim. Acta* **2011**, 75, 645 – 656.
- [26] a) J. C. Aponte, M. R. Alexandre, Y. Wang, A. J. Brearley, C. M. O. D. Alexander, Y. Huang, *Geochim. Cosmochim. Acta* **2011**, 75, 2309 – 2323; b) J. C. Aponte, J. P. Dworkin, J. E. Elsila, *Geochim. Cosmochim. Acta* **2014**, 141, 331 – 345.
- [27] S. Pizzarello, Y. Wang, G. M. Chaban, *Geochim. Cosmochim. Acta* **2010**, 74, 6206 – 6217.
- [28] a) U. J. Meierhenrich, *Amino Acids and the Asymmetry of Life*, Springer, Heidelberg, **2008**; b) A. Guijarro, M. Yus, *The Origin of Chirality in the Molecules of Life*, Royal Society of Chemistry, Cambridge, **2009**.
- [29] D. W. Deamer, R. Dick, W. Thiemann, M. Shinitzky, *Chirality* **2007**, 19, 751 – 763.
- [30] S. Pizzarello, *Antarct. Meteorite Res.* **2003**, 17, 65.
- [31] M. H. Engel, B. Nagy, *Nature* **1982**, 296, 837 – 840.
- [32] S. Pizzarello, J. R. Cronin, *Nature* **1998**, 394, 236 – 236.
- [33] S. Pizzarello, J. R. Cronin, *Geochim. Cosmochim. Acta* **2000**, 64, 329 – 338.
- [34] J. R. Cronin, S. Pizzarello, *Science* **1997**, 275, 951 – 955.
- [35] E. Anders, E. Zinner, *Meteoritics* **1995**, 28, 490 – 514.
- [36] D. Despois, H. Cottin in *Lectures in Astrobiology* (Eds.: M. Gargaud, B. Barbier, H. Martin, J. Reisse), Springer, Heidelberg, **2005**, pp. 289 – 352.
- [37] a) S. A. Sandford, J. Aléon, C. M. D. Alexander, T. Araki, S. A. Bajt, G. A. Baratta, J. Borg, J. P. Bradley, D. E. Brownlee, J. R. Brucato, et al., *Science* **2006**, 314, 1720 – 1724; b) J. E. Elsila, D. P. Glavin, J. P. Dworkin, *Meteorit. Planet. Sci.* **2009**, 44, 1323.

- [38] L. Colangeli, J. R. Brucato, A. Bar-Nun, R. L. Hudson, M. H. Moore, *Comets II* (Eds.: M. C. Festou, H. U. Keller, H. A. Weaver), University of Arizona Press, **2004**, pp. 695 – 717.
- [39] a) J. M. Greenberg in *Comets* (Ed.: L. L. Wilkening), University of Arizona Press, Tucson, **1982**, pp. 131 – 163; b) J. M. Greenberg, *Origin Life* **1984**, 14, 25 – 36; c) J. M. Greenberg, *Nature* **1986**, 321, 385 – 385; d) J. M. Greenberg, A. Kouchi, W. Nissan, H. Irth, J. v. Paradijs, M. d. Groot, W. Hemsén, *J. Biol. Phys.* **1994**, 20, 61 – 70.
- [40] a) R. T. Garrod, S. L.W. Weaver, A. J. E. Herbst, *Astrophys. J.* **2008**, 682, 283 – 302; b) W.W. Duley, *Astrophys. J.* **2000**, 528, 841 – 848; c) M. H. Moore, B. Donn, R. Khanna, M. F. A’Hearn, *Icarus* **1983**, 54, 388 – 405.
- [41] a) G. Strazzulla, *Adv. Space Res.* **1997**, 19, 1077 – 1084; b) G. Strazzulla, G. A. Baratta, R. E. Johnson, B. Donn, *Icarus* **1991**, 91, 101 – 104; c) L. J. Allamandola, S. A. Sandford, G. J. Valero, *Icarus* **1988**, 76, 225 – 252; d) H. Cottin, M. H. Moore, Y. Benilan, *Astrophys. J.* **2003**, 590, 874 – 881.
- [42] M. P. Bernstein, J. P. Dworkin, S. A. Sandford, G. W. Cooper, L. J. Allamandola, *Nature* **2002**, 416, 401 – 403.
- [43] G. M. Muñoz Caro, U. J. Meierhenrich, W. A. Schutte, B. Barbier, A. Arconas Segovia, H. Rosenbauer, W. H.-P. Thiemann, A. Brack, J. M. Greenberg, *Nature* **2002**, 416, 403 – 406.
- [44] C. Meinert, J.-J. Filippi, P. de Marcellus, L. Le Sergeant d’Hendecourt, U. J. Meierhenrich, *ChemPlusChem* **2012**, 77, 186 – 191.
- [45] R. Briggs, G. Ertem, J. P. Ferris, J. M. Greenberg, P. J. McCain, C. X. Mendoza-Gomez, W. Schutte, *Origin Life* **1992**, 22, 287 – 307.
- [46] a) U. J. Meierhenrich, G. M. Muñoz Caro, W. A. Schutte, W. H. P. Thiemann, B. Barbier, A. Brack, *Chem. Eur. J.* **2005**, 11, 4895 – 4900; b) C. N. Matthews, R. D. Minard, *Farraday Discuss.* **2006**, 133, 393 – 401.
- [47] a) M. Nuevo, J. H. Bredeho, U. J. Meierhenrich, L. d’Hendecourt, W. H.-P. Thiemann, *Astrobiology* **2010**, 10, 245 – 256; b) M. Nuevo, S. N. Milam, S. A. Sandford, *Astrobiology* **2012**, 12, 295 – 314.
- [48] a) E. Rubenstein, W. A. Bonner, H. P. Noyes, G. S. Brown, *Nature* **1983**, 306, 118 – 118; b) W. A. Bonner, E. Rubenstein, *Biosystems* **1987**, 20, 99 – 111; c) W. A. Bonner, *Origins Life Evol. Biospheres* **1991**, 21, 59 – 111; d) J. Bailey, A. Chrysostomou, J. H. Hough, T. M. Gledhill, A. McCall, S. Clark, F. Ménard, M. Tamura, *Science* **1998**, 281, 672 – 674.
- [49] M. Nuevo, U. J. Meierhenrich, G. M. Muñoz Caro, E. Dartois, L. d’Hendecourt, D. Deboffle, G. Auger, D. Blanot, J. H. Bredehoft, L. Nahon, *Astron. Astrophys.* **2006**, 457, 741 – 751.
- [50] P. de Marcellus, C. Meinert, M. Nuevo, J.-J. Filippi, G. Danger, D. Deboffle, L. Nahon, L. d’Hendecourt, U. J. Meierhenrich, *Astrophys. J. Lett.* **2011**, 727, L27.
- [51] P. Modica, C. Meinert, P. de Marcellus, L. Nahon, U. J. Meierhenrich, L. Le Sergeant d’Hendecourt, *Astrophys. J.* **2014**, 788, 79 – 90.
- [52] J. Monod, *Le hasard et la nécessité: essai sur la philosophie naturelle de la biologie moderne*, Seuil, Paris, **1970**.

- [53] a) L. D. Barron, *J. Am. Chem. Soc.* **1986**, *108*, 5539 – 5542; b) M. Avalos, R. Babiano, P. Cintas, J. L. Jiménez, J. C. Palacios, L. D. Barron, *Chem. Rev.* **1998**, *98*, 2391 – 2404; c) L. Barron, *Chem. Soc. Rev.* **1986**, *15*, 189 – 223.
- [54] L. D. Barron, *Nature* **2000**, *405*, 895 – 896.
- [55] a) U. J. Meierhenrich, L. Nahon, C. Alcaraz, J. H. Bredehöft, S. V. Hoffmann, B. Barbier, A. Brack, *Angew. Chem. Int. Ed.* **2005**, *44*, 5630 – 5634; *Angew. Chem.* **2005**, *117*, 5774 – 5779; b) U. J. Meierhenrich, J. J. Filippi, C. Meinert, S. V. Hoffmann, J. H. Bredehöft, L. Nahon, *Chem. Biodiversity* **2010**, *7*, 1651 – 1659; c) U. J. Meierhenrich, J.-J. Filippi, C. Meinert, S. V. Hoffmann, J. H. Bredehöft, L. Nahon in *D-Amino Acids in Chemistry, Life Sciences, and Biotechnology* (Eds.: H. Brückner, N. Fujii), Wiley-VCH, Weinheim, **2011**, pp. 341 – 349.
- [56] a) A. C. Evans, C. Meinert, C. Giri, F. Goesmann, U. J. Meierhenrich, *Chem. Soc. Rev.* **2012**, *41*, 5447 – 5458; b) C. Meinert, P. de Marcellus, L. Le Sergeant d’Hendecourt, L. Nahon, N. C. Jones, S. V. Hoffmann, J. H. Bredehöft, U. J. Meierhenrich, *Phys. Life Rev.* **2011**, *8*, 307 – 330; c) C. Meinert, J. H. Bredehöft, J. J. Filippi, Y. Baraud, L. Nahon, F. Wien, N. C. Jones, S. V. Hoffmann, U. J. Meierhenrich, *Angew. Chem. Int. Ed.* **2012**, *51*, 4484 – 4487; *Angew. Chem.* **2012**, *124*, 4562 – 4565; d) C. Meinert, S. V. Hoffmann, P. Cassam-Chenai, A. C. Evans, C. Giri, L. Nahon, U. J. Meierhenrich, *Angew. Chem. Int. Ed.* **2014**, *53*, 210 – 214; *Angew. Chem.* **2014**, *126*, 214 – 218; e) A. C. Evans, C. Meinert, J. H. Bredehöft, C. Giri, N. C. Jones, S. V. Hoffmann, U. J. Meierhenrich in *Differentiation of Enantiomers II*, Vol. 341 (Ed.: V. Schurig), Springer, Berlin, **2013**, pp. 271 – 299.
- [57] J. Kwon, M. Tamura, P. W. Lucas, J. Hashimoto, N. Kusakabe, R. Kandori, Y. Nakajima, T. Nagayama, T. Nagata, J. H. Hough, *Astrophys. J. Lett.* **2013**, *765*, L6.
- [58] T. Fukue, M. Tamura, R. Kandori, N. Kusakabe, J. Hough, J. Bailey, D. B. Whittet, P. Lucas, Y. Nakajima, J. Hashimoto, *Origins Life Evol. Biospheres* **2010**, *40*, 335 – 346.
- [59] G. Rikken, E. Raupach, *Nature* **2000**, *405*, 932 – 935.
- [60] a) G. L. J. A. Rikken, E. Raupach, *Phys. Rev. E* **1998**, *58*, 5081 – 5084; b) G. L. J. A. Rikken in *Chiral Photochemistry* (Eds.: Y. Inoue, V. Ramamurthy, M. Dekker), CRC Press, New York **2004**, p. 107.
- [61] a) D. K. Kondepudi, R. J. Kaufman, N. Singh, *Science* **1990**, *250*, 975 – 976; b) W. S. Kipping, W. J. Pope, *J. Chem. Soc. Trans.* **1898**, *73*, 606 – 617.
- [63] J. M. McBride, R. L. Carter, *Angew. Chem. Int. Ed. Engl.* **1991**, *30*, 293 – 295; *Angew. Chem.* **1991**, *103*, 298 – 300.
- [64] a) C. Viedma, *Phys. Rev. Lett.* **2005**, *94*, 065504; b) C. Viedma, J. E. Ortiz, T. de Torres, T. Izumi, D. G. Blackmond, *J. Am. Chem. Soc.* **2008**, *130*, 15274 – 15275.
- [65] T. Lee, Y. K. Lin, *Cryst. Growth Des.* **2010**, *10*, 1652 – 1660.
- [66] C. Viedma, W. L. Noorduin, J. E. Ortiz, T. de Torres, P. Cintas, *Chem. Commun.* **2011**, *47*, 671 – 673.
- [67] P. Cintas, C. Viedma, *Chirality* **2012**, *24*, 894.
- [68] T. D. Lee, C. N. Yang, *Phys. Rev.* **1956**, *104*, 254 – 258.

- [69] L. D. Barron, *Rend. Fis. Acc. Lincei* **2013**, *24*, 179 – 189.
- [70] C. S. Wu, E. Ambler, R.W. Hayward, D. D. Hoppes, R. P. Hudson, *Phys. Rev.* **1957**, *105*, 1413 – 1415.
- [71] a) Y. Yamagata, *J. Theor. Biol.* **1966**, *11*, 495 – 498; b) R. Wesendrup, J. K. Laerdahl, R. N. Compton, P. Schwerdtfeger, *J. Phys. Chem. A* **2003**, *107*, 6668 – 6673.
- [72] R. Berger in *Theoretical and Computational Chemistry*, Vol. 14 (Ed.: S. Peter), Elsevier, Amsterdam, **2004**, pp. 188 – 288.
- [73] M. Quack, *Angew. Chem. Int. Ed.* **2002**, *41*, 4618 – 4630; *Angew. Chem.* **2002**, *114*, 4812 – 4825.
- [74] D. Campbell, P. Farago, *J. Phys. B* **1987**, *20*, 5133.
- [75] W. A. Bonner, M. A. van Dort, M. R. Yearian, H. D. Zeman, G. C. Li, *Isr. J. Chem.* **1976**, *15*, 89 – 95.
- [76] W. Darge, I. Laczko, W. Thiemann, *Nature* **1976**, *261*, 522 – 524.
- [77] a) M. Akaboshi, M. Noda, K. Kawai, H. Maki, K. Kawamoto, *Origins Life* **1979**, *9*, 181 – 186; b) M. Akaboshi, M. Noda, K. Kawai, H. Maki, K. Kawamoto, *Origins Life* **1982**, *12*, 395 – 399.
- [78] a) T. Ulbricht, F. Vester, *Tetrahedron* **1962**, *18*, 629 – 637; b) T. L. V. Ulbricht, *Origins Life* **1975**, *6*, 303 – 315.
- [79] A. Garay, *Nature* **1968**, *219*, 338 – 340.
- [80] a) W. A. Bonner, *J. Mol. Evol.* **1974**, *4*, 23 – 39; b) D.W. Gidley, A. Rich, J. V. House, P.W. Zitzewitz, *Nature* **1982**, *297*, 639 – 643.
- [81] a) W. A. Bonner, Y. Liang, *J. Mol. Evol.* **1984**, *21*, 84 – 89; b) L. A. Hodge, F. B. Dunning, G. K. Walters, R. H. White, G. J. Schroepfer, *Nature* **1979**, *280*, 250 – 252.
- [82] A. S. Garay, J. A. Ahigren-Beckendorf, *Nature* **1990**, *346*, 451 – 453.
- [83] D. G. Blackmond, *Cold Spring Harbor Perspect. Biol.* **2010**, *2*, a002147.
- [84] F. C. Frank, *Biochim. Biophys. Acta* **1953**, *11*, 459 – 463.
- [85] K. Soai, T. Shibata, H. Morioka, K. Choji, *Nature* **1995**, *378*, 767 – 768.
- [86] a) T. Shibata, J. Yamamoto, N. Matsumoto, S. Yonekubo, S. Osanai, K. Soai, *J. Am. Chem. Soc.* **1998**, *120*, 12157 – 12158; b) K. Soai, T. Shibata, I. Sato, *Acc. Chem. Res.* **2000**, *33*, 382 – 390.
- [87] a) D. G. Blackmond, *Tetrahedron: Asymmetry* **2006**, *17*, 584 – 589; b) D. G. Blackmond, C. R. McMillan, S. Ramdeehul, A. Schorm, J. M. Brown, *J. Am. Chem. Soc.* **2001**, *123*, 10103 – 10104.
- [88] J. R. Islas, D. Lavabre, J.-M. Grevy, R. H. Lamonedá, H. R. Cabrera, J.-C. Micheau, T. Buhse, *Proc. Natl. Acad. Sci. USA* **2005**, *102*, 13743 – 13748.
- [89] D. D. Medina, A. Gedanken, Y. Mastai, *Chem. Eur. J.* **2011**, *17*, 11139 – 11142.
- [90] C. Viedma, *Origins Life Evol. Biospheres* **2001**, *31*, 501 – 509.
- [91] M. Levine, C. S. Kenesky, D. Mazori, R. Breslow, *Org. Lett.* **2008**, *10*, 2433 – 2436.
- [92] C. Viedma, *Astrobiology* **2007**, *7*, 312 – 319.
- [93] a) M. Klussmann, H. Iwamura, S. P. Mathew, D. H. Wells, U. Pandya, A. Armstrong, D. G. Blackmond, *Nature* **2006**, *441*, 621 – 623; b) S. P. Mathew, H.

Iwamura, D. G. Blackmond, *Angew. Chem. Int. Ed.* **2004**, *43*, 3317 – 3321; *Angew. Chem.* **2004**, *116*, 3379 – 3383.

[95] J. E. Hein, E. Tse, D. G. Blackmond, *Nat. Chem.* **2011**, *3*, 704 – 706.

[96] a) F. Goesmann, H. Rosenbauer, R. Roll, C. Szopa, F. Raulin, R. Sternberg, G. Israel, U. Meierhenrich, W. Thiemann, G. Muñoz-Caro, *Space Sci. Rev.* **2007**, *128*, 257 – 280; b) F. Goesmann, H. Rosenbauer, R. Roll, H. Böhnhardt, *Astrobiology* **2005**, *5*, 622 – 631.

[97] a) W. H.-P. Thiemann, U. Meierhenrich, *Origins Life Evol. Biospheres* **2001**, *31*, 199 – 210; b) U. Meierhenrich, W. H.-P. Thiemann, H. Rosenbauer, *J. Anal. Appl. Pyrolysis* **2001**, *60*, 13 – 26.

[99] W.-P. Thiemann, H. Rosenbauer, U. Meierhenrich, *Adv. Space Res.* **2001**, *27*, 323 – 328.

[100] a) U. J. Meierhenrich, W. H. P. Thiemann, F. Goesmann, R. Roll, H. Rosenbauer, *Chirality* **2001**, *13*, 454 – 457; b) U. J. Meierhenrich, M. J. Nguyen, B. Barbier, A. Brack, W. H. P. Thiemann, *Chirality* **2003**, *15*, S13 – S16; c) C. Giri, F. Goesmann, C. Meinert, A. C. Evans, U. J. Meierhenrich in *Biochirality*, Springer, Heidelberg **2013**, pp. 41 – 82.

The previous section explored in details the existing theories of enantiomeric enrichment with regards to their classification. In particular, the astrophysical scenario of the original symmetry breaking received special attention. The interaction of circularly polarized light with chiral organic matter is a crucial part of the hypothesis under question. To predict the behavior of a racemic mixture upon exposure with CPL their chiroptical properties have to be understood. The following article explains how circular dichroism and anisotropy spectroscopy can be used to predict sign and degree of enantiomeric enrichment. An overview regarding chiroptical properties of specific classes of prebiotic molecules i.e. amino acids, aldehydes, sugars, amines and carboxylic acids is proposed below.



Article 2. Light on Chirality: Absolute Asymmetric Formation of Chiral Molecules Relevant in Prebiotic Evolution

Iuliia Myrgorodska, Cornelia Meinert, Søren V. Hoffmann, Nykola C. Jones, Laurent Nahon, , and Uwe J. Meierhenrich

Abstract

Homochirality is a distinct property of living matter manifested by the unichiral molecular units of genetic material and of proteins, D-deoxyribose and L-amino acids. These molecular subunits, or their precursors, have been proven to form under various prebiotic conditions in racemic form. However, the nature of the chiral influence, resulting in the first molecular symmetry breaking, remains unclear. The photochemical model of enantioselection has gained particular importance in recent years. In this model, the interaction of circularly polarized light with racemic molecules generated in the interstellar medium is considered as the main driving force of enantiomeric discrimination in early prebiotic evolution. Cometary ice simulations, L-enantioenriched amino acids in meteorites and the detection of circularly polarized electromagnetic radiation in star-forming regions provide evidence for photochirogenesis. The recent discovery of aldehydes in the cometary nucleus of 67P/Churyumov-Gerasimenko by the COSAC experiment on board the Rosetta lander Philae, along with the detection of aldehydes and aldopentoses, including the chiral ribose, in simulated interstellar ice analogues, provide a direct link between laboratory simulations and cometary composition. In the context of these new findings this review will provide an overview on the role of chiral molecules in prebiotic evolution with special emphasis on their chiroptical properties and absolute asymmetric photosynthesis.

Published article: *ChemPlusChem* (2016) 81, DOI: 10.1002/cplu.201600214R1

1. Introduction

One of the most intriguing questions in modern science addresses the origin of life and concerns the first chemical processes producing the simplest precursors of biomolecules. Proteins and nucleic acids are central to the emergence of self-replicating systems, and are made up exclusively of homochiral units: L-amino acids and D-sugars.^[1] However, the driving force behind the original enantio discrimination preceding the homochiral state remains obscure, generating a new puzzle in chemical evolution: how the selection of “one-handedness” has occurred? Is this the result of deterministic chemical or physical laws?

In a larger sense, chirality is a geometrical property of symmetry by which objects differ only as an image in a mirror from the object that produces it. This concept, embraces several disciplines including physics, chemistry, mathematics and biology. Unlike in biological systems, in synthetic chemistry enantiospecific reactions which produce only one chiral image of the molecule are rare, thus enantiopure products are mainly generated by the means of asymmetric synthesis or asymmetric catalysis. Absolute asymmetric synthesis/formation is a branch of asymmetric reactions that refers to a large group of enantio-enriching processes induced by truly chiral systems.

One should not forget that chirality does not only apply to stationary objects, but also to time-dependent physical entities, which may present a transient chirality. As a consequence we can distinguish between true and false chirality.^[2] A system is called truly chiral when it exists in two distinct enantiomeric states which can be interconverted by space inversion (parity P), but not by time reversal (T) (see L. D. Barron^[3] and A. Guijarro, M. Yus^[4] for an elaborated explanation). Among the truly chiral systems are: circularly polarized electromagnetic radiation,^[5] uniform magnetic field collinear with the propagation vector of a light beam^[6] and spin polarized elections.^[7] Since organocatalysts and chiral auxiliaries typically used in classical asymmetric synthesis are not compatible with prebiotic chemistry, the answer to the “handedness” puzzle is assumed to originate from a truly chiral entity capable of absolute asymmetric discrimination under prebiotic settings.

The above-mentioned approach is commonly referred to as *deterministic* and includes parity violation in the weak nuclear force^[8] and the application of chiral fields^[5-7] to generate a chiral bias. Deterministic mechanisms are opposite to random mechanisms for symmetry breaking^[9], where the chiral sign in the biosphere evolved by mere chance. As it is difficult to test any random theory, and as the energy gap between enantiomers produced by parity violation cannot currently be recorded by any technique, in this review we will focus on the last remaining experimentally testable group of theories: asymmetry induction by chiral forces.

Among possible chiral forces,^[6,7] inter- and circumstellar circularly polarized light (CPL) is thought to be a highly plausible factor of the initial symmetry breaking. Differential absorption of circularly polarized photons by chiral biological building blocks results in photosynthetic or photolytic selection of one enantiomer over the other.^[10] According to the photochemical model^[11] the asymmetry of life originated in interstellar space where the simplest chiral organic molecules

could be produced. Following exogenous delivery^[12] of enantioenriched organic matter during late accretion, the inventory of meteoritic and cometary objects have triggered the origin of biological homochirality through an autocatalytic amplification of the initial enantiomeric imbalance^[13] on primitive Earth.

Similar to circularly polarized light, unpolarized light in an oriented magnetic field was found to be absorbed differently by left and right enantiomers (magneto-chiral dichroism). It was shown experimentally that the combination of oriented magnetic with electromagnetic fields may induce an enantiomeric excess of the less absorbing enantiomer. The handedness of which depends on the sign of the scalar $\vec{k} \cdot \vec{B}$ product.^[6b, 6c] As magnetic fields and unpolarized light are known to be more common than circularly polarized light in the cosmos, it could be expected that magneto-chiral dichroism would play a significant role in the formation of *ee*. However, the formation of any substantial amount of *ee* depends upon very high magnetic fields, for example only 10⁻⁵ % *ee* can be reached for a magnetic field of 1 T.^[6b] Consequently, further studies, including synchrotron radiation experiments, are needed to provide more evidence for the role of magneto-chiral phenomena in any enantioselection process. While this field continues to develop we will focus our attention on circularly polarised electromagnetic radiation as a source of initial symmetry breaking.

In order to explain molecular asymmetry from the point of view of photochirogenesis, one has to understand the interaction of CPL with chiral molecules relevant in prebiotic evolution. In this review we will highlight the origin of the first biological building blocks and systematically describe their chiroptical response to interstellar/circumstellar CPL.

1. Chiroptical response and absolute asymmetric formation of amino acids

Amino acids are one of the key players in early chemical evolution, as they polymerize to become proteins – the main catalytic units of cells. There are several hypotheses to *where* prebiotic amino acids may have been generated; one involves the synthesis of organic matter in interstellar molecular clouds and its subsequent delivery to Earth,^[14] another hypothesis refers to hydrothermal vents as a suitable environment for prebiotic chemistry.^[15] While both approaches have been validated for amino acid formation, only the exogenous model includes an external source of chirality and is therefore capable of explaining the origin of molecular asymmetry. The discovery of L-enantioenriched amino acids in carbonaceous chondrites,^[16] together with the observation of partially circularly polarized radiation in the Orion Nebula,^[5, 11, 17] strengthened the astrophysical scenario where the “one-handedness” of amino acids was triggered by the preferred “handedness” of interstellar CPL.

The chiroptical features of chiral molecules such as amino acids can be characterized via several techniques including circular dichroism (CD) spectroscopy and anisotropy spectroscopy (AIS)^[18] as well as Photoelectron Circular Dichroism (PECD)^[19]. The spectra obtained via the former two techniques provide valuable information on both the rate and the degree of photochemical enantio-enrichment, while PECD could have been involved in a photophysical enantio-

richment in a given direction of space.^[20] Herein we will present the theoretical and experimental background of CD and anisotropy spectroscopy, historically extensively studied for amino acids. Those spectra will be further discussed in the context of absolute asymmetric photosynthesis and chiral symmetry breaking.

1.1. Circular Dichroism spectroscopy

In general, dichroism is a polarization-dependent property of matter linked to its symmetry characteristics. When chiral molecules are exposed to circularly polarized light, unequal absorption of *left*- and *right*-circularly polarized electromagnetic radiation takes place and circular dichroism is observed. CPL is known to travel through an optically active medium with different velocities. The differential extinction coefficient $\Delta\epsilon$ measured in CD spectroscopy is defined as $\Delta A = (\Delta\epsilon)cl$ where ΔA is the difference in absorption of *left*- and *right*-CPL, c is the sample concentration and l is the sample's optical path length. The CD spectrum itself can be used to estimate both rate and degree of an asymmetric photochemical reaction.

A typical spectropolarimeter used in CD spectroscopy is illustrated in Fig. 2.1. It consists of a light source producing UV and visible radiation (commonly xenon arc lamps), a monochromating unit for wavelength selection followed by a polarizer which produces linear polarized light, which is transformed by a photoelastic modulator (PEM) into electromagnetic radiation which is alternatively *left*- or *right*-circularly polarized. The light is passed through the analyte and a photo-multiplier tube (PMT) detector determines the energy-dependent differential absorption for the two circular polarizations. The PMT signal is dependent on the light intensity and also the high tension voltage (HV) applied to the detector. The detector HV is directly related to the sample absorbance, and can be converted into an absorption spectrum.^[18] This setup is commonly used to study the chiroptical response of simple organic molecules. However, it presents a number of limitations when applied to short wavelengths. The recorded spectra contain little structural information mainly due to low light flux in the VUV range and consequently low signal-to-noise data.

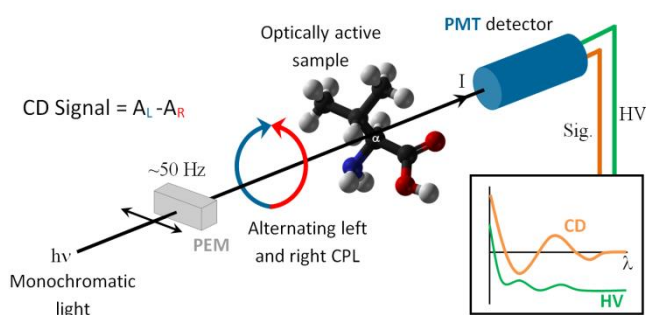


Figure 2.1. Experimental configuration for measuring CD spectra.^[21] The photoelastic modulator (PEM) converts monochromatic light into alternating *left* and *right-handed* CPL. Optically active organic molecules have differential absorptions of chiral photons. This differential absorption as well as the high-tension voltage (HV) are recorded by the photo-multiplier tube (PMT) detector.

As the UV-extension of the wavelength range requires a source of higher brightness, the replacement of the xenon arc lamp by a synchrotron light source gives rise to a modern spectroscopic technique called synchrotron radiation circular dichroism (SRCD) spectroscopy.^[22] In contrast to conventional CD, SRCD spectra provide much more accurate data at lower wavelengths, allowing for the interpretation of more energetic electronic transitions within the chiral molecule.

To complement and/or interpret experimentally recorded CD or SRCD spectra, one may attempt to theoretically predict the interaction of electromagnetic radiation with chiral organic molecules. Quantum mechanical calculations are able to compute theoretical CD spectra based on the Hamiltonian operator \hat{H}^{int} of interaction between light and matter. The Hamiltonian operator is calculated as follows:

$$\hat{H}^{int} = -\hat{\mu} \cdot E - \hat{m} \cdot B \quad (2.1)$$

Where μ is the analyte's electric dipole momentum, E is the light's electric field vector, m is the magnetic dipole momentum and B is the magnetic field vector.^[23]

Such a theoretical calculation for the $n \rightarrow \pi^*$ electronic transition for amino acids in aqueous solution has been anticipated to produce a CD signal at around 200 nm.^[24] This agrees quite well with CD studies of amino acids^[25] and diamino acids,^[26] where the spectral maximum was observed around 205 nm. It soon became evident that even though CD spectra of amino acid solutions were easily accessible, they did not provide full information on the electronic molecular transitions. Water absorption, beginning at 190 nm, is cutting off all the signals at lower wavelengths.^[27] Moreover, the liquid state appeared to be rather irrelevant in the context of an astrophysical scenario.

By taking into consideration the above-mentioned drawbacks, researchers interested in VUV CD spectra moved from liquid samples to condensed amorphous films that were prepared in a specially assembled sublimation chamber by thermal deposition onto a MgF₂ window. Intense CD-active transitions of amino acids became visible when CD spectroscopy was extended to the VUV spectral range between 140 and 190 nm, with intensities much higher than the previously known CD bands between 190 and 330 nm.^[28] All the studied α -H amino acids showed the same CD magnitude and sign over a large wavelength range (Fig. 2.2), thus indicating the possibility of photochemically-inducible enantiomeric excesses (*ees*) of the same handedness within the proteinogenic amino acids. DFT calculations of Nakagawa et al.^[29] match these experimentally obtained UV and VUV spectra allowing the assignment of electronic transitions to individual CD signals. As an example, the major peak observed in most amino acids between 165 and 180 nm was interpreted as a $\pi \rightarrow \pi^*$ transition.^[30]

What came as a surprise from the studies of condensed amino acid CD spectra^[28] is that the α -methylated amino acids, isovaline and α -methyl valine, those showing the highest *ees* of left-handed enantiomers in meteorites, were giving CD signals of the opposite sign compared to the family of α -H amino acids (Fig. 2.2). The higher steric hindrance due to the methyl group in the α -position is assumed to provide dramatic changes in the preferred realized amino acid confor-

mation^[31] and its molecular orbitals, probably leading to reversal of the CD band. It was further shown that the molecular environment of amino acids has a great impact on the CD structure, giving a significant difference in the peak shape and sometimes leading to inversion of the $n \rightarrow \pi^*$ band by passing from liquid to amorphous state.^[21]

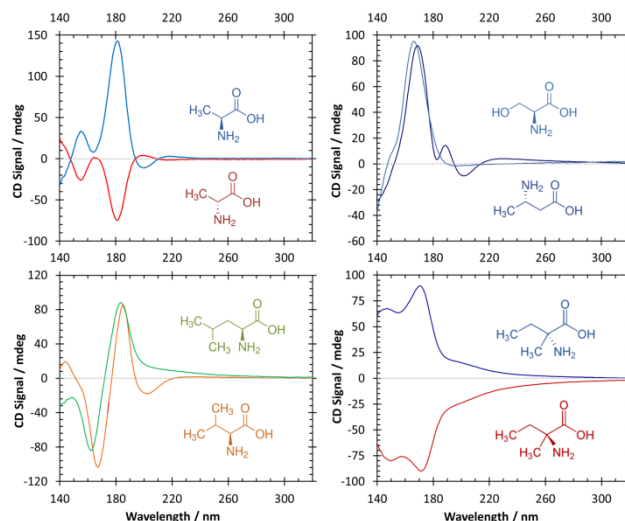


Figure 2.2. VUV SRCD spectra of amorphous solid-state amino acids immobilized on MgF₂: a) CD spectra between 140 and 330 nm of isotropic amorphous D-Ala (red) and L-Ala (blue) of different film thicknesses; b) L-Val (orange), and L-Leu (green) c) L-3-Aba (dark blue) and L-Ser (light blue); d) D-Iva (red), L-Iva (black).^[28]

While the CD spectrum for any given molecule can be used to predict how it will behave upon CPL exposure, CD spectra alone are insufficient to predict the maximum ee -value inducible upon CPL irradiation, as the induced asymmetry depends on both $\Delta\epsilon$ and ϵ . Therefore, a new spectroscopic technique known as anisotropy spectroscopy (AIS) was introduced.

1.2. Anisotropy spectroscopy

The chiroptical response of a molecule interacting with monochromatic CPL can be quantified by the anisotropy factor g , defined as $g = \Delta\epsilon/\epsilon$.^[16, 32] This term was introduced by W. Kuhn as "...the factor by which the contribution to ordinary refraction has to be multiplied in order to get the contribution to the optical activity".^[33] Kuhn also indicated that g attains its highest value if the vibrating moment corresponding to the absorption band has components vertical to each other and are of equal magnitude in distant parts of the molecule.^[34] Thus, high anisotropy values are typically observed for weak absorption bands. In molecular quantum physics g is usually approximated as $4R/D$, where R is the rotational strength and D is the dipole strength of the molecule.^[32b]

The dependence of the optical yield upon the anisotropy factor was later established by W. Kuhn and E. Knopf.^[35] Subsequent studies of Balavoine et al.^[32c] evaluated three possible chemical routes of enantioenrichment: asymmetric

photodestruction, partial photoresolution, and asymmetric photosynthesis and kinetic models were generated for each particular case. The most commonly encountered scenario of introducing the chiral bias with CPL is preferential enantiodestruction. During the asymmetric photolysis of a racemate, the *R*- and *S*-enantiomers photodegrade at different rates. These two reactions can be described as pseudo-first order reactions defined by the following equation:

$$g = 2 \frac{\varepsilon_R - \varepsilon_S}{\varepsilon_R + \varepsilon_S} = 2 \frac{k_R - k_S}{k_R + k_S} \quad (2.2)$$

Where k_R and k_S correspond to rate constants for the photodestruction of *R*- and *S*-enantiomers, respectively.^[32c]

From kinetic studies, Balovine et al. deduced quantitatively the enantiomeric purity achievable during photolysis of a racemate as a function of the magnitude of g and the extent of the reaction ζ . Thus showing that an optical purity of 100% can be obtained with a sufficiently large g value and ζ . This means that the optical purity increases as the chemical yield approaches zero.

In early studies the anisotropy factor was calculated for a given wavelength only, however, the sign and magnitude of g depend on the wavelength. By determining g for every λ of the CPL, it becomes possible to generate anisotropy spectra that afford full and direct characterization of the photodiscrimination of a given molecule. In practice, anisotropy spectra can be obtained by dividing the differential excitation coefficient recorded^[22a] during CD measurements by the excitation coefficient recorded during absorption measurements.^[36] For high quality recording of g , simultaneous measurement of the CD signal and absorption is essential. The anisotropy can then be directly evaluated as $g = \Delta A/A$ without knowing the pathlength and concentration, which can be difficult to determine with, e.g., films. The use of high brightness sources, such as synchrotron radiation, is not only necessary for the acquisition of the VUV part of the anisotropy spectrum, but also for accurate measurements when CD and absorption are low, but still yield a high g value.

As outlined above, anisotropy spectra allow the quantitative prediction of the inducible ee into a racemic sample by enantioselective photolysis. At a given extent of reaction, ζ , the upper limit of inducible ee can be determined by equation 2.3^[36]:

$$ee \geq (1 - (1 - \xi)^{g/2}) \times 100\% \quad (2.3)$$

As the more photoabsorbing enantiomer is destroyed during CPL irradiation, the concentration of the opposite enantiomer increases. The final ee depends on both the extent of reaction and the anisotropy factor of a given molecule.

Once recorded, anisotropy data allow for: 1) the prediction of the sign of the induced ee , especially at astrophysically-relevant wavelengths, 2) the determination of the kinetics and the ee values of the enantioselective photolysis and 3) the selection of the wavelength most suitable for inducing high enantioenrichments.

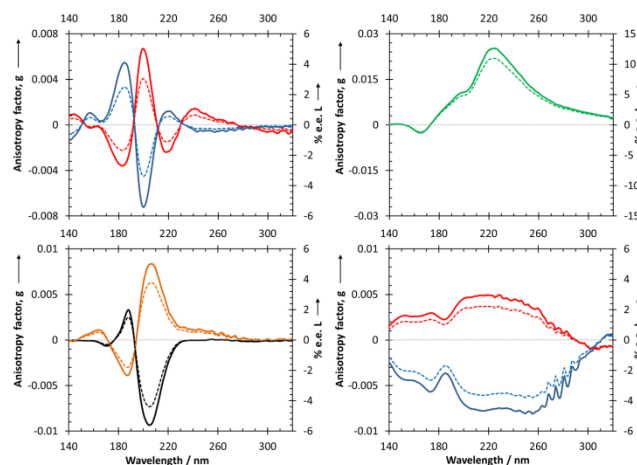


Figure 2.3. Anisotropy spectra (thick lines) of α -amino acids in the vacuum-UV and UV spectral region. a) Anisotropy spectra of isotropic amorphous D-Ala (red) and L-Ala (blue); b) D-Val (orange) and L-Val (black); c) L-Leu (dark green); d) D-Iva (red), L-Iva (blue). Dashed lines represent the corresponding ee plots inducible by either left or right circularly polarized light at $\xi = 0.999$.^[36]

By comparing CD spectra of amino acids (Fig. 2.2) with corresponding anisotropy spectra (Fig. 2.3), it becomes obvious that even though the highest CD signal is located in the 165–180 nm area, it does not necessarily correspond to the highest g value and consequently to the highest inducible ee . As ϵ becomes lower at longer wavelengths the spectral region around 200 nm turns out to be a more attractive choice for asymmetric photolysis. For example, optical purities greater than 5% can be photochemically induced into racemic alanine, assuming that the extent of the reaction $\xi = 0.9999$ is reached.^[37] In a recent study^[38] on the energy and polarization-controllable symmetry breaking in amorphous films of *rac*-alanine, it was shown that anisotropy spectra proved to be essential for determining the optimal wavelengths of asymmetric photolysis. Therefore both CD and anisotropy spectra have to be recorded ahead of absolute asymmetric photolysis with intense chiral light.

1.3. Absolute asymmetric photolysis

First results on chirality transfer from CPL to racemic organic molecules appeared in the work of Kuhn and Braun^[39], as they induced optical activity in α -bromopropanoic acid ethyl ester upon irradiation with CPL. Follow-up experiments demonstrated similar effects for α -cyanopropanoic acid dimethylamide in *n*-hexane^[40], α -azido-*N,N*-dimethylpropionamide and camphor^[32c]. Inspired by these results, Bonner et al.^[41] were the first to apply asymmetric photochemistry to prebiotically relevant molecules in the form of a racemic mixture of amino acids. They showed that at a chosen energy, the *R*-enantiomer of *rac*-leucine, was degraded more intensively than the opposite enantiomer. In this study an enantiomeric excess of approximately 2% was determined by enantioselective gas chromatography. The analytical method applied presented numerous advantages over previously used techniques, namely polarimetry.^[42]

Another study on the asymmetric photoresolution of *rac*-leucine was conducted by Inoue et al. as they demonstrated the pH dependence of the anisotropy factor g and achieved a maximal optical purity of 0.2%.^[43] The selection of leucine as a target molecule was by no means a coincidence as it has a large anisotropy at 211 nm ($g = 0.0244$), thus providing a higher probability of producing a significant *ee*.

Alanine and glutamic acid are two other genetically encoded amino acids partially resolved under CPL irradiation in earlier studies. The wavelengths for irradiation were selected based on recorded CD spectra, resulting in a maximum optical purity of 0.06% for alanine ($g = 0.007$) and 0.22% for glutamic acid ($g = 0.008$).^[44]

As discussed in Section 2.1., CPL irradiation of liquid samples show limited astrophysical relevance. Furthermore, due to solvent absorption below 200 nm, such studies have been restricted to excitations of $n \rightarrow \pi^*$ electronic transitions, so that only a part of the UV/VUV absorption spectrum was accessible. This is somewhat unfortunate, as in general amino acids exhibit stronger absorption cross-sections and higher CD values for the $\pi \rightarrow \pi^*$ electronic transition in the VUV range, which is accessible by investigating solid state samples only.

The first transition from liquid to solid samples was made by Meierhenrich et al.^[45] The authors induced 2.6% *ee* into a solid sample of leucine by *right*-CPL at 182 nm. The results obtained for the opposite helicity were three times lower, probably due to the difference in the spatial transverse flux density between *left*- and *right*-CPL. Following experiments, on the photolysis of racemic amorphous films lacking long-range order and of defined film thickness, resulted in a greater enantiomeric purity of 5.2% *ee* but were not confirmed by the opposite helicity.^[46] Recently, the same group reported CPL-induced *ee* values of up to 4% for both helicities of incident light in alanine accompanied by TDDFT calculations.^[47] Another sophisticated experimental set-up to study the asymmetric photolysis of solid state amino acids was introduced by Takahashi et al.^[48] as they compared CD spectra before and after CPL exposure.

The astrophysical scenario, however envisions interstellar ices as a mixture of organic molecules embedded in a complex matrix, rather than a homogeneous amorphous film of amino acids. According to the Greenberg core-mantle-grain model,^[49] small volatile molecules condense from the gas phase on the cold surface of interstellar dust grains, thereby forming an icy mantle. During the deposition, grain and mantle are subjected to energy in the form of UV photons and cosmic-ray particles, creating free radicals that can recombine and form complex organic molecules, so icy grains are considered as efficient astrochemical micro-reactors. Cometary ice simulation experiments were proven to be successful in recreating organic matter potentially present in the interstellar medium. The UV irradiation of the key volatile interstellar species under high vacuum on a cold surface gives rise to a remarkable diversity of organic compounds. Among them are amino acids, sugars in form of ribose and its sister aldopentoses arabinose, xylose and lyxose along with aldehydes, nucleobases etc.^[50] All chiral molecules in the experiments listed above were detected as racemates since no chiral influence was introduced.

It should not be overlooked that all the above-mentioned molecules were detected by either liquid or gas chromatography, which involve a hydrolysis and/or derivatization step prior to analysis. Heating and pH changes during derivatization have been shown to produce significant alterations in molecular composition of the initial mixture.^[51] However, in this case hydrolysis and heating release the analytes, e.g. amino acids, from a complex matrix of the sample, and do not produce new molecular species. Validation of this method^[52] has been performed for amino acid analytes and the analytical procedure has proven to be effective without modifying the initial composition.

Recently, it has been shown that partially circularly polarized radiation is present in the star forming regions^[5] and therefore the interstellar medium could contain a certain degree of asymmetry. In this regard, the logical extension of the ice simulation experiments was to replace the classical unpolarized UV source by intense circularly polarized synchrotron radiation from an undulator beamline^[53], as done by de Marcellis et al.^[54] The resulting photoprocessed astrophysical ices contained alanine with 1.34% optical purity. It was later found that an elaborate set-up can be replaced by two steps: achiral formation of astrophysical ices and subsequent irradiation with chiral photons at the synchrotron radiation source.^[55]

In 2007, K. Kobayashi and his team^[56] simulated the formation of interstellar amino acid precursor molecules in a similar manner, by irradiating carbon monoxide, ammonia, and water with 3.0 MeV protons. The resulting organic material was then subjected individually to *right*- and *left*-handed CPL produced at a synchrotron radiation source. An enantiomeric enrichment of 0.65% in alanine was detected by enantioselective liquid chromatography. Recent investigations by Modica et al.^[55] revealed statistically relevant *ee* values, all of the same sign, in five enantiomeric pairs of amino acids, with a maximum value of -2.54% *ee_L* for 2-aminobutyric acid.

Ice simulation experiments provide indirect evidence for the photochemical model proposed by Greenberg, further strengthened by *in situ* analysis of a cometary nucleus in the frame of the Rosetta-Philae mission.

2. Aldehydes as prebiotic precursor molecules

Deoxyribonucleic acid (DNA) is the genetic source code for all known living organisms. Monomers of DNA display distinct chirality defined by the asymmetric sugar subunit within the nucleotide structure. The sugar subunit of DNA – deoxyribofuranose – has been found exclusively in D-configuration. Currently it is believed that DNA evolved from the more fragile ribonucleic acid (RNA). In this hypothesis, known as RNA World state^[55], D-ribofuranose replaces D-deoxyribofuranose as the stereo-dictating element. Nevertheless, the ultimate origin of the sugar subunits as well as the original process of enantioselection remains unknown.

It is fascinating that the stereodictating elements of nucleic acids and proteins, sugars and amino acids, may have had a common precursor, chiral aldehydes. In this section we will emphasize the synthetic relationship between aldehydes, amino acids and sugars and the implications for prebiotic chemistry.

2.1. Aldehydes as amino acid precursors

Based on the observed relative abundance of organic precursors in meteorites and the interstellar medium, a number of synthetic routes have been proposed for amino acid formation in space^[56]. The discovery of high proportions of α -amino acids in the Murchison meteorite correlated well with Miller's Strecker-cyanohydrin synthesis work^[57], which demonstrated that reactions of aldehydes and ketones with NH_3 and HCN yielded α -amino acids (Fig. 2.4).

Due to the high HCN and ammonia abundances, together with various carbonyls detected in the Murchison meteorite, the Strecker synthesis has become generally accepted as responsible for both α -amino and α -hydroxy acid formation within a meteorite parent body.^[58] However β -, γ - , δ -amino acids as well as diamino acids cannot be formed by cyanide addition to carbonyl compounds. Furthermore, compound specific D/H measurements^[59] suggest diverse synthetic mechanisms of interstellar amino acids. Alternatively, reductive amination of α -keto acids^[60], radical-radical mechanisms^[61] and ion-molecule reactions in the gas-phase^[62] have been proposed.

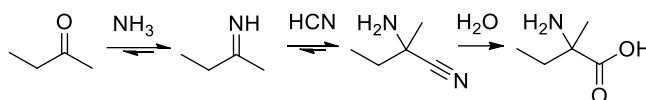


Figure 2.4. Formation pathway for meteoritic α -amino acids: The Strecker-cyanohydrin pathway is the generally accepted synthetic route to α -amino acids inside aqueously altered meteorites.

Regardless of the diversity of chemical reactions occurring within a meteorite parent body and on the surface of dust grains, aldehydes are still thought to be the major precursors for the production of amino acids. This synthetic relation is capable of explaining certain contentious enantiomeric excesses detected within Murchison extracts. For example Pizzarello et al.^[63] reported on the pristine non-racemic isoleucine showing the opposite sign of enantioenrichment as its diastereomer *allo*-isoleucine. This contradictory result can be explained through the synthetic origin of the molecules concerned. When the cyanohydrin reaction of a chiral five-carbon (*R*)(*S*)-2-methylbutyraldehyde occurs, four amino acid diastereomers are formed. If the initial aldehyde was racemic the diastereomers are formed in equal proportions, but if some *ee* is present those amino acids that carried a *S*-portion of the initial molecule through their synthesis will be more abundant than their respective enantiomers. In the above example, this would be the (*RS*)-*allo*-isoleucine and (*SS*)-isoleucine, which agrees with the observation of opposite signs of *ee* in these meteoritic amino acids

Another point that deserves to be discussed is the high optical purity of meteoritic α -methylated amino acids.^[64] As mentioned in Section 2.1 the CD spectra of α -methylated amino acids show relatively low anisotropies that result at maximum of 4% inducible *ee* under the photolysis rate of 99.99%, thus indicating that asymmetric photolysis of α -methylated amino acids could not be directly responsible for the high optical purities found in meteorites. One possible interpretation may be an aqueous alteration of the meteorite parent body that amplified the initial CPL induced molecular asymmetry.^[64c] Another explanation may come from investigation of CD and anisotropy spectra of chiral aldehydes, precursors

for α -methylated amino acids. Since no g value has ever been reported for those molecules, one can so far only hypothesize that reported ees have originated from enantioselective photodecomposition of chiral aldehydes.

2.2. Aldehydes as nucleic acid precursors

When considering asymmetric nucleotide synthesis under prebiotic conditions, several issues have to be addressed. Firstly, even though both nucleobases and sugars can be formed from prebiotic precursors, nucleobase-sugar covalent bond formation is energetically unlikely. Purines are insufficiently reactive with ribose and ribose derivatives and pyrimidines do not react at all with preformed sugars.^[65] Moreover, ribose is difficult to form selectively.^[66] Recently, an alternative synthetic pathway bypassing the classical free ribose and nucleobase reaction was proposed by Sutherland et al.^[67] (Fig. 5). Starting materials for the synthesis included glycolaldehyde and glyceraldehyde, which were further condensed to amino-oxazolines in the presence of cyanamide, cyanoacetylene and inorganic phosphate. Currently this route is considered an attractive mechanism of ribonucleotide formation on early Earth.

In the Sutherland model, glyceraldehyde is the first chiral molecule on the way to nucleic acids. The asymmetry of nucleotides can therefore be driven by chiral catalysis governed by enantioenriched amino acids^[68], or it could also have been directly promoted by interstellar CPL. To evaluate the astrophysical relevance of the proposed scenario one would estimate the abundance of the molecules concerned in the interstellar medium and evaluate their chiroptical properties by recording CD and anisotropy spectra.

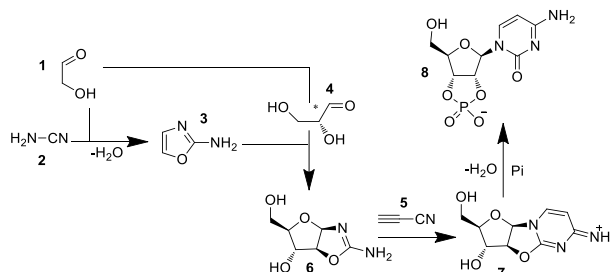


Figure 2.5. Glyceraldehyde **4** stereodictates the prebiotic synthesis of activated pyrimidine nucleotides. Pi, inorganic phosphate. Arabinose derivative **6** is formed by the addition of 2-amino-oxazoline **3** to glyceraldehydes **4**. Further reactions to anhydronucleoside **7** are stereospecific; the stereochemistry of glyceraldehydes **4** controls the chirality of the pyrimidine ribonucleotide **8**.

Glycolaldehyde has been detected in emission and/or in absorption by radio astronomy toward the galactic center source, Sagittarius B2(N)^[69], in the hot molecular core, G31.41+0.31^[70], in the solar-type protostellar binary, IRAS 16293–2422^[71], and its upper limit could be determined in the Hale–Bopp comet^[72], in the C/2012 F6 and C/2013 R1 comets^[73] as well as in the comet C/2014 Q2 (Lovejoy)^[73].

Glyceraldehyde is readily produced via a self-aldol reaction from glycolaldehyde, which is itself formed from formaldehyde. Taking into account their

synthetic relationship, one would expect to find glyceraldehyde together with glycolaldehyde in the interstellar medium. Indirect evidence for this came from studies of de Marcellis et al.^[50c] as they detected 10 aldehydes, including the sugar-related glycolaldehyde and glyceraldehyde, in interstellar ice analogues resulting from a $\text{H}_2\text{O}:\text{}^{13}\text{CH}_3\text{OH}:\text{NH}_3$ gas mixture condensation. Notably, the same molecular composition was used to produce amino acids in previous works^[50e, 74] suggesting that bodies such as comets contain all molecules necessary for early prebiotic chemistry and the generation of life. Moreover, recent analyses of a simulated interstellar ice produced from the same gas mixture revealed the presence of ribose and its sister aldopentoses arabinose, lyxose and xylose in large amounts.^[75] The total quantity of sugars detected adds up to 3.5% of the entire sample, with ribose giving the higher yields among the sugars.^[75] The presence of alcohols and the sugar acids hydroxymethylglycerol and hydroxymethyltetritol in the same sample indicate a formose type-reaction mechanism.^[76]

The above mentioned results are in agreement with organic molecules found via *in situ* analysis of the cometary nucleus of Churyumov/Gerasimenko 67P performed by the COSAC experiment on the Rosetta^[77] lander Philae^[78]. This provides a direct link between the laboratory simulation and cometary composition.

3. Other chiral species relevant for prebiotic enantiomeric discrimination

Often amino acids, sugars, and nucleotides are considered as the main molecular precursors of life, leaving a large group of structurally related organic molecules out of the discussion. In this section we will focus on the origin and significance of other chiral organic molecules such as amines and carboxylic acids for prebiotic evolution and more importantly for the generation of an enantiomeric bias.

3.1. The evolution and detection of chiral amines

Aliphatic amines and amino acids share structural features such as carbon backbones and chiral centres. ^{13}C isotopic studies^[79] suggested direct synthetic connections between these two classes of compounds, either through the loss or the addition of a carboxylic group. Both aliphatic amines and amino acids were found in meteorites^[79-80], simulated interstellar ices^[50e, 81] and even in interstellar dust grains^[78, 82]. C1 and C2 aliphatic amines (methylamine and ethylamine) were detected in comet-exposed material from the Stardust sample return mission to comet Wild 2^[82a] and by the COSAC instrument on board the Rosetta-Philae Mission^[78]. Another great achievement of the Stardust mission approaching comet Wild 2 was the detection of the amino acid glycine.^[82b, 82c] Knowing the high *ee* values detected for meteoritic amino acids and taking into account their structural similarities and their common origin with chiral amines, one would expect to find a similar enantiomeric distribution within chiral amines. Nevertheless, recent investigation of Aponte et al.^[79] revealed no *ee* within 2-aminobutane while its structurally related homologue isovaline showed an $ee_L = 9.8\%$. Two more amines 2-

aminopentane and 2-amino-3-methylbutane gave R/S ratios close to 1. These, at first sight contradictory, results question the possibility of CPL enantioenrichment in the interstellar medium.

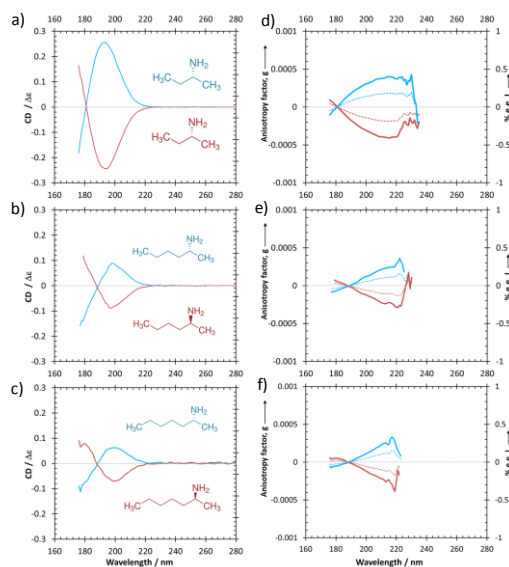


Figure 2.6. Circular dichroism (a–c) and anisotropy spectra $g(\lambda)$ (d–f) of 2-aminobutane, 2-aminohexane and 2-aminoheptane, in aqueous solution. The R -enantiomers are blue curves; the S -enantiomers are shown as brown curves. Dashed lines on the right-hand side represent the inducible L -enantiomeric excesses $\% ee_L$ by either *left*- or *right*-circularly polarized light as a function of g and an extent of reaction ξ of 0.9999.

The disagreement was resolved in a recent investigation on CD and anisotropy spectra of chiral amines. Meinert et al.^[83] provided quantitative predictions of inducible ee_L -values at a given photolysis rate of 99.99% based on selected anisotropies g_{\max} in aqueous solution. Three chiral aliphatic amines were selected for this study: S -2-aminobutane, S -2-aminohexane, and S -2-amino-heptane. The shapes of the recorded CD and anisotropy spectra of the investigated amines were quite similar: all displaying a negative CD and g band for the S enantiomer at 195 ± 4 nm and 218 ± 3 nm respectively (see Fig. 2.6). This band was assigned as the transition of one of the unshared electrons of nitrogen to an antibonding σ^* orbital ($n \rightarrow \sigma^*$). The maximum g values deduced from the anisotropy spectra were relatively small ($g = 0.0003$ – 0.00004) and consequently predicted ee values were below 1%. These values may be compared with anisotropy spectra recorded for water solutions of amino acids^[20] where the maximum g -value varies between 0.01 and 0.015, which corresponds to theoretically inducible ee of 8–10% of the same sign. All in all the presence of racemic amines does not contradict the CPL driven asymmetric induction mechanism, but rather supports it.

3.2. The evolution and detection of chiral hydroxycarboxylic acids

Similar to aliphatic amines, monocarboxylic and α -hydroxycarboxylic acids are structurally related to amino acids, suggesting a possible link between these compounds. Chiral molecules from both classes have been detected in carbonaceous chondrites^[84] and simulated interstellar ices^[85].

Hydroxycarboxylic acids were first identified in Murchison extracts by Peltzer and Bada^[86], as a suite of several compounds having a general molecular and chiral distribution comparable to those of the amino acid. Further studies on the chiral distribution of hydroxycarboxylic acids were undertaken by Pizzarello et al.^[84b] In this work up to 20 hydroxycarboxylic acids were identified, and for 6 of them enantioresolution was achieved. Interestingly, the α -hydroxy analogue of alanine – lactic acid – appears to be the only hydroxyl carboxylic acid species displaying molecular asymmetry ($ee_L = 3\text{--}12\%$). At the same time the authors underline that L-lactic acid is common in the terrestrial biosphere and therefore can be introduced as contamination during the analytical procedure. Several polyhydroxycarboxylic acids, also known as sugar acids, were detected by Cooper in the Murchison meteorite^[87], but no enantiomeric resolution was reported. The absence of CD and anisotropy data complicates the interpretation of ee -values. Further investigations of the chiroptical properties of hydroxycarboxylic acids will shed light on the optical purities in meteorites.

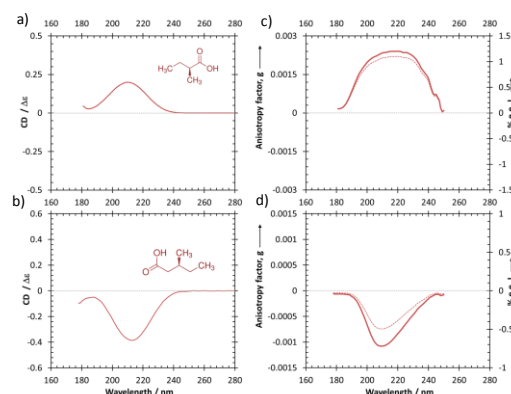


Figure 2.7. Circular dichroism (a–b) and anisotropy spectra $g(\lambda)$ (c–d) of *S*-2-methylbutanoic acid and *S*-3-methylpentanoic acid in aqueous solution. Dashed lines on the right-hand side represent the inducible L-enantiomeric excesses % ee_L by right-circularly polarized light as a function of g and an extent of reaction ξ of 0.9999.

New insights on the enantiomeric distribution of free monocarboxylic acids (MCA) and aliphatic side chains present in meteoritic insoluble organic matter were given by Aponte et al.^[84a], as they showed no enantiomeric excess within the studied samples of CM2 and CR2 meteorites. As a possible explanation the authors suggested that UV-CPL might have a different effect on the MCAs and amino acids resulting in no observable asymmetry in the free carboxylic acids. Meinert et al.^[83] examined this hypothesis by recording CD and anisotropy spectra of two carboxylic acids, *S*-2-methylbutanoic acid and *S*-3-methylpentanoic acid

(Fig. 2.7). The maximum anisotropy $g = 0.0024$ was observed at 220 nm for *S*-2-methylbutanoic acid, while *S*-3-methylpentanoic acid exhibited a minimal value of $g = -0.0011$ at 213 nm. Such differences in sign and anisotropy values suggest that the carboxyl group adopts a preferred conformation with respect to the rest of the molecule, thereby inverting the sign of rotational strength R and CD bands. Recorded g values correspond to an enantiomeric excess below 1% for both *S*-2-methylbutanoic acid and *S*-3-methylpentanoic acid. Again, the low anisotropies of MCAs in this study, as in the case of aliphatic amines, are assumed to explain their racemic distribution in meteoritic samples.

4. Outlook

The photochemical model of symmetry breaking in the interstellar environment remains as one of the most pertinent explanations for how biomolecular homochirality arose on early Earth. There exist many indirect sources of evidence including the enantioselective analysis of meteorites and laboratory simulations of interstellar ices. The straightforward interpretation of the reported ee values becomes possible through the systematic analysis of VUV and UV CD spectra and anisotropy data. AIS provides a predictive tool for the degree to which a molecule can be CPL-enantioenriched for a given extent of reaction and at a given wavelength. As discussed in this review the amino acids show CD maxima and minima in the spectral VUV range from 160 to 220 nm and anisotropy extrema in the UV range from 185 to 220 nm, which correspond to reasonably achievable ee -values of ~5%. Closely related to amino acids, amines and carboxylic acids on the other hand show very low anisotropies and consequently would yield very low enantioenrichment by asymmetric photolysis in any spectral range. This agrees with the racemic values detected for meteoritic amines and monocarboxylic acids.

Until now, photochemically induced ees correlate well with those found in meteorites. The results which stand out, e.g., high ees in α -methylated amino acids can be explained by the synthetic relationship between aldehydes and amino acids. New data originating from CD and anisotropy spectra of aldehydes, sugars, and hydroxycarboxylic acids are required to further evaluate the role of asymmetric photolysis or photosynthesis in triggering the selection of the handedness of the molecular building blocks of life.

References

- [1] U. J. Meierhenrich, *Amino Acids and the Asymmetry of Life*, Springer-Verlag, Heidelberg, **2008**.
- [2] L. D. Barron, *J. Am. Chem. Soc.* **1986**, *108*, 5539-5542.
- [3] L. D. Barron, *Rend. Fis. Acc. Lincei*, **2013**, *24*, 179-189.
- [4] A. Guijarro, M. Yus. *The origin of chirality in the molecules of life: a revision from awareness to the current theories and perspectives of this unsolved problem*, Royal Society of Chemistry, Cambridge, **2009**.
- [5] J. Bailey, A. Chrysostomou, J. H. Hough, T. M. Gledhill, A. McCall, S. Clark, F. Ménard, M. Tamura, *Science* **1998**, *281*, 672-674.
- [6] a) G. L. J. A. Rikken, E. Raupach, *Nature*, **1997**, *390*, 493-494; b) G. L. J. A. Rikken, E. Raupach, *Nature* **2000**, *405*, 932-935; c) L. D. Barron, *Nature*, **2000**, *405*, 895-896.
- [7] a) W. A. Bonner, M. A. van Dort, M. R. Yearian, H. D. Zeman, G. C. Li, *Isr. J. Chem.* **1976**, *15*, 89-95; b) J. M. Dreiling, T. J. Gay, *Phys. Rev. Lett.* **2014**, *113*, 118103.
- [8] M. Quack, *Angew. Chem., Int. Ed.* **2002**, *41*, 4618-4630.
- [9] D. K. Kondepudi, R. J. Kaufman, N. Singh, *Science* **1990**, *250*, 975-976.
- [10] a) E. Rubenstein, W. A. Bonner, H. P. Noyes, G. S. Brown, *Nature* **1983**, *306*, 118-118; b) W. A. Bonner, E. Rubenstein, *Biosystems* **1987**, *20*, 99-111.
- [11] W. Bonner, *Origins Life Evol. Biosphere* **1991**, *21*, 59-111.
- [12] C. Chyba, C. Sagan, *Nature* **1992**, *355*, 125-132.
- [13] a) K. Soai, T. Shibata, H. Morioka, K. Choji, *Nature* **1995**, *378*, 767-768; b) K. Soai, T. Shibata, I. Sato, *Acc. Chem. Res.* **2000**, *33*, 382-390.
- [14] A. C. Evans, C. Meinert, C. Giri, F. Goesmann, U. J. Meierhenrich, *Chem. Soc. Rev.* **2012**, *41*, 5447-5458.
- [15] a) R. J. C. Hennet, N. G. Holm, M. H. Engel, *Naturwissenschaften* **1992**, *79*, 361-365; b) A. Brack, *The molecular origins of life: assembling pieces of the puzzle*, Cambridge University Press, Cambridge **1998**; c) G. Proskurowski, M. D. Lilley, J. S. Seewald, G. L. Früh-Green, E. J. Olson, J. E. Lupton, S. P. Sylva, D. S. Kelley, *Science* **2008**, *319*, 604-607; d) W. Martin, J. Baross, D. Kelley, M. J. Russell, *Nat. Rev. Microbiol.* **2008**, *6*, 805-814.
- [16] a) I. Myrgorodska, C. Meinert, Z. Martins, L. Le Sergeant d'Hendecourt, U. J. Meierhenrich, *Angew. Chem., Int. Ed.* **2015**, *54*, 1402-1412; b) J. R. Cronin, S. Pizzarello, *Science* **1997**, *275*, 951-955.
- [17] a) K. Jungmi, T. Motohide, W. L. Phil, H. Jun, K. Nobuhiko, K. Ryo, N. Yasushi, N. Takahiro, N. Tetsuya, H. H. James, *Astrophys. J., Lett.* **2013**, *765*, L6; b) M. Buschermöhle, D. C. B. Whittet, A. Chrysostomou, J. H. Hough, P. W. Lucas, A. J. Adamson, B. A. Whitney, M. J. Wolff, *Astrophys. J.* **2005**, *624*, 821-826; c) K. Jungmi, T. Motohide, H. H. James, K. Nobuhiko, N. Tetsuya, N. Yasushi, W. L. Phil, N. Takahiro, K. Ryo, *Astrophys. J., Lett.* **2014**, *795*, L16.
- [18] A. C. Evans, C. Meinert, J. H. Bredehöft, C. Giri, N. C. Jones, S. V. Hoffmann, U. J. Meierhenrich, in *Differentiation of Enantiomers II, Vol. 341* (Ed.: V. Schurig), Springer International Publishing, Heidelberg, **2013**, pp. 271-299.

- [19] a) L. Nahon, G. A. Garcia, I. Powis, *J. Electron Spectrosc. Relat. Phenom.* **2015**, *204, Part B*, 322-334; b) L. Nahon, L. Nag, G. A. Garcia, I. Myrgorodska, U. Meierhenrich, S. Beaulieu, V. Wanie, V. Blanchet, R. Geneaux, I. Powis, *Phys. Chem. Chem. Phys.*, **2016**, *18*, 12696-12706.
- [20] a) M. Tia, B. Cunha de Miranda, S. Daly, F. Gaie-Levrel, G. A. Garcia, I. Powis, L. Nahon, *J. Phys. Chem. Lett.* **2013**, *4*, 2698-2704; b) M. Tia, B. Cunha de Miranda, S. Daly, F. Gaie-Levrel, G. A. Garcia, L. Nahon, I. Powis, *J. Phys. Chem. A* **2014**, *118*, 2765-2779.
- [21] J. H. Bredehöft, N. C. Jones, C. Meinert, A. C. Evans, S. V. Hoffmann, U. J. Meierhenrich, *Chirality* **2014**, *26*, 373-378.
- [22] a) F. Wien, A. Giuliani, F. Jamme, V. Rouam, M. Refregiers, *Eur. Biophys. J.*, **2011**, *40*, 146-146; b) A. J. Miles, S. V. Hoffmann, Y. Tao, R. W. Janes, B. A. Wallace, *Spectroscopy* **2007**, *21*, 245-255.
- [23] a) R. Woody, in *Circular Dichroism and the Conformational Analysis of Biomolecules* (Ed.: G. Fasman), Springer US, New York, **1996**, pp. 25-67; b) P. J. Stephens, N. Harada, *Chirality* **2010**, *22*, 229-233; c) C. Diedrich, S. Grimme, *J. Phys. Chem. A* **2003**, *107*, 2524-2539.
- [24] a) A. Osted, J. Kongsted, K. V. Mikkelsen, O. Christiansen, *Chem. Phys. Lett.* **2006**, *429*, 430-435; b) T. Fukuyama, K. Matsuo, K. Gekko, *J. Phys. Chem. A* **2005**, *109*, 6928-6933.
- [25] a) L. I. Katzin, E. Gulyas, *J. Am. Chem. Soc.* **1968**, *90*, 247-251; b) P. A. Snyder, P. M. Vipond, W. C. Johnson, *Biopolymers* **1973**, *12*, 975-992.
- [26] J. H. Bredehöft, K. Breme, U. J. Meierhenrich, S. V. Hoffmann, W. H. P. Thiemann, *Chirality* **2007**, *19*, 570-573.
- [27] W. C. Johnson, N. Berova, K. Nakanishi, R. Woody, *Circular dichroism: Principles and applications*, Wiley-VCH, New York **2000**.
- [28] U. J. Meierhenrich, J. J. Filippi, C. Meinert, J. H. Bredehöft, J. i. Takahashi, L. Nahon, N. C. Jones, S. V. Hoffmann, *Angew. Chem., Int. Ed.* **2010**, *49*, 7799-7802.
- [29] M. Tanaka, K. Yagi-Watanabe, F. Kaneko, K. Nakagawa, *J. Phys. Chem. A* **2010**, *114*, 11928-11932.
- [30] F. Kaneko, K. Yagi-Watanabe, M. Tanaka, K. Nakagawa, *J. Phys. Soc. Jap.* **2008**, *78*, 013001.
- [31] M. Adrian-Scotto, S. Antonczak, J. H. Bredehöft, S. V. Hoffmann, U. J. Meierhenrich, *Symmetry* **2010**, *2*, 935-949.
- [32] a) O. Buchardt, *Angew. Chem., Int. Ed.* **1974**, *13*, 179-185; b) L. D. Barron, *Molecular light scattering and optical activity*, Cambridge University Press, Cambridge, **2004**; c) G. Balavoine, A. Moradpour, H. B. Kagan, *J. Am. Chem. Soc.* **1974**, *96*, 5152-5158; d) H. Rau, in *Chiral Photochemistry*, Vol. 11 (Ed. Y. Inoue, V. Ramamuehry), Marcel Dekker, New York, **2004**, pp. 1-44.
- [33] W. Kuhn, *Trans. Faraday Soc.* **1930**, *26*, 293-308.
- [34] W. Kuhn, *Annu. Rev. Phys. Chem.* **1958**, *9*, 417-438.
- [35] W. Kuhn, E. Knopf, *Z. Phys. Chem.* **1930**, *7*, 292-310
- [36] C. Meinert, J. H. Bredehöft, J.-J. Filippi, Y. Baraud, L. Nahon, F. Wien, N. C. Jones, S. V. Hoffmann, U. J. Meierhenrich, *Angew. Chem., Int. Ed.* **2012**, *51*, 4484-4487.

- [37] C. Meinert, U. J. Meierhenrich, *Angew. Chem., Int. Ed.* **2012**, *51*, 10460-10470.
- [38] C. Meinert, S. V. Hoffmann, P. Cassam-Chenaï, A. C. Evans, C. Giri, L. Nahon, U. J. Meierhenrich, *Angew. Chem., Int. Ed.* **2014**, *53*, 210-214.
- [39] W. Kuhn, E. Braun, *Naturwissenschaften* **1929**, *17*, 227-228.
- [40] W. Kuhn, E. Knopf, *Naturwissenschaften* **1930**, *18*, 183-183.
- [41] J. J. Flores, W. A. Bonner, G. A. Massey, *J. Am. Chem. Soc.* **1977**, *99*, 3622-3625.
- [42] W. A. Bonner, *J. Chromatogr. Sci.* **1973**, *11*, 101-104.
- [43] a) H. Nishino, A. Kosaka, G. A. Hembury, K. Matsushima, Y. Inoue, *J. Chem. Soc., Perkin Trans.* **2002**, *2*, 582-590; b) H. Nishino, A. Kosaka, G. A. Hembury, H. Shitomi, H. Onuki, Y. Inoue, *Org. Lett.* **2001**, *3*, 921-924.
- [44] B. Norden, *Nature* **1977**, *266*, 567-568.
- [45] U. J. Meierhenrich, L. Nahon, C. Alcaraz, J. H. Bredehöft, S. V. Hoffmann, B. Barbier, A. Brack, *Angew. Chem., Int. Ed.* **2005**, *44*, 5630-5634.
- [46] U. J. Meierhenrich, J.-J. Filippi, C. Meinert, S. V. Hoffmann, J. H. Bredehöft, L. Nahon, *Chem. Biodiversity* **2010**, *7*, 1651-1659.
- [47] C. Meinert, P. Cassam-Chenaï, N. Jones, L. Nahon, S. Hoffmann, U. Meierhenrich, *Origins Life Evol. Biosphere* **2015**, *45*, 149-161.
- [48] J.-i. Takahashi, H. Shinojima, M. Seyama, Y. Ueno, T. Kaneko, K. Kobayashi, H. Mita, M. Adachi, M. Hosaka, M. Katoh, *Int. J. Mol. Sci.* **2009**, *10*, 3044-3064.
- [49] a) J. Greenberg, in *Comets* (Ed.: L. L. Wilkening), University of Arizona Press, Tucson, **1982**, pp. 131-163; b) J. M. Greenberg, *Origins Life Evol. Biosphere* **1984**, *14*, 25-36; c) J. M. Greenberg, A. Kouchi, W. Niessen, H. Irth, J. van Paradijs, M. de Groot, W. Hermsen, *J. Biol. Phys.* **1995**, *20*, 61-70.
- [50] a) M. Nuevo, J. H. Bredehöft, U. J. Meierhenrich, L. Le Sergeant d'Hendecourt, W. H. P. Thiemann, *Astrobiology* **2010**, *10*, 245-256; b) M. Nuevo, S. N. Milam, S. A. Sandford, *Astrobiology* **2012**, *12*, 295-314; c) P. de Marcellus, C. Meinert, I. Myrgorodska, L. Nahon, T. Buhse, L. L. S. d'Hendecourt, U. J. Meierhenrich, *Proc. Natl. Acad. Sci. U. S. A.* **2015**, *112*, 965-970; d) C. Meinert, J.-J. Filippi, P. De Marcellus, L. Le Sergeant d'Hendecourt, U. J. Meierhenrich, *ChemPlusChem* **2012**, *77*, 186-191; e) G. M. Munoz Caro, U. J. Meierhenrich, W. A. Schutte, B. Barbier, A. Arcones Segovia, H. Rosenbauer, W. H. P. Thiemann, A. Brack, J. M. Greenberg, *Nature* **2002**, *416*, 403-406.
- [51] M. Fang, J. Ivanisevic, H. P. Benton, C. H. Johnson, G. J. Patti, L. T. Hoang, W. Uritboonthai, M.E. Kurczy, G. Siuzdak, *Anal. Chem.*, **2015**, *87*, 10935-10941.
- [52] I. Myrgorodska, C. Meinert, Z. Martins, L. le Sergeant d'Hendecourt, U. J. Meierhenrich, *J. Chrom. A* **2016**, *1433*, 131-136.
- [53] L. Nahon, N. de Oliveira, G. A. Garcia, J.-F. Gil, B. Pilette, O. Marcouille, B. Lagarde, F. Polack, *J. Synchrotron Radiat.* **2012**, *19*, 508-520.
- [54] P. De Marcellus, C. Meinert, M. Nuevo, J.-J. Filippi, G. Danger, D. Debouffle, L. Nahon, L. Le Sergeant d'Hendecourt, U. J. Meierhenrich, *Astrophys. J., Lett.* **2011**, *727*, L27.

- [55] P. Modica, C. Meinert, P. De Marcellus, L. Nahon, U. J. Meierhenrich, L. Le Sergeant d'Hendecourt, *Astrophys. J.* **2014**, 788, L79.
- [56] Y. Takano, J.-i. Takahashi, T. Kaneko, K. Marumo, K. Kobayashi, *Earth Planet. Sci. Lett.* **2007**, 254, 106-114.
- [57] W. Gilbert, *Nature* **1986**, 319, 618-618.
- [58] O. Botta, D. P. Glavin, G. Kminek, J. L. Bada, *Origins Life Evol. Biosphere* **2002**, 32, 143-163.
- [59] A. Strecker, *Justus Liebigs Ann. Chem.* **1850**, 75, 27-45.
- [60] E. T. Peltzer, J. L. Bada, G. Schlesinger, S. L. Miller, *Adv. Space Res.* **1984**, 4, 69-74.
- [61] T. E. Bunch, S. Chang, *Geochim. Cosmochim. Acta* **1980**, 44, 1543-1577.
- [62] S. Pizzarello, G. Cooper, G. Flynn, in *Meteorites and the early solar system II, Voll* (Ed. D. S. Lauretta, H. Y. McSween) The University of Arizona Press, Tuscon, **2006**, pp. 625-651.
- [63] J. E. Elsila, J. P. Dworkin, M. P. Bernstein, M. P. Martin, S. A. Sandford, *Astrophys. J.* **2007**, 660, 911-918.
- [64] a) V. Blagojevic, S. Petrie, D. K. Bohme, *Mon. Not. R. Astron. Soc.* **2003**, 339, L7-L11; b) A. Largo, P. Redondo, C. Barrientos, *Int. J. Quantum Chem.* **2004**, 98, 355-360.
- [65] S. Pizzarello, Y. Huang, M. R. Alexandre, *Proc. Natl. Acad. Sci. U. S. A.* **2008**, 105, 3700-3704.
- [66] a) S. Pizzarello, J. R. Cronin, *Geochim. Cosmochim. Acta* **2000**, 64, 329-338; b) S. Pizzarello, M. Zolensky, K. A. Turk, *Geochim. Cosmochim. Acta* **2003**, 67, 1589-1595; c) D. P. Glavin, J. P. Dworkin, *Proc. Natl. Acad. Sci. U. S. A.* **2009**, 106, 5487-5492.
- [67] a) W. D. Fuller, R. A. Sanchez, L. E. Orgel, *J. Mol. Bio.* **1972**, 67, 25-33; b) O. Leslie E, *Crit. Rev. Biochem. Mol. Bio.* **2004**, 39, 99-123.
- [68] a) J. Kofoed, J.-L. Reymond, T. Darbre, *Org. Biomol. Chem.* **2005**, 3, 1850-1855; b) A. Ricardo, M. A. Carrigan, A. N. Olcott, S. A. Benner, *Science* **2004**, 303, 196.
- [69] M. W. Powner, B. Gerland, J. D. Sutherland, *Nature* **2009**, 459, 239-242.
- [70] a) S. Pizzarello, A. Weber, *Orig Life Evol. Biosph* **2010**, 40, 3-10; b) S. Pizzarello, A. L. Weber, *Science* **2004**, 303, 1151.
- [71] J. M. Hollis, F. J. Lovas, P. R. Jewell, *Astrophys. J. Lett.* **2000**, 540, L107.
- [72] M. T. Beltrán, C. Codella, S. Viti, R. Neri, R. Cesaroni, *The Astrophys. J. Lett.* **2009**, 690, L93.
- [73] J. K. Jørgensen, C. Favre, S. E. Bisschop, T. L. Bourke, E. F. Van Dishoeck, M. K. Schmalzl, *Astrophys. J. Lett.* **2012**, 757, L4.
- [74] J. Crovisier, D. Bockelée-Morvan, P. Colom, N. Biver, D. Despois, D. C. Lis, *Astron. Astrophys.* **2004**, 418, 1141-1157.
- [75] N. Biver, D. Bockelée-Morvan, V. Debout, J. Crovisier, J. Boissier, D. C. Lis, N. Dello Russo, R. Moreno, P. Colom, G. Paubert, R. Vervack, H. A. Weaver, *Astron. Astrophys.* **2014**, 566, L5.
- [76] M. P. Bernstein, J. P. Dworkin, S. A. Sandford, G. W. Cooper, L. J. Allamandola, *Nature* **2002**, 416, 401-403.

- [77] C. Meinert, I. Myrgorodska, P. de Marcellus, T. Buhse, L. Nahon, S.V Hoffmann, L. Le Sergeant d'Hendecourt, U. J. Meierhenrich, *Science* **2016**, 352, 208-212.
- [78] a) Y. Shigemasa, Y. Matsuda, C. Sakazawa, T. Matsuura, *Bull. Chem. Soc. Jap.* **1977**, 50, 222-226; b) T. Zweckmair, S. Böhmendorfer, A. Bogolitsyna, T. Rosenau, A. Potthast, S. Novalin, *J. Chromatogr. Sci.* **2014**, 52, 169-175.
- [79] U. Meierhenrich, *Comets And Their Origin: The Tools To Decipher A Comet*, John Wiley & Sons, Weinheim, **2015**.
- [80] F. Goesmann, H. Rosenbauer, J. H. Bredehöft, M. Cabane, P. Ehrenfreund, T. Gautier, C. Giri, H. Krüger, L. Le Roy, A. J. MacDermott, S. McKenna-Lawlor, U. J. Meierhenrich, G. M. M. Caro, F. Raulin, R. Roll, A. Steele, H. Steining, R. Sternberg, C. Szopa, W. Thiemann, S. Ulamec, *Science* **2015**, 349, aab0689.
- [81] J. C. Aponte, J. P. Dworkin, J. E. Elsila, *Geochim. Cosmochim. Acta* **2014**, 141, 331-345.
- [82] a) J. C. Aponte, J. P. Dworkin, J. E. Elsila, *Meteorit. Planet. Sci.* **2015**, 50, 1733-1749; b) J. R. Cronin, S. Pizzarello, *Adv. Space Res.* **1983**, 3, 5-18.
- [83] Y. S. Kim, R. I. Kaiser, *Astrophys. J.* **2011**, 729, L68.
- [84] a) D. P. Glavin, J. P. Dworkin, S. A. Sandford, *Meteorit. Planet. Sci.* **2008**, 43, 399-413; b) J. E. Elsila, D. P. Glavin, J. P. Dworkin, *Meteorit. Planet. Sci.* **2009**, 44, 1323-1330; c) S. A. Sandford, J. Aléon, C. M. O. D. Alexander, T. Araki, S. a. Bajt, G. A. Baratta, J. Borg, J. P. Bradley, D. E. Brownlee, J. R. Brucato, M. J. Burchell, H. Busemann, A. Butterworth, S. J. Clemett, G. Cody, L. Colangeli, G. Cooper, L. D'Hendecourt, Z. Djouadi, J. P. Dworkin, G. Ferrini, H. Fleckenstein, G. J. Flynn, I. A. Franchi, M. Fries, M. K. Gilles, D. P. Glavin, M. Gounelle, F. Grossemy, C. Jacobsen, L. P. Keller, A. L. D. Kilcoyne, J. Leitner, G. Matrajt, A. Meibom, V. Mennella, S. Mostefaoui, L. R. Nittler, M. E. Palumbo, D. A. Papanastassiou, F. Robert, A. Rotundi, C. J. Snead, M. K. Spencer, F. J. Stadermann, A. Steele, T. Stephan, P. Tsou, T. Tylliszczak, A. J. Westphal, S. Wirick, B. Wopenka, H. Yabuta, R. N. Zare, M. E. Zolensky, *Science* **2006**, 314, 1720-1724.
- [85] C. Meinert, N. Jones, S. V. Hoffmann, U. J. Meierhenrich, *J. Photochem. Photobiol. A* **2016**, DOI: 10.1016/j.jphotochem.2015.12.018.
- [86] a) J. C. Aponte, R. Tarozo, M. R. Alexandre, C. M. O. D. Alexander, S. B. Charnley, C. Hallmann, R. E. Summons, Y. Huang, *Geochim. Cosmochim. Acta* **2014**, 131, 1-12; b) S. Pizzarello, Y. Wang, G. M. Chaban, *Geochim. Cosmochim. Acta* **2010**, 74, 6206-6217.
- [87] a) V. K. Agarwal, W. Schutte, J. M. Greenberg, J. P. Ferris, R. Briggs, S. Connor, C. P. E. M. Van de Bult, F. Baas, *Origins Life Evol. Biosphere* **1985**, 16, 21-40; b) C. K. Materese, M. Nuevo, P. P. Bera, T. J. Lee, S. A. Sandford, *Astrobiology* **2013**, 13, 948-962.
- [88] E. T. Peltzer, J. L. Bada, *Nature* **1978**, 272, 443-444.
- [89] G. Cooper, N. Kimmich, W. Belisle, J. Sarinana, K. Brabham, L. Garrel, *Nature* **2001**, 414, 879-883.



Any hypotheses, as well as hypothesis regarding the origin of life, require experimental methods to test them. The photochemical model of enantioenrichment implies very small enantiomeric excesses to be produced by means of CPL irradiation. Since the optical purity increases together with the photolysis rate, eventually the amount of sample drastically decreases to provide reliable quantification. Another way to test the photochemical model is to analyze meteoritic samples, where enantioenriched amino acids have been found previously. The precisely determined ee values may shed some light on the origin of molecular asymmetry.

In this regard, the following section is dedicated to development of an analytical protocol for the quantitative enantioseparation of amino acids.



CHAPTER II: Analytical methods

Article 3. Quantitative enantioseparation of amino acids by comprehensive two-dimensional gas chromatography applied to non-terrestrial samples

Iuliia Myrgorodska, Cornelia Meinert, Zita Martins, Louis le Sergeant d'Hendecourt, Uwe J. Meierhenrich

Abstract

This work presents an improved analytical procedure for the resolution and quantification of amino acid enantiomers by multidimensional gas chromatography. The procedure contains a derivatization step, by which amino acids were transformed into *N*(O,S)-ethoxycarbonylheptafluorobutyl esters. It was optimized for the resolution of non-proteinogenic amino acids in the matrix of complex non-terrestrial samples. The procedure has proven to be highly sensitive and shows a wide linearity range with 0.005–3 pmol detection limits for quantitative determinations. The developed procedure was tested on a sample of the Murchison meteorite, for which obtained chromatograms show excellent peak resolution, minimal co-elution and peak overlap. We conclude that comprehensive two dimensional chromatography, in combination with the optimized derivatization method is a highly suitable technique for the analysis of samples with very limited quantities and containing potentially prebiotic molecules, such as interstellar ice analogs and meteorites.

Key words: GC × GC, chirality, enantioseparation, amino acids, non-terrestrial samples

Published article: *The Journal of Chromatography A* (2016) 1433, 131–136.

1. Introduction

The search for prebiotic organic compounds of non-terrestrial origin such as amino acids, is one of the major tasks of numerous space missions [1,2] and meteorite studies [3]. Once found, they open a window into the chemical evolution of organic matter—possible precursors to the origin of life and further biological evolution [4]. It has been shown that some of the key molecules in terrestrial biology, e.g. amino acids [5,6], nucleobases [7–9], and sugar acids [10] are present in ppb to ppm level within a specific class of meteorites—carbonaceous chondrites, thus suggesting an exogenous delivery of prebiotic organic matter to Earth. In this context the enantiomeric resolution of chiral species is of a primary relevance as the ratio between two optical isomers can be viewed as a signature of their biotic versus abiotic origin. Additionally, small enantiomeric excesses (*ee*) are often interpreted as the result of a molecular symmetry breaking event, e.g., driven by achiral force [11]. The first detection of an enantiomeric enrichment in L-amino acids within the Murchison meteorite opened a debate on the indigeneity of the observed *ees* and the efficiency of the applied analytical separation technique [12]. Since then, demands for the analytical procedure with high precision *ee* measurement and increased separation power have raised significantly.

Gas chromatography (GC) has a long track record in the analysis of extraterrestrial samples [13]. Given the complex nature of extraterrestrial organic matter and its low available quantity [14], an analytical procedure for the enantioselective analysis of amino acids has to meet certain requirements such as: (i) low detection and quantification limits; (ii) high enantiomeric resolution; (iii) complete absence of racemization following the analytical protocol; (iv) minimal co-elution. While some of the mentioned limitations are linked to the derivatization step (e.g., the degree of racemization) others are mainly related to the separation power of conventional GC. As the monodimensional capillary GC technique has reached its limits for complete analyte separation, further improvement of gas chromatographic resolution has been achieved as a result of the development of comprehensive multidimensional gas chromatography (GC \times GC). Since its first introduction in the 1990s [15] the innovative technique has been successfully applied to detect and quantify trace-level constituents and contaminants in various types of samples [16]. In this study we emphasize the advantages of enantioselective multidimensional gas chromatography applied to samples of astrobiological relevance, including a sample of the Murchison meteorite. The developed analytical method is compared to previously reported HPLC, GC–MS and GC \times GC–MS methods [17–21] for the separation of amino acid enantiomers.

Furthermore, the classical optimization and validation of analytical procedures for amino acid separation is generally limited to 20 genetically encoded units, keeping a much larger group of non-proteinogenic amino acids out of the picture. However, the enantiomeric separation of non-proteinogenic amino acids gains more and more attention in a number of fields of bioanalytical chemistry, metabolomics, medicinal chemistry, and pharmacology [22]. Regarding an outer space origin of these molecules, the newly developed analytical procedure is of primary interest in meteoritic and planetary research. In spite of their importance

to the field, only a few researchers have studied their resolution and analytical response [23,24]. Thus, this work contains an elaborated list of amino acids taking into account their relevance for the chemical evolution of organic matter in solar system objects. Additionally, high precision measurements of amino acid *ees* in a Murchison meteorite extract were performed.

2. Experiments

2.1. Chemicals, reagents, and tools

Different groups of amino acids were analyzed: proteinogenic amino acids (Gly, Ala, Ser, Asp, Val, Pro, Glu, Met, Leu, Ile, and Phe), α -non-proteinogenic amino acids (2-aminobutyric acid, norvaline, norleucine, and *tert*-leucine), β -amino acids (β -alanine, 3-aminobutyric acid, 3-aminoisobutyric acid, 3-aminopentanoic acid, and β -leucine), a γ -amino acid (4-aminobutyric acid), α -dialkylated amino acids (2-aminoisobutyric acid, isovaline, and 2-methylglutamic acid), *N*-alkylated amino acids (sarcosine, *N*-methylalanine, and *N*-ethylglycine), an iminodiacid (iminodiacetic acid), and diamino acids (2,3-diaminopropanoic acid and 2,3-diaminobutanoic acid). All the chemicals used in this study were purchased from Sigma-Aldrich, Fluka, or Acros Organics. To prepare the amino acid stock solution (1.25×10^{-3} M), the individual 30 amino acids were weighted, mixed, and dissolved in 0.1 M HCl solution prepared by dilution of 6 M HCl (Fluka) in ultrapure water (HPLC grade). Serial dilutions (from 10^{-5} M to 10^{-9} M) were prepared for the generation of the calibration curves (supplementary information Fig. S3.1 (1–8)). Due to their low response, two amino acids – isovaline and α -aminoisobutyric acid – were prepared separately with serial dilution from 10^{-3} M to 10^{-6} M. All glassware used was wrapped in aluminum foil, and heated at 500 °C for at least 3 hours to eliminate possible terrestrial contamination.

2.2. Derivatization

Diluted series of the standard solution were transformed into *N*(O,S)-ethoxy-carbonylheptafluorobutylester derivatives (ECHFBE) according to the modified standard procedure of Abe et al. [25] described elsewhere [19, 20]. Arguments for the choice of the derivatization method were reviewed by Meinert and Meierhenrich [26]. The reagents were added into a reaction vial in the following order: 25 μ L of a 2,2,3,3,4,4,4-heptafluoro-1-butanol/pyridine mixture (3:1, *v/v*) followed by 5 μ L of ethyl chloroformate. The reaction mixture was vigorously shaken for 10 seconds to form the ECHFBE derivatives. The amino acid derivatives were extracted from the reaction mixture by adding 40 μ L of chloroform and 10 μ L solution of pyrene in chloroform ($2 \mu\text{g mL}^{-1}$), the last serving as an internal standard (IS). The organic phases were withdrawn and transferred into 1 mL GC vials equipped with 100 μ L inserts for enantioselective GC \times GC analyses.

This derivatization method was also applied to an extract of the Murchison meteorite. The detailed extraction procedure is described in the supplementary information and can be found in the literature [6].

2.3. GC × GC–TOFMS

The enantioselective multidimensional analysis was carried out by a GC × GC Pegasus IV D instrument coupled to a time-of-flight mass spectrometer (LECO, Michigan, USA). The MS system operated at a storage rate of 150 Hz, with a 50–400 amu mass range, detector voltage of 1.8 kV, and solvent delay of 15 min. Ion source and injector temperatures were set to 230 °C.

The column set consisted of two Press-Tight[®] connected Varian-Chrompack Chirasil-L-Val columns (49.2 m × 0.25 mm, 0.12 μm film thickness) in the first dimension and a DB Wax as secondary column (1.4 m × 0.1 mm, 0.1 μm film thickness). Helium was used as carrier gas at a constant flow of 1 mL min⁻¹. All samples were injected in the splitless mode with an identical temperature program. The temperature of the primary column was held at 40 °C for 1 min then increased to 80 °C at a rate of 10 °C min⁻¹ and held for 10 min, finally it was heated up to 180 °C with a 2 °C min⁻¹ rate and held for 15 min. The secondary oven used a temperature offset of 20 °C. It stayed at 60 °C for 1 min, warmed up to 100 °C with a 10 °C min⁻¹ rate, and held for 10 min, then heated up to 150 °C at a rate of 2 °C min⁻¹ and finally it was increased to 210 °C at a rate of 4 °C min⁻¹ and held for 30 min. A modulation period of 3 seconds was applied. All samples were injected 3 to 5 times in order to accurately calculate peak areas with reliable statistical error bars. Data were processed using the LECO Corp ChromaTOF[™] software. Volume peak integration was performed, taking into account possible modulation-induced errors.

3. Result and discussion

3.1. Mass spectra of the derivatives

Mass spectra of amino acids were interpreted based on the previously described fragmentation mechanism [18]. The ECHFBE derivatives allow for compound specific characterization as it demonstrate class specific mass losses: [M-227-44]⁺ is a fingerprint of *N*-alkylated amino acids and [M-199]⁺ resulting in the formation of cyclic ion is a characteristic signature of the β, γ and δ-amino acids. The common characteristic ion masses for the majority of amino acids are: [M-227]⁺, [M-227-28]⁺, [M-227-46]⁺, [M-227-72]⁺, [M-88]⁺. The loss of *m/z* = 227 corresponds to the loss of the acylium ion [CO₂CH₂(CF₂)₂CF₃]⁺ derived from *α*-cleavage. The loss of the neutral fragment [CH₃CH₂OCONH₂] formed by the cleavage of C–N bond in the *α*-position to the NH₂ functional group results in the characteristic ion [M-88]⁺. Fragments *m/z* = 28 and *m/z* = 46, are attributed to [CH₂CH₂]⁺ and [CH₃CH₂OH]⁺ molecular ions, respectively. The interpretation of the mass spectra for all 30 amino acids is listed in the supporting information-Fig. S3.2 (1–31). The applied derivatization provides new insights into the identification of unknown peaks based on the interpretation of mass fragmentation patterns. Table 3.1 summarizes the characteristic mass fragments for all analyzed amino acids.

Table 3.1. Characterization of amino acids by mass spectra, detection (LOD) and quantification limits (LOQ) and resolution values (R_s) for enantiomeric pairs.

#	Compound	Characteristic ions ^[a]	LOD, μM	LOQ, μM	R_s
1	Glycine	256, 102 , 56	0.24	0.71	
2	Sarcosine	270, 116 , 88	$4.50 \cdot 10^{-3}$	0.01	
3	α -Alanine	270, 116 , 70	0.03	0.09	4.00
4	β -Alanine	270, 242 ^[b] , 228, 144, 115, 102 , 98, 70,	0.78	2.36	
5	Serine ^[c]	256, 204, 129, 114 , 101, 86, 60	8.80	26.67	2.00
6	2,3-Diaminopropanoic acid ^[h]	341, 313, 256, 157, 129, 102 , 85	0.16	0.49	4.00
7	<i>N</i> -Methylalanine	284, 130 , 102, 86, 58	0.13	0.40	
8	<i>N</i> -Ethylglycine	284, 270, 242 ^[b] , 130 , 116, 102, 86, 58	0.17	0.51	
9	2-Aminoisobutyric acid	284, 130, 84, 58	41.67	126.27	
10	2-Aminobutyric acid	284, 256, 130 , 84, 58	0.16	0.48	3.80
11	3-Aminoisobutyric acid	256, 158, 129, 112, 102 , 84, 56	0.06	0.19	
12	3-Aminobutyric acid	284, 270, 242, 158, 129, 116 , 84, 70	0.43	1.30	1.83
13	Iminodiacetic acid	369, 342, 298, 270 , 242, 213, 86, 69	0.60	1.82	
14	4-Aminobutyric acid	284, 158, 129, 116, 112, 102 , 86 , 84, 56	3.71	11.26	
15	Aspartic acid	342 ^[d] , 296, 270, 254, 228, 142, 98, 70 , 56	1.08	3.27	2.25
16	2,4-Diaminobutanoic acid ^[h]	329, 282, 171, 128, 116 , 102, 88, 56	9.65	29.23	2.60
17	Isovaline	342, 270, 227, 144 , 98, 72, 55	122.92	372.51	1.67
18	Valine	298, 256, 144 , 129, 116, 101, 98, 72, 55	0.09	0.28	3.20
19	Proline	296, 142 ^[e] , 114, 98, 70	0.24	0.72	
20	Norvaline	298, 256, 144 , 100, 98, 72, 55	0.34	1.04	4.50

Table 3.1. *Continued*

#	Compound	Characteristic ions ^[a]	LOD, μM	LOQ, μM	R_s
21	3-Aminopentanoic acid	298, 270, 172, 130 , 98, 84, 70, 56	3.81	11.55	2.00
22	Pyroglutamic acid ^[f]	84 , 56	11.31	34.28	3.20
23	Glutamic acid	356, 312, 156, 128, 84	10.09	30.57	3.67
24	Methionine ^[h]	329, 256, 201, 146, 129, 101 , 74	0.80	2.42	2.16
25	<i>tert</i> -Leucine	329, 312, 256, 158 , 129, 112, 101, 57	0.53	1.61	5.50
26	Isoleucine	312, 283, 256, 158 , 129, 101, 83, 57, 56	0.11	0.33	9.00
27	Leucine	312, 256, 158 , 129, 112, 102 , 86, 58	0.33	1.01	4.75
28	β -Leucine	342, 270, 228, 186, 144, 116, 98, 70 , 56	1.20	3.62	4.50
29	Norleucine	312, 256, 158 , 142, 130, 112, 84, 70	0.15	0.45	4.57
30	Methylpyroglutamic acid ^[g]	98 , 82, 55	2.09	6.34	3.60
31	Phenylalanine	330, 256, 192, 131, 103, 91 , 65, 59	0.15	0.46	4.00

^[a] Numbers designated in boldface are the main mass fragments. ^[b] McLafferty rearrangement. ^[c] Bis-acylated. ^[d] Cyclic oxonium ion. ^[e] Cyclic iminium ion. ^[f] Dehydration product of glutamic acid. ^[g] Dehydration product of methylglutamic acid. ^[h] Amino acids that were not detected in the Murchison extract.

3.2. Method validation

The developed method was tested for quantitative analysis in terms of linearity and working range. At least 5 concentrations of the standard solution were used in this study. The calibration curves were plotted as the logarithm of A_{AA}/A_S , versus logarithm of C_A/C_{IS} , to provide visual confirmation of the linear range (see supporting information Fig. S3.1 (1–8)). Each point of the curve represents the average value of three replicated measurements. The linear relationship was evaluated by the calculation of a regression line by the method of least squares for the plot of peak area as a function of analyte concentration. The squared correlation coefficient values are close to 1, which certify good agreement with generated linear equation (Table 3.2). The upper limit of the working range was determined by the saturation of the detector response and the lower limit corresponds to the method detection limit (Table 3.2) [27]. Additional information on the regression parameters and the working range for all studied amino acids can be found in the supporting information.

Table 3.2. The parameters characterizing regression line (S , σ , R^2) and working range (C_{max} , C_{min}) of the developed method.

Compound	$S^{[a]}$	$\sigma^{[b]}$	$R^2^{[c]}$	$C_{max}^{[d]}$, μM	$C_{min}^{[e]}$, μM
Glycine	$3.0 \cdot 10^{12}$	$2.1 \cdot 10^5$	1.000	33.3	0.17
β -Alanine	$7.7 \cdot 10^{11}$	$1.8 \cdot 10^5$	1.000	130.1	0.56
Serine	$8.7 \cdot 10^{10}$	$2.3 \cdot 10^5$	0.976	1158	6.27
2,3-Diaminopropanoic acid	$9.7 \cdot 10^{12}$	$4.9 \cdot 10^5$	1.000	10.2	0.17
<i>N</i> -Methylalanine	$3.2 \cdot 10^{12}$	$1.3 \cdot 10^5$	1.000	31.5	0.09
Iminodiacetic acid	$8.8 \cdot 10^{12}$	$1.6 \cdot 10^5$	1.000	114.4	0.43
4-Aminobutyric acid	$1.2 \cdot 10^{11}$	$1.3 \cdot 10^5$	0.982	843.6	2.65
Isovaline	$1.8 \cdot 10^9$	$6.8 \cdot 10^4$	1.000	54970	87.65
3-Aminopentanoic acid	$3.5 \cdot 10^{11}$	$4.1 \cdot 10^5$	0.984	283.9	2.72
Pyroglutamic acid	$8.1 \cdot 10^{11}$	$2.9 \cdot 10^6$	0.971	120.3	8.06
Glutamic acid	$3.0 \cdot 10^{11}$	$9.2 \cdot 10^5$	0.971	332.1	7.19
Methionine	$3.0 \cdot 10^{12}$	$7.2 \cdot 10^5$	1.000	33.5	0.57
Phenylalanine	$1.4 \cdot 10^{12}$	$6.6 \cdot 10^5$	1.000	7.3	0.11

^[a] S – slope of the calibration curve. ^[b] σ – standard deviation of response. ^[c] R^2 – coefficient of determination. ^[d] The upper limit of working range calculated from the regression equation as a concentration of the detector response saturation. ^[e] The lower limit of working range.

In the developed protocol the limit of detection (LOD) and the limit of quantification (LOQ) were calculated based on the standard deviation of the response (σ) and the slope of the calibration curve (S) at levels approximating the LOD and LOQ according to the formulas: $\text{LOD} = 3.3\sigma/S$, $\text{LOQ} = 10\sigma/S$ [28]. The standard deviation of the response was determined based on the standard deviation

of y -intercepts of regression lines. Most of the studied amino acids showed adequate sensitivity with detection limits ranging from 0.005–3 pmol. Exceptions are 2-AIB, isovaline, 3-aminopentanoic acid, 4-aminobutanoic acid, 2,3-aminobutanoic acid, serine, glutamic, pyroglutamic, and iminodiacetic acid, where the LOD is above 3 pmol (Table 3.1). Based on the obtained data we can conclude that the reaction yield decreases with the addition of a new functional group, moving the amine group from the α - to γ -position, and most prominently with addition of an additional alkyl group in α -position.

In GC \times GC analysis the thermal modulator compresses the analytes before they are released into the secondary column. This feature of the modulator, also known as focusing effect results in narrow peaks with enhanced peak height [16]. Consequently, the calculated LOD and LOQ exceed previously reported values [18, 21] (ranging from 0.18 pmol to 6 nmol) by an order of magnitude, hence indicating the enhanced sensitivity of the developed procedure. Remarkably, even the lowest LOQ values of α -dialkylated amino acids are above the concentrations found in carbonaceous meteorites [29], and therefore the procedure can be used for further quantifications.

3.3. Enantioseparation

The one-step, achiral chloroformate derivatization combined with the separation on a chiral stationary phase provides substantial advantages versus the widely used chiral derivatization followed by diastereomer separation via an achiral stationary phase. It eliminates sources of errors in the quantitative enantioseparation related to the derivatization procedure, e.g. enantiomeric impurities of the derivatization auxiliary, partial racemization of both reactants during derivatization, and the difference in reaction kinetics of enantiomers with a chiral reagent [29]. Chiral OPA/NAC was used in recently reported nano-electrospray ionization high resolution orbitrap mass spectrometry coupled to HPLC [17]. It was proven to detect amino acids with concentrations as low as 10^{-10} M. However, errors resulting from chiral derivatization and incomplete resolution of several amino acids make this technique less suitable for quantification of small enantiomeric excesses in complex matrices.

The here-developed analytical method was investigated for the enantioseparation of 23 enantiomeric pairs of amino acids. Out of these, 13 pairs of non-proteinogenic amino acids have been previously viewed as particularly important target molecules [30] due to their rare occurrence in the biosphere, and therefore indigenous *ee* distribution within carbonaceous meteorites. Additionally, our results show that the Chirasil-L-Val stationary phase in combination with the applied derivatization was not able to separate *N*-methylalanine, proline, and 3-aminoisobutyric acid (Figure 3.1). The chemical structure of the stationary phase is known to be crucial for the resolution of amino acid enantiomers. The interaction between analytes and the Chirasil-Val stationary phase is mainly based on hydrogen-bridged intermediate diastereomeric associates. Consequently such interaction cannot take place if the asymmetric carbon bonds to the substituted amino group. To achieve better resolution of proline and *N*-alkylated amino acid enantiomers, Chirasil- β -Dex or mixed phases such as Chirasil-Val/Chirasil- β -Dex

were described to be useful [23]. Previous studies of the resolution of α -alkyl and α -dialkyl amino acids demonstrated that the presence of an alkyl chain in α -position complicates enantiomeric separation [21]. Both enantiomers were resolved for all other amino acids. All of them display baseline separation, i.e. resolution higher than 1.5 (Table 3.1). The best separation of the α -dialkyl amino acid isovaline was achieved using a temperature program with a 10 min plateau at 80 °C.

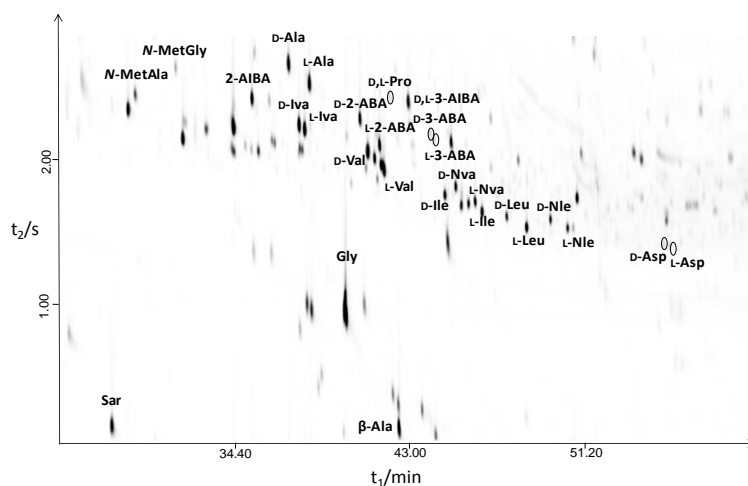


Figure 3.1 Two dimensional surface plot of GC \times GC-TOFMS for the Murchison extract. Selected atomic masses are: 102, 116, 130, 142, 144, 158, and 342.

On the studied stationary phase (Chirasil-L-Val), the elution order was constant for all the enantiomeric pairs: the D-form always elutes first. The exception is pyroglutamic acid where it is inverse.

3.4. Method application

In one-dimensional GC, peak overlapping of amino acid enantiomers with the sample matrix is a common problem. Therefore, enantioselective comprehensive two-dimensional gas chromatography with different column sets has previously been tested on complex natural samples providing narrower peaks and better detection limits. The lowest values reported are in the order of 10^{-2} mg L⁻¹ [20,21]. However, no method validation and resolution data have been reported.

In this study, the separation power of GC \times GC and the developed analytical procedure were applied to an amino acid extract of the Murchison meteorite. The method was proven to produce results coherent with previous findings [29] for amino acids in the presence of interfering compounds and a complex matrix. The two-dimensional counter plot shown in Fig. 3.1 demonstrates complete resolution of the main enantiomeric species. In total, the baseline separation was achieved for more than 200 signals. Fig. 3.2 represents a segment of the two-dimensional chromatogram superposed to its one-dimensional reconstruction, emphasizing the benefits of GC \times GC analysis. The addition of a second separation

dimension in combination with the focusing effect of the modulator and the powerful mass spectrometer drastically increase the amount of information one can deduce from a single gas chromatogram. As an example, the separation of glutamic and pyroglutamic acid would be impossible in 1D GC as they present nearly identical first dimension retention times (Fig. S3.4). Furthermore, the L-enantiomer of 3-aminopentanoic acid co-elutes with numerous compounds having the same main mass fragment in conventional 1D GC (Fig. S3.5), thereby contributing to an ee_1 while two-dimensional analysis discriminates against all sorts of co-elution and gives the precise racemic value of 3-aminopentanoic acid. Summarizing, GC \times GC analysis minimizes errors resulting from the interference through peak overlap and/or co-extracted matrix impurities. Moreover, the produced structured chromatograms result in similar elution patterns for structurally related homologues. Diamino acids, for example, elute in the upper right corner of the chromatogram due to the high polarity, while amino dicarboxylic acids have a shorter second dimension retention time, therefore eluting in the lower right corner. The clustering in this case can provide additional insights for future identifications.

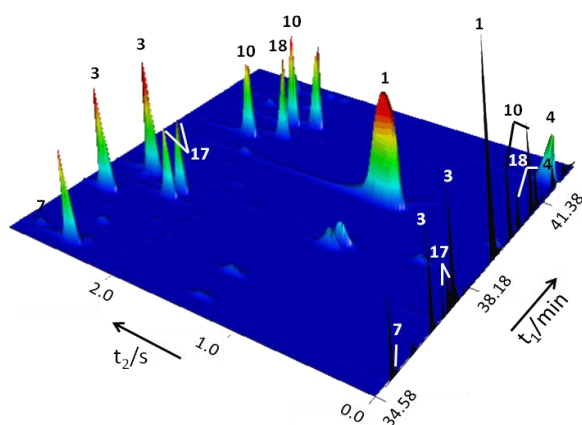


Figure 3.2 Close-up view of the two-dimensional and reconstructed one dimensional enantioselective gas chromatogram depicting standard amino acids identified in a sample of the Murchison meteorite. Numeration of amino acid corresponds to numeration in Table 3.1 Each point in the 3D chromatogram is accompanied by its individual mass spectrum. Atomic mass units 102, 116, 130, 144, 142, 158, and 324 were selected for the above representation. Individual signal intensities were modified for better representation.

The determined ee values of meteoritic chiral amino acids are summarized in Table 3.3. The maximum enantioenrichments were observed for the proteinogenic amino acids leucine and isoleucine. Here, further isotopic ratio studies are needed to determine the origin of the observed asymmetry; high ee_1 values are an indicator of terrestrial contamination. Among the non-proteinogenic amino acids, α -methylated amino acids showed the highest ee values that is consistent with data reported by Pizzarello et al. [31].

Table 3.3. Enantiomeric excesses (*ee*) identified in the Murchison meteorite

#C ^[a]	Amino acid	ee _L (%) ± 3σ ^[b]	Corrected ee _L (%) ^[c]
3	Alanine	3.51 ± 0.74	3.16 ± 0.80
4	2-Aminobutyric acid	2.04 ± 0.86	2.04 ± 0.86
	3-Aminobutyric acid	5.95 ± 0.62	–
	Aspartic acid	4.97 ± 0.44	4.31 ± 0.59
5	Isovaline	4.61 ± 0.83	–
	Valine	5.94 ± 0.52	4.88 ± 0.73
	Norvaline	0.55 ± 0.21	–
	3-Aminopentanoic acid	0.52 ± 0.32	–
	Pyroglutamic acid	4.75 ± 0.52	3.85 ± 0.78
	Glutamic acid	5.99 ± 0.95	3.79 ± 1.07
6	<i>tert</i> -Leucine	0.00 ± 0.23	–
	Isoleucine	13.85 ± 0.31	9.49 ± 1.16
	<i>allo</i> -Isoleucine	-9.55 ± 0.70	–
	Leucine	35.55 ± 1.06	26.33 ± 0.76
	Norleucine	-0.04 ± 0.39	–
	β-Leucine	-0.01 ± 0.45	–
	Methylpyroglutamic acid	0.61 ± 0.03	–
7	Methylleucine	6.16 ± 0.26	–
9	Phenylalanine	28.23 ± 3.24	0.27 ± 3.32

^[a] Number of carbon atoms. ^[b] ± gives the standard deviation 3σ of multiple injections *n* (*n* = 5–8). ^[c] ± corrected against L-amino acid abundances quantified in serpentine blank.

4. Conclusions

This study provides an improved multidimensional analytical method for enantiomeric separation of amino acids in samples potentially relevant for the origin of homochirality on Earth, such as meteorites, comets, and interstellar ices. The present procedure provides several distinct advantages for the quantitative enantioselective analysis. Firstly, the method sensitivity, linearity, and separation power tested on the diverse groups of amino acids including non-proteinogenic amino acids showed improved LOD and LOQ resulting from the multiplication of the individual peak capacities of the two single columns. Secondly, most of the studied enantiomeric pairs were baseline separated and demonstrated excellent resolution in combination with minimal co-elution with the complex matrix of extraterrestrial samples. The high data acquisition of TOF-MS instruments combined with improved mass spectral deconvolution software allow for clean, unambiguous spectra to be produced, even for partially co-eluting compounds. Additionally,

the alkyl chloroformate derivatives of amino acids demonstrate class specific mass fragmentation enabling the identification of so far unknown amino acid structures in such samples.

The combination of two distinct chromatographic separations allowed us to detect and resolve more than 200 peaks within a single fraction of the Murchison meteorite sample. It was shown that co-elution of analytes with interfering compounds and the complex meteoritic matrix can be minimized by performing GC \times GC analysis. We anticipate that our method will be employed for the precise quantification of organic compounds and/or calculation of small *ees* in meteorites, simulated interstellar ice analogs, and potentially interplanetary dust and cometary particles.

References

- [1] F. Goesmann, F. Raulin, J.H. Bredehöft, M. Cabane, P. Ehrenfreund, A.J. MacDermott, S. McKenna-Lawlor, U.J. Meierhenrich, G.M. Muñoz Caro, C. Szopa, R. Sternberg, R. Roll, W.H.P. Thiemann, S. Ulamec, *COSAC, Planetary and Space Science* 103 (2014) 318–330.
- [2] U.J. Meierhenrich, *Comets and their Origin - The Tool to Decipher a Comet*, Wiley-VCH, Weinheim, 2015.
- [3] Z. Martins, M.A. Sephton, Extraterrestrial amino acids, in: A.B. Hughes (Ed.), *Amino Acids, Peptides and Proteins in Organic Chemistry*, Wiley-VCH Verlag GmbH & Co. KGaA, Weinheim, 2009, pp. 1–42.
- [4] U.J. Meierhenrich, *Amino Acids and the Asymmetry of Life*, Springer, Heidelberg, 2008.
- [5] D.P. Glavin, M.P. Callahan, J.P. Dworkin, J.E. Elsila, The effects of parent body processes on amino acids in carbonaceous chondrites, *Meteoritics & Planetary Science* 45 (2010) 1948–1972.
- [6] Z. Martins, P. Modica, B. Zanda, L. Le Sergeant d'Hendecourt, The amino acid and hydrocarbon contents of the Paris meteorite: Insights into the most primitive CM chondrite, *Meteoritics & Planetary Science* 50 (2015) 926–943.
- [7] P.G. Stoks, A.W. Schwartz, Uracil in carbonaceous meteorites, *Nature* 282 (1979) 709–710.
- [8] Z. Martins, O. Botta, M.L. Fogel, M.A. Sephton, D.P. Glavin, J.S. Watson, J.P. Dworkin, A.W. Schwartz, P. Ehrenfreund, Extraterrestrial nucleobases in Murchison meteorite, *Earth and Planetary Science Letters* 270 (2008) 130–136.
- [9] M.P. Callahan, K.E. Smith, H.J. Cleaves, J. Ruzicka, J.C. Stern, D.P. Glavin, C.H. House, J.P. Dworkin, Carbonaceous meteorites contain a wide range of extraterrestrial nucleobases, *Proceedings of the National Academy of Sciences* 108 (2011) 13995–13998.
- [10] G. Cooper, N. Kimmich, W. Belisle, J. Sarinana, K. Brabham, L. Garrel, Carbonaceous meteorites as a source of sugar-related organic compounds for the early Earth, *Nature* 414 (2001) 879–883.
- [11] I. Myrgorodska, C. Meinert, Z. Martins, L. Le Sergeant d'Hendecourt, U.J. Meierhenrich, Molecular Chirality in Meteorites and Interstellar Ices, and the Chirality Experiment on Board the ESA Cometary Rosetta Mission, *Angewandte Chemie International Edition* 54 (2015) 1402–1412.
- [12] M.H. Engel, B. Nagy, Distribution and enantiomeric composition of amino acids in the Murchison meteorite, *Nature* 296 (1982) 837–840.
- [13] V. Brazhnikov, L. Mukhin, Gas chromatography and space research, *Chromatographic Reviews* 15 (1971) 151–194.
- [14] P. Schmitt-Kopplin, Z. Gabelica, R.D. Gougeon, A. Fekete, B. Kanawati, M. Harir, I. Gebefuegi, G. Eckel, N. Hertkorn, High molecular diversity of extraterrestrial organic matter in Murchison meteorite revealed 40 years after its fall, *Proceedings of the National Academy of Sciences* 107 (2010) 2763–2768.
- [15] Z. Liu, J.B. Philips, Comprehensive two-dimensional gas chromatography using an on-column thermal modulator interface, *Journal of Chromatographic Science* 29 (1991) 227–231.

- [16] C. Meinert, U.J. Meierhenrich, A New Dimension in Separation Science: Comprehensive Two-Dimensional Gas Chromatography, *Angewandte Chemie International Edition* 51 (2012) 10460–10470.
- [17] M.P. Callahan, M.G. Martin, A.S. Burton, D.P. Glavin, J.P. Dworkin, Amino acid analysis in micrograms of meteorite sample by nanoliquid chromatography–high-resolution mass spectrometry, *Journal of Chromatography A* 1332 (2014) 30–34.
- [18] M. Zampolli, G. Basaglia, F. Dondi, R. Sternberg, C. Szopa, M. Pietrogrande, Gas chromatography–mass spectrometry analysis of amino acid enantiomers as methyl chloroformate derivatives: application to space analysis, *Journal of Chromatography A* 1150 (2007) 162–172.
- [19] M. Junge, H. Huegel, P.J. Marriott, Enantiomeric analysis of amino acids by using comprehensive two-dimensional gas chromatography, *Chirality* 19 (2007) 228–234.
- [20] R. Mayadunne, T-T. Nguyen, P.J. Marriott, Amino acid analysis by using comprehensive two-dimensional gas chromatography, *Analytical Bioanalytical Chemistry* 382 (2005) 836–847.
- [21] M. Pietrogrande, G. Basaglia, Enantiomeric resolution of biomarkers in space analysis: Chemical derivatization and signal processing for gas chromatography–mass spectrometry analysis of chiral amino acids, *Journal of Chromatography A* 1217 (2010) 1126–1133.
- [22] I. Ilisz, A. Aranyi, Z. Pataj, A. Péter, Enantiomeric separation of nonproteinogenic amino acids by high-performance liquid chromatography, *Journal of Chromatography A* 1269 (2012) 94–121.
- [23] S. Fox, H. Strasdeit, S. Haasmann, H. Brückner, Gas chromatographic separation of stereoisomers of non-protein amino acids on modified γ -cyclodextrin stationary phase, *Journal of Chromatography A* 1411 (2015) 101–109.
- [24] V. Schuring, Gas chromatographic enantioseparation of derivatized α -amino acids on chiral stationary phases—Past and present, *Journal of Chromatography B* 879 (2011) 3122–3140.
- [25] I. Abe, N. Fujimoto, T. Nishihara, K. Terada, T. Nakahara, Rapid analysis of amino acid enantiomers by chiral-phase capillary gas chromatography, *Journal of Chromatography A* 722 (1996) 221–227.
- [26] C. Meinert, U.J. Meierhenrich, Derivatization and Multidimensional Gas-Chromatographic Resolution of α -Alkyl and α -Dialkyl Amino Acid Enantiomers, *ChemPlusChem* 79 (2014) 781–785.
- [27] L. van Reeuwijk, Guidelines for quality management in soil and plant laboratories, Food & Agriculture Org., FAO, Rome, 1998.
- [28] E. Bernal, Limit of Detection and Limit of Quantification Determination in Gas Chromatography, in: X. Guo (Ed.), *Advances in Gas Chromatography*, InTech, 2014, pp. 57–81.
- [29] C. Reiner, G.J. Nicholson, U. Nagel, V. Schurig, Evaluation of enantioselective gas chromatography for the determination of minute deviations from racemic composition of α -amino acids with emphasis on tyrosine: Accuracy and precision of the method, *Chirality* 19 (2007) 401–414.

- [30] J.R. Cronin, S. Pizzarello, Amino acid enantiomer excesses in meteorites: origin and significance, *Advances in Space Research* 23 (1999) 293–299.
- [31] S. Pizzarello, M. Zolenski, K.A. Turk, Nonracemic isovaline in the Murchison meteorite: Chiral distribution and mineral association, *Geochimica et Cosmochimica Acta* 67 (2003) 1589–1595.

Supporting information

1. Method validation

The linearity of the calibration curves was verified for more than three orders of magnitude with concentrations of amino acids varying from 10^{-5} to 10^{-10} M. For amino acids with lower response (isovaline and 2-aminoisobutyric acid) individual standard solutions with a concentration ranging from 10^{-3} to 10^{-5} M were prepared. To correct the errors derived from analyte loss during sample preparation, the sample inlet, and changes in the detector response; the calibration was done by using an internal standard (IS). An IS solution of pyrene in chloroform ($2 \mu\text{g mL}^{-1}$) was added into all samples including the Murchison extract. To demonstrate the linearity, calibration curves were plotted in double-logarithmic scale (Figure S3.1). We have chosen to present one amino acid for each class analyzed: alanine for proteinogenic amino acids, 2-aminobutyric acid for α -non-proteinogenic amino acids, β -alanine for β -amino acids, 4-aminobutyric acid for γ -amino acid, isovaline for α -dialkylated amino acids, sarcosine for *N*-alkylated amino acids, iminodiacetic acid for iminodiacides, and 2,3-diaminopropanoic acid (DAP) for diamino acids. For the majority of the studied amino acids four different concentrations (in some cases 3) provide a good agreement with the linear model.

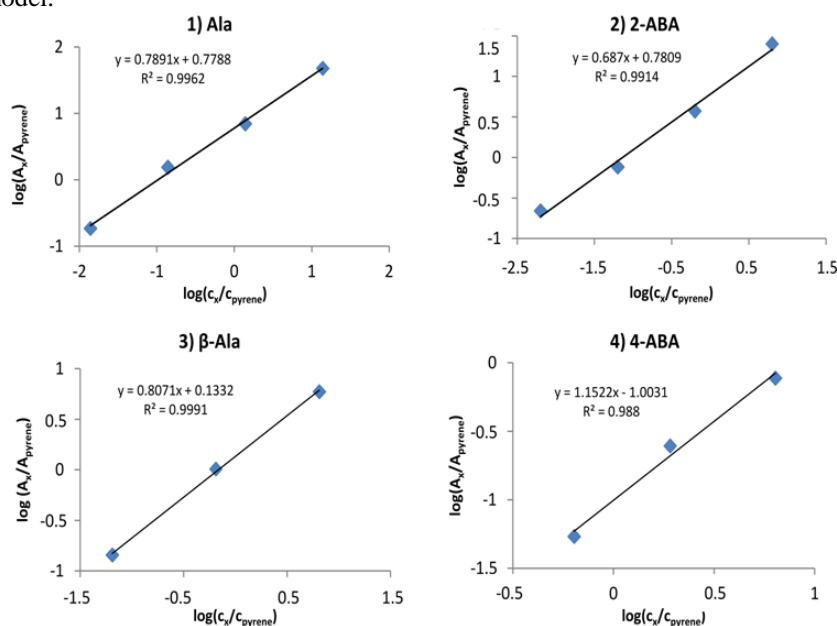


Figure S3.1a Calibration curves of 1) alanine, 2) 2-aminobutyric acid, 3) β -alanine, and 4) 4-aminobutyric acid plotted as function of $\log(A_s/A_{\text{pyrene}})$ over $\log(c_s/c_{\text{pyrene}})$ with calibration line equation and squared correlation coefficient.

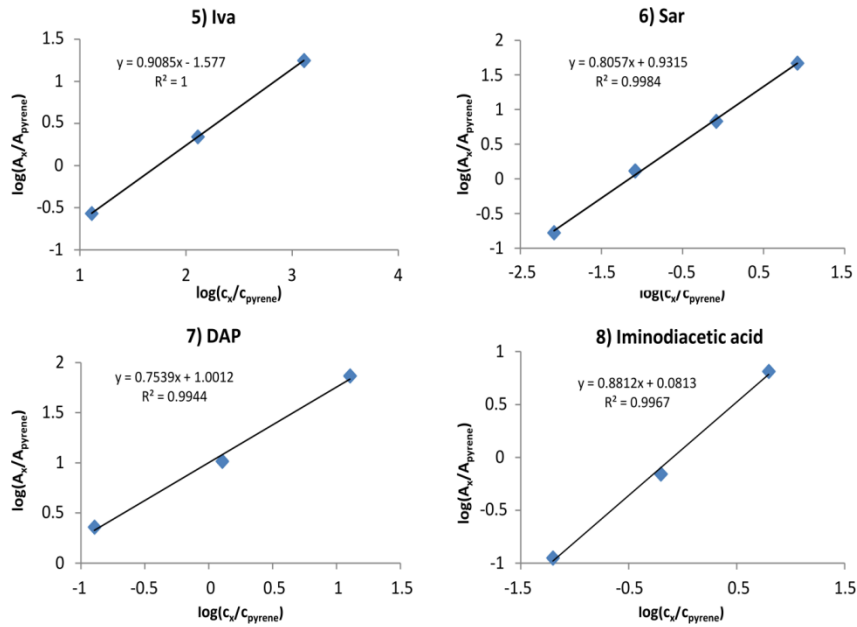


Figure S3.1b Calibration curves of 5) isovaline, 6) sarcosine, 7) 2,3-diaminopropanoic acid, and 8) 4-aminobutyric acid plotted as function of $\log(A_x/A_{\text{pyrene}})$ over $\log(C_s/C_{\text{pyrene}})$ with calibration line equation and squared correlation coefficient.

To calculate LOD and LOQ, the calibration curves were plotted as concentration versus peak area. Coefficient of determination (R^2), standard deviation of the response (σ) and the slope of the mentioned calibration curve (S) are listed in Table S3.1 as well as retention time in both dimensions.

Table S3.1. Regression parameters of the studied calibration curves.

#	Compound	σ	S	R^2	t_1 , min	t_2 , sec
1	Glycine	$3.0 \cdot 10^{12}$	$2.1 \cdot 10^5$	1.000	39.82	3.98
2	Sarcosine	$4.7 \cdot 10^{12}$	$1.4 \cdot 10^5$	1.000	28.58	3.13
3	α -Alanine	$5.7 \cdot 10^{12}$	$5 \cdot 10^4$	1.000	D-37.07; L-38.07	D-2.76; L-2.62
4	β -Alanine	$7.7 \cdot 10^{11}$	$1.8 \cdot 10^5$	1.000	42.31	3.13
5	Serine ^[c]	$8.7 \cdot 10^{10}$	$2.3 \cdot 10^5$	0.976	D-60.75; L-61.09	D-2.36; L-2.38
6	2,3-Diaminopropanoic acid	$9.7 \cdot 10^{12}$	$4.9 \cdot 10^5$	1.000	D-76.70; L-77.70	D-1.96; L-1.96
7	<i>N</i> -Methylalanine	$3.2 \cdot 10^{12}$	$1.3 \cdot 10^5$	1.000	29.73	2.52
8	<i>N</i> -Ethylglycine	$2.5 \cdot 10^{12}$	$1.3 \cdot 10^5$	1.000	31.68	2.73
9	2-Aminoisobutyric acid	$2.0 \cdot 10^{10}$	$2.5 \cdot 10^5$	1.000	35.33	2.50
10	2-Aminobutyric acid	$3.3 \cdot 10^{12}$	$1.6 \cdot 10^5$	1.000	D-40.47; L-41.42	D-2.36; L-2.16

Table S3.1. Continued

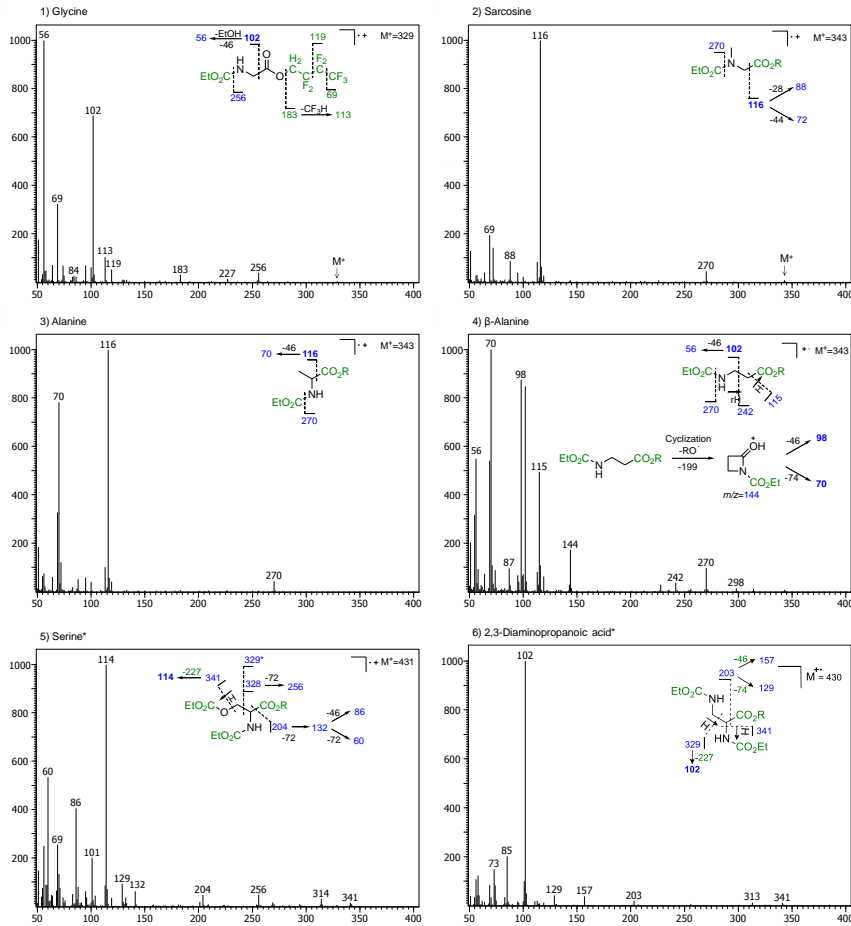
#	Compound	σ	S	R ²	t ₁ , min	t ₂ , sec
11	3-Aminoisobutyric acid	4.8·10 ¹²	9.2·10 ⁴	1.000	42.77	2.49
12	3-Aminobutyric acid	9.7·10 ¹¹	1.3·10 ⁵	1.000	D-43.76; L-44.02	D-2.25; L-2.22
13	Iminodiacetic acid	8.8·10 ¹²	1.6·10 ⁵	1.000	48.31	1.70
14	4-Aminobutyric acid	1.2·10 ¹¹	1.3·10 ⁵	0.982	51.06	2.10
15	Aspartic acid	1.3·10 ¹²	4.3·10 ⁵	1.000	D-55.00; L-55.30	D-1.43; L-1.42
16	2,4-Diaminobutanoic acid	3.8·10 ¹¹	1.1·10 ⁶	0.991	D-81.60; L-82.25	D-0.81; L-0.81
17	Isovaline	1.8·10 ⁹	6.8·10 ⁴	1.000	D-37.57; L-37.82	D-2.30; L-2.28
18	Valine	5.1·10 ¹²	1.4·10 ⁵	1.000	D-40.82; L-41.62	D-2.11; L-1.98
19	Proline	3.6·10 ¹²	2.7·10 ⁵	1.000	37.57	2.30
20	Norvaline	6.9·10 ¹²	7.2·10 ⁵	1.000	D-45.06; L-45.96	D-1.86; L-1.75
21	3-Aminopentanoic acid	3.5·10 ¹¹	4.1·10 ⁵	0.984	D-47.66; L-47.91	D-1.82; L-1.79
22	Pyroglutamic acid	8.1·10 ¹¹	2.9·10 ⁶	0.971	D-62.14; L-62.94	D-2.66; L-2.65
23	Glutamic acid	3.0·10 ¹¹	9.2·10 ⁵	0.971	D-62.39; L-62.94	D-1.66; L-1.66
24	Methionine	3.0·10 ¹²	7.2·10 ⁵	1.000	D-62.70; L-63.35	D-2.30; L-2.30
25	tert-Leucine	1.0·10 ¹²	1.6·10 ⁵	0.999	D-40.72; L-41.27	D-2.01; L-1.91
26	Isoleucine	3.9·10 ¹²	1.3·10 ⁵	1.000	D-44.51; L-46.31	D-1.79; L-1.67
27	Leucine	5.1·10 ¹²	5.1·10 ⁵	1.000	D-47.56; L-48.46	D-1.63; L-1.56
28	β-Leucine	1.7·10 ¹¹	6.1·10 ⁴	1.000	D-49.61; L-50.31	D-1.62; L-1.57
29	Norleucine	5.7·10 ¹²	3.5·10 ⁵	1.000	D-49.60; L-50.41	D-1.62; L-1.55
30	Methylpyroglutamic acid	6.1·10 ¹¹	3.9·10 ⁵	0.999	D-61.69; L-62.59	D-1.93; L-1.92
31	Phenylalanine	1.4·10 ¹²	6.6·10 ⁵	1.000	D-65.39; L-65.79	D-2.70; L-2.68

2. Extraction of amino acids from the Murchison meteorite

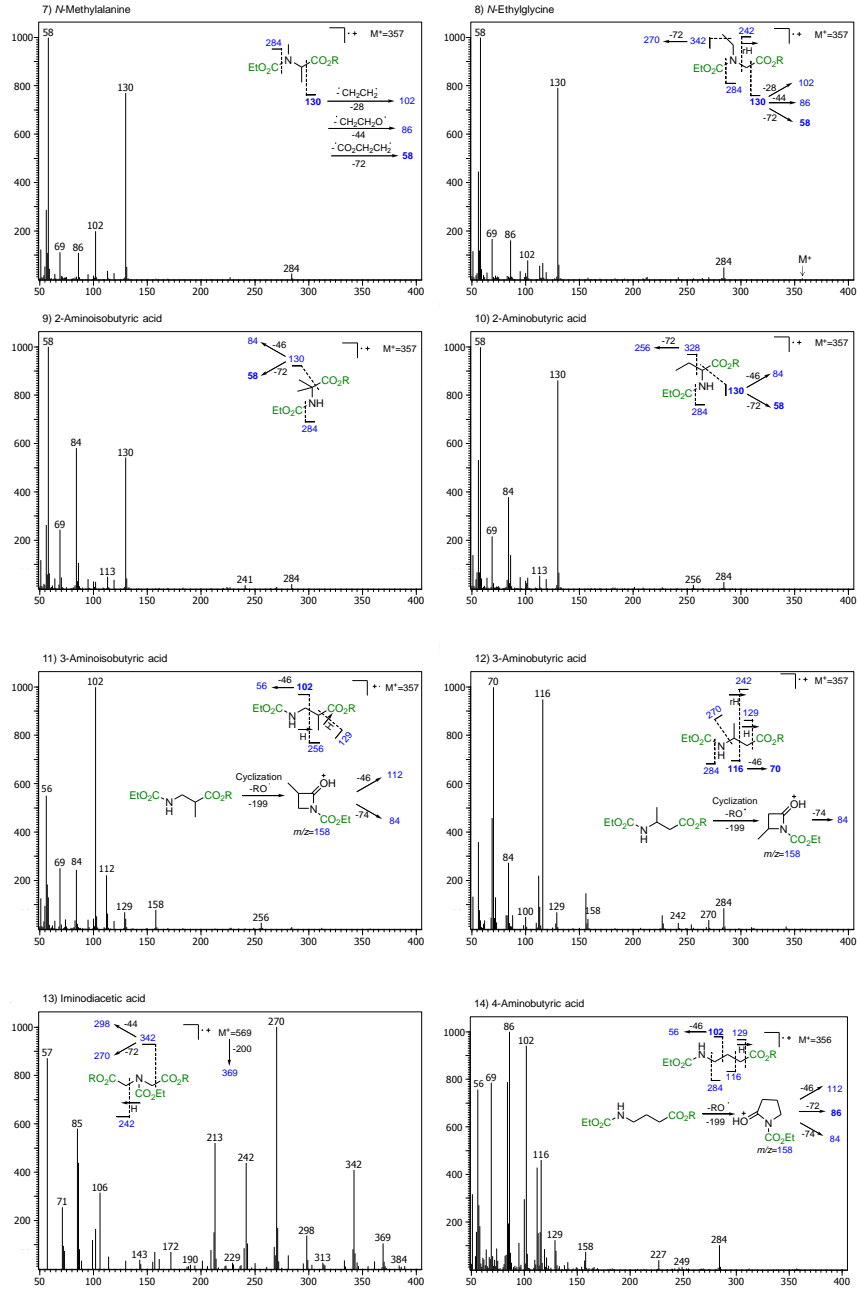
An interior piece of 1.0105 g of the Murchison meteorite (USNM 5451) provided by the Smithsonian National Museum of Natural History as well as 0.9966 g of serpentinite used as a procedural blank (heated to 500°C for more than 3 h) were separately crushed into powder using ceramic mortars and pestles. Samples were transferred into glass ampoules and 2 mL of water (HPLC grade) were added to each ampoule before they were flame-sealed and placed in a heating block for 24 h at 100 °C. The ampoules were then opened, centrifuged, and each supernatant was transferred into a small test tube. Each supernatant was dried under vacuum, and subjected to a 6 M HCl acid vapor hydrolysis (150 °C for 3 h). The acid-hydrolyzed fractions were desalted on a cation exchange resin, the amino acids eluted with 5 ml of 2 M ammonium hydroxide, and the eluates dried under vacuum before being derivatised.

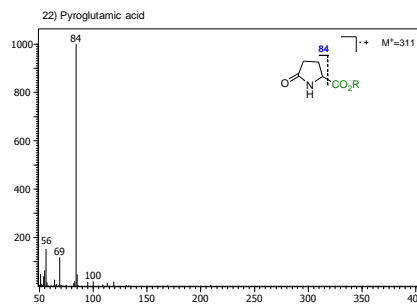
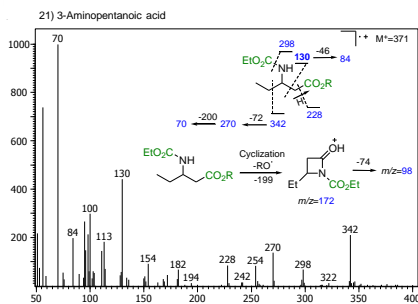
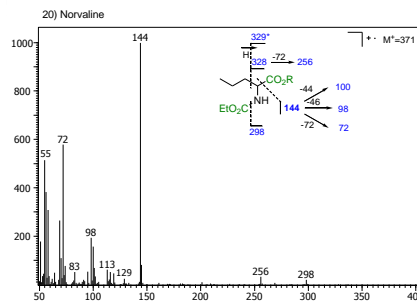
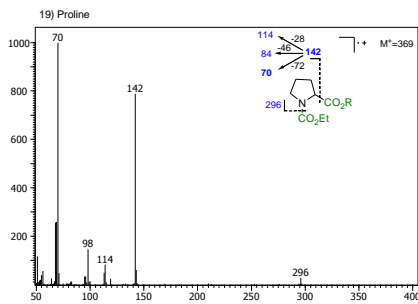
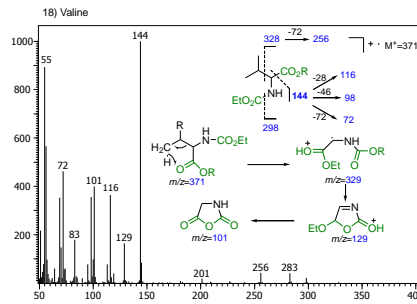
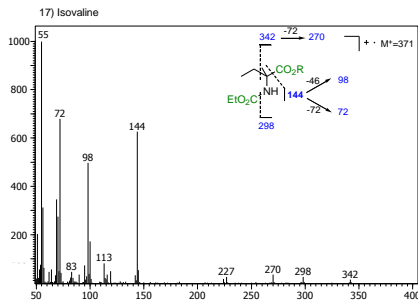
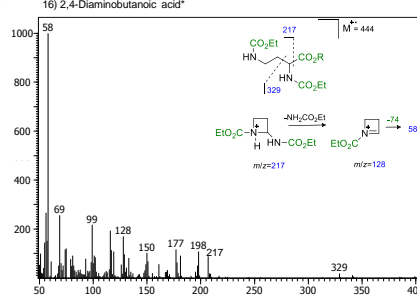
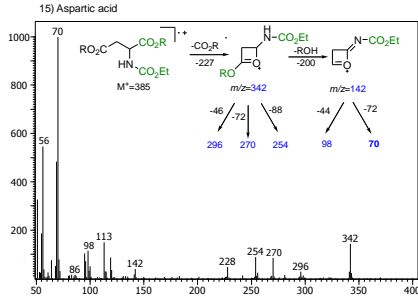
3. Interpretation of mass spectra

The individual mass spectra of the *N*-ethoxycarbonylheptafluorobutyl esters of 31 amino acids and the interpretation of their most prominent mass spectrometric fragments are shown in Figure S3.2 (1-31).



70 CHAPTER II: Analytical methods





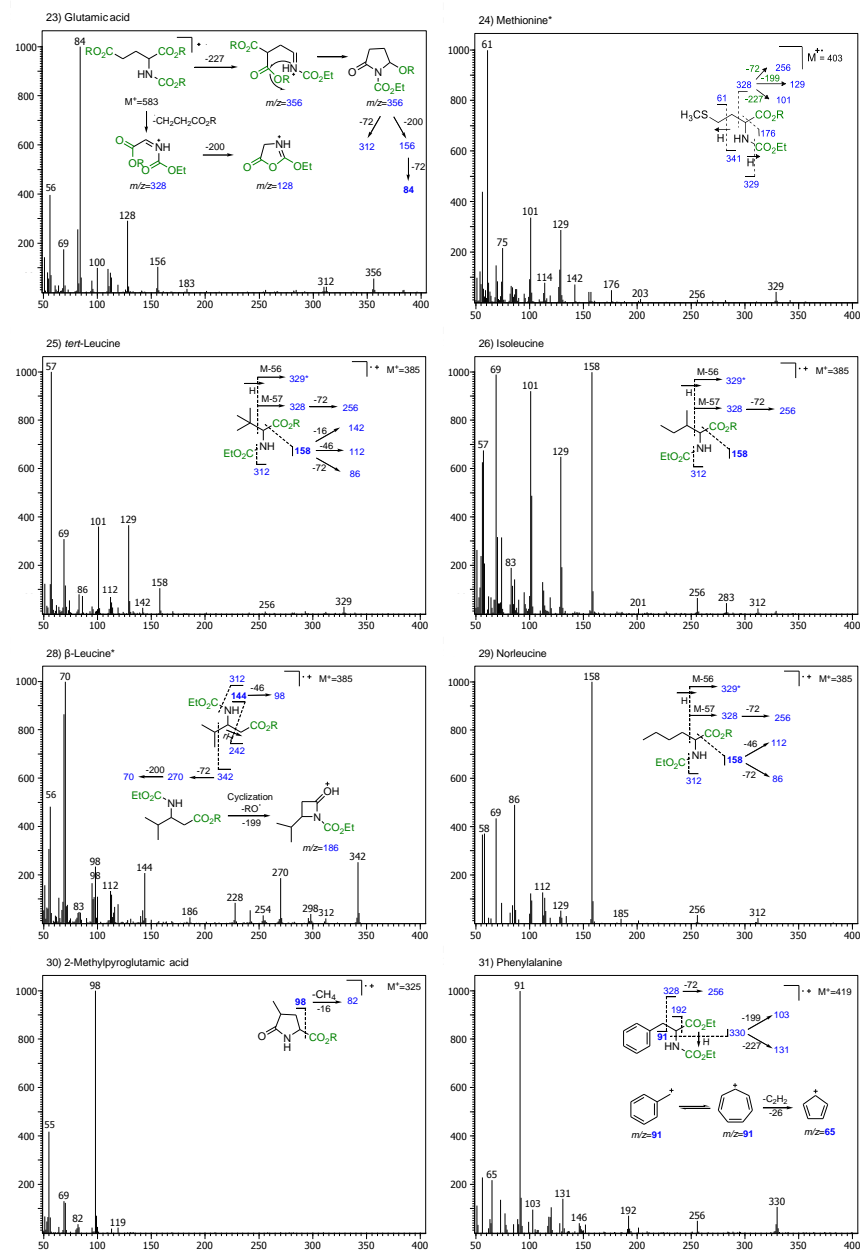


Figure S3.2 (1-31) Proposed fragmentation mechanism of amino acid ECHFBE derivatives and their mass spectra, numeration on the spectra corresponds to numeration of the amino acids in the Table 3.1. Asterisk under the compound name indicate that the mass spectra correspond to the mass spectra of the standard, while for all the others amino acids the mass spectra is taken from the Murchison sample. Formation mechanism for characteristic ions $m/z=129$ and $m/z=101$ from ion $m/z=329$ is presented in the Fig. S3.2 (18)

4. GC×GC chromatograms of a standard solution of amino acids

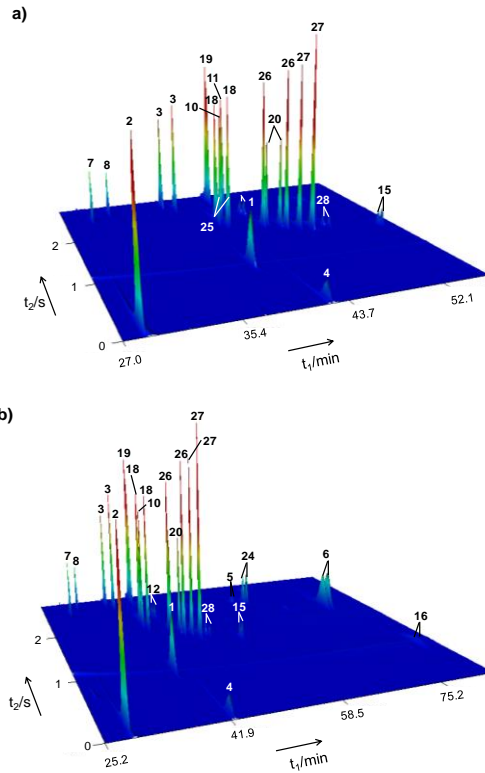


Figure S3.3 The two-dimensional enantioselective gas chromatogram depicting standard amino acids: a) overall view b) close-up view. Numeration of amino acid corresponds to numeration in Table 3.1. Each point in the 3D chromatogram is accompanied by its individual mass spectrum. Atomic mass units 102, 114, 116, 130, 144, 142, 158, 172, and 270 were selected for the above representation. Individual signal intensities were modified for improved visualization.

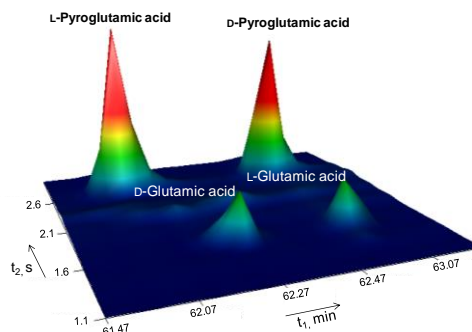


Figure S3.4 The two-dimensional enantioselective gas chromatogram of glutamic and pyroglutamic acids in Murchison meteorite extract. Atomic mass unit 84 was selected for the above representation.

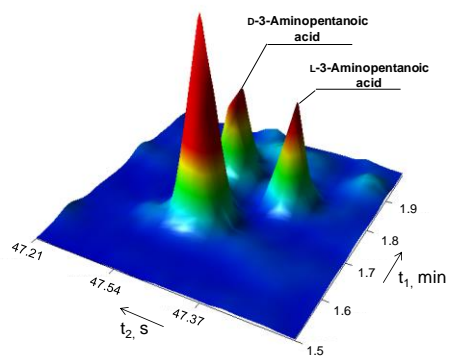


Figure S3.5 The two-dimensional enantioselective gas chromatogram of 3-aminopropanoic acids in Murchison meteorite extract. Atomic mass unit 130 was selected for the above representation.

Once the analytical method has been tested and validated it can be further applied to a sample of choice. In the following study several samples of simulated interstellar ices have been analyzed by comprehensive two-dimensional gas chromatography. As a result several aldehydes and carbonyls have been detected. Among the identified species are glyceraldehyde and glycoaldehyde two intermediate species of the formose reaction. They are also necessary intermediates in the synthesis of activated nucleotides. Moreover, glyceraldehyde is the first chiral aldehyde detected in simulated interstellar ices.

This study became possible because of an accurate and sensitive analytical method developed to target specifically organic molecules with carbonyl groups. The following publications will explain the relevance of this discovery in the context of the origin of life.



CHAPTER III: Prebiotic chemistry of interstellar ice analogues

Article 4. Aldehydes and sugars from evolved precometary ice analogs: Importance of ices in astrochemical and prebiotic evolution

Pierre de Marcellus, Cornelia Meinert, Iuliia Myrgorodska, Laurent Nahon, Thomas Buhse, Louis Le Sergeant d'Hendecourt, and Uwe J. Meierhenrich

Abstract

Evolved interstellar ices observed in dense protostellar molecular clouds may arguably be considered as part of precometary materials that will later fall on primitive telluric planets, bringing a wealth of complex organic compounds. In our laboratory, experiments reproducing the photo/thermochemical evolution of these ices are routinely performed. Following previous amino acid identifications in the resulting room temperature organic residues, we have searched for a different family of molecules of potential prebiotic interest. Using multidimensional gas chromatography coupled to time-of-flight mass spectrometry, we have detected 10 aldehydes, including the sugar-related glycolaldehyde and glyceraldehydes—two species considered as key prebiotic intermediates in the first steps toward the synthesis of ribonucleotides in a planetary environment. The presence of ammonia in water and methanol ice mixtures appears essential for the recovery of these aldehydes in the refractory organic residue at room temperature, although these products are free of nitrogen. We finally point out the importance of detecting aldehydes and sugars in extraterrestrial environments, in the gas phase of hot molecular clouds, and, more importantly, in comets and in primitive meteorites that have most probably seeded the Earth with organic material as early as 4.2 billion years ago.

Key words: glyceraldehydes, glycolaldehyde, astrochemistry, precometary ices, prebiotic evolution

Published article: *Proceedings of the National Academy of Sciences of the U.S.A.* (2015), 112: 965–970.

Significance statement

In molecular clouds out of which stars and planetary systems form, simple solid-state molecules made in large part of H₂O, CO, CO₂, CH₃OH, and NH₃ are abundantly present. In these environments, energetic and thermal processes on these ices, which can be simulated in the laboratory, lead to complex organic matter. Possibly at the origin of the organic matter in our Solar System and incorporated into planetesimals, this material may be considered as a potential source for prebiotic chemistry on telluric planets, following a process that may be quite universal. The composition of these laboratory-evolved ices includes potentially prebiotic species such as amino acids and, as presented in this paper, aldehydes and sugars.

1. Introduction

In dense molecular clouds, interstellar ices are by far the most abundant molecular fraction in the solid state compared with the gas-phase molecules. They are observed in the mid-infrared range around protostars, from which planets, but also much debris, such as comets and asteroids, eventually form. Their composition is dominated by H₂O, followed by CO, CO₂, CH₃OH, NH₃, CH₄, and some less abundant molecules, although their respective abundances can vary from one (type of) source to another [1]. Ices are subjected to various energetic processes such as cosmic rays and UV irradiation [2] as well as thermal reactions, which initiate a rich solid-state chemistry from diffusion within the bulk of reactive species such as ions and radicals, which ultimately recombine to form new and more complex molecules. This molecular complexity is difficult to trace in astrophysical settings and to characterize in the solid state by in situ infrared spectroscopy alone because of the presence of the dominant simple ice species as well as the deep and broad silicate feature along the line of sight that hide minor features expected from complex molecules. However, in warmer regions such as hot molecular cores, icy mantles can sublimate, and complex molecules become more easily detectable and identifiable by radio astronomy due to their rotational spectra [3]. Detected gas-phase molecules are thus more complex than those observed in the solid phase, but models show that an important initial solid-state (ice) chemistry is usually required to explain the measured abundances, which cannot result from gas-phase reactions alone [4, 5].

Laboratory experiments that simulate the photochemical evolution of simple interstellar ices (including C, H, O, and N elements) lead to the production of a complex semirefractory organic residue after warming up to room temperature [6, 7], which is often considered as an analog of precometary matter. Such residues display a macromolecular structure, including a large variety of chemical functions such as alcohols, amines, amides, esters, carboxylic acids, etc. [8, 9]. Among the numerous individual molecules detected in these residues, hexamethylenetetramine (HMT) is a dominant species [10–13], although it seems not to have any direct prebiotic implication [14]. On the other hand, several molecules of potential prebiotic interest have been found, such as amino and diamino acids [14–18], hydantoin [19], urea and glycolic acid [6, 20], lipid precursors [21], quinines

when polycyclic aromatic hydrocarbons are irradiated in water ice [22], and even nucleobases—however, only when pyrimidine is added to the initial ice mixture [23–25]. The presence of sugars, in particular those included in nucleotides that are the building blocks of nucleic acids, has never been reported in these residues.

In this study, we report the first to our knowledge detection of aldehydes in room temperature organic residues, including glycolaldehyde and the chiral glyceraldehyde. We discuss their potential implications for prebiotic chemistry within an astrophysical scenario that emphasizes the central role of extraterrestrial ice photo/thermochemistry as an ubiquitous phenomenon in protostellar media and protoplanetary disk environments [26].

2. Results

Ten different aldehydes, ranging from one to four carbon atoms (Table 4.1), were detected in the organic residue resulting from the processing of an initial $\text{H}_2\text{O}:\text{}^{13}\text{CH}_3\text{OH}:\text{NH}_3$ (12:3.5:1) ice mixture: formaldehyde (H_2CO), glycolaldehyde (CH_2OHCHO), acetaldehyde (CH_3CHO), propanal ($\text{CH}_3\text{CH}_2\text{CHO}$), propenal (CH_2CHCHO), lactaldehyde ($\text{CH}_3\text{CHOHCHO}$), glyceraldehydes ($\text{CH}_2\text{OHCHOHCHO}$), glyoxal (OCHCHO), methylglyoxal [$\text{CH}_3\text{C}(\text{O})\text{CHO}$], and butyraldehyde [$\text{CH}_3(\text{CH}_2)_2\text{CHO}$]. Our analysis of aldehydes in the organic residues uses a definitive means of detection, 2D gas chromatography, coupled to time-of-flight mass spectrometry (GC \times GC–TOFMS). All of these aldehydes—some of them exhibiting additional functional group (Fig. 4.1)—were identified as their *O*-pentafluorobenzyl oxime (PFBO) and *O*-pentafluorobenzyl oxime-trimethylsilyl ether (PFBO-TMS) derivatives, respectively, using aqueous-phase derivatization with *O*-(pentafluorobenzyl)hydroxylamine (PFBHA). Nine out of ten aldehydes were identified by their mass fragmentation patterns, along with the chromatographic elution time in both dimensions of individual PFBHA-TMS-reacted authentic standard injections. Due to the lack of a lactaldehyde reference standard, the structural elucidation of lactaldehyde is solely based on the interpretation of its mass spectrum and its predicted retention time.

For glyceraldehyde, the mass spectrum of the detected molecule is displayed just above the mass spectrum of the corresponding standard (Fig. 4.2). We remind the reader here that organic residues were made with ^{13}C only, whereas standards are composed of ^{12}C . Thus molecular ions and fragments containing one or more carbon atom(s) are shifted accordingly and lead to unambiguous detections.

80 CHAPTER III: Prebiotic chemistry of interstellar ice analogues

Table 4.1. Aldehydes and sugar-related molecules identified in simulated pre-cometary organic residues. Data were obtained from a VUV-irradiated ice mixture at 78 K containing water, ¹³C-labeled methanol, and ammonia; H₂O:¹³CH₃OH:NH₃, in molar composition of 12:3.5:1. After water extraction of the residue at room temperature, the aldehydes were derivatized to form 1-(O-pentafluorobenzyl)oxime derivatives and identified by enantioselective GC×GC-TOFMS analysis.

#C ^[a]	Compound	R _{t1} ^[b] [min]	R _{t2} ^[c] [sec]	MS-fragmentation / ¹³ C sample		MS-fragmentation / ¹² C standard	
				[M ^{**}]	Other important ions, <i>m/z</i>	[M ^{**}]	Other important ions, <i>m/z</i>
1	Formaldehyde	17.08	1.80	226 ^[d]	196, 181	225	195, 181
2	(<i>Z</i>)-Acetaldehyde	20.35	1.94	241 ^[d]	211, 181	239	209, 181
	(<i>E</i>)-Acetaldehyde	21.20	1.92	241 ^[d]	211, 181	239	209, 181
3	(<i>Z</i>)-Glycolaldehyde	41.81	2.24	329 ^[e]	314, 181, 132, 104, 73	327	312, 181, 130, 103, 73
	(<i>E</i>)-Glycolaldehyde	42.14	2.32	329 ^[e]	314, 181, 132, 104, 73	327	312, 181, 130, 103, 73
	(<i>Z</i>)-Glyoxal	72.12	5.21	450 ^[f]	420, 255, 253, 237, 181	448	418, 253, 251, 235, 181
	(<i>E</i>)-Glyoxal	74.54	5.14	450 ^[f]	420, 255, 253, 237, 181	448	418, 253, 251, 235, 181
	(<i>Z</i>)-Propanal	25.49	1.94	256 ^[d]	239, 226, 239, 181	253	236, 223, 181
	(<i>E</i>)-Propanal	25.99	1.94	256 ^[d]	239, 226, 181	253	236, 223, 181
4	(<i>E,Z</i>)-Propenal	25.98	2.20	254 ^[d]	237, 224, 181	251	234, 221, 181
	(<i>E,Z</i>)-Propenal	26.66	2.33	254 ^[d]	237, 224, 181	251	234, 221, 181
	(<i>Z</i>) Lactaldehyde	46.39	2.54	344 ^[e]	329, 181, 73		
	(<i>E</i>) Lactaldehyde	46.81	2.54	344 ^[e]	329, 181, 73		
	(<i>Z</i>) Glyceraldehyde	51.47	2.55	431 ^[g]	417, 328, 251, 220, 181, 147, 104, 73	429	414, 326, 248, 218, 181, 147, 103, 73
	(<i>E</i>) Glyceraldehyde	52.89	2.44	431 ^[g]	417, 328, 251, 220, 181, 147, 104, 73	429	414, 326, 248, 218, 181, 147, 103, 73
	(<i>Z</i>)-Methylglyoxal	71.12	3.84	465 ^[f]	435, 284, 268, 181	463	432, 281, 265, 181
	(<i>E</i>)-Methylglyoxal	74.54	4.14	465 ^[f]	435, 284, 268, 181	462	432, 281, 265, 181
4	(<i>Z</i>) Butyraldehyde	31.65	1.99	271 ^[d]	241 ^[h] , 181	267	239 ^[f] , 181
	(<i>E</i>) Butyraldehyde	31.74	2.04	271 ^[d]	241 ^[h] , 181	267	239 ^[f] , 181

[a] Quantity of carbon atoms. [b] GC×GC retention time 1st dimension. [c] GC×GC retention time 2nd dimension. [d] Molecular ion *m/z* value of 1-(O-pentafluorobenzyl) oxime (PFBO) derivatives. [e] Molecular ion *m/z* value of PFBO trimethylsilyl ether derivatives. [f] Molecular ion *m/z* value of di-PFBO derivatives. [g] Molecular ion *m/z* value of PFBO-bis(trimethylsilyl) ether derivatives. [h] McLafferty rearrangement.

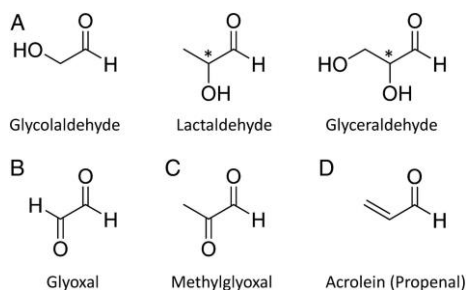


Figure 4.1. Selected aldehydes identified at room temperature in simulated precometary organic residues: (A) hydroxyaldehydes, (B) dialdehyde, (C) ketoaldehyde, and (D) an unsaturated aldehyde.

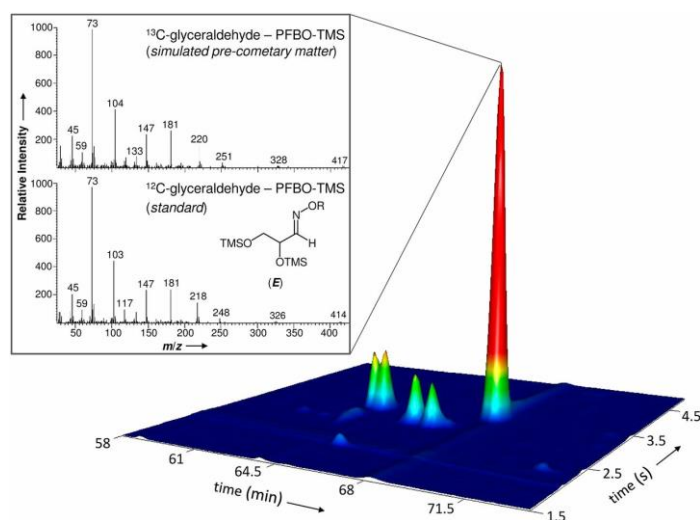


Figure 4.2. Glycer-aldehyde detected in simulated precometary organic residues. Identification of glycer-aldehyde as *O*-pentafluorobenzyl (*R*) oxime bis(trimethylsilyl) ether (PFBO-TMS) in laboratory organic residues using multidimensional gas chromatography. The corresponding external glycer-aldehydes standard shows identical retention times and ^{12}C isotopic signatures in its mass spectra. The mass fragmentation reveals that glycer-aldehyde formed in the residue is entirely composed of ^{13}C -isotopes provided by the $^{13}\text{CH}_3\text{OH}$ reactant present in the original ice mixture. Note that all aldehyde derivatives, except formaldehyde PFBO, can form syn (*Z*) and anti (*E*) stereoisomers of the oximes because the carbon nitrogen double bond (imine) formed during derivatization prevents rotation.

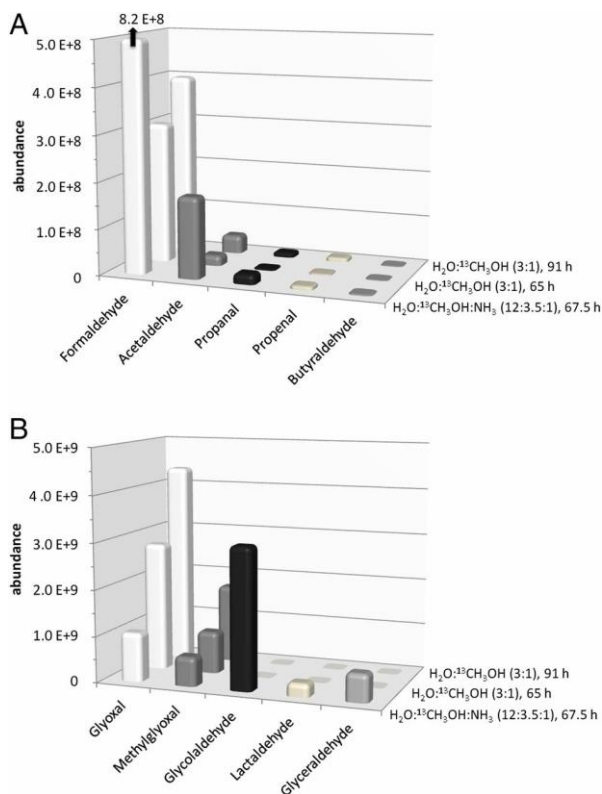


Figure 4.3. Abundances of (A) aldehydes, (B) dialdehydes, keto- and hydroxyaldehydes in the room temperature samples with and without ammonia in the initial ice mixtures.

In the homologous series of aldehydes detected in the organic residues, the lower-molecular-weight members are usually more abundant (Fig. 4.3)—the exception here of formaldehyde may be due to its higher volatility and its gradual loss while heating the vacuum chamber up to room temperature after forming in the ices. The abundances of aldehydes (Fig. 4.3A) and hydroxyaldehydes (Fig. 4.3B) are decreasing with increasing carbon number, as previously observed for amino acids in such ice simulation experiments [13, 17]. Three different samples were analyzed in this study: one containing ammonia ($\text{H}_2\text{O}:\text{}^{13}\text{CH}_3\text{OH}:\text{NH}_3 = 12:3.5:1$, with a simultaneous deposition and irradiation time of 67.5 h) and two without ammonia ($\text{H}_2\text{O}:\text{}^{13}\text{CH}_3\text{OH} = 3:1$, one made during 65 h and one during 91 h, resulting in a higher quantity of organic residue for the second one). Relative aldehyde abundances for the two samples without ammonia follow the trend of the total experiment duration (the global amount of organic residue), although not strictly proportional to it (Fig. 4.3). Interestingly, the abundances of the simple aldehydes (formaldehyde, acetaldehyde, propanal, and butyraldehyde) are lower in the absence of ammonia in the initial ice mixture. Even more striking, the hydroxyaldehydes, including glycolaldehyde, lactaldehyde, and glycerinaldehyde, are completely absent in the samples without ammonia (Figs. 4.3 and 4.4). In contrast,

the abundances of the dialdehydes, glyoxal and methylglyoxal, are reduced in the presence of ammonia, an effect that we do not explain at this stage.

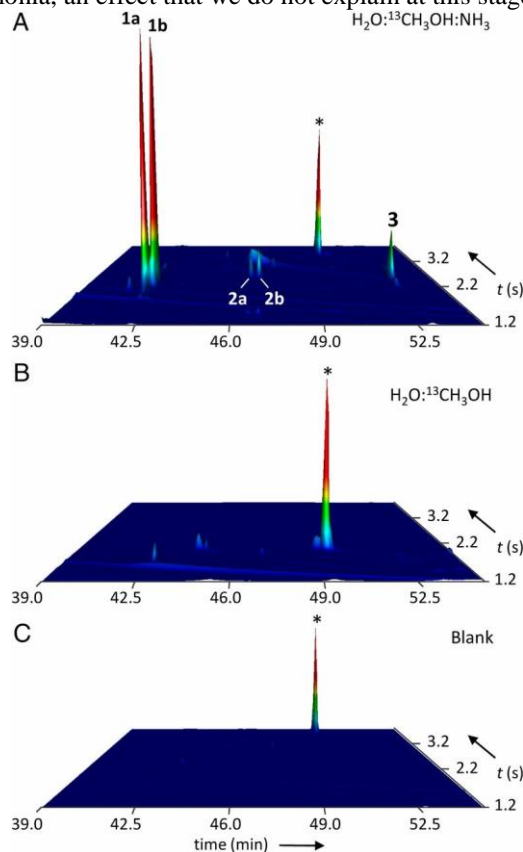


Figure 4.4. Nitrogen allows aldehyde retention at room temperature in simulated precometary organic residues. (A) Identification of glycolaldehyde (1a, b), lactaldehyde (2a, b), and (*E*)-glyceraldehyde (3) as *O*-pentafluorobenzoyloxime-trimethylsilylether derivatives from a VUV-irradiated ice mixture containing ammonia. Double peaks occur because two isomers are formed. (B) Complex aldehydes are absent in samples without ammonia in the initial ice mixture. Peaks marked with an asterisk are interferences caused by the derivatization protocol revealed by running (C) a blank sample of the derivatization reagents.

3. Astrophysical discussion

Six out of the ten molecules in Table 4.1 have been detected in extraterrestrial environments, which include protostellar media but also Solar System objects such as comets and asteroids, including meteorites on the Earth's surface. Formaldehyde is actually ubiquitous, observed in many places of the interstellar medium [3, 27], but also in the gas originating from comets [28] and in meteorites [29]. Acetaldehyde, propanal (propionaldehyde), and propenal (acraldehyde) are detected in the hot molecular core Sagittarius B2 [30, 31], the well-known "Large Molecular Heimat" (LMH) of radio astronomers, as well as, for the first two, in meteorites [29]. Butyraldehyde has been reported in the Murchison mete-

orite as well [29]. Additionally, Cooper et al. [32] identified several sugars, sugar alcohols, and sugar acids, some of them with up to six carbon atoms, in the Murchison and Murray meteorites. Because of the prebiotic importance of sugar-related molecules, the following discussion will focus on glycolaldehyde and glyceraldehyde.

Glycolaldehyde has been detected in emission and/or in absorption by radio astronomy toward the galactic center source, Sagittarius B2(N) [33–37], in the hot molecular core, G31.41+0.31 [38], and in the solar-type protostellar binary, IRAS 16293–2422 [39]. However, glycolaldehyde has never been detected in Solar System objects, for which only an upper limit could be determined in the Hale–Bopp comet [40, 41], as well as in the C/2012 F6 and C/2013 R1 comets [42]. Glyceraldehyde has been searched for in the interstellar medium by Hollis et al. [31] toward Sgr B2 (*N*-LMH), but no lines were detected. Note, however, that aldehydes of higher molecular weights are more difficult and uncertain to search for because of the intrinsic complexity of their rotational spectra associated with the likely presence of several conformers/tautomers.

In the laboratory, only glycolaldehyde has been detected, in the ice phase. An infrared study of glycolaldehyde and its tentative identification in a proton-irradiated CO:CH₃OH 100:1 ice mixture was reported in 2005 by Hudson et al. [43]. In 2009, Öberg et al. [44] reported the formation of acetaldehyde and minor contributions of glycolaldehyde in UV-irradiated CH₃OH-rich ice analogs. Bennett et al. [45] provided an upper limit for the formation rate of glycolaldehyde during ion bombardment of pure CH₃OH ice. IR spectroscopy and mass spectrometry allowed Bennett and Kaiser [46] to establish the formation of glycolaldehyde in CH₃OH:CO ices irradiated with energetic electrons.

The first formation mechanism speculated for glycolaldehyde was an interstellar equivalent of the formose reaction in solid or gas phase based on the polymerization of formaldehyde [35]. Recently, Woods et al. [47, 48] considered several different reaction mechanisms in solid or gas phase, most of them previously suggested in the literature [33, 38, 46, 49, 50], and, from a theoretical point of view, studied their effectiveness at 10 K. To our knowledge, no formation mechanism in extraterrestrial conditions has been proposed for glyceraldehyde or higher-mass aldehydes, although the speculative “interstellar formose reaction” may again apply.

The favored mechanisms, involving CH₃OH, H₂CO, and HCO in the solid state, are applicable to our experimental protocol. Indeed, CH₃OH is a component of the initial ice mixture and a major component of interstellar ices, and H₂CO and HCO are some of the UV photoproducts, detected by in situ IR spectroscopy during the experiment. H₂CO is observed in interstellar ices but not HCO, probably because of its instability as a radical coupled to its absorption range (1,850 cm⁻¹), inaccessible from the ground and with very poor infrared spectroscopic data from the Infrared Space Observatory and Spitzer satellites. Moreover, observations support the idea that glycolaldehyde is sublimated into the gas phase from the grains’ ice mantles [35, and references therein].

An important point to underscore here is that all of these experimental and theoretical studies are made at 10–20 K, mainly in the ice phase. Moreover,

Hudson et al. [43] reported that glycolaldehyde sublimates completely after 10 min at 195 K. In our case, we have searched for the aldehydes, in the organic residues only, at 300 K. Remarkably, the samples still contain aldehydes, including glycolaldehyde, in a free form because our samples were not acid-hydrolyzed before analysis, which is the usual protocol for extracting amino acids. Indeed, the aldehydes should have been evaporated from the substrate well before reaching room temperature.

However, we did not detect the 10 aldehydes in each sample. As underlined above, organic residues made by irradiation of $\text{H}_2\text{O}:\text{}^{13}\text{CH}_3\text{OH}:\text{NH}_3$ contain all of the aldehydes. On the other hand, when NH_3 was not present in the initial ice mixture ($\text{H}_2\text{O}:\text{}^{13}\text{CH}_3\text{OH} = 3:1$), the hydroxyaldehydes glycolaldehyde, lactaldehyde, and glyceraldehyde were not detected, suggesting an essential role of NH_3 for their presence in the residues. This importance of NH_3 was already mentioned in the literature in similar experiments involving the photochemistry of interstellar ice analogs, for the formation of amphiphilic compounds [21] or polyoxymethylene [51, 52] within the organic residue. Although the underlying mechanism(s) in these experiments (including ours) may not be the same, they all point to the crucial role of NH_3 for the formation and the final composition of the organic residues.

Finally, and independently of the exact understanding of the mechanism maintaining the aldehydes up to 300 K, one should remember that ammonia is actually present in protostellar ices [53], and aldehydes may indeed be formed and preserved on the grains' surface, as observed in our laboratory simulations, to later become incorporated in planetesimals and various parent bodies of meteorites.

4. Implications for prebiotic chemistry

Sugars are carbohydrates, components of nucleic acids (DNA, RNA). D-2-Deoxyribofuranose is the sugar subunit present in DNA, but it is currently thought that DNA was not actually the original genetic material and that our present DNA genomic composition evolved from a primordial RNA World state, with D-ribofuranose sugar subunits dictating genetic stereochemistry [54–56]. However, the ultimate origin of the ribose sugar subunit essential to the RNA structure still remains unknown. Recently, experimental evidence was given, revealing that the origin of ribonucleotides could have bypassed the classical chemical synthesis and proceeded from the starting materials, glycolaldehyde and glyceraldehyde, via pentose aminooxazolines [57]. These data suggest that glyceraldehyde and its derivatives were the fundamental asymmetric building blocks, from which enantiomerically enriched oligonucleotide intermediates were synthesized in a prebiotic RNA World.

The detection of glycolaldehyde and glyceraldehyde in our laboratory analogs of extraterrestrial organic residues may thus be of importance from a prebiotic point of view when considering the scenario of an exogenous delivery of organics to the early Earth's surface by small Solar System bodies [58, 59]. Furthermore, as for some meteoritic amino acids [60–62], glyceraldehydes may have been enantiomerically enriched by the same process, but with an opposite excess (D instead of L, as is the case in biological sugars and amino acids, respec-

tively). These excesses could have originated from UV circularly polarized light irradiation, as previously suggested [for a review, see ref. 63] and recently experimentally shown by our group in the case of amino acids formed from precometary ices [64, 65], experiments in which a similar procedure to the one reported in this paper was used.

We emphasize here that such laboratory organic residues, as long as their initial ice mixture is composed of the simple molecules, H_2O , CH_3OH , and NH_3 , contain, in a single residue, a wide variety of organic molecules, including the important molecular bricks linked to the origin of life: amino acids, sugars, lipid precursors, urea, hydantoin, etc. All of these molecules could have thus simultaneously seeded individual comets and asteroids and have then been delivered at the same moment and location on the early Earth.

Finally, the search for glyceraldehyde, for which spectroscopic data exist in the millimeter range [66], should be attempted with the new Atacama Large Millimeter Array (ALMA) in the various astronomical gas-phase environments where glycolaldehyde is already detected. However, the lack of positive detection of the simplest amino acid, glycine, in the gas phase [67] underscores the lack of stability against cosmic or UV irradiation of such complex molecules in this gas phase. This was shown in laboratory experiments [68] for various amino acids in rare gas matrices, proxy for gas-phase media, and glyceraldehyde may well be similarly unstable in the gas phase of molecular clouds. Molecular complexity does need the protection offered by the solid-state environment [69]. In fact, much more significant for prebiotic inference, glycolaldehyde and glyceraldehyde should be searched for in comets and in the Soluble Organic Matter (SOM) of the less possibly aqueously altered carbonaceous chondrites, such as the “Paris” meteorite [70]. These proposed detections must be seen as the next step for supporting a scenario in which chemically evolved cosmic ices played a major role in the feeding of organic materials to the primitive solar nebula.

5. Conclusions

In this paper, we show that the UV irradiation of astrophysically relevant ice mixtures leads to the detection of a new family of molecules, the aldehydes, within the room temperature organic residues. Our results show that the formation of a large range of aldehydes in the solid phase of dense molecular clouds is likely. Among them, two are of particular importance for prebiotic processes: glycolaldehyde and glyceraldehyde are indeed chemical intermediates in ribonucleotide synthesis.

By changing the initial ice composition we observe the apparently essential role of NH_3 in stabilizing light aldehydes within the refractory organic residues. This phenomenon could have been of a fundamental importance to allow these molecules to remain trapped in grains and later be incorporated into small Solar System bodies, from which meteorites found on the Earth originate. The recovery of these aldehydes in comets and in primitive chondrites may constitute a test, bridging our experimental simulations to the SOM of meteorites, linking molecular clouds' ice chemistry to primitive materials in the solar nebula and further playing a significant role in prebiotic chemistry at the surface of telluric planets.

Finally, the reported data will be of importance for the Rosetta mission that landed on a cometary nucleus in November 2014 [71] to perform in situ measurements of cometary ices, particularly with the Cometary Sampling and Composition (COSAC) instrumentation, which contains a GC-MS device specifically designed for the characterization of organic molecules.

Material and Methods

The experimental setup has already been described in detail elsewhere [e.g., ref. 72]. In brief, it consists of a high-vacuum chamber (10^{-7} mbar), in which an infrared (IR) transparent MgF_2 window is cooled down to 78 K. A gas mixture, previously prepared in an independent stainless steel gas line pumped down to about $5 \cdot 10^{-6}$ mbar, is then injected into the chamber where it condenses on the cold MgF_2 substrate to form a thin film of “ices.” These ices are, simultaneously to their deposition, irradiated by UV photons using a H_2 microwave-discharge lamp [73]. In our experiments the ratio of UV photons to deposited molecules is around 1. The entire experiment (deposition rate, ice mixture, and effect of UV photolysis) is monitored by IR spectroscopy.

For this study, we prepared one mixture composed of H_2O , $^{13}\text{CH}_3\text{OH}$, and NH_3 in relative proportions 12:3.5:1, qualitatively representative of interstellar/precometary ices. We also made mixtures without ammonia ($\text{H}_2\text{O}:^{13}\text{CH}_3\text{OH} = 3:1$), to examine the effect of a different ice mixture on the chemical composition of the final residues. Methanol, our unique source of carbon, was labeled with ^{13}C to avoid any confusion with potential biological contamination in the handling and analysis processes of the samples. H_2O (water, liquid) was purified by using a Millipore Direct Q5 system, $^{13}\text{CH}_3\text{OH}$ (methanol, liquid) was purchased from Aldrich (99.9% purity), and NH_3 (ammonia, gas) was purchased from Messer (99.98% purity). The ratios between the components were determined by their partial pressures in the gas line, measured by an absolute pressure gauge (Baratron).

Note that the physicochemical state of the initial sample (temperature and ice composition) is used as a template of preaccretionary ices and not fully representative of interstellar conditions. At 78 K, enhanced diffusion of reactants allows for a faster chemical evolution than at 10 K without significantly affecting the nature of the organic residue, as noted by Muñoz Caro and Schutte [8]. For the initial ice composition, we observe that CO and CO_2 do appear during the photochemical process and are thus part of the icy molecular chemical reservoir.

After a total of 65–91 h of deposition and simultaneous irradiation, the samples were slowly warmed up to room temperature (about 0.15 K min^{-1}), then removed from the vacuum chamber and kept under argon atmosphere in special sample holders for storage and transportation until their analysis at the Université de Nice-Sophia Antipolis, Institut de Chimie de Nice, Nice, France.

Samples were water-extracted from their substrate, derivatized, and then analyzed by 2D gas chromatography–time-of-flight mass spectrometry ($\text{GC} \times \text{GC-TOFMS}$) using a LECO Pegasus IV D system. Supporting information provides the detailed procedure.

References

- [1] Öberg KI, et al. (2011) The Spitzer ice legacy: Ice evolution from cores to protostars. *Astrophys J* 740(2):109.
- [2] Shen CJ, Greenberg JM, Schutte WA, van Dishoeck EF (2004) Cosmic ray induced explosive chemical desorption in dense clouds. *Astron Astrophys* 415(1):203–215.
- [3] Belloche A, Müller HSP, Menten KM, Schilke P, Comito C (2013) Complex organic molecules in the interstellar medium: IRAM 30 m line survey of Sagittarius B2(N) and (M). *Astron Astrophys* 559: A47.
- [4] Garrod RT, Widicus Weaver SL, Herbst E (2008) Complex chemistry in star-forming regions: An expanded gas-grain warm-up chemical model. *Astrophys J* 682(1):283–302.
- [5] Belloche A, Garrod RT, Müller HSP, Menten KM (2014) Detection of a branched alkyl molecule in the interstellar medium: Iso-propyl cyanide. *Science* 345(6204):1584–1587.
- [6] Agarwal VK, et al. (1985) Photochemical reactions in interstellar grains photolysis of CO, NH₃, and H₂O. *Orig Life Evol Biosph* 16(1):21–40.
- [7] Briggs R, et al. (1992) Comet Halley as an aggregate of interstellar dust and further evidence for the photochemical formation of organics in the interstellar medium. *Orig Life Evol Biosph* 22(5):287–307.
- [8] Muñoz Caro GM, Schutte WA (2003) UV-photoprocessing of interstellar ice analogs: New infrared spectroscopic results. *Astron Astrophys* 412:121–132.
- [9] Danger G, et al. (2013) Characterization of laboratory analogs of interstellar/cometary organic residues using very high resolution mass spectrometry. *Geochim Cosmochim Acta* 118:184–201.
- [10] Bernstein MP, Sandford SA, Allamandola LJ, Chang S, Scharberg MA (1995) Organic compounds produced by photolysis of realistic interstellar and cometary ice analogs containing methanol. *Astrophys J* 454:327–344.
- [11] Muñoz Caro GM, Meierhenrich U, Schutte WA, Thiemann WH-P, Greenberg, JM (2004) UV-photoprocessing of interstellar ice analogs: Detection of hexamethylenetetraminebased species. *Astron Astrophys* 413:209–216.
- [12] Vinogradoff V, Duvernay F, Danger G, Theulé P, Chiavassa T (2011) New insight into the formation of hexamethylenetetramine (HMT) in interstellar and cometary ice analogs. *Astron Astrophys* 530:A128.
- [13] Vinogradoff V, et al. (2013) Importance of thermal reactivity for hexamethylenetetramine formation from simulated interstellar ices. *Astron Astrophys* 551:A128.
- [14] Muñoz Caro GM, et al. (2002) Amino acids from ultraviolet irradiation of interstellar ice analogues. *Nature* 416(6879):403–406.
- [15] Bernstein MP, Dworkin JP, Sandford SA, Cooper GW, Allamandola LJ (2002) Racemic amino acids from the ultraviolet photolysis of interstellar ice analogues. *Nature* 416(6879):401–403.
- [16] Elsila JE, Dworkin JP, Bernstein MP, Martin MP, Sandford SA (2007) Mechanisms of amino acid formation in interstellar ice analogs. *Astrophys J* 660(1):911–918.

- [17] Nuevo M, Auger G, Blanot D, d'Hendecourt L (2008) A detailed study of the amino acids produced from the vacuum UV irradiation of interstellar ice analogs. *Orig Life Evol Biosph* 38(1):37–56.
- [18] Meinert C, Filippi J-J, de Marcellus P, Le Sergeant d'Hendecourt L, Meierhenrich UJ (2012) *N*-(2-aminoethyl)glycine and amino acids from interstellar ice analogues. *ChemPlusChem* 77(3):186–191.
- [19] de Marcellus P, Bertrand M, Nuevo M, Westall F, Le Sergeant D'Hendecourt L (2011) Prebiotic significance of extraterrestrial ice photochemistry: Detection of hydantoinin organic residues. *Astrobiology* 11(9):847–854.
- [20] Nuevo M, Bredehöft JH, Meierhenrich UJ, D'Hendecourt L, Thiemann WH-P (2010) Urea, glycolic acid, and glycerol in an organic residue produced by ultraviolet irradiation of interstellar/pre-cometary ice analogs. *Astrobiology* 10(2):245–256.
- [21] Dworkin JP, Deamer DW, Sandford SA, Allamandola LJ (2001) Special feature—Self-assembling amphiphilic molecules: Synthesis in simulated interstellar/precometary ices. *Proc Natl Acad Sci USA* 98(3):815–819.
- [22] Bernstein MP, et al. (1999) UV irradiation of polycyclic aromatic hydrocarbons in ices: Production of alcohols, quinones, and ethers. *Science* 283(5405):1135–1138.
- [23] Nuevo M, Milam SN, Sandford SA (2012) Nucleobases and prebiotic molecules in organic residues produced from the ultraviolet photo-irradiation of pyrimidine in NH₃ and H₂O+NH₃ ices. *Astrobiology* 12(4):295–314.
- [24] Nuevo M, Milam SN, Sandford SA, Elsila JE, Dworkin JP (2009) Formation of uracil from the ultraviolet photo-irradiation of pyrimidine in pure H₂O ices. *Astrobiology* 9(7):683–695.
- [25] Nuevo M, Materese CK, Sandford SA (2014) The photochemistry of pyrimidine in realistic astrophysical ices and the production of nucleobases. *Astrophys J* 793(2):125.
- [26] Ciesla FJ, Sandford SA (2012) Organic synthesis via irradiation and warming of ice grains in the solar nebula. *Science* 336(6080):452–454.
- [27] Snyder LE, Buhl D, Zuckerman B, Palmer P (1969) Microwave detection of interstellar formaldehyde. *Phys Rev Lett* 22(13):679–681.
- [28] Snyder LE, Palmer P, de Pater I (1989) Radio detection of formaldehyde emission from comet Halley. *Astron J* 97(1):246–253.
- [29] Jungclauss GA, Yuen GU, Moore CB, Lawless JG (1976) Evidence for the presence of low molecular weight alcohols and carbonyl compounds in the Murchison meteorite. *Meteoritics* 11(3):231–237.
- [30] Gottlieb CA (1973) *Molecules in the Galactic Environment*, eds Gordon MA, Snyder LE (Wiley-Interscience, New York), pp 181–186.
- [31] Hollis JM, Jewell PR, Lovas FJ, Remijan A, Møllendal H (2004) Green Bank telescope detection of new interstellar aldehydes: Propenal and propanal. *Astrophys J* 610(1):L21–L24.
- [32] Cooper G, et al. (2001) Carbonaceous meteorites as a source of sugar-related organic compounds for the early Earth. *Nature* 414(6866):879–883.

- [33] Halfen DT, Apponi AJ, Woolf N, Polt R, Ziurys LM (2006) A systematic study of glycolaldehyde in Sagittarius B2(N) at 2 and 3 mm: Criteria for detecting large interstellar molecules. *Astrophys J* 639(1):237–245.
- [34] Hollis JM, Jewell PR, Lovas FJ, Remijan A (2004) Green Bank telescope observations of interstellar glycolaldehyde: Low-temperature sugar. *Astrophys J* 613(1):L45–L48.
- [35] Hollis JM, Lovas FJ, Jewell PR (2000) Interstellar glycolaldehyde: The first sugar. *Astrophys J* 540(2):L107–L110.
- [36] Hollis JM, Vogel SN, Snyder LE, Jewell PR, Lovas FJ (2001) The spatial scale of glycolaldehyde in the galactic center. *Astrophys J* 554(1):L81–L85.
- [37] Requena-Torres MA, Martín-Pintado J, Martín S, Morris MR (2008) The galactic center: The largest oxygen-bearing organic molecule repository. *Astrophys J* 672(1):352–360.
- [38] Beltrán MT, Codella C, Viti S, Neri R, Cesaroni R (2009) First detection of glycolaldehyde outside the galactic center. *Astrophys J* 690(2):L93–L96.
- [39] Jørgensen JK, et al. (2012) Detection of the simplest sugar, glycolaldehyde, in a solar type protostar with ALMA. *Astrophys J* 757(1):L4.
- [40] Crovisier J, et al. (2004) The composition of ices in comet C/1995 O1 (Hale-Bopp) from radio spectroscopy. Further results and upper limits on undetected species. *Astron Astrophys* 418:1141–1157.
- [41] Despois D, Biver N, Bockelée-Morvan D, Crovisier J (2005) *Observations of molecules in comets. Astrochemistry: Recent Successes and Current Challenges*, IAU Symposium, eds Lis DC, Blake GA, Herbst E (Cambridge Univ Press, Cambridge), pp 469–478.
- [42] Biver N, et al. (2014) Complex organic molecules in comets C/2012 F6 (Lemmon) and C/2013 R1 (Lovejoy): Detection of ethylene glycol and formamide. *Astron Astrophys* 566:L5.
- [43] Hudson RL, Moore MH, Cook AM (2005) IR characterization and radiation chemistry of glycolaldehyde and ethylene glycol ices. *Adv Space Res* 36(2):184–189.
- [44] Öberg KI, Garrod RT, van Dishoeck EF, Linnartz H (2009) Formation rates of complex organics in UV irradiated CH₃OH-rich ices. I. Experiments. *Astron Astrophys* 504(3):891–913.
- [45] Bennett CJ, Chen S-H, Sun B-J, Chang AHH, Kaiser RI (2007) Mechanistical studies on the irradiation of methanol in extraterrestrial ices. *Astrophys J* 660(2):1588–1608. Bennett CJ, Kaiser RI (2007) On the formation of glycolaldehyde (HCOCH₂OH) and methyl formate (HCOOCH₃) in interstellar ice analogs. *Astrophys J* 661(2):899–909.
- [47] Woods PM, et al. (2012) On the formation of glycolaldehyde in dense molecular cores. *Astrophys J* 750(1):19.
- [48] Woods PM, et al. (2013) Glycolaldehyde formation via the dimerization of the formyl radical. *Astrophys J* 777(2):90.
- [49] Sorrell WH (2001) Origin of amino acids and organic sugars in interstellar clouds. *Astrophys J* 555(2):L129–L132.

- [50] Charnley SB, Rodgers SD (2005) *Pathways to molecular complexity. Astrochemistry: Recent Successes and Current Challenges*, IAU Symposium, eds Lis DC, Blake GA, Herbst E (Cambridge Univ Press, Cambridge), pp 237–246.
- [51] Schutte WA, Allamandola LJ, Sandford SA (1993) An experimental study of the organic molecules produced in cometary and interstellar ice analogs by thermal formaldehyde reactions. *Icarus* 104(1):118–137.
- [52] Duvernay F, Danger G, Theulé P, Chiavassa T (2014) Formaldehyde chemistry in cometary ices: On the prospective detection of $\text{NH}_2\text{CH}_2\text{OH}$, HOCH_2OH , and POM by the on-board ROSINA instrument of the Rosetta mission. *Astrophys J* 791(2):75.
- [53] Bottinelli S, et al. (2010) The c2d Spitzer spectroscopic survey of ices around low-mass young stellar objects. IV. NH_3 and CH_3OH . *Astrophys J* 718(3):1100–1117.
- [54] Woese C (1967) *The Genetic Code: the Molecular basis for Genetic Expression*, ed. Harper R (Harper & Row, New York), pp 179–195.
- [55] Crick FH (1968) The origin of the genetic code. *J Mol Biol* 38(3):367–379.
- [56] Orgel LA (1968) Evolution of the genetic apparatus. *J Mol Biol* 38(3):381–393.
- [57] Powner MW, Gerland B, Sutherland JD (2009) Synthesis of activated pyrimidine ribonucleotides in prebiotically plausible conditions. *Nature* 459(7244):239–242.
- [58] Oró J (1961) Comets and the formation of biochemical compounds on the primitive Earth. *Nature* 190(4774):389–390.
- [59] Chyba C, Sagan C (1992) Endogenous production, exogenous delivery and impactshoc synthesis of organic molecules: An inventory for the origins of life. *Nature* 355(6356):125–132.
- [60] Cronin JR, Pizzarello S (1997) Enantiomeric excesses in meteoritic amino acids. *Science* 275(5302):951–955.
- [61] Glavin DP, Dworkin JP (2009) Enrichment in L-isovaline by aqueous alteration on CI and CM meteorite parent bodies. *Proc Natl Acad Sci USA* 106(14):5487–5492.
- [62] Glavin DP, et al. (2012) Unusual nonterrestrial L-proteinogenic amino acid excesses in the Tagish Lake meteorite. *Meteorit Planet Sci* 47(8):1347–1364.
- [63] Meinert C, et al. (2011) Photochirogenesis: Photochemical models on the absolute asymmetric formation of amino acids in interstellar space. *Phys Life Rev* 8(3):307–330.
- [64] de Marcellus P, et al. (2011) Non-racemic amino acid production by ultraviolet irradiation of achiral interstellar ice analogs with circularly polarized light. *Astrophys J Letters* 727(2):L27.
- [65] Modica P, et al. (2014) Enantiomeric excesses induced in amino acids by ultraviolet circularly polarized light irradiation of extraterrestrial ice analogs: A possible source of asymmetry for prebiotic chemistry. *Astrophys J* 788(1):79–89.
- [66] Lovas FJ, Suenram RD, Plusquellic DF, Møllendal H (2003) The microwave spectrum of the C 3 sugars: Glyceraldehyde and 1,3-dihydroxy-2-propanone and the dehydration product 2-hydroxy-2-propen-1-al. *J Mol Spectrosc* 222(2):263–272.

- [67] Snyder LE, et al. (2005) A rigorous attempt to verify interstellar glycine. *Astrophys J* 619(2):914–930.
- [68] Ehrenfreund P, Bernstein MP, Dworkin JP, Sandford SA, Allamandola LJ (2001) The photostability of amino acids in space. *Astrophys J* 550(1):L95–L99.
- [69] Le Sergeant d’Hendecourt L (2011) Molecular complexity in astrophysical environments: From astrochemistry to “astrobiology“? *Chemistry in Astrophysical Media, Astr OHP 2010, EPJ Web Conf*, 18, 6001.
- [70] Hewins RH, et al. (2014) The Paris meteorite, the least altered CM chondrite so far. *Geochim Cosmochim Acta* 124:190–222.
- [71] Meierhenrich UJ (2015) *Comets and their Origin* (Wiley-VCH, Weinheim, Germany).
- [72] Nuevo M, et al. (2007) Enantiomeric separation of complex organic molecules produced from irradiation of interstellar/circumstellar ice analogs. *Adv Space Res* 39(3):400–404.
- [73] Chen Y-J, et al. (2014) Vacuum ultraviolet emission spectrum measurement of a microwave-discharge hydrogen-flow lamp in several configurations: Application to photodesorption of CO ice. *Astrophys J* 781(1):15.

Supporting information

Extraction, Derivatization, and GC×GC Analysis

Sample-handling glassware was wrapped in aluminum foil and heated at 500 °C for 3 h before use. Eppendorf tips were sterile, and the water used for extraction, standard solutions, reagent solutions, and blanks had been prepared by a Millipore Super-Q water filter system (4 ppb total organic carbon). The organic residues were water-extracted from their MgF₂ windows and transferred into conical reaction vials. The samples were derivatized in a two-step derivatization procedure that begins with the initial formation of pentafluorobenzyl oximes of aldehyde functional groups, followed by trimethylsilylation of protic groups to enhance the resolution of hydroxyaldehydes on the secondary polar column in our gas chromatographic analysis. The first reaction used freshly prepared aqueous *O*-(2,3,4,5,6-pentafluorobenzyl) hydroxylamine (PFBHA) to selectively transform aldehydes into the corresponding PFB oximes at room temperature [1, 2]. After 45 min, concentrated sulfuric acid was added to each vial to prevent excess of PFBHA from being extracted into the organic solvent together with the PFBHA reaction products. The oxime derivatives were then extracted twice with dichloromethane and pooled into new conical vials. The dichloromethane extracts were evaporated to dryness using a gentle stream of nitrogen and then silylated with 50 μL BSTFA [*N,O*-bis-(trimethylsilyl)trifluoroacetamide] for 1.5 h at 80 °C. The mixtures were cooled to room temperature and transferred into GC vials prior their analyses by 2D gas chromatography–time-of-flight mass spectrometry (GC × GC–TOFMS) using a LECO Pegasus IV D system. Procedural blanks were run in sequence to each sample to monitor significant background interferences.

The GC×GC column set consisted of a Chirasil-Dex CB primary column (24.85 m × 0.25 mm internal diameter, 0.25-μm film thickness) modulator coupled to a DB-Wax secondary column (1.42 m × 0.1 mm ID, 0.1-μm film thickness). Helium was used as carrier gas at a constant flow of \bar{u} = 1 mL min⁻¹. Sample volumes of 1 μL were injected in the splitless mode at an injector temperature of 230 °C. The primary oven was operated as follows: 40 °C for 1 min, temperature increase of 10 °C min⁻¹ to 80 °C and held for 2 min, followed by 2 °C min⁻¹ to 180 °C and an isothermal hold at 180 °C for 20 min. The secondary oven used the same temperature program with a constant temperature offset of 30 °C. A modulation period of 5 s was applied. The TOFMS was operated at a storage rate of 150 Hz with a 25–450 atomic mass unit (amu) mass range. Data were acquired and processed with LECO Corp ChromaTOF software. Compound identification was performed by comparison with the chromatographic retention in both dimensions and mass spectra of authentic standards. The mass spectra of unknown aldehydes were interpreted based on their fragmentation patterns. Compounds were quantified using the characteristic mass fragment m/z 181, corresponding to the C₆F₅CH₂⁺ (or substituted-tropylium) ion.

References

- [1] Kobayashi K, Tanaka M, Kawai S (1980) Gas chromatographic determination of low-molecular-weight carbonyl compounds in aqueous solution as their *O*-(2,3,4,5,6-pentafluorobenzyl) oximes. *J Chromatogr A* 187(2):413–417.
- [2] Glaze WH, Koga M, Cancilla D (1989) Ozonation by-products 2 improvements of an aqueous phase derivatization method for the detection of formaldehyde and other carbonyl compounds formed by the ozonation of drinking water. *Environ Sci Technol* 23(7):838–847.

Glyceraldehyde and glycolaldehyde, detected in the previous study, are both products of formaldehyde condensation, also known as the formose reaction. Their identification in interstellar ices gave a hint to the possible presence of other products of the formose reaction within the solid-state sample. The following study is focused on the analysis of similar interstellar ice analogues with the analytical protocol developed for the sugar detection.

This time we were able to detect ribose as well as other related aldopentoses within interstellar ices and therefore could infer that chemical sub-units of nucleotides can be formed in the precisely described physico-chemical conditions of space. Their mechanism of formation and their relevance in prebiotic evolution is discussed in details in the following section.



Article 5. Ribose and related sugars from ultraviolet irradiation of interstellar ice analogs

Cornelia Meinert, Iuliia Myrgorodska, Pierre de Marcellus, Thomas Buhse, Laurent Nahon, Søren V. Hoffmann, Louis Le Sergeant d'Hendecourt, and Uwe J. Meierhenrich

Abstract

Ribose is the central molecular subunit in RNA, but the prebiotic origin of ribose remains unknown. We observed the formation of substantial quantities of ribose and a diversity of structurally related sugar molecules such as arabinose, xylose, and lyxose in the room-temperature organic residues of photo-processed interstellar ice analogs initially composed of H₂O, CH₃OH, and NH₃. Our results suggest that the generation of numerous sugar molecules, including the aldopentose ribose, may be possible from photochemical and thermal treatment of cosmic ices in the late stages of the solar nebula. Our detection of ribose provides plausible insights into the chemical processes that the generation of numerous sugar molecules, including the aldopentose ribose, may be possible from photochemical and thermal treatment of cosmic ices in the late stages of the solar nebula. Our detection of ribose provides plausible insights into the chemical processes that could lead to formation of biologically relevant molecules in suitable planetary environments.

Published article: *Science* (2016), 352: 208–212.

DNA is the genetic source code for all known living organisms. It is currently thought that DNA evolved from a primordial ribonucleic acid RNA world state (1, 2), in which ribose chemically binds and orientates the complementary purine and pyrimidine nucleobases for efficient base pairing. Ribose thereby forms the essential part of the RNA backbone. However, ribose is difficult to form, and the source of the ribose subunits in the sugars that constitute the key stereodictating elements in nucleic acid structure remained unknown (3, 4). We describe here the identification of precursor molecules, including ribose, in simulated precometary ices using the sensitive two-dimensional gas chromatography time-of-flight mass spectrometry (GC \times GC-TOFMS) technique.

Our astrophysical scenario involves the simulation of the photo- and thermo-chemistry of precometary ices. It is based on the assumption that planetesimals (including asteroids, comets, and the parent bodies of meteorites) were formed in the solar nebula from the aggregation of icy grains already present and processed at the late molecular cloud stages. This also took place within the protoplanetary disk phase, owing to vertical/radial mixing of the protostellar materials (5). As a model, these dust particles are composed of silicate (or carbon) grains surrounded by icy mantles containing H₂O, CH₃OH, NH₃, and other volatile species (6). In this environment, dust particles and icy mantles are expected to be subjected to ultraviolet photons and cosmic-ray irradiation, leading to a complex chemistry in the condensed phase. We empirically simulated this process in the laboratory at low temperature ($T = 78$ K) and low pressure ($p = 10^{-7}$ mbar). Volatile molecules H₂O, ¹³CH₃OH, and NH₃ in a 10:3.5:1 ratio were condensed on the cooled surface, while being irradiated with ultraviolet photons, and then warmed up to room temperature, leading to the formation of an organic residue (7). ¹³C isotopic labeling of the methanol allowed us to distinguish between the reaction products and potential contamination during manipulation of the sample and through the analytical procedure. A precise description of the experimental setup is provided in the supplementary materials.

The samples were extracted with water, derivatized, and submitted to GC \times GC-TOFMS analysis (8). The analytical multidimensional separation apparatus consisted of a 0.25-mm capillary column with a β -cyclodextrin stationary phase in the first dimension and a polyethylene glycol capillary column of 100 mm inner diameter in the second dimension. A cryogenic modulator connected both capillary columns (7). A reflectron time-of-flight (TOF) mass spectrometer has been used for recording retention times and mass spectra. The GC \times GC-TOFMS analysis in combination with our derivatization protocol (7) provided the simultaneous resolution and identification of the sugar and sugar-related compounds, which has not been possible with classical chromatographic devices because of coelution of analytes.

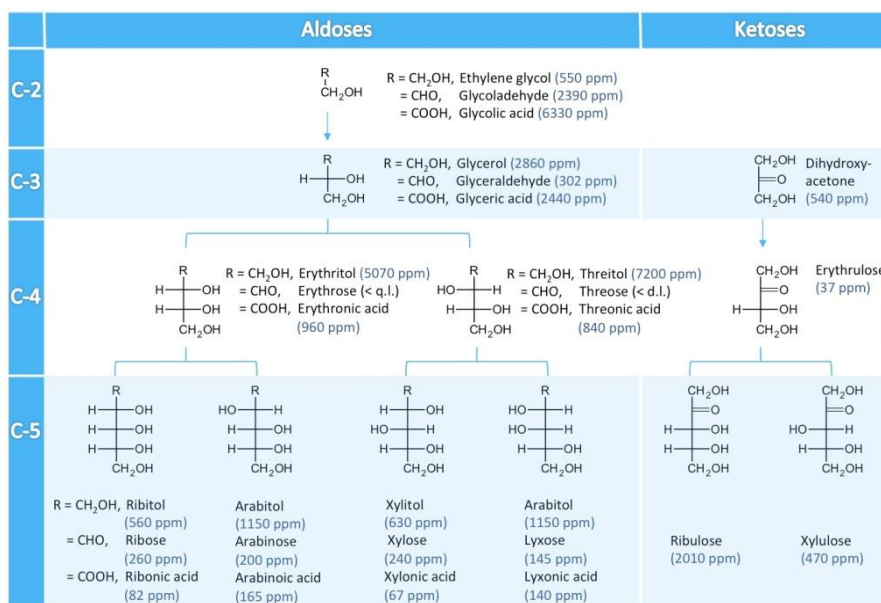


Figure 5.1. Aldoses and ketoses as identified in a sample generated under simulated precometary conditions. The structures of sugar alcohols, monosaccharides, and saccharinic acids are indicated along with the amount of the identified analyte in the simulated ice sample. Identified C-6 analytes are not included. The Fischer projections indicate the D-enantiomer form only. ppm, parts per million by mass; q.l., quantification limit; d.l., detection limit.

We detected aldoses and ketoses in these simulated interstellar ice analogs as schematically represented by the Fischer projections in Fig. 5.1. The monosaccharides ribose, arabinose, xylose, and lyxose belong to the aldopentoses; ribulose and xylulose are ketopentoses. The aldopentoses were resolved and identified in both α - and β -pyranose form (Fig. 5.2), and the ketopentoses show ketol form. Besides aldopentoses and ketopentoses, we identified the ketotetrose erythrulose. Mass spectra of the analytes and the interpretation of characteristic fragmentation pathways leading to unambiguous identification are provided (supplementary text), along with details on the quantification of the analytes.

The corresponding saccharinic acids (sugar acids) were identified. We also detected the corresponding sugar alcohols, along with threitol, erythritol, mannitol, and sorbitol. We further found the related series of hydroxycarboxylic acids.

A systematic representation of the identified molecular species is given in Table 5.1, which indicates the analytes' retention times in the first and second chromatographic dimension and mass spectra of analyzed sample and standard. The analytes detected in the organic residue were found to contain ¹³C isotopes, whereas the standard samples used for identification were made of the natural isotopic composition dominated by ¹²C (figs. S5.3 to S5.5). We therefore exclude experimental contamination and conclude that all described analytes were formed by

the H_2O , $^{13}\text{CH}_3\text{OH}$, and NH_3 volatile reactants that were deposited under simulated interstellar precometary conditions (fig. S5.2).

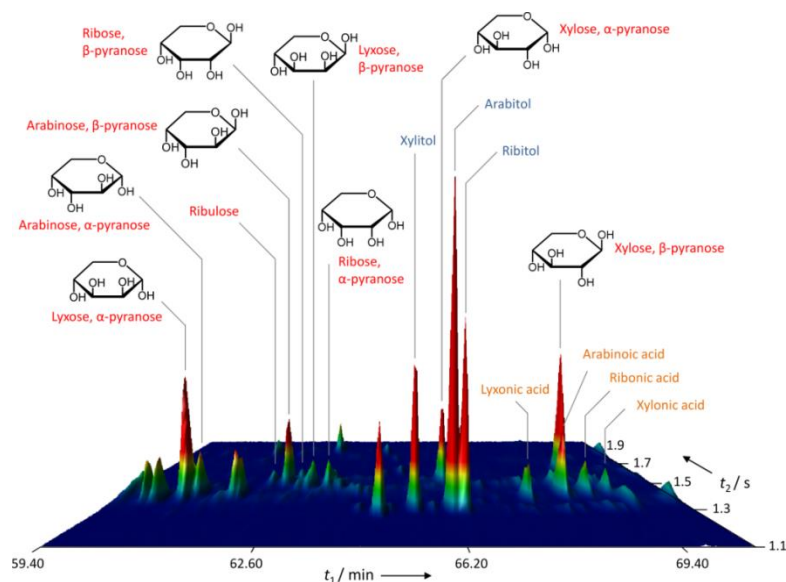


Figure 5.2. Multidimensional gas chromatogram showing ribose and other monosaccharides in the organic residue from an evolved precometary ice analog. See also fig. S5.1 (7). The atomic mass units 206 and 294 were selected for the multidimensional chromatographic representation. D- and L-enantiomers of the monosaccharides were not resolved.

The molecular complexity in the evolved ices reported here suggests a far larger similarity to meteoritic organic materials than previously assumed. Thus, molecular evolution of meteoritic organic species available for planetary environments could have benefited from accretion of protostellar material. The sugars, dicarboxylic acids, C-4 hydroxycarboxylic acids, and branched-chain molecules described here have not previously been identified, although aldehydes, including glycolaldehyde and glyceraldehyde, have been found in similar laboratory residues (9), along with lower hydroxycarboxylic acids (10). Sugar-related alcohols and acids have previously been detected in the Murchison meteorite (11). Glycolaldehyde has been found sublimating from the nucleus of comet Lovejoy (C/2014 Q2) (12) and by means of millimeter wave rotational transitions in emission toward the Galactic center source Sagittarius B2(N) (13). Glycolaldehyde was recently also detected in solar-type protostars (14). Moreover, glycolaldehyde and ethylene glycol were characterized by means of infrared spectroscopy in radiation chemistry of laboratory ices (15).

Table 5.1. Identified compounds in H₂O: ¹³CH₃OH: NH₃ (10:3.5:1) at 78 K.

#C ^[a]	Compound	R _{t1} ^[b] [min]	R _{t2} ^[c] [sec]	MS-fragmentation / ¹³ C sample		MS-fragmentation / ¹² C standard	
				[M ⁺]	Other important ions, <i>m/z</i>	[M ⁺]	Other important ions, <i>m/z</i>
Monosaccharides							
3	L-Glyceraldehyde	33.48	1.78	237	207, 206, 191, 147, 119, 104, 73, 29	234	205, 204, 189, 147, 117, 103, 73, 28
	D-Glyceraldehyde	34.03	1.74				
	Dihydroxyacetone	43.37	1.88	237	222, 191, 147, 104, 73	234	219, 189, 147, 103, 73
4	D,L-Erythrose, α-furanose	49.46	1.52	340	235, 221, 220, 206, 192, 147, 104, 73	336	231, 218, 217, 203, 191, 147, 103, 73
	D,L-Erythrulose	54.51	1.82	340	309, 235, 207, 191, 147, 119, 104, 73	336	306, 231, 205, 189, 147, 117, 103, 73
5	D,L-Lyxose, α-pyranose	60.90	1.41	443	<i>see Ribose</i>		
	D,L-Arabinose, α-pyranose	61.15	1.42		<i>see Ribose</i>		
	D,L-Ribulose, ketol	62.50	1.46	443	339, 310, 249, 220, 192, 147, 132, 104, 73	438	335, 307, 245, 218, 191, 147, 129, 103, 73
	D,L-Arabinose, β-pyranose	62.85	1.51		<i>see Ribose</i>		
	D,L-Ribose, β-pyranose	63.15	1.45	443	308, 294, 220, 206, 192, 147, 119, 104, 103, 73	438	305, 291, 217, 204, 191, 147, 117, 103, 101, 73
	D,L-Lyxose, β-pyranose	63.40	1.48	443	<i>see Ribose</i>		
	D,L-Ribose, α-pyranose	63.70	1.46	443	308, 294, 220, 206, 192, 147, 119, 103, 73	438	305, 291, 217, 204, 191, 147, 117, 103, 101, 73
	D,L-Xylulose, ketol ^[d,e]	64.30	1.54	443	339, 310, 249, 220, 192, 147, 132, 104, 73	438	335, 307, 245, 218, 191, 147, 129, 103, 73
	D,L-Xylose, α-pyranose	66.20	1.52	443	<i>see Ribose</i>		
	D,L-Xylose, β-pyranose	69.04	1.61	443	<i>see Ribose</i>		

102 CHAPTER III: Prebiotic chemistry of interstellar ice analogues

#C ^[a]	Compound	R ₁ ^[b] [min]	R ₂ ^[c] [sec]	MS-fragmentation / ¹³ C sample		MS-fragmentation / ¹² C standard	
				[M ⁺]	Other important ions, m/z	[M ⁺]	Other important ions, m/z
Sugar acids (saccharinic acids)							
3	D,L-Glyceric acid	44.42	1.64	325	310, 294 ^[f] , 220, 207, 191, 177, 147, 119, 103, 73	322	307, 292 ^[f] , 217, 205, 189, 175, 147, 117, 102, 73
4	D,L-Erythronic acid	56.96	1.47	428	413, 382, 294 ^[f] , 222, 207, 147, 104, 73	424	409, 379, 292 ^[f] , 220, 205, 147, 103, 73
	D,L-Threonic acid	58.10	1.49	428	413, 382, 294 ^[f] , 222, 207, 147, 104, 73	424	409, 379, 292 ^[f] , 220, 205, 147, 103, 73
5	D,L-Lyxonic acid ^[e]	67.79	1.39	531	<i>see Ribonic acid</i>		
	D,L-Arabinic acid ^[e]	68.59	1.41	531	<i>see Ribonic acid</i>		
	D,L-Ribonic acid ^[e]	69.09	1.41	531	337, 310, 294 ^[f] , 279, 220, 207, 191, 147, 119, 104, 73	526	333, 307, 292 ^[f] , 277, 217, 205, 189, 147, 117, 103, 73
	D,L-Xylonic acid ^[e]	69.54	1.42	531	<i>see Ribonic acid</i>		
Sugar alcohols							
3	Glycerol	40.58	1.43	311	296, 221, 207, 147, 119, 104, 73	308	293, 218, 205, 147, 117, 103, 73
4	D,L-Threitol	54.56	1.38	414	324, 310, 295, 220, 207, 191, 147, 119, 104, 73	410	320, 307, 293, 217, 205, 189, 147, 117, 103, 73
	Erythritol	54.86	1.38	414	324, 310, 295, 220, 207, 191, 147, 119, 104, 73	410	320, 307, 293, 217, 205, 189, 147, 117, 103, 73
5	D,L-Xylitol	65.54	1.33	517	337, 323, 310, 220, 207, 191, 147, 119, 104, 73	512	332, 319, 307, 217, 205, 189, 147, 117, 103, 73
	D,L-Arabitol	66.29	1.32	517	337, 323, 310, 220, 207, 191, 147, 119, 104, 73	512	332, 319, 307, 217, 205, 189, 147, 117, 103, 73
	D,L-Ribitol (Adonitol) ^[d,e]	66.49	1.31	517	337, 323, 310, 220, 207, 191, 147, 119, 104, 73	512	332, 319, 307, 217, 205, 189, 147, 117, 103, 73

#C ^[a]	Compound	<i>R</i> ₁ ^[b] [min]	<i>R</i> ₂ ^[c] [sec]	MS-fragmentation / ¹³ C sample		MS-fragmentation / ¹² C standard	
				[M ⁺]	Other important ions, <i>m/z</i>	[M ⁺]	Other important ions, <i>m/z</i>
<i>Sugar alcohols (continued)</i>							
6	D,L-Mannitol	82.54 ^[g]	1.63	620	426, 323, 310, 220, 207, 147, 104, 73	614	421, 319, 307, 217, 205, 147, 103, 73
	D,L-Sorbitol	83.24 ^[g]	1.65	620	426, 323, 310, 220, 207, 147, 104, 73	614	421, 319, 307, 217, 205, 147, 103, 73
	D,L-Allitol ^[d]	83.49 ^[g]	1.67	620	<i>see Mannitol</i>		
	D,L-Dulcitol (Galactitol)	83.69 ^[g]	1.67	620	426, 323, 310, 220, 207, 147, 104, 73	614	421, 319, 307, 217, 205, 147, 103, 73
	D,L-Talitol (Altritol) ^[d]	84.04 ^[g]	1.67	620	<i>see Mannitol</i>		
<i>Branched-chain sugar acids & polyols</i>							
4	2-Methylglycerol ^[e]	40.03	1.31	326	311, 235, 222, 147, 104, 73	322	307, 232, 219, 147, 103, 73
	2-Methylglyceric acid ^[d]	43.02	1.48	340	325, 309 ^[f] , 296, 236, 222, 206, 191, 147, 104, 73	336	321, 306 ^[f] , 293, 233, 219, 203, 189, 147, 103, 73
	2-Hydroxymethyl glycerol ^[d]	52.81	1.33	414	310, 220, 191, 147, 132, 104, 73		
5	2-Hydroxymethyl tetritol ^[d]	64.90	1.29	517	323, 310, 220, 147, 104, 73		
<i>Hydroxycarboxylic acids</i>							
2	Glycolic acid	31.39	1.69	222	207, 178 ^[f] , 162, 147, 104, 73	220	205, 177 ^[f] , 161, 147, 103, 73
3	D-Lactic acid	24.94	1.66	237	222, 193, 147, 119, 103, 73	234	219, 191, 147, 117, 101, 73
	L-Lactic acid	25.24	1.66	237	222, 193, 147, 119, 103, 73	234	222, 191, 147, 117, 101, 73
	3-Hydroxypropanoic acid	36.63	1.60	237	222, 178, 147, 118, 103, 73	234	219, 177, 147, 116, 101, 73
4	2-Hydroxyisobutyric acid	24.00	1.52	252	237, 208 ^[f] , 147, 134, 73	248	233, 205 ^[f] , 147, 131, 73
	(<i>R</i>)-2-Hydroxy-butyric acid	29.54	1.65	252	237, 208 ^[f] , 147, 134, 73	248	233, 205 ^[f] , 147, 131, 73

104 CHAPTER III: Prebiotic chemistry of interstellar ice analogues

#C ^[a]	Compound	R_{t1} ^[b] [min]	R_{t2} ^[c] [sec]	MS-fragmentation / ¹³ C sample		MS-fragmentation / ¹² C standard		
				[M ⁺]	Other important ions, m/z	[M ⁺]	Other important ions, m/z	
	(S)-2-Hydroxy-butyric acid	29.79	1.63	252	237, 208 ^[f] , 147, 134, 73	248	233, 205 ^[f] , 147, 131, 73	
	3-Hydroxy-isobutyric acid ^[e]	34.73	1.58	252	237, 221, 208, 178, 162, 147, 104, 73	248	233, 218, 205, 177, 158, 147, 103, 73	
	(R)-3-Hydroxy-butyric acid	35.63	1.57	252	237, 206 ^[f] , 193, 147, 119, 73	248	233, 204 ^[f] , 191, 147, 117, 73	
	(S)-3-Hydroxy-butyric acid	36.13	1.55					
	4-Hydroxybutyric acid	42.52	1.62	252	237, 206, 147, 119, 73	248	233, 204, 147, 117, 73	
	D,L-Malic acid	55.81	1.77	354	339, 310, 249, 236, 191, 147, 119, 73	350	335, 307, 245, 233, 189, 147, 117, 73	
	Dicarboxylic acids							
4	Succinic acid	48.37	2.05	266	251, 176, 147, 132, 73	262	247, 172, 147, 129, 73	
	Fumaric acid	51.76	1.96	264	249, 220, 147, 118, 73	260	245, 217, 147, 115, 73	
	Miscellaneous							
2	Ethylene glycol	16.00 ^[h]	1.38	208	193, 147, 104, 73	206	191, 147, 103, 73	
	Oxamic acid ^[d,e]	37.68	1.61	235	220, 191, 147, 117, 73	233	218, 190, 147, 116, 73	
	Glycolaldehyde ^[i]	36.18	2.16		304, 288, 215, 191, 147, 73		302, 286, 214, 189, 147, 73	
		36.48	2.12		304, 288, 215, 191, 147, 73		302, 286, 214, 189, 147, 73	
3	D,L-1,3-Propanediol	27.69	1.36	223	208, 178, 147, 133, 73	220	205, 177, 147, 130, 73	

^[a] Quantity of carbon atoms. ^[b] GC × GC retention time 1st dimension and ^[c] 2nd dimension. ^[d] Identification based on literature data on the formose reaction, former ice simulation experiments, as well as chromatographic retention properties of sugar and sugar-related molecules (see SI). ^[e] Identification based on NIST mass spectral database and retention time prediction. ^[f] McLafferty and McLafferty-type (ester migration) rearrangement. ^[g] Retention time shift by +3 min due to changes in column flow. ^[h] Temperature program of first dimension: 40 °C (1'), 10 °C min⁻¹, 80 °C (10'), 2 °C min⁻¹, 180 °C (5'). ^[i] Stereoisomers of dimeric or anhydrol form.

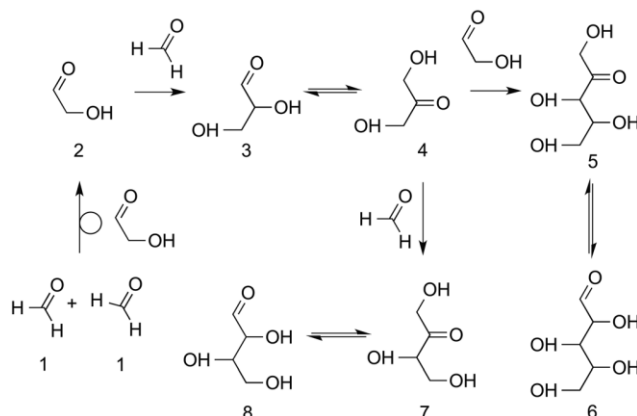


Figure 5.3. The formose reaction. Formaldehyde 1 condenses under autocatalytic reaction kinetics to form glycolaldehyde 2, which undergoes an aldol reaction by forming glyceraldehydes 3. Dihydroxyacetone 4 is formed by aldoseketose isomerization of 3 and reacts with 2, forming pentulose 5, which isomerizes to an aldopentose 6 such as ribose. In an alternative pathway, dihydroxyacetone 4 reacts with 1, producing ketotetrose 7 and aldotetrose 8 (18).

The diversity of sugar molecules formed from H_2O , $^{13}\text{CH}_3\text{OH}$, and NH_3 under interstellar conditions can be understood in the framework of a photochemically initiated formose-type reaction. Reactant and intermediate species of the formose reaction (16–18) are formaldehyde and glycolaldehyde that undergo aldol condensations to produce hydroxyl aldehydes and hydroxyl ketones with linear and branched structures (Fig. 5.3 and fig. S5.6). As in our case, sugar alcohols and sugar acids typically accompany the sugars formed by the formose reaction. We further detected the branched chain molecules hydroxymethylglycerol and hydroxymethyltetritol, which indicate a formose type reaction mechanism (19, 20). The classical formose reaction is known to require a divalent metal catalyst such as Ca^{2+} , Pb^{2+} , or Tl^{2+} for the stabilizing effect of chelating ions on enediols (18), a condition not needed in the present work. Final steps of the formose-type reaction might have occurred above 78 K during temperature increase of the sample to room temperature, in which reactants diffuse and react within the labile and sublimating ice matrix.

The parts-per-million values of the photoproducts described in Fig. 5.1 sum up to greater than 35,000 (table S5.1), which corresponds to a value $>3.5\%$ (by mass) (7). Thus, sugars, sugar alcohols, and sugar acids are present notably above trace or ultratrace quantities and are therefore considered major molecular constituents of the condensed interstellar organics. The relative yield of ribose, which is known to be very small in the classical formose reaction, resulted in higher values during our cold scenario. We regard this result as central for an implication for prebiotic chemistry because it shows that even at this initial level of molecular “simplicity,” we observe an autocatalytic reaction. This, in turn, may be interpreted as a link between astrochemistry and astrobiology. The acquisition of kinetic data and enantioseparation will be necessary to rationalize the reaction

mechanism of the sugar formation and to search for asymmetric autocatalytic effects.

The identification of ribose in the organic residues obtained from evolved precometary ices does not necessarily indicate the prebiotic evolutionary pathway. Besides ribose, we identified threose in its oxidized and reduced form, threonic acid and threitol, respectively. Threose is the molecular component of threose nucleic acid (TNA), a nucleic acid analog discussed to have preceded RNA (21). We further detected glycol and glycerol, which provide the molecular backbones of glycol and glycerol nucleic acids (GNAs) (22, 23). The molecular building blocks of peptide nucleic acids (PNAs), *N*-(2-aminoethyl) glycine and 2,4-diaminobutanoic acid, were previously detected in organic residues from similar ice experiments (24). In this experimental frame, precursors of both proteins (amino acids) (25) and genetic material (sugars and their derivatives) are produced in large amounts so that if delivered from meteorites in the Earth's environment, their co-evolution may be considered one of the standing issues in prebiotic chemistry (26).

Our samples are fully soluble in water (as well as in other polar solvents), a condition that is essential for any further prebiotic activity. In aqueous solution, sugar molecules, including ribose, develop chemical equilibria between the open form (Fig. 5.1), the cyclic furanose and pyranose forms (Fig. 5.2), and in between the various constitutional isomers such as ribose and arabinose. Our experiments demonstrate plausible physical and chemical environmental conditions that allow for abiotic ribose synthesis.

Our findings support the identification of organic molecules in cometary samples taken in situ by the Philae Lander (27, 28) part of the cometary Rosetta mission (29). Our analytical results demonstrate the usefulness of multidimensional chromatographic techniques for the chemical analyses of extraterrestrial samples, which are often available only in small quantities, in which sugar molecules including ribose may be present.

References

1. R. F. Gesteland, T. R. Cech, J. F. Atkins, *The RNA World* (Cold Spring Harbor Laboratory Press, 2005).
2. C. Woese, *The Genetic Code* (Harper & Row, 1967), pp. 179–195.
3. F. H. C. Crick, *J. Mol. Biol.* **38**, 367–379 (1968).
4. L. E. Orgel, *J. Mol. Biol.* **38**, 381–393 (1968).
5. F. J. Ciesla, S. A. Sandford, *Science* **336**, 452–454 (2012).
6. J. M. Greenberg, in *The Chemistry of Life's Origins*, J. M. Greenberg, Ed. (Kluwer, Dordrecht, 1993) pp. 195–207.
7. Materials and methods are available as supplementary materials on Science Online.
8. C. Meinert, U. J. Meierhenrich, *Angew. Chem. Int. Ed. Engl.* **51**, 10460–10470 (2012).
9. P. de Marcellus et al., *Proc. Natl. Acad. Sci. U.S.A.* **112**, 965–970 (2015).
10. V. K. Agarwal et al., *Orig. Life Evol. Biosph.* **16**, 21–40 (1985).
11. G. Cooper et al., *Nature* **414**, 879–883 (2001).
12. N. Biver et al., *Sci. Adv.* **1**, e1500863 (2015).
13. J. M. Hollis, F. J. Lovas, P. R. Jewell, *Astrophys. J.* **540**, L107–L110 (2000).
14. J. K. Jørgensen et al., *Astrophys. J.* **757** (L4), 1–6 (2012).
15. R. L. Hudson, M. H. Moore, A. M. Cook, *Adv. Space Res.* **36**, 184–189 (2005).
16. M. A. Butlerow, *C. R. Séances Acad. Sci.* **53**, 145–147 (1861).
17. M. A. Butlerow, *Ann. Chem.* **120**, 295–298 (1861).
18. R. Breslow, *Tetrahedron Lett.* **21**, 22–26 (1959).
19. Y. Shigemasa, Y. Matsuda, C. Sakazawa, T. Matsuura, *Bull. Chem. Soc. Jpn.* **50**, 222–226 (1977).
20. T. Zweckmair et al., *J. Chromatogr. Sci.* **52**, 169–175 (2014).
21. H. Yu, S. Zhang, J. C. Chaput, *Nat. Chem.* **4**, 183–187 (2012).
22. L. Zhang, A. Peritz, E. Meggers, *J. Am. Chem. Soc.* **127**, 4174–4175 (2005).
23. C.-H. Tsai, J. Chen, J. W. Szostak, *Proc. Natl. Acad. Sci. U.S.A.* **104**, 14598–14603 (2007).
24. C. Meinert, J.-J. Filippi, P. de Marcellus, L. le Sergeant d'Hendecourt, U. J. Meierhenrich, *ChemPlusChem* **77**, 186–191 (2012).
25. G. M. Muñoz Caro et al., *Nature* **416**, 403–406 (2002).
26. D. J. Ritson, J. D. Sutherland, *Angew. Chem. Int. Ed. Engl.* **52**, 5845–5847 (2013).
27. F. Goesmann et al., *Science* **349**, aab0689 (2015).
28. I. P. Wright et al., *Science* **349**, aab0673 (2015).
29. U. J. Meierhenrich, *Comets and their Origin* (Wiley-VCH, 2015).

Supplementary materials

Materials and Methods

1. Preparation of the interstellar pre-cometary ice analogue

The experimental setup has already been described in detail elsewhere (30). It consists of a high vacuum chamber (10^{-7} mbar) in which an infrared (IR) transparent MgF_2 window is cooled down to 78 K. A gas mixture, previously prepared in an independent stainless steel gas line pumped down to about 5.10^{-6} mbar, is then injected into the chamber where it condenses on the cold MgF_2 substrate to form a thin film of “ices”. These ices were, simultaneously to their deposition, irradiated by UV photons for 142 h, using an H_2 discharge lamp providing essentially Lyman- α photons at 122 nm with a tail including an H_2 recombination line at approximately 160 nm and a continuum down to the visible range. In our experiments the ratio of ultraviolet photons to deposited molecules is around 1, meaning approximately 10 eV per deposited molecule to obtain the soluble organic matter sample. The sample was further irradiated, at room temperature, with right-hand circularly polarized synchrotron radiation (CPSR) at 10.2 eV for 2 h at the beamline DESIRS (31) of the SOLEIL synchrotron because we initially intended to induce asymmetric photochemical reactions. At this level of interpretation, no stereochemical effects induced by CPSR could be definitely identified yet in our samples. The entire experiment in terms of deposition rate, ice mixture, and the effect of UV photolysis is constantly monitored by IR spectroscopy which reveals the presence of a few photochemical produced molecules and radicals such as CO, CO_2 , HCO, and H_2CO , trapped in the ice phase. Photon-molecule interactions are assumed to occur predominantly in the condensed phase but in rare events UV photons may have initiated gas-phase reactions, with the photo-products being subsequently trapped on the ices.

For this study, we prepared one mixture composed of H_2O , $^{13}\text{CH}_3\text{OH}$, and NH_3 in relative proportions 10:3.5:1, qualitatively representative of interstellar/pre-cometary ices. Methanol, our only source of carbon, was labelled with ^{13}C in order to avoid any confusion with potential biological contamination in the handling and analysis processes of the samples. H_2O (water, liquid) was purified by using a Millipore Direct Q5 system, $^{13}\text{CH}_3\text{OH}$ (methanol, liquid) was purchased from Aldrich (99.9% purity), and NH_3 (ammonia, gas) from Messer (99.98% purity). The ratios between the components were determined by their partial pressures in the gas line, measured by an absolute pressure gauge (Baratron). The physico-chemical state of the initial sample (temperature and ice composition) is used as a template of pre-accretionary ices and is not fully representative of interstellar conditions. At 78 K, enhanced diffusion of reactants allows for a faster chemical evolution than at 10 K without significantly affecting the nature of the organic residue (32). The organic residue is always extracted after warm-up to room temperature as when considering the chemical composition of meteorites. For the initial molecular ice composition, we observed that CO and CO_2 ^{13}C isotopologues appear during the photochemical process, formed and trapped in the ice and are thus part

of the icy molecular chemical reservoir. During the preparation of the samples infrared monitoring is used to control deposition rate and UV efficiency by using the apparition of a weak HCO band and a reasonably strong H₂CO band, which falls at 1720 cm⁻¹. The 3.4- μ m feature, which consists of two subfeatures at 2925 cm⁻¹ (3.42 μ m) and 2875 cm⁻¹ (3.48 μ m) indicative to the presence of CH₂OH groups (33), was recorded in our ice during temperature increase to 230 K when the sublimation of water, methanol, and ammonia is almost finished. Below 230 K the sample is optically too thick for the detection of the 3.4- μ m feature.

2. Analysis of the interstellar pre-cometary ice analogue

Sample-handling glassware was wrapped in aluminum foil, and heated at 500 °C for 3 h prior to usage. Eppendorf tips® were sterile and the water used for extraction, standard solutions, reagent solutions, and blanks had been prepared by a Milipore Super-Q water filter system (4 ppb total organic carbon). The organic residues were extracted with 150 μ L high-performance liquid chromatography grade water from their MgF₂ windows and transferred into conical reaction vials. The samples were silylated with 10 μ L *N,O*-bis(trimethylsilyl)trifluoroacetamide (BSTFA) and 25 μ L pyridine for 2 h at 80 °C. The samples were evaporated to dryness using a gentle stream of nitrogen and 30 μ L of the internal standard methyl laurate in *n*-hexane (5·10⁻⁵ M) were added. The mixtures were transferred into GC vials prior their analyses by two-dimensional gas chromatography–time-of-flight mass spectrometry (GC \times GC–TOFMS) using a LECO Pegasus IV D system. Procedural blanks were run in sequence to each sample in order to monitor significant background interferences.

The GC \times GC column set consisted of a Chirasil-Dex chemically bonded primary column (24.5 m \times 0.25 mm inner diameter (ID), 0.25 μ m film thickness) modulator-coupled to an Agilent Wax secondary column (1.40 m \times 0.1 mm ID, 0.1 μ m film thickness). Helium was used as carrier gas at a constant flow rate \bar{u} = 1 mL min⁻¹. Sample volumes of 1 μ L were injected in the splitless mode at an injector temperature of 230 °C. The primary oven was operated as follows: 40 °C for 1 min, temperature increase of 10 °C min⁻¹ to 80 °C and held for 15 min, followed by 2 °C min⁻¹ to 180 °C, and an isothermal hold at 180 °C for 5 min. The secondary oven used the same temperature program with a constant temperature offset of 15 °C. A modulation period of 3 seconds was applied. The TOF-MS was operated at a storage rate of 150 Hz, with a 25–500 amu mass range. Data were acquired and processed with LECO Corp ChromaTOF™ software. Compound identification was performed by comparison with the chromatographic retention in both dimensions and mass spectra of authentic standards. All reference compounds were purchased from Sigma Aldrich including the monosaccharides: glycolaldehyde dimer, D,L-, D-, and L-glyceraldehyde, dihydroxyacetone, erythrose, erythrulose, ribose, arabinose, lyxose, xylose, and ribulose; the saccharinic acids: glyceric and threonic acid; the polyols: ethylene glycol, 1,3-propanediol, glycerol, threitol, erythritol, xylitol, arabitol, mannitol, sorbitol, and dulcitol; the hydroxycarboxylic acids: glycolic, D,L-, D-, and L-lactic, 3-hydroxypropanoic, 2-hydroxyisobutyric, *S*-2-hydroxybutyric, *S*-3-hydroxybutyric, 4-hydroxybutyric,

malic, dicarboxylic acid: succinic, and fumaric acid as well as the dialdehyde: glyoxal. The mass spectra of unknown analytes were interpreted based on their fragmentation patterns. Compounds were quantified using external standards.

Arabitol can be formed by the reduction of either arabinose or lyxose. Therefore, arabitol is sometimes but less often called lyxitol. In Figure 5.1 we used the name arabitol for both, the reduced arabinose and for the reduced lyxose.

3. Analyte quantification

The simulated interstellar pre-cometary ice samples were deposited onto magnesium fluoride (MgF_2) windows. The condensation was performed on two rectangles of 4 mm to 9 mm providing a sample surface $A = 72 \text{ mm}^2$ and a sample mass $m = 100 \pm 50 \text{ }\mu\text{g}$. To avoid sample loss while weighting, the mass and its estimated error were deduced from IR spectroscopy by comparison with a similar sample previously measured as a standard at the Institute d'Astrophysique Spatiale (IAS) (34). The quantification of each analyte indicated in ppm by mass (Figure 5.1) corresponds to the mass of the analyte in a 100- μg ice sample. Relative quantities from one molecular species to another are reliable to within the indicated error bars. Absolute quantities vary within $\pm 50\%$. Note however that the absolute errors are less important if one considers the final conclusion that the detected sugars are abundant within this sample.

The quantities of the analytes were calculated based on the relative response factors (*RRF*) using standard solutions with known concentration of the internal standard and the compound of interest. The *RRF* was calculated as follows: $RRF = A_X \cdot c_{IS} / A_{IS} \cdot c_X$, where A_X is the peak area of the analyte, A_{IS} the peak area of the internal standard, c_X and c_{IS} are the concentrations of the analyte and internal standard, respectively. The approximations for the compounds without corresponding standard were based on the *RRF* of structurally related compounds, i.e. $RRF(\text{threonic acid}) = RRF(\text{erythronic acid}) = RRF(\text{ribonic acid}) = RRF(\text{lyxonic acid}) = RRF(\text{xylonic acid})$; $RRF(\text{ribulose}) = RRF(\text{xylulose})$, and $RRF(\text{xylitol}) = RRF(\text{ribitol})$.

The *RRFs* of ribose, arabinose, lyxose and xylose were calculated for mass/charge (m/z) 204 (^{12}C) and 206 (^{13}C), respectively, to avoid any contribution from co-eluting compounds. For xylulose and ribulose, m/z 335 and 339, respectively, were used for the same reason. As for the other analytes, the peak area and *RRFs* were calculated for the most abundant mass fragment m/z 73. For arabinose, lyxose, and xylose the sum of both anomeric forms (α - and β -pyranose) was used. The calculated concentrations of the identified sugar and sugar-related compounds (Fig. 5.2) accompanied by their experimental 3σ errors ($n = 6$) are given in Table S5.1.

Figure S5.1 provides a supplementary view on the multidimensional gas chromatographic separation of ribose and other monosaccharides and sugar-related molecules. Potential ^{13}C -contamination from biological and/or laboratory sources was determined by analyzing a blank sample. Therefore, 150 μL HPLC grade water was dried in a conical reaction vial, derivatized with BSTFA and pyridine, and analyzed under identical analytical conditions as the pre-cometary ice

sample. Figure S5.2 shows the GC \times GC–TOFMS chromatogram of the blank sample, in which monosaccharides are clearly absent.

4. Identification of organic molecules in the interstellar pre-cometary ice analogue

Compound identification was performed by comparison with the chromatographic retention in both dimensions of authentic standards and mass spectra. For those compounds that were not available as standard solution, e.g. 3-hydroxyisobutyric acid, we utilized the mass selectivity of the fragments of silylated derivatives, provided by the characteristic electron impact (EI) mass spectra, present in the NIST library (35).

Comparison with previously reported data on the photoproducts formed in the organic residues of interstellar ice mixtures (10) let us identify oxamic acid (36). 2-Hydroxymethylglycerol – one of the major products in the photochemically induced formose reaction – was identified from its reported spectral and analytical data (19) as well as 2-hydroxymethyltetritol (20).

4.1. Identification of monosaccharides in the interstellar pre-cometary ice analogue

Monosaccharides with an anomeric center can yield mixtures of α - and β -anomeric derivatives. The possibility of both pyranose (6-membered ring) and furanose (5-membered ring) forms of sugar molecules increases the number of potential derivatives. Mass spectra, however, allow pyranose derivatives to be unambiguously distinguished from furanose derivatives (37, 38). Pyranose trimethylsilyl ethers produce characteristic ions by electron impact sugar degradation at: m/z 217 ($^{13}\text{C} = 220$) $[(\text{CH}_3)_3\text{SiOCH}=\text{CH}-\text{CH}=\text{OSi}(\text{CH}_3)_3]^+$, m/z 204 ($^{13}\text{C} = 206$) $[(\text{CH}_3)_3\text{SiOCH}=\text{CHOSi}(\text{CH}_3)_3]^{+}$, and m/z 191 ($^{13}\text{C} = 192$) $[(\text{CH}_3)_3\text{SiOCH}=\text{OSi}(\text{CH}_3)_3]^+$. The ion at m/z 217 ($^{13}\text{C} = 220$) is generally very intense for the furanose form whereas the relative intensity of the ion at m/z 204 ($^{13}\text{C} = 206$) is always less than 5%. Based on our recorded mass spectra we thus conclude that the majority of the extracted and derivatized C5-sugar molecules from the interstellar ice sample is present in the pyranose ring form. Since the known fragmentation pattern for trimethylsilyl derivatives is almost identical for all of the C5-sugar pyranosides, the assignment was confirmed by the retention time and comparison with authentic standards. We used the following observations to distinguish between the α - and β -anomeric derivatives. Figure S5.3 shows the mass spectra and the characteristic mass fragmentation pathway of ribose, representative for all other C–5 monosaccharides.

10 Rules for monosaccharides identification

Anomerization occurring in pyridine during preparation of TMS derivatives is minimal (39).

Each anomer yields one peak. All free OH groups are thus converted to TMS derivatives (39).

α - and β -composition of equilibrium mixtures of sugars in a) aqueous solution: arabinose: $\alpha = 51\%$, $\beta = 44\%$; lyxose: $\alpha = 74\%$, $\beta = 26\%$; ribose: $\alpha = 89\%$ & xylose: $\alpha = 41\%$, $\beta = 55\%$ and in b) pyridine: arabinose: $\alpha = 32\%$, $\beta = 53\%$; lyxose: $\alpha = 72\%$, $\beta = 28\%$; ribose: $\alpha = 19\%$, $\beta = 63\%$ & xylose: $\alpha = 46\%$, $\beta = 43\%$ (39, 40).

Excellent resolution of anomeric forms. Structural properties imparted by pyranose and furanose ring account for their excellent separation of various stereoisomers.

α - and β -pyranose separation factor: ribose (1.08) < arabinose (1.2) < lyxose (1.4) < xylose (1.4) (39, 40).

α -Anomer elutes before β -anomer in case of glucose, galactose, mannose, talose, xylose, lyxose, and arabinose (39, 41).

Pyranosides having planar structures are more strongly retained (39). The first peaks eluted are always α -lyxo- and α -arabinopyranoses; they are also the less planar pyranose forms. Maximum retention is always attained for β -xylose, whose TMS groups are all equatorial.

Elution order of pyranoses: α -lyxose \approx α -arabinose < β -arabinose = β -ribose < β -lyxose \approx α -ribose < α -xylose < β -xylose (41).

Retention times of ketoses in ring form are often lower than those of the analogues aldoses whereas the open form (ketol) is more strongly retained (42).

Replacement of OH by H in deoxysugars leads to decreased relative retention times (39).

4.2. Identification of sugar alcohols in the interstellar pre-cometary ice analogue

The trimethylsilyl derivatives of alditols with three to six carbon atoms including glycerol, erythritol, threitol, arabinitol, glucitol, xylitol, ribitol, galactitol, and mannitol – that were all detected in the organic residue of the simulated interstellar ices – were studied in detail (43). The mass spectra and corresponding fragmentation pattern of arabitol (arabinitol) are illustrated in Figure S5.4. Favoured α -cleavage with charge retention followed by rearrangement loss of trimethylsilanol $[(\text{CH}_3)_3\text{Si-OH}]^+$ has been shown as the predominant fragmentation pathway. For the alditols this type of resonance stabilization favors cleavage of all other C-C bonds. The abundance of these α -cleavage ions is explained by the stabilization of the positive charge by the unshared electron pairs on the oxygen atoms. The differentiation of diastereomeric derivatives, however, is nearly impossible due to the small differences between these spectra.

For sugar alcohols that were not commercially available, we compared their reported retention indices with the proposed structures detected in our study with GC \times GC-TOFMS. The elution order and final peak assignment was thus possible for the C-5-alditols: ribitol and alditol (42) as well as for the C-6 sugar alcohols: allitol and talitol (altritol) (39).

4.3. Identification of saccharinic, hydroxycarboxylic, and dicarboxylic acids in the interstellar pre-cometary ice analogue

Fragmentation studies on the aliphatic hydroxycarboxylic acids (44, 45) glycolic acid, lactic acid, and 2-hydroxybutyric acid:

$m/z = 147$: through rearrangement decomposition of the $[M-15]^+$ ions, which can be described as cyclic oxonim ions and subsequent loss of CO and CH_2O for glycolic acid and CO and CH_3CHO for lactic acid

$m/z = 147$: for 2-hydroxybutyric acids direct migration of the ester trimethylsiloxy group to a positive charge site at the other silicon atom

Fragmentation studies on the aliphatic dicarboxylic & hydroxy dicarboxylic acids (45) succinic acid and malic acid:

the molecular ion $[M]^{*+} = 262$ (266 for ^{13}C) and $[M]^{*+} = 350$ (354) – often absent in trimethylsilyl derivatives – is observed for succinic and malic acid, respectively

Fragmentation studies on the saccharinic acids (44) glyceric acid, erythronic acid, threonic, lyxonic, ribonic (Figure S5.5), xylonic and arabinic acid:

$m/z = 292$ (294): all acids with OH in C2 and C3 position; McLafferty-type rearrangement (ester migration) of a trimethylsilyl group with aldehyde loss (2-deoxyaldonic acid disclose that formation)

$m/z = 205$ (207): indicative of a vicinal diol group

$[M-15-90]$: glyceric acid 217 (220) and erythronic acid 319 (323)

$m/z = 189$ (191): characteristic for glyceric acid by stepwise loss from $[M-15]^+$ of both trimethylsilanol and carbon monoxide $[M-15-118]$

Fragmentation studies on C5 sugar acids:

$m/z = 307$ (310): decomposes by loss of formaldehyde to $m/z = 277$ (279)

$m/z = 307$ (310): decomposes by rearrangement loss of trimethylsilanol to $m/z = 217$ (220)

$m/z = 423$ (427): metastable peak formed from loss of the end group with electron withdrawing effect of the ester group: $[M]^{*+} = 527$ (532) - $[103/104\text{-H}]$, further decomposes to $m/z = 333$ (337) by loss of trimethylsilanol

Fragmentation studies on the branched-chain saccharinic acid (44) 2-methylglyceric acid:

$[M-15]$: 321 (325)

$m/z = 306$ (308): McLafferty-type rearrangement

$m/z = 233$ (236) & $m/z = 219$ (222): chain cleavage ions with charge retention at C2

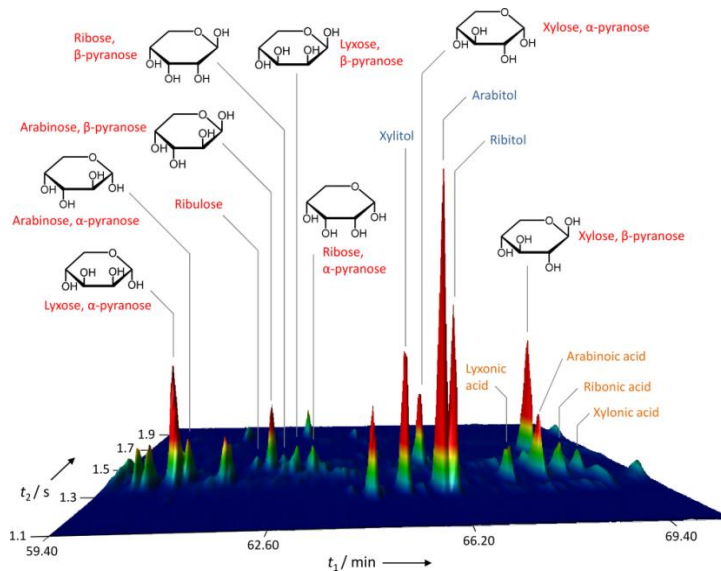


Fig. S5.1. Supplementary view on the multidimensional gas chromatographic separation of ribose and other monosaccharides and sugar-related molecules. Experimental conditions are identical as compared to Figure 5.2. This view better allows for the visual separation of the α - and β -pyranose of xylose and arabinonic acid. Atomic mass units 206 and 294 were selected for the above representation with z-scaling = 10^5 .

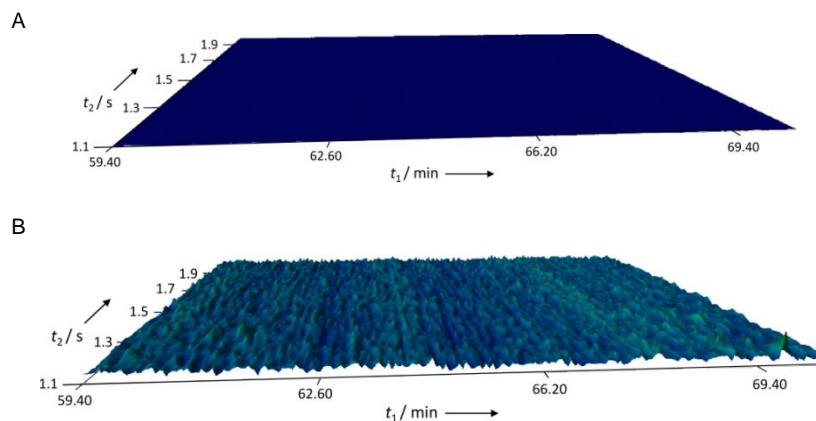


Fig. S5.2. Analytical blank. A: Representative enantioselective GCxGC-TOFMS chromatogram of the blank sample submitted to the entire analytical protocol. Atomic mass units 206 and 294 ($\times 5$) were selected for the above representation and the primary and secondary temperature program was identical to Figure S5.1. B: Reduced z-scaling (z-axis = 5,000) illustrates the absence of monosaccharides and other related compounds in the blank sample.

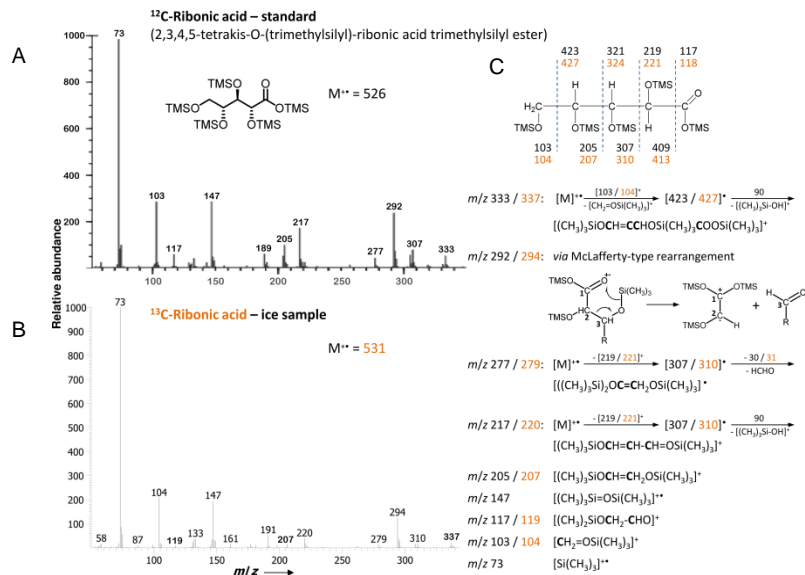


Fig. S5.5. Mass spectra of the ¹²C-ribonic acid standard (A) and the ¹³C-ribonic acid in the pre-cometary ice sample (B). The ribonic acid fragmentation pattern is indicated (C) by representing the individual mass shifts for each fragment of the ¹²C standard (black) and the ¹³C sample (orange). The mass spectrum of ribonic acid was taken from the NIST database (35).

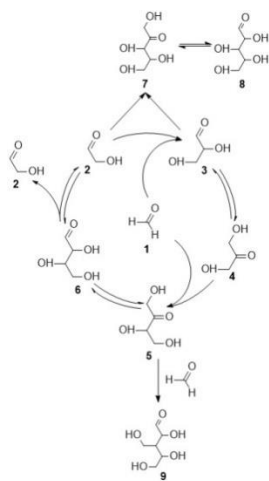


Fig. S5.6. The formose reaction. Formaldehyde 1 undergoes self-condensation under autocatalytic reaction kinetics to form glycolaldehyde 2, which undergoes an aldol reaction with an equivalent of 1 by forming glyceraldehydes 3. Dihydroxyacetone 4 is formed by aldose-ketose isomerization, a tautomerization, of 3. Dihydroxyacetone 4 reacts with 1 producing ketotetrose (erythulose) 5 and aldotetrose 6 (18). The aldol condensation of 2 and 4 forms the 2-ketopentoses 7 that isomerize to an aldopentose 8 such as ribose, arabinose, xylose, and lyxose. Branched aldotetroses 9 are formed by aldol condensation of 5 and 1.

Table S5.1. Summary of the total abundances of sugar and sugar-related compounds in the water extract of a pre-cometary interstellar ice analogue.^[a] Quantity of carbon atoms.^[b] The data are mean values given with their standard deviation of 3 σ .

#C ^[a]	Compound	Quantity [ppm] ^[b]	#C ^[a]	Compound	Quantity [ppm] ^[b]
Aldoses / aldehydes			Ketoses		
2	Glycolaldehyde	2390 \pm 100	2	-	
3	D,L-Glyceraldehyde	302 \pm 30	3	Dihydroxyacetone	540 \pm 40
4	D,L-Erythrose	LOQ*	4	Erythrulose	37 \pm 4
5	D,L-Ribose	260 \pm 20	5	Ribulose	2010 \pm 110
	D,L-Arabinose	200 \pm 20		Xylulose	470 \pm 50
	D,L-Xylose	240 \pm 15			
	D,L-Lyxose	145 \pm 11			
Sugar acids (saccharinic acids)			Sugar alcohols / polyols		
2	Glycolic acid	6330 \pm 750	2	Ethylene glycol	550 \pm 50 [†]
3	D,L-Glyceric acid	2440 \pm 30	3	Glycerol	2860 \pm 90
4	D,L-Erythronic acid	960 \pm 40	4	Erythritol	5070 \pm 500
	D,L-Threonic acid	840 \pm 50		D,L-Threitol	7200 \pm 680
5	D,L-Ribonic acid	82 \pm 7	5	D,L-Ribitol	560 \pm 50
	D,L-Arabinic acid	165 \pm 9		D,L-Xylitol	630 \pm 40
	D,L-Xylonic acid	67 \pm 5		D,L-Arabitol	1150 \pm 90
	D,L-Lyxonic acid	140 \pm 15			

[*] Limit of quantification. [†] The low relative abundance of ethylene glycol as compared to the corresponding C2 aldehyde and C2 acid is due to its high volatility resulting in its loss during sample preparation and analysis.



It has been previously demonstrated that chiral prebiotic molecules such as amino acids and sugars are present in photoprocessed interstellar ices, and therefore may be present in the actual cometary nucleus of 67P and/or interstellar dust particles. The following step in the astrophysical scenario of the photodependent symmetry breaking would be the interaction of chiral racemic molecules with interstellar CPL. This interaction is directed by the CD of the chiral molecule under investigation, while PECD could have been involved in a photophysical gas phase enantioenrichment in a given direction of space.

In the context of asymmetric photodynamics, PECD properties of chiral molecules have to be understood in details and benchmarked versus theory. The following article describes, besides its striking sensitivity to isomer, the analytical aspects of PECD, which enable the detection of relative enantiomeric excesses in the gas phase as precisely as a comprehensive two dimensional gas chromatography.



CHAPTER IV: Photo Electron Circular Dichroism

Article 6. Determination of accurate electron chiral asymmetries in fenchone and camphor in the VUV range: sensitivity to isomerism and enantiomeric purity

Laurent Nahon, Lipsa Nag, Gustavo A. Garcia, Iuliia Myrgorodska, Uwe Meierhenrich, Samuel Beaulieu, Vincent Wanie, Valérie Blanchet, Romain Géneaux and Ivan Powis

Abstract

Photoelectron circular dichroism (PECD) manifests itself as an intense forward/backward asymmetry in the angular distribution of photoelectrons produced from randomly-oriented enantiomers by photoionization with circularly-polarized light (CPL). As a sensitive probe of both photoionization dynamics and of the chiral molecular potential, PECD attracts much interest especially with the recent performance of related experiments with visible and VUV laser sources. Here we report, by use of quasi-perfect CPL VUV synchrotron radiation and using a double imaging photoelectron/photoion coincidence (i^2 PEPICO) spectrometer, new and very accurate values of the corresponding asymmetries on showcase chiral isomers: camphor and fenchone. These data have additionally been normalized to the absolute enantiopurity of the samples measured by a chromatographic technique. They can therefore be used as benchmarking data for new PECD experiments, as well as for theoretical models. In particular we found, especially for the outermost orbital of both molecules, a good agreement with CMS- $X\alpha$ PECD modeling over the whole VUV range. We also report a spectacular sensitivity of PECD to isomerism for slow electrons, showing large and opposite asymmetries when comparing *R*-camphor to *R*-fenchone (respectively -10% and $+16\%$ around 10 eV). In the course of this study, we could also assess the analytical potential of PECD. Indeed, the accuracy of the data we provide are such that limited departure from perfect enantiopurity in the sample we purchased could be detected and estimated in excellent agreement with the analysis performed in parallel via a chromatographic technique, establishing a new standard of accuracy, in the $\pm 1\%$ range, for enantiomeric excess measurement via PECD. The i^2 PEPICO technique allows correlating PECD measurements to specific parent ion masses, which would allow its application to analysis of complex mixtures.

Published article: *Physical Chemistry Chemical Physics* (2016), 18, 12696 – 12706.

1. Introduction

Since its formal prediction in 1976,¹ its first precise calculated values in 2000,^{2,3} and its first experimental evidence in 2001,⁴ Photoelectron Circular Dichroism (PECD) has been the subject of a large number of both theoretical and experimental studies,⁵⁻⁷ mainly carried out with Synchrotron Radiation (SR), for valence and core-shell ionization. PECD is an orbital-specific chiroptical effect which manifests itself as a forward/backward asymmetry, with respect to the photon axis, of the electron angular distribution produced by the photoionization with Circularly Polarized Light (CPL) of randomly-oriented pure enantiomers of a chiral system. More precisely, PECD asymmetry can be defined, for a given light helicity and molecular handedness, as the normalized difference between the electron flux in the forward vs. backward direction which will equal $2b_1$ in the case of one-photon ionization, where b_1 is the so-called dichroic parameter. The corresponding asymmetry factors are large (up to a few tens of %) because PECD emerges in the pure electric-dipole approximation, and PECD is therefore orders of magnitude more intense than other chiroptical probes, such as circular dichroism absorption, requiring interaction with weaker (magnetic and quadrupolar) terms.⁸ As found for other chiroptical parameters, b_1 is anti-symmetric with the switching of either enantiomers or light helicity.

In the context of molecular photoionization, b_1 depends on both the initial-state (orbital) and final state (continuum).^{9,10} However, unlike the usual cross section σ or the asymmetry parameter β , this new observable has a pure quantum origin in the scattering of the outgoing electron by an intrinsically chiral potential, being also fully dependent on the sine of the relative phase between adjacent outgoing partial wave continuum functions.⁵ This phase dependence makes b_1 a very sensitive probe of the whole molecular potential, much more so than σ or β , with a demonstrated dependence on conformers,¹¹⁻¹⁵ chemical substitution,^{16,17} dimerization¹⁸ and clustering,^{19,20} and even vibrational-dynamics.^{21,22}

PECD possesses, therefore, a real analytical potential in the gas phase (*i.e.* in a solvent-free environment) which has recently been the driving force for a new emerging field of table-top PECD experiment based on fs laser ionization: UV-resonance enhanced multi-photon ionization (REMPI) PECD²³⁻²⁸ or 1-photon VUV PECD by High Harmonic Generation (HHG).²⁹ These experiments are paving the way towards a potentially very sensitive analytic use of PECD for enantiomeric separation on mass-selected samples,³⁰ competing with other promising and emerging enantiomeric probes in the gas phase such as the one based upon phase-sensitive microwave spectroscopy.³¹⁻³³ A natural step further will be the development of Time-Resolved (TR)-PECD to probe stereo-chemical reactions of chiral systems in real time.

Most of the pioneering SR-based experiments³⁴⁻³⁶ as well as the new generation of laser-based PECD experiments, were performed on the monoterpenes camphor and/or fenchone,^{24-26,30,37} two isomeric forms of a rigid, single-conformer, bi-cyclic ketone, quite easy to bring in the gas phase, and that can both be considered as showcases for molecular chirality. Note that fenchone has also been used to demonstrate a pioneering chiroptical method based upon High Har-

monic Generation (HHG) from a chiral molecule,³⁸ and both isomers have been studied by REMPI-UV Ion Yield CD.³⁹ To be validated insensitivity and reliability laser-based PECD experiments need benchmarking with data obtained with more well-established and controlled experiments such as the one that can be carried out with pure-CPL SR sources. This is one of the motivations for the present study, which provides for the first time complete and very accurate measurements of b_1 parameters for the two outermost orbitals of camphor and fenchone up to $h\nu \sim 16$ eV. Indeed, in the past some of us^{34,36,40} and other authors³⁵ published some data for these molecules but, because of technical SR light source limitations at the time, there were uncovered regions of the spectrum—notably in the crucial 10 to 15 eV photon energy range for which theoretical models^{36,41} predict large oscillations of b_1 . The benchmarking of theory *versus* experiment, in this specific range, with very accurate data obtained with a state-of-the-art double imaging electron/ion coincidence (i²PEPICO) spectrometer set-up and quasi-perfect CPL is the second motivation of the present study, especially in a context where multiphoton/high field PECD modeling has just been initiated on these showcase molecules.^{42,43} The precision of the measurements we provide are such that departures from perfect enantiopurity in the sample we purchased could be detected, quantified, and corrections applied to the measured b_1 parameter, all perfectly corroborated by an independent analysis performed *via* chromatographic techniques. Establishing this new standard of accuracy, in terms of enantiomeric excess measurement *via* PECD, became an important issue that we also focused on in the course of the data analysis.

Finally, and this is an important goal of this work, the observation of PECD for various valence orbitals for both fenchone and camphor, which only differ by the position of two methyl groups, will allow us to expand our previous knowledge⁴⁰ on the sensitivity of valence-shell PECD to isomerism which in this case cannot be detected from the shape of the photoelectron spectra.

2. Experimental methods

Both *R*- and *S*-fenchone and *R*- and *S*-camphor were obtained from Sigma-Aldrich with a chemical purity above 98%. In the case of fenchone, the optical rotations quoted in the bottle labels for both enantiomers ($[\alpha]_D^{24} = -51.5$ for the *R* and $[\alpha]_D^{24} = +62$ for the *S*) suggested a difference in enantiopurity, with an *R/S* ratio of 0.81. For camphor, the optical rotations quoted in the chemical analysis of the particular lots used ($[\alpha]_D^{24} = +44.6$ for the *R* and $[\alpha]_D^{24} = -43.5$ for the *S*), led to an *R/S* ratio of 1.02. Therefore, we decided to analyze the exact enantiopurity of the purchased samples with multi-dimensional gas chromatography coupled to time-of-flight mass spectrometry (GC \times GC-TOFMS).⁴⁴ The GC \times GC column set consisted of a Chirasil-Dex CB (for fenchone) or Hydrodex- β -6-TBDM (for camphor) primary column modulator-coupled to a DB Wax secondary column. Temperature program was adapted to achieve maximum peak resolution. Secondary column was operated with 30 °C off-set. Modulation period of 3 s was applied. Helium was used as carrier gas at a constant flow of $\bar{u} = 1$ mLmin⁻¹. Sample volumes of 1 mL were injected in the split mode at an injector temperature of

230 °C. The TOF-MS was operated at a storage rate of 150 Hz, with a 25–500 amu mass range. Data were acquired and processed with LECO Corp Chroma-TOF™ software. Samples of *S*- and *R*-enantiomers with the concentration 10^{-3} M were injected several times in order to obtain statistically relevant *ee* values.

PECD experiments were performed on the SAPHIRS endstation⁴⁵ of the VUV synchrotron beamline DESIRS,⁴⁶ at the French synchrotron facility SOLEIL. Each enantiomer of each molecule was directly placed into a temperature-controlled in-vacuum stainless steel oven. The reservoir was gently heated at 40°C and the resulting vapor was mixed with 0.5 bars of He and adiabatically expanded through a 70 μm nozzle. After traversing a differentially pumped chamber with two $\phi = 1$ mm skimmers, the collimated molecular beam crossed the synchrotron radiation at a right angle.

Tailored polarized light was provided by the HU640 electromagnetic undulator of DESIRS, set in the so-called “pure CPL mode” and monochromatised with the 200 lines per mm grating of the 6.65 m normal incidence monochromator. For photon energies below 15 eV, a gas filter located upstream the monochromator was filled with Kr or Ar to remove the high harmonics from the undulator.⁴⁷ The monochromator slits were merely set to avoid saturation of the charged particle detectors, providing energy resolutions between 6 meV at the lowest photon energy, and 11 meV at the highest. The full polarization ellipse, including the unpolarized component, was measured *in situ* at the sample level with a dedicated polarimeter,⁴⁸ and was found to be quasi-purely circular, with absolute circular polarization rates (S_3) values of 0.99 ± 0.01 over the whole photon energy range⁴⁶ which we have used to normalize the experimental PECD values. Further and more complicated corrections to the PECD values due to S_1 and S_2 terms can be neglected in view of the polarization purity. In addition, the stability of S_3 over time is routinely confirmed by frequent polarimetry checks.

Electrons and ions formed in the interaction region are accelerated in opposite directions by a continuous electric field perpendicular to the molecular and synchrotron beams. A complete description of the DELICIOUS3 i^2 PEPICO spectrometer used in this work and its performances has been reported elsewhere.^{45,49} Briefly, it consists of an electron velocity map imaging (VMI) analyser coupled to a modified ion Wiley–McLaren imaging spectrometer. Electron and ion arrivals are correlated in time and therefore the photoelectron VMI images can be obtained and filtered as a function of ion mass and translational energy. Photoelectron spectra (PES) and angular parameters are then extracted from the Abel inversion of the VMI image using a least squares fitting of previously computed forward Abel functions.⁵⁰ For the PECD measurements, typically a total of around 20 images are obtained at a given fixed photon energy for a given enantiomer with alternating light helicities, switched every 15 min. The images are then summed according to the light helicity to provide a single pair composed of the left (LCP) and right (RCP) circularly polarized measurements. The PES is then obtained by Abel inversion of the LCP + RCP image with a kinetic energy resolution of 3% for the fastest electrons, while the $b_0 b_1$ term, where b_0 is the total cross-section of ionization of a given electronic band as given by the integral of the PES, is obtained from the LCP–RCP difference, leading to the final PECD, $2b_1$, through normalization by b_0

(see ref. 36 for a complete description of the procedure). The statistical error bars are given as the standard error on the principle that each image pixel acts as an independent counter that follows a Poisson distribution, with the associated error properly propagated through all subsequent operations. Systematic errors are estimated by comparison of both enantiomers' data, which should exhibit perfect mirroring behavior.

3. Results and discussions

3.1. Camphor data

Fig. 6.1 shows the typical data recorded in these experiments, in this case for *R*- and *S*-camphor at 12.3 eV. Several features mentioned in the introduction can be readily observed in the figure. Indeed the large asymmetry observed with PECD up to 12% means that it is readily visible even in the raw non-inverted 2D-difference images shown in Fig. 6.1a and b. The strong initial orbital dependency is also appreciated with the sign and magnitude changing for different electronic bands across the image radius. Moreover, the PECD value in Fig. 6.1c oscillates several times between IE = 10 and 12 eV. These oscillations, although not seen in the VMI-PES concurrently recorded with our spectrometer, are real and exceed our error bars. They are perfectly mirrored in the *R*- and *S*-enantiomer curves as anticipated from the anti-symmetry of the b_1 coefficients for the two enantiomers, showing the high quality of the data. The mirroring is explored in Fig. 6.1d, by plotting the mean value or baseline

$$BL = \frac{PECD_R - PECD_S}{2}$$

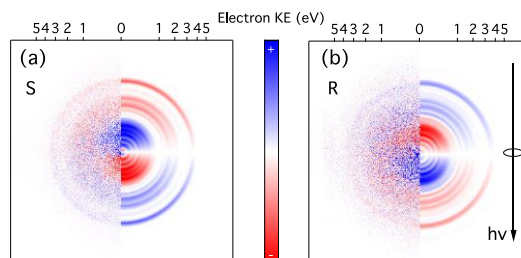


Figure 6.1 VMI difference images (LCP–RCP) recorded at $h\nu = 12.3$ eV for 1*S*,4*S*-camphor (a) and 1*R*,4*R*-camphor (b) enantiomers. The left-half images show raw 2D-projections, and the right half the corresponding Abel inverted image (c) PECD (open and filled circles) and PES (solid line) extracted from inversion of the total and difference images. For clarity, the PECD is only shown for energies where the PES signal is higher than 10% of the maximum. The data have been normalized by S_3 and the ee measured by GC \times GC-TOFMS. (d) PECD baseline (BL) obtained as the mean value of the *S* and *R* PECD curves. Error bars are obtained according to the description written at the end of the experimental section. A higher resolution PES obtained at $h\nu = 95$ eV is also represented (dashed line) along with the calculated values (arrows), both taken from ref. ⁵¹

Deviation from the ideal value of zero could be ascribed to statistical error (different S/N), to systematic error (*e.g.* residual instrumental asymmetry), or to different enantiopurity. In the higher resolution PES recorded by Rennie *et al.*⁵¹

with a hemi spherical analyzer the electronic band structure is slightly more-marked and seen to correlate with the PECD changes. The OVGf calculations published by Rennie *et al.* also correspond to the observed oscillations, which highlights the enhanced sensitivity of PECD to electronic structure when compared to usual observables such as ionization cross-sections—even in the case of congested electronic bands as already observed in camphor³⁶ and glycidol.¹³

The onset of camphor parent ion fragmentation is ~ 9.7 eV, with the parent ion rapidly disappearing as photon energy is increased (less than 10% of parent yield remains at 10.0 eV). The first electronic band seen in Fig. 6.1c, which corresponds to ionization of the HOMO orbital localized onto the carbonyl oxygen lone pair, results solely in the production of parent ion. Thus, by filtering the electron images according to the coincident parent ion mass, the electrons ejected from the HOMO can be better isolated. This becomes³⁶ extremely useful at high photon energies where the moderate resolution of the VMI leads to overlap between the HOMO and the inner orbital bands. Fig. 6.2 illustrates the result of applying the filtering for the parent ions at $h\nu = 12.3$ eV, and can be directly compared to Fig. 6.1. It is clear that the mass-filtering removes the contribution from inner orbitals since these lead to fragmentation. Conversely, to obtain the PECD of the deeper-lying orbitals, we have obtained the electron images correlated to the fragmentations only, so ensuring removal of any contribution from the HOMO orbital electron data. This treatment is especially effective when the HOMO and HOMO-1 orbitals have b_1 parameters of opposite sign, and so might tend to cancel if unresolved, as happens here in certain regions of photon energy. For instance, at $h\nu = 12.3$ eV the weighted HOMO $|b_1|$ values obtained from Fig. 6.1c (unfiltered) and Fig. 6.2 (filtered) are 0.055 and 0.058, respectively, a discrepancy in the unfiltered data of 5% due to the small overlap between HOMO and HOMO-1.

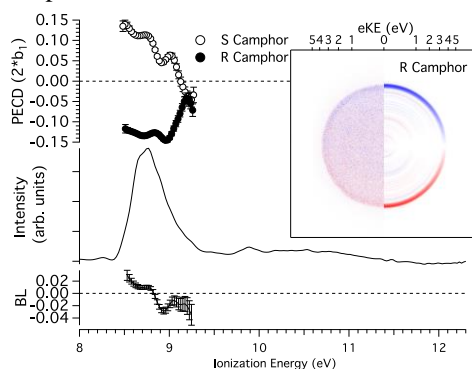


Figure 6.2 PECD (open and filled circles) and PES (solid line) extracted in coincidence with parent ions (m/z 152, plus 153 and 154 to take into account the ^{13}C contributions) recorded for 1*R*,4*R*- and 1*S*,4*S*-camphor at $h\nu = 12.3$ eV. The data have been normalized by S_3 and the ee measured by GC \times GC-TOFMS. The bottom-left axis represents the PECD baseline (BL) extracted as the mean value of the *R* and *S* PECD curves. The inset shows the raw (left) and Abel inverted (right) difference image for 1*R*,4*R*-camphor corresponding only to photoelectrons correlated to parent ions.

In addition, the double imaging coincidence scheme permits removing common background impurities such as water, N_2 , O_2 , which would increase the achiral content in the total signal used for normalization and therefore decrease the

observed PECD. Overall, the procedure dramatically increases the signal-to-noise ratio with respect to previous non-coincident data^{36,40} recorded for camphor and fenchone, as evidenced with the low error bars and excellent mirror behavior. Indeed, in Fig. 6.1c the PECD baseline, BL, barely deviates from the ideal zero value over the whole kinetic energy range, with a weighted mean value of 0.0003 ± 0.0005 . Deviations from zero outside of the given error bars are ascribed to systematic errors. It is worth noting that the *R* and *S* measurements correspond to two different experiments spaced by one month. In Fig. 6.2, the parent-coincident data show small deviations from perfect mirroring behavior, associated to the lower overall signal. Even in this case, however, the PES intensity weighted integral of the baseline, BL, over the FWHM of the HOMO band is very close to zero, 0.0005, so that the mean b_1 values across the HOMO and HOMO-1 regions (see text below and Fig. 6.3 and 6.4) will have very similar absolute values for both enantiomers within the given error bars—provided both have the same enantiopurity

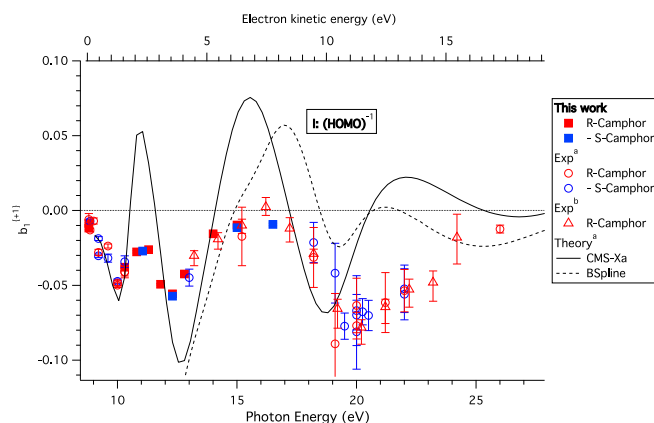


Figure 6.3 Mean chiral parameter (b_1) for ionization of the HOMO orbital of camphor obtained at different photon energies. The markers represent experimental measurements while the lines correspond to two different scattering models. The *S*-enantiomer data have been negated. For some of the data points, the statistical error bars are not visible because they are smaller than the point width (see Table S6.1, Sup. Inf.). The values in this work have been normalized by S_3 and the ee measured by GC \times GC-TOFMS. ^a From ref. 36. ^b From ref. 35.

However, at the photon energies where both enantiomers were recorded (12.3 and 15.0 eV), we initially found that the raw, uncorrected magnitude of the HOMO band PECD measured for the *R* enantiomer was slightly smaller than that of the *S*, leading to a $PECD_R/PECD_S$ average ratio of 0.97 ± 0.02 , as derived from the uncorrected data presented in Fig. S6.1(a) (Sup. Inf.). It is known that the magnitude of measured asymmetries will scale linearly with the absolute value of the enantiomeric excess (ee) as defined by $([R] - [S])/([R] + [S])$ where $[R]$ (resp. $[S]$) corresponds to the concentration of the *R* (resp. *S*) enantiomer, and this therefore suggests some variation of the relative enantiopurity of the two commercial samples with an ee ratio of 0.97 ± 0.02 , surprisingly quite different from the value of 1.02 that could be inferred from the optical rotation data provided by Aldrich

(see Experimental methods above). We therefore took additional steps to verify purity of our samples analyzing them by chiral-sensitive GC \times GC-TOF MS to obtain a precise value of the ee. The results of the chromatographic analysis are shown in Table 6.1. The agreement between ee ratio deduced from these PECD data and the absolute ee obtained by GC \times GC-TOFMS is remarkable, as are the experimental PECD error bars. The presented data of Fig. 6.1, and that discussed further below discussed were subsequently corrected for these reduced ee ratios, to represent the enantiopure values for PECD.

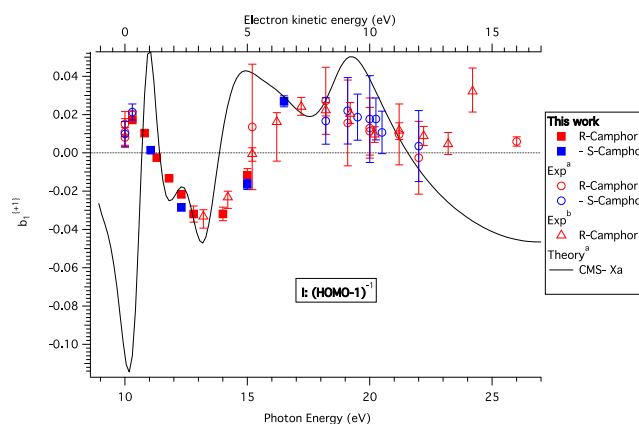


Figure 6.4 Mean chiral parameter (b_1) for ionization of the HOMO-1 orbital of camphor, corresponding to the binding energy region 10–10.3 eV, obtained at different photon energies. The markers represent experimental measurements while the line correspond to the CMS-X α scattering models. The *S*-enantiomer data have been negated. For some of the data points, the statistical error bars are not visible because they are smaller than the point width (see Table S6.1, Sup. Inf.). The values in this work have been normalized by S_3 and the ee measured by GC \times GC-TOFMS. ^a From ref. 36. ^b From ref. 35.

The importance of the quality of the circular polarization needs also to be highlighted because the measured b_1 is directly proportional to S_3 . A low absolute value of S_3 will at best—when it is known—lead to a decreased sensitivity to chirality by increasing the error bar on b_1 and, at worst—if not recognized—lead to incorrect PECD amplitudes. The argument must be also extended to cases where the Stokes parameters S_1 and S_2 defining respectively the linear polarization rates with respect to normal and 45° tilted axis, are non-zero. In such cases, if the usual anisotropy parameter β is non-zero, the S_1 and S_2 contributions to the photoelectron angular distribution (PAD) need to be taken into account. This would be a severe issue in the case of a VMI spectrometer relying on Abel inversion of a 2D image (*i.e.* without electron time-of-flight available to provide a direct 3D momentum determination) since only the cases where the axis of symmetry given by the light’s polarization state is contained within the detector plane can be properly treated. However, in the case of the present experiments, the DESIRS beamline delivers quasi-perfect CPL and the undesirable effects cited above do not apply here. Also, the error bars on the S_3 measurement are negligible and do not increase those of b_1 .

The data shown in Fig. 6.1 and 6.2 can be obtained at different photon energies in order to study dynamical effects such as the dependence on electron

kinetic energy or the effects of continuum resonances. For this, the orbital-specific PECD has been extracted by taking the PES intensity weighted average of b_1 over the FWHM of the corresponding electronic band. The results are given in Fig. 6.3 and 4 for the HOMO and HOMO-1 of camphor, which also compile the data from previous works. The HOMO-1 data have been obtained by filtering the electron images on the sum of the camphor fragments (discarding therefore the parent contribution) and by considering the binding energy range 10.0–10.3 eV as in ref. 36. Note that for the sake of providing highly accurate benchmarking PECD data, we list in Table 6.1. of the Sup. Inf. the corresponding new b_1 values.

The new data on the HOMO orbital of camphor, as given by the solid squares in Fig. 6.3, fit very well with previous existing data recorded below 10 eV and above 13 eV although they have much better accuracy. The completion of the 10–13 eV photonenergy range is extremely useful since in this range the CMS-X α model³⁶ made predictions of oscillations in the PECD which are now clearly evident in the experimental data. While these fixed equilibrium geometry calculations appear to over emphasize the magnitude of the swings experimentally observed in the 10–17 eV range, they do capture the essence of the energy dependent variation in b_1 . One may speculate that allowance for vibrational motion averaging in such calculated PECD might attenuate the swing in b_1 values suggested by experiment. An alternative calculation, the density functional based B-spline model of Stener *et al.*⁴¹ has previously been reported and compared. In the case of coreshell C1s ionization of camphor, both models give very comparable results in close agreement with the experimental data.⁴¹ Unfortunately, due to limitations in the LB94 exchange–correlation potential employed for these B-spline calculations the scattering potential generated for the valence ionization was too attractive, and consequently the available B-spline model predictions do not cover this crucial first few eV above the HOMO ionization threshold.

In the case of the HOMO-1 orbital, as shown in Fig. 6.4, the new data in the 10–13 eV range display a reversed PECD asymmetry, as compared to the HOMO orbital, as the b_1 parameter flips sign. This experimentally observed behavior is well reproduced by the CMS-X α model calculations until, in the first eV above threshold, the model predicts a spurious unobserved swing in b_1 . Such low-energy electrons will, of course be especially sensitive to the subtleties of the molecular potential, making this region specially challenging for calculation. Nevertheless, the overall experiment/theory is satisfactory.

3.2. Fenchone data

In Fig. 6.5 and 6.6 we present photon energy dependent PECD data for the HOMO and the HOMO-1 orbital ionizations of fenchone, obtained following a similar procedure outlined for camphor. In particular, the same PEPICO filtering treatment, to decipher the HOMO and HOMO-1 contribution has been applied to fenchone since the two molecules exhibit the same fragmentation pattern with HOMO orbital ionization leaving an intact molecular ion, while the inner orbitals leads to the cation fragmentation.

Pre-alerted by previous reports^{25,37} that similarly sourced commercial fenchone samples may not be enantiopure, and by our own experience with camphor (above), we took additional steps to verify purity of our fenchone samples. The two different enantiomeric samples of fenchone were analyzed by GC × GC-TOFMS to obtain a precise value of the ee. The results of the chromatographic analysis are shown in Table 6.1. While the *S*-fenchone sample was perfectly enantiopure, the nominal *R*-fenchone sample, had an ee of $82.1 \pm 0.5\%$. Note that here the error bars are given by the 3σ statistical distribution analysis of the ee measurements over 10 injections into the GC × GC-TOFMS apparatus.

Table 6.1 GC × GC-TOFMS analysis of the supplied fenchone samples, along with the relative ee measured by PECD

Sample	GC×GC-TOFMS			PECD
	Enantiomeric excess (%)	Chemical purity (%) ^b	$ ee_R/ee_S $	$ ee_R/ee_S $
<i>R</i> (+)-Camphor	$+96.7 \pm 0.9^a$	> 99.9	0.979(9) ^a	0.97(2) ^c
<i>S</i> (-)-Camphor	-98.7 ± 0.1^a	> 99.9		
<i>R</i> (-)-Fenchone	$+82.1 \pm 0.5^a$	> 99.9	0.821(5) ^a	0.82(1) ^c
<i>S</i> (+)-Fenchone	-99.90 ± 0.03^a	> 99.9		

^a 3σ error bars. ^b Not considering non-volatile or solvent species. ^c 1σ error bars.

While treating the fenchone PECD data we could infer such an enantiopurity difference between the two samples of fenchone since at the three photon energies for which we had measured the PECD for both enantiomers (9.4, 15.5 and 18.6 eV) we observed systemically lower magnitudes for the b_1 values of the *R*-sample. The average ratio of the b_1 absolute values for the *R*-, *S*-enantiomer pairs at these three photon energies, weighted by the standard deviation, provides us with $ee[R]/ee[S]$ ratio of 0.82 ± 0.01 , as deduced from data presented in Fig. S6.1(b) (Sup. Inf.), in perfect agreement to the 0.821 ± 0.005 obtained from the GC × GC-TOFMS analysis (see Table 6.1). All the new data presented here in figures (and including Table S6.2, Sup. Inf.) have been corrected for the reduced sample enantiopurity, as was done earlier with our camphor data.

In a more extensive study using REMPI-PECD Kastner *et al.*⁵² have similarly demonstrated relative ee determinations with better than 1% uncertainty for fenchone mixtures spanning the full range (0–100%). However, as compared to this latter method, the i^2 PEPICO experiment provides the capability for ion mass-tagged PECD measurement. This allows for the simultaneous enantiomer specific analysis of multi-component mixtures which was proposed and demonstrated for a mixture of chiral and non-chiral species – spurious achiral decomposition product of alanine¹⁵ – and for prepared mixtures of chiral compounds by Rafie Fanood *et al.*³⁰ In that later case an ee measurement on a component present in chiral mixture was made with 20% uncertainty, the limitation being the restricted data rate in that work. The present result confirms that this is not a fundamental restriction and that mass-selected PECD can be used for analyzing gas phase enan-

tiomeric excess with precision in the $\pm 1\%$ range. This is not far below chiral chromatographic measurement precision and very competitive with other gas phase chiroptical methods for relative ee determination, such as the one based upon microwave three-wave mixing.^{33,53} Note that in addition, PECD-PICO may as well provide the chemical purity (by MS-TOF analysis of the coincident cation) at the same time as the relative enantiopurity for each mass-selected species (by PECD).

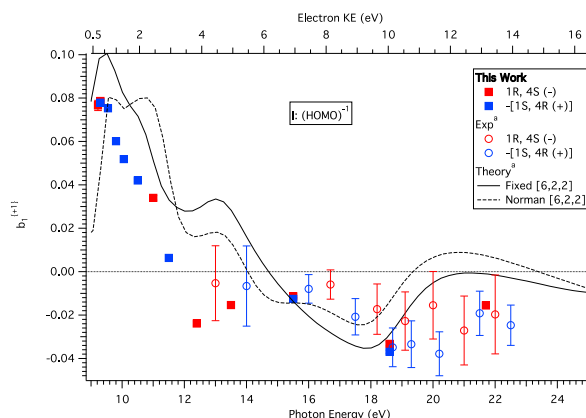


Figure 6.5 Mean chiral parameter (b_1) for ionization of the HOMO orbital of fenchone obtained at different photon energies. The values in this work are normalized to S_3 and to the absolute ee as provided by GC \times GC-TOFMS. The markers represent experimental measurements while the lines correspond to two different CMS- $X\alpha$ models. The S -enantiomer data have been negated. For some of the data points, the statistical error bars are not visible because they are smaller than the point width (see Table S6.2, Sup. Inf.).^a From ref. 40.

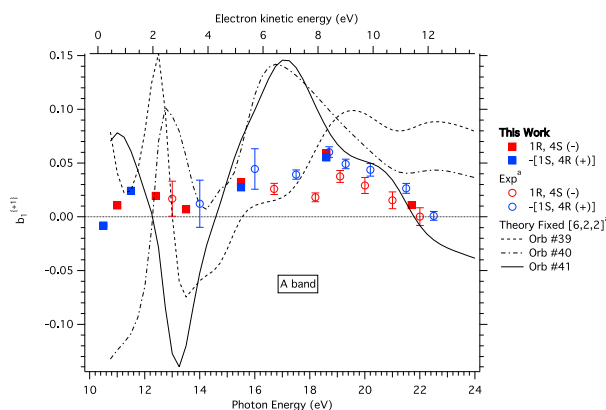


Figure 6.6 Mean chiral parameter (b_1) of the A band, corresponding to the binding energy region 10.05–10.61 eV of fenchone obtained at different photon energies. The data in this work are normalized to S_3 and to the absolute ee as provided by GC \times GC-TOFMS. The markers represent experimental measurements while the lines correspond to two different CMS- $X\alpha$ models. The S -enantiomer data have been negated. For some of the data points, the statistical error bars are not visible because they are smaller than the point width (see Table S6.2, Sup. Inf.).^a From ref. 40.

The new measurements provide b_1 data for fenchone below 12 eV photon energy, where previously none had been published. The CMS- $X\alpha$ modeling pre-

dicts for the HOMO orbital (Fig. 6.5) an intense asymmetry in the first few eV kinetic energy (KE) range, followed by a sign change of the asymmetry at increasing photon energies. These features are reproduced by the experimental data. However, and unlike the clearer case of camphor, the situation of the ‘‘HOMO–1’’ orbital in fenchone (Fig. 6.6) is more complex since due to our limited electron energy resolution and to the congestion of the PES, what we labeled as ‘‘HOMO–1’’ is in fact a mixture of several closely lying electronic orbitals such as the one labeled 39, 40 and 41 in ref. 40. In consequence the b_1 value observed in the A band (10.05–10.61 eV binding energy range) represents a blend of these individual ionizations. The comparison with the theoretical modelling of the various contributing orbitals is consequently not straightforward, although at high energy all calculations agree toward the same sign of b_1 , corresponding to the experimental observations *i.e.* fixing the absolute configuration.

3.3. Camphor/fenchone comparison: sensitivity to isomerism

The sensitivity of PECD to chemical substitution in oxirane derivatives has been studied in the past theoretically¹⁶ as well as experimentally¹⁷ and strong effects upon substitution were reported even when the initial orbital appeared identical for all molecules and not centered onto the substituted chemical group. Even more spectacular are effects, as seen here, concerning pure isomers with the same chemical formula and the same localization of the HOMO orbitals as shown in Fig. S6.2 (Sup. Inf.). In this respect, Powis *et al.*⁴⁰ already commented on the different PECD values measured on camphor and fenchone, albeit in an energy range restricted to electron KE 4.4 eV for the HOMO orbital. Here we can now extend this comparison to the threshold energy regions, which are known to be the most sensitive to the molecular potential.⁷ The HOMO orbital in both molecules is a localized 2p lone pair of the carbonyl oxygen (see Fig. S6.2, Sup. Inf.). The corresponding hole in the unrelaxed cation potentials used for the CMS- $X\alpha$ calculations is consequently similarly localized. The good CMS- $X\alpha$ theory/experiment agreement that is evident, even within a few eV of the ionization threshold (Fig. 6.3 and 6.5) is then possibly attributable to relative accuracy with which the atomic-site partitioning of the multiple scattering potential model can reproduce this potential. Supporting this, ionization of the highly localized C1s orbital by soft X-ray SR in early studies of camphor and fenchone is similarly well described by the CMS- $X\alpha$ calculations. In contrast, the more delocalized HOMO–1 ionizations give rise to PECD behavior which as discussed above is less well described by the CMS- $X\alpha$ calculations in the low energy region.

Turning to a broader comparison of these molecules, both are rigid single-conformer structures whose isomerism can be reduced to the shift of two methyl groups (see Scheme 1) from a top position to a side one, none of them being directly connected to the asymmetric carbons (C1, C4) nor to the carbonyl group—in other words the isomeric changes are remote from the chiral centers and the localized HOMO orbitals. Fig. 6.7 shows the PES and PECD obtained at photon energies of 10.3 and 10.5 eV for 1*R*,4*R*-(+)-camphor and 1*R*,4*S*-(-)-fenchone respectively. The two photon energies are close enough so that dynam-

ical effects would be marginal, so we can compare directly the data. The figure shows similar PES for both molecules, except for an energy shift due to the small ionization energy difference (fenchone is 180 meV lower than camphor^{40,51}). The PECD curves, however, show a striking difference with opposite sign for the same absolute configuration of the two molecules. Here, note that absolute configuration of the C4 asymmetric carbon is fixed by the rigid cycle; the change in labeling from 4*R* (camphor) to 4*S* (fenchone) is due to a change in priority assigned by the Cahn–Ingold–Prelog nomenclature rules rather than a rearranged molecular configuration. Therefore, the natural comparison is shown in Fig. 6.7 and Scheme 6.1, *i.e.* between 1*R*,4*R*-(+)-camphor and 1*R*,4*S*-(−)-fenchone. In this respect the quasi-mirroring of the PECD curves appearing in Fig. 6.3 is quite spectacular since it shows, that at 10.3/10.5 eV photon energy the two isomers behave nearly as opposite enantiomers while they have in fact the same absolute configuration!

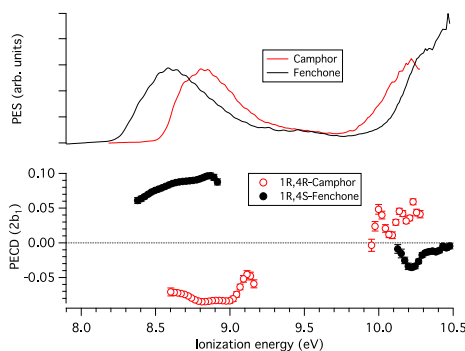
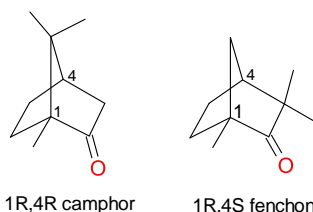


Figure 6.7 PES and PECD for *R*-camphor (red) and *R*-fenchone (black) recorded at $h\nu = 10.3$ eV and 10.5 eV respectively. The data have been normalized to S_3 and the absolute ee as provided by GC \times GC-TOFMS.



Scheme 6.1 Structure of the camphor and fenchone molecules

A marked difference between REMPI-PECD measurements on fenchone and camphor at a single given energy was also reported by Lux *et al.*,^{24,25} especially for the odd C_n ($n > 1$) parameters describing the high-order multi-photon electron angular distribution. Of course the role of the intermediate resonant state adds additional complexity to the interpretation of such results. Indeed, in the REMPI-PECD case, the origin may also lie in the resonant excited intermediate state which can also differently select, and align, the two isomers. Such a structure specificity in REMPI experiments is a well known process which has been recently applied to measure conformer-specific response in absorption CD.⁵⁴ In the pre-

sent work, the b_1 sign inversion makes this isomerism phenomenologically quite striking but its origin is also very clear being, in a one-photon ionization regime, purely due to the multiple scattering of the outgoing electron in the chiral potential of the molecule.

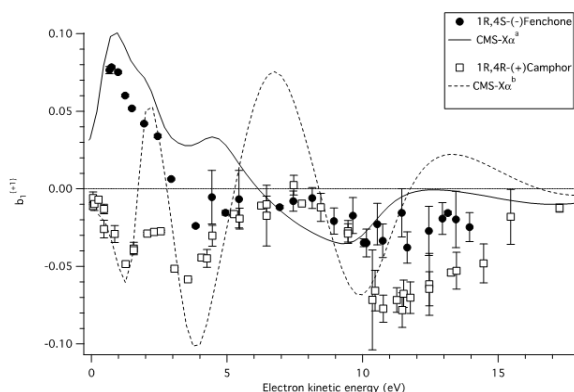


Figure 6.8 Chiral parameter ($b_1^{(+1)}$) for ionization from the HOMO orbital of *R*-fenphone and *R*-camphor (*S* enantiomers negated). The points represent all the available experimental data in the literature, including the present work, while the lines correspond to CMS- $X\alpha$ calculations. The data have been normalized to the absolute ee as provided by GC \times GC-TOFMS. ^a From ref. 40. ^b From ref. 36.

The comparison between *1R*-camphor and *1R*-fenphone PECD spectra is shown across the full photon energy range studied in Fig. 6.8 and 6.9 for respectively the first (HOMO–1 channel) and second PES bands. In a previous study carried out with photon energies above 13 eV,⁴⁰ a difference between the b_1 curve for the HOMO orbitals of fenphone versus camphor was observed mainly as a difference in amplitude in the 18–22 eV range, i.e. KE of B9–13 eV, corresponding to a shape resonance. These are known to be sensitive to molecular structures. Here (Fig. 6.8) the new PECD data show a far more striking signature of isomerism, in the KE = 0–5 eV region. Although it is also quite evident in the A band PECD (Fig. 6.9), this enhanced sensitivity is especially marked for electrons ejected from the HOMO orbital. There is a totally different behavior of the b_1 parameter, in terms of oscillation pattern and sign, for the same absolute configuration. With caveats discussed above, b_1 is very well reproduced by the CMS- $X\alpha$ modeling.

In a more general context the enhanced sensitivity of the chiral parameter b_1 to the molecular potential—and thus to effects such as isomerism, chemical substitution, conformers, vibrational dynamics, clustering—has been discussed previously^{3,6,7} and arises from the strong dependence on the phase shifts of the different outgoing partial waves that interfere in the scattering process.⁵ This dependency has been shown to be much more marked in the dichroic parameter b_1 than in the anisotropy parameter β or in the cross section,¹⁶ so that tiny changes in the molecular potential will have a much larger effect on this new observable (b_1) accessible on randomly-oriented chiral targets. In contrast to b_1 , numerical computations of the β parameter of fenphone⁴⁰ and camphor⁴¹ lead to very similar, non-distinguishable behaviour with photon energy. The present results also confirm

that the enhanced sensitivity of PECD to the molecular potential is especially marked for slow electrons as already pointed out in the case of conformers^{14,15} and dimers.¹⁸ Finally, this sensitivity to isomerism confirms also that PECD is a long-range effect, at least for slow electrons, since in the case of camphor the methyl groups are localized quite far from the site of the ionized orbital.

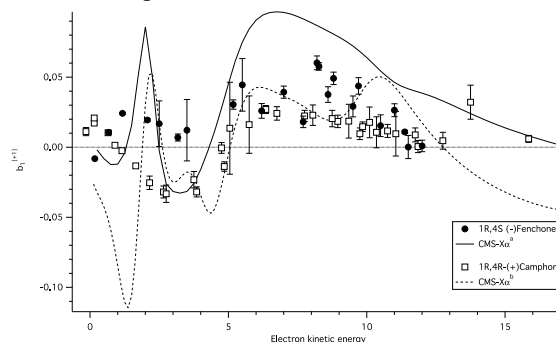


Figure 6.9 Chiral parameter (b_1) for the A region of *R*-fenphone and ionization from the HOMO-1 orbital of *R*-camphor. The points represent all the available experimental data in the literature (*S* enantiomers negated), including the present work, while the lines correspond to CMS- $X\alpha$ calculations. In the case of fenphone, an average theoretical curve of three orbitals (#39, #40 and #41) weighted by their cross sections is shown. The data have been normalized to the absolute ee as provided by GC \times GC-TOFMS. ^a From ref. 40. ^b From ref. 36.

Because PECD happens during the scattering process, it also observed upon inner-shell ionization from spherical orbitals, and some difference have also been found in the PECD from C1s ionization of camphor and fenphone.⁵⁵ However these differences, mainly observed along the shape resonance above 10 eV KE, are much smaller than what is observed here for outer valence shell electrons. This difference of sensitivity to isomerism between core and valence ionization, clearly observed experimentally and simulated by theory, is *a priori* unexpected since in both cases the initial orbital is very localized, and in the same area in the molecule.

In a broader context of chiroptical spectroscopies, note that the microwave 3 wave-mixing technique has been shown to be also sensitive to isomerism able for instance to distinguish menthone from isomenthone.⁵⁶

4. Conclusions and future prospects

In this work we have experimentally studied the chiroptical PECD effect induced by one-photon valence-shell ionization in the VUV range of randomly-oriented enantiomers. We provide b_1 values on showcase chiral isomers camphor and fenphone with high accuracy since sources of systematic errors such as imperfect CPL or enantiopurity have been taken into account. We expect these data to be useful for the development and benchmarking of new PECD experiments, especially those involving VUV radiation based upon HHG and probably in the near future Free Electron Lasers (FELs).

In addition, in the context of a growing development of VUV/XUV CPL sources from FELs,⁵⁷ HHG,^{29,58,59} plasma-based laser⁶⁰ and associated polarizing

optics,⁶¹ PECD could, like other dichroic effects,⁶² be used as a “molecular polarimeter template”, especially when either the β parameter is null or known, or when the linear polarization components of light (S_1 and S_2) are negligible, in which case accurate PECD benchmarking with the present data would allow the disentangling of the unpolarized component (S_4) from the circular one (S_3). This would be a complementary approach from the molecular polarimetry data deduced from molecular-frame photoelectron angular distributions (MF-PADs), recently demonstrated⁶³ and valid in the dissociative ionization continuum range of small molecules, *i.e.*, above 20 eV or so. We therefore hope in this context, to contribute to the expansion of the active field of polarization dependent short wavelength photodynamics with short pulses.

In the more fundamental context of the understanding of the PECD process itself, we found a remarkable agreement between the experimental data and the CMS- $X\alpha$ modeling of the HOMO orbital of both camphor and fenchone, even in the challenging low KE energy range. On the other hand some clear discrepancies remain. Owing to the size and lack of symmetry simplifications in these molecules, current methods rely on solving independent electron dynamics in single reference derived potential (either semi-empirical as in CMS- $X\alpha$ or DFT as in the B-spline method).⁴¹ Future developments are likely to introduce electron correlations into the $N - 1$ electron potential model, and the current experimental data could serve as a benchmark for judging performance of such developments. Equally, there is accumulating evidence of the need to take fuller account of vibrational motions in refining out understanding of PECD,²¹ something which is absent from the current capabilities of fixed-geometry computations.

Besides, the accuracy of the data we provide is such that limited departure from perfect enantiopurity in the samples we purchased could be detected, by the non-perfect mirroring of the R/S PECD data. The benchmarking versus a conventional chromatographic analytical method, highlights the interest and high accuracy, in the % range, of PECD as a precise enantiomeric analytical tool in the gas phase. Especially when combined in with TOF mass spectrometry of the photoions, recorded in coincidence with the photoelectrons, via the so-called PECD-PICO scheme, we stress the ability to analyze a mixture of compounds simultaneously and to provide highly accurate relative ee measurement of each of these compounds, now with significantly improved accuracy over the first demonstrations of this capability.^{15,30} As compared to the well-established GC type of technique, PECD is a direct method with no derivatization, nor use of reagents, directly applicable in the gas phase, and which provides additional electronic information, as a multi-dimensional chiroptical probe (photon energy, electron energy, coincident ion mass). Also as compared to the REMPI-PECD-PICO technique, there is no need here, in the VUV one-photon PECD-PICO approach for any chromophore absorbing in the UV range, so that the method is genuinely universal. We intend therefore in the near future to apply such a PECD-PICO scheme to disentangle the enantiomeric composition of a complex mixture of samples.

Finally, our experimental data show a very striking signature of the profound sensitivity of PECD to isomerism with large and opposite asymmetries measured on the HOMO orbital of the same enantiomers of camphor and fen-

chone. This feature, especially marked for slow electrons, is very well reproduced by theory, while the same theory shows that the two isomers have similar anisotropy parameter β . This ability of PECD could be applied in the future in the field of gas phase chemical reactivity, in order to probe and disentangle isomers in chemical reactions involving chiral products, as for instance in combustion of bio-fuels. PECD, with its exquisite sensitivity to isomers would be, in this context of gas phase chemical reactions probed by photoionization, an additional observable to products appearance energies,⁶⁴ or even to the full PES of mass-selected species.^{65,66}

References

- 1 B. Ritchie, *Phys. Rev. A: At., Mol., Opt. Phys.*, 1976, **13**, 1411–1415.
- 2 I. Powis, *J. Phys. Chem. A*, 2000, **104**, 878–882.
- 3 I. Powis, *J. Chem. Phys.*, 2000, **112**, 301–310.
- 4 N. Böwering, T. Lischke, B. Schmidtke, N. Müller, T. Khalil and U. Heinzmann, *Phys. Rev. Lett.*, 2001, **86**, 1187–1190.
- 5 I. Powis, *Adv. Chem. Phys.*, 2008, **138**, 267–329.
- 6 L. Nahon and I. Powis, in *Chiral recognition in the gas phase*, ed. A. Zehnacker, CRC Press – Taylor & Francis, Boca Raton, 2010, pp. 1–26.
- 7 L. Nahon, G. A. Garcia and I. Powis, *J. Electron Spectrosc. Relat. Phenom.*, 2015, **204**, 322–334.
- 8 N. Berova, K. Nakanishi and R. Woody, *Circular dichroism principles and applications*, Wiley-VCH, New York, 2nd edn, 2000.
- 9 S. Stranges, S. Turchini, M. Alagia, G. Alberti, G. Contini, P. Decleva, G. Fronzoni, M. Stener, N. Zema and T. Prospero, *J. Chem. Phys.*, 2005, **122**, 244303.
- 10 D. Catone, M. Stener, P. Decleva, G. Contini, N. Zema, T. Prospero, V. Feyrer, K. C. Prince and S. Turchini, *Phys. Rev. Lett.*, 2012, **108**, 083001.
- 11 S. Turchini, D. Catone, G. Contini, N. Zema, S. Irrera, M. Stener, D. Di Tommaso, P. Decleva and T. Prospero, *ChemPhysChem*, 2009, **10**, 1839–1846.
- 12 S. Turchini, D. Catone, N. Zema, G. Contini, T. Prospero, P. Decleva, M. Stener, F. Rondino, S. Piccirillo, K. C. Prince and M. Speranza, *ChemPhysChem*, 2013, **14**, 1723–1732.
- 13 G. Garcia, L. Nahon, C. J. Harding and I. Powis, *Phys. Chem. Chem. Phys.*, 2008, **10**, 1628–1639.
- 14 G. Garcia, H. Soldi-Lose, L. Nahon and I. Powis, *J. Phys. Chem. A*, 2010, **114**, 847.
- 15 M. Tia, B. Cunha de Miranda, S. Daly, F. Gaie-Levrel, G. A. Garcia, L. Nahon and I. Powis, *J. Phys. Chem. A*, 2014, **118**, 2765–2779.
- 16 M. Stener, G. Fronzoni, D. Di Tommaso and P. Decleva, *J. Chem. Phys.*, 2004, **120**, 3284–3296.
- 17 G. A. Garcia, H. Dossmann, L. Nahon, S. Daly and I. Powis, *Phys. Chem. Chem. Phys.*, 2014, **16**, 16214–16224.
- 18 L. Nahon, G. Garcia, H. Soldi-Lose, S. Daly and I. Powis, *Phys. Rev. A: At., Mol., Opt. Phys.*, 2010, **82**, 032514.
- 19 S. Daly, I. Powis, G. A. Garcia, H. Soldi-Lose and L. Nahon, *J. Chem. Phys.*, 2011, **134**, 064306.
- 20 I. Powis, S. Daly, M. Tia, B. Cunha de Miranda, G. Garcia and L. Nahon, *Phys. Chem. Chem. Phys.*, 2014, **16**, 467–476.
- 21 G. Garcia, L. Nahon, S. Daly and I. Powis, *Nat. Commun.*, 2013, **4**, 2132.
- 22 I. Powis, *J. Chem. Phys.*, 2014, **140**, 111103.
- 23 M. H. M. Janssen and I. Powis, *Phys. Chem. Chem. Phys.*, 2014, **16**, 856–871.
- 24 C. Lux, M. Wollenhaupt, T. Bolze, Q. Q. Liang, J. Kohler, C. Sarpe and T. Baumert, *Angew. Chem., Int. Ed.*, 2012, **51**, 5001–5005.
- 25 C. Lux, M. Wollenhaupt, C. Sarpe and T. Baumert, *ChemPhysChem*, 2015, **16**, 115–137.

- 26 C. S. Lehmann, N. B. Ram, I. Powis and M. H. M. Janssen, *J. Chem. Phys.*, 2013, **139**, 234307.
- 27 M. M. Rafiee Fanood, I. Powis and M. H. M. Janssen, *J. Phys. Chem. A*, 2014, **118**, 11541–11546.
- 28 M. M. Rafiee Fanood, M. H. M. Janssen and I. Powis, *Phys. Chem. Chem. Phys.*, 2015, **17**, 8614–8617.
- 29 A. Ferré, C. Handchin, M. Dumergue, F. Burgy, A. Comby, D. Descamps, B. Fabre, G. A. Garcia, R. Géneaux, L. Merceron, E. Mével, L. Nahon, S. Petit, B. Pans, D. Staeder, S. Weber, T. Ruchon, V. Blanchet and Y. Mairesse, *Nat. Photonics*, 2015, **9**, 93–98.
- 30 M. M. Fanood, N. B. Ram, C. S. Lehmann, I. Powis and M. H. M. Janssen, *Nat. Commun.*, 2015, **6**, 7511.
- 31 D. Patterson, M. Schnell and J. M. Doyle, *Nature*, 2013, **497**, 475–477.
- 32 D. Patterson and J. M. Doyle, *Phys. Rev. Lett.*, 2013, **111**, 023008.
- 33 V. A. Shubert, D. Schmitz, D. Patterson, J. M. Doyle and M. Schnell, *Angew. Chem., Int. Ed.*, 2014, **53**, 1152–1155.
- 34 G. A. Garcia, L. Nahon, M. Lebech, J. C. Houver, D. Doweck and I. Powis, *J. Chem. Phys.*, 2003, **119**, 8781–8784.
- 35 T. Lischke, N. Böwering, B. Schmidtke, N. Müller, T. Khalil and U. Heinzmann, *Phys. Rev. A: At., Mol., Opt. Phys.*, 2004, **70**, 022507.
- 36 L. Nahon, G. A. Garcia, C. J. Harding, E. A. Mikajlo and I. Powis, *J. Chem. Phys.*, 2006, **125**, 114309.
- 37 C. Lux, A. Senfleben, C. Sarpe, M. Wollenhaupt and T. Baumert, *J. Phys. B: At., Mol. Opt. Phys.*, 2016, **49**, 02LT01.
- 38 R. Cireasa, A. E. Boguslavskiy, B. Pons, M. C. H. Wong, D. Descamps, S. Petit, H. Ruf, N. Thiré, A. Ferré, J. Suarez, J. Higuier, B. E. Schmidt, A. F. Alharbi, F. Légraré, V. Blanchet, B. Fabre, S. Patchkovskii, O. Smirnova, Y. Mairesse and V. R. Bhardwaj, *Nat. Phys.*, 2015, **11**, 654–658.
- 39 C. Loge and U. Boesl, *ChemPhysChem*, 2011, **12**, 1940–1947.
- 40 I. Powis, C. J. Harding, G. Garcia and L. Nahon, *ChemPhysChem*, 2008, **9**, 475–483.
- 41 M. Stener, D. D. Tommaso, G. Fronzoni, P. Decleva and I. Powis, *J. Chem. Phys.*, 2006, **124**, 024326.
- 42 I. Dreissigacker and M. Lein, *Phys. Rev. A: At., Mol., Opt. Phys.*, 2014, **89**, 053406.
- 43 A. N. Artemyev, A. D. Muller, D. Hochstuhl and P. V. Demekhin, *J. Chem. Phys.*, 2015, **142**, 244105.
- 44 C. Meinert and U. J. Meierhenrich, *Angew. Chem., Int. Ed.*, 2012, **51**, 10460–10470.
- 45 X. Tang, G. Garcia, G. Jean-Francois and L. Nahon, *Rev. Sci. Instrum.*, 2015, **86**, 123108.
- 46 L. Nahon, N. de Oliveira, G. Garcia, J. F. Gil, B. Pilette, O. Marcouille, B. Lagarde and F. Polack, *J. Synchrotron Radiat.*, 2012, **19**, 508–520.
- 47 B. Mercier, M. Compin, C. Prevost, G. Bellec, R. Thissen, O. Dutuit and L. Nahon, *J. Vac. Sci. Technol., A*, 2000, **18**, 2533–2541.
- 48 L. Nahon and C. Alcaraz, *Appl. Opt.*, 2004, **43**, 1024–1037.

- 49 G. Garcia, B. Cunha de Miranda, M. Tia, S. Daly and L. Nahon, *Rev. Sci. Instrum.*, 2013, **84**, 053112.
- 50 G. A. Garcia, L. Nahon and I. Powis, *Rev. Sci. Instrum.*, 2004, **75**, 4989–4996.
- 51 E. E. Rennie, I. Powis, U. Hergenhahn, O. Kugeler, G. Garcia, T. Lischke and S. Marburger, *J. Electron Spectrosc. Relat. Phenom.*, 2002, **125**, 197–203.
- 52 A. Kastner, C. Lux, T. Ring, S. Zullighoven, C. Sarpe, A. Senftleben and T. Baumert, *ChemPhysChem*, 2016, DOI: 10.1002/cphc.201501067.
- 53 D. Patterson and M. Schnell, *Phys. Chem. Chem. Phys.*, 2014, **16**, 11114–11123.
- 54 A. Hong, C. M. Choi, H. J. Eun, C. Jeong, J. Heo and N. J. Kim, *Angew. Chem., Int. Ed.*, 2014, **53**, 7805–7808.
- 55 V. Ulrich, S. Barth, S. Joshi, U. Hergenhahn, E. Mikajlo, C. J. Harding and I. Powis, *J. Phys. Chem. A*, 2008, **112**, 3544–3549.
- 56 V. Alvin Shubert, D. Schmitz and M. Schnell, *J. Mol. Spectrosc.*, 2014, **300**, 31–36.
- 57 E. Allaria, B. Diviacco, C. Callegari, P. Finetti, B. Mahieu, J. Vieffhaus, M. Zangrando, G. De Ninno, G. Lambert, E. Ferrari, J. Buck, M. Ilchen, B. Vodungbo, N. Mahne, C. Svetina, C. Spezzani, S. Di Mitri, G. Penco, M. Trovó, W. M. Fawley, P. R. Rebernik, D. Gauthier, C. Grazioli, M. Coreno, B. Ressel, A. Kivimäki, T. Mazza, L. Glaser, F. Scholz, J. Seltmann, P. Gessler, J. Grünert, A. De Fanis, M. Meyer, A. Knie, S. P. Moeller, L. Raimondi, F. Capotondi, E. Pedersoli, O. Plekan, M. B. Danailov, A. Demidovich, I. Nikolov, A. Abrami, J. Gautier, J. Lüning, P. Zeitoun and L. Giannessi, *Phys. Rev. X*, 2014, **4**, 041040.
- 58 D. D. Hickstein, F. J. Dollar, P. Grychtol, J. L. Ellis, R. Knut, C. Hernández-García, D. Zusin, C. Gentry, J. M. Shaw, T. Fan, K. M. Dorney, A. Becker, A. Jaroń-Becker, H. C. Kapteyn, M. M. Murnane and C. G. Durfee, *Nat. Photonics*, 2015, **9**, 743–750.
- 59 O. Kfir, P. Grychtol, E. Turgut, R. Knut, D. Zusin, D. Popmintchev, T. Popmintchev, H. Nembach, J. M. Shaw, A. Fleischer, H. Kapteyn, M. Murnane and O. Cohen, *Nat. Photonics*, 2014, **9**, 99–105.
- 60 A. Depresseux, E. Oliva, J. Gautier, F. Tissandier, G. Lambert, B. Vodungbo, J. P. Goddet, A. Tafzi, J. Nejd, M. Kozlova, G. Maynard, H. T. Kim, K. T. Phuoc, A. Rousse, P. Zeitoun and S. Sebban, *Phys. Rev. Lett.*, 2015, **115**, 083901.
- 61 J. Schmidt, A. Guggenmos, M. Hofstetter, S. H. Chew and U. Kleineberg, *Opt. Express*, 2015, **23**, 33564.
- 62 T. Mazza, M. Ilchen, A. J. Rafipoor, C. Callegari, P. Finetti, O. Plekan, K. C. Prince, R. Richter, M. B. Danailov, A. Demidovich, G. De Ninno, C. Grazioli, R. Ivanov, N. Mahne, L. Raimondi, C. Svetina, L. Avaldi, P. Bolognesi, M. Coreno, P. O’Keeffe, M. Di Fraia, M. Devetta, Y. Ovcharenko, T. Moller, V. Lyamayev, F. Stienkemeier, S. Dusterer, K. Ueda, J. T. Costello, A. K. Kazansky, N. M. Kabachnik and M. Meyer, *Nat. Commun.*, 2014, **5**, 3648.
- 63 K. Veyrinas, C. Elkharrat, S. Marggi Poullain, N. Saquet, D. Doweck, R. R. Lucchese, G. A. Garcia and L. Nahon, *Phys. Rev. A: At., Mol., Opt. Phys.*, 2013, **88**, 063411.

- 64 D. L. Osborn, P. Zou, H. Johnsen, C. C. Hayden, C. A. Taatjes, V. D. Knyazev, S. W. North, D. S. Peterka, M. Ahmed and S. R. Leone, *Rev. Sci. Instrum.*, 2008, **79**, 104103.
- 65 A. Bodi, P. Hemberger, D. L. Osborn and B. Sztáray, *J. Phys. Chem. Lett.*, 2013, **4**, 2948–2952.
- 66 J. Kruger, G. A. Garcia, D. Felsmann, K. Moshhammer, A. Lackner, A. Brockhinke, L. Nahon and K. Kohse-Hoinghaus, *Phys. Chem. Chem. Phys.*, 2014, **16**, 22791–22804

Supplementary information

Table S6.1: Compilation of literature values, and those obtained in this work of the mean $b_1^{(+1)}$ values for ionization from the HOMO and HOMO-1 orbitals of 1*R*,4*R*-(+)-camphor. The Nahon *et al.* corresponds to Ref.¹ and Lischke *et al.* to Ref.². The table contains also the negated *S* enantiomer data. At photon energies where several b_1 values have been measured at the same photon energy and with the same experimental setup, the b_1 is presented as the weighted average of these measurements plus or minus its standard deviation. In this work, the binding energy region of the HOMO-1 orbital has been chosen as 10.15 ± 0.15 eV, whereas Lischke *et al.* use 10.45 eV. The values in this work have been normalized by S_3 and the e.e. measured by GC x GC-TOFMS.

HOMO			HOMO-1		
$b_1^{(+1)}$	hν	Ref.	$b_1^{(+1)}$	hν	Ref.
-0.011 ± 0.002	8.8	This Work	0.011 ± 0.003	10	Nahon et al.
-0.006 ± 0.004	8.8	Nahon et al.	0.0172 ± 0.0009	10.3	This Work
-0.010 ± 0.004	8.85	Nahon et al.	0.0209 ± 0.0009	10.3	Nahon et al.
-0.007 ± 0.002	9	Nahon et al.	0.010 ± 0.001	10.8	This Work
-0.013 ± 0.003	9.2	Garcia et al.	0.001 ± 0.001	11.05	This Work
-0.026 ± 0.006	9.2	Nahon et al.	-0.0024 ± 0.0009	11.3	This Work
-0.029 ± 0.005	9.6	Nahon et al.	-0.013 ± 0.001	11.8	This Work
-0.049 ± 0.001	10	Nahon et al.	-0.025 ± 0.005	12.3	This Work
-0.038 ± 0.004	10.3	Nahon et al.	-0.032 ± 0.004	12.8	This Work
-0.0396 ± 0.0007	10.3	This Work	-0.033 ± 0.006	13.2	Lischke et al.
-0.0289 ± 0.0009	10.8	This Work	-0.032 ± 0.004	14	This Work
-0.0278 ± 0.0007	11.05	This Work	-0.023 ± 0.006	14.2	Lischke et al.
-0.0273 ± 0.0007	11.3	This Work	-0.014 ± 0.003	15	This Work
-0.0515 ± 0.0009	11.8	This Work	0.01 ± 0.03	15.2	Nahon et al.
-0.0584 ± 0.0003	12.3	This Work	-0.001 ± 0.004	15.2	Lischke et al.
-0.044 ± 0.002	12.8	This Work	0.02 ± 0.02	16.2	Lischke et al.
-0.045 ± 0.006	13	Nahon et al.	0.027 ± 0.003	16.5	This Work
-0.030 ± 0.007	13.2	Lischke et al.	0.024 ± 0.005	17.2	Lischke et al.
-0.016 ± 0.001	14	This Work	0.022 ± 0.004	18.2	Lischke et al.
-0.019 ± 0.007	14.2	Lischke et al.	0.023 ± 0.007	18.2	Nahon et al.
-0.011 ± 0.001	15	This Work	0.018 ± 0.004	19.1	Nahon et al.
-0.02 ± 0.02	15.2	Nahon et al.	0.020 ± 0.006	19.2	Lischke et al.
-0.010 ± 0.005	15.2	Lischke et al.	0.02 ± 0.01	19.5	Nahon et al.
0.002 ± 0.006	16.2	Lischke et al.	0.015 ± 0.003	20	Nahon et al.
-0.0095 ± 0.0008	16.5	This Work	0.010 ± 0.004	20.2	Lischke et al.
-0.012 ± 0.009	17.2	Lischke et al.	0.02 ± 0.01	20.25	Nahon et al.

-0.027 ± 0.007	18.2	Nahon et al.	0.01 ± 0.01	20.5	Nahon et al.
-0.029 ± 0.006	18.2	Lischke et al.	0.01 ± 0.02	21.2	Nahon et al.
-0.07 ± 0.03	19.1	Nahon et al.	0.012 ± 0.005	21.2	Lischke et al.
-0.07 ± 0.01	19.2	Lischke et al.	0.000 ± 0.004	22	Nahon et al.
-0.077 ± 0.009	19.5	Nahon et al.	0.009 ± 0.005	22.2	Lischke et al.
-0.072 ± 0.008	20	Nahon et al.	0.005 ± 0.006	23.2	Lischke et al.
-0.08 ± 0.01	20.2	Lischke et al.	0.03 ± 0.01	24.2	Lischke et al.
-0.068 ± 0.009	20.25	Nahon et al.	0.006 ± 0.002	26	Nahon et al.
-0.07 ± 0.01	20.5	Nahon et al.			
-0.06 ± 0.02	21.2	Nahon et al.			
-0.06 ± 0.01	21.2	Lischke et al.			
-0.054 ± 0.002	22	Nahon et al.			
-0.05 ± 0.01	22.2	Lischke et al.			
-0.05 ± 0.01	23.2	Lischke et al.			
-0.02 ± 0.02	24.2	Lischke et al.			
-0.012 ± 0.003	26	Nahon et al.			

Table S6.2: Compilation of literature values, and those obtained in this work of the mean b_1^{+1} values for ionization from the HOMO orbital and A band of 1*R*,4*S*-(-)-fenchone. The Powis *et al.* corresponds to Ref.³. The table contains also the negated *S* enantiomer data. At photon energies where several b_1 values have been measured at the same photon energy and with the same experimental setup, the b_1 is presented as the weighted average of these measurements plus or minus its standard deviation. In this work, the binding energy boundaries of the A region have been chosen as 10.05–10.61 eV, whereas Powis *et al.* used 9.9–11.0 eV. The values in this work have been normalized by S_3 and the e.e. measured by GC x GC-TOFMS.

HOMO			A band		
$b_1^{(+1)}$	$h\nu$	Ref.	$b_1^{(+1)}$	$h\nu$	Ref.
0.077 ± 0.002	9.22	This Work	-0.0082 ± 0.0007	10.5	This Work
0.078 ± 0.001	9.3	This Work	0.011 ± 0.001	11	This Work
0.0753 ± 0.0009	9.54	This Work	0.0242 ± 0.0007	11.5	This Work
0.0601 ± 0.0007	9.8	This Work	0.019 ± 0.001	12.4	This Work
0.0519 ± 0.0006	10.05	This Work	0.02 ± 0.02	13	Powis et al.
0.0420 ± 0.0006	10.5	This Work	0.007 ± 0.003	13.5	This Work
0.034 ± 0.001	11	This Work	0.01 ± 0.02	14	Powis et al.
0.0063 ± 0.0006	11.5	This Work	0.031 ± 0.003	15.5	This Work
-0.0239 ± 0.0008	12.4	This Work	0.04 ± 0.02	16	Powis et al.
-0.01 ± 0.02	13	Powis et al.	0.026 ± 0.005	16.7	Powis et al.
-0.015 ± 0.001	13.5	This Work	0.039 ± 0.004	17.5	Powis et al.

-0.01 ± 0.02	14	Powis et al.	0.018 ± 0.004	18.2	Powis et al.
-0.0118 ± 0.0009	15.5	This Work	0.058 ± 0.003	18.6	This Work
-0.008 ± 0.007	16	Powis et al.	0.060 ± 0.005	18.7	Powis et al.
-0.006 ± 0.007	16.7	Powis et al.	0.038 ± 0.006	19.1	Powis et al.
-0.021 ± 0.008	17.5	Powis et al.	0.049 ± 0.004	19.3	Powis et al.
-0.02 ± 0.01	18.2	Powis et al.	0.029 ± 0.007	20	Powis et al.
-0.035 ± 0.003	18.6	This Work	0.044 ± 0.006	20.2	Powis et al.
-0.035 ± 0.009	18.7	Powis et al.	0.015 ± 0.008	21	Powis et al.
-0.02 ± 0.01	19.1	Powis et al.	0.026 ± 0.005	21.5	Powis et al.
-0.03 ± 0.01	19.3	Powis et al.	0.011 ± 0.001	21.7	This Work
-0.02 ± 0.02	20	Powis et al.	0.000 ± 0.008	22	Powis et al.
-0.04 ± 0.01	20.2	Powis et al.	0.001 ± 0.004	22.5	Powis et al.
-0.03 ± 0.02	21	Powis et al.			
-0.02 ± 0.01	21.5	Powis et al.			
-0.016 ± 0.001	21.7	This Work			
-0.02 ± 0.02	22	Powis et al.			
-0.025 ± 0.009	22.5	Powis et al.			

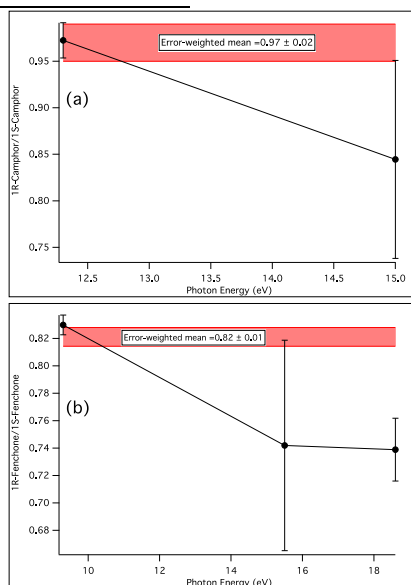


Figure S6.1: Observed PECD ratio for (a) camphor and (b) fenchone at the photon energies where both enantiomers were measured. The error-weighted mean values are given as red transparent band. Note that the error bars will increase for small absolute values of b_1 , and for increasing photon energies where the HOMO relative cross-section is smaller, so that the more precise values are generally obtained at low photon energies.

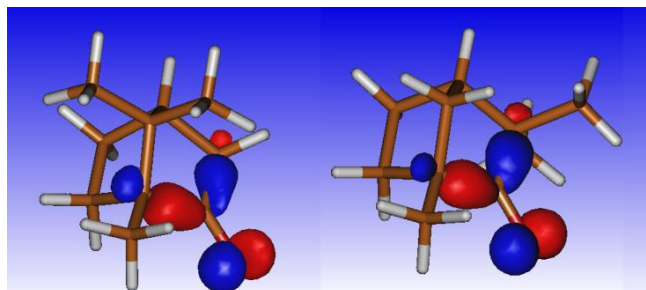


Figure S6.2: Computed (HF/6-31G**) isosurface plots showing the electronic density for the HOMO orbitals of 1*R*,4*R*-camphor (left) and 1*R*,4*S*-fenchone (right).

References

- 1 L. Nahon, G. A. Garcia, C. J. Harding, E. A. Mikajlo and I. Powis, *J. Chem. Phys.*, 2006, **125**, 114309.
- 2 T. Lischke, N. Böwering, B. Schmidtke, N. Muller, T. Khalil and U. Heinzmann, *Phys. Rev. A*, 2004, **70**, 022507.
- 3 I. Powis, C. J. Harding, G. Garcia and L. Nahon, *ChemPhysChem*, 2008, **9**, 475-483.

CONCLUSIONS (FR)

Il existe deux grandes catégories de théories expliquant l'origine de l'homochiralité du vivant: les théories *déterministes* et les théories *basées sur le hasard*. Selon les premières l'asymétrie des biomolécules serait liée soit à une asymétrie interne (différence énergétique entre deux énantiomères gouvernée par la violation de parité dans l'interaction faible) soit à l'influence de forces chirales comme une lumière circulairement polarisée (LCP) ou un champ magnétique collinéaire avec le vecteur de propagation d'un faisceau lumineux. Les théories basées sur le hasard, au contraire, expliquent l'origine d'homochiralité par une brisure spontanée de symétrie, conduisant, par le simple fruit du hasard, à un type d'énantiomères qui sont prédominants dans la biosphère,

Les théories déterministes, contrairement aux théories « aléatoires » peuvent être testées expérimentalement, notamment en terme de reproductibilité. Parmi celles-ci, seule l'influence de forces chirales peut être mesurée par les instruments analytiques tandis que la violation de parité au niveau moléculaire est trop ténue pour être détectée par les techniques spectroscopiques existantes. Ensuite, si on compare les deux forces la LCP et un champ magnétique associé à un rayonnement non polarisé, on s'aperçoit que les deux sont présentes dans l'espace mais seule la LCP est en mesure d'induire les excès énantiomériques de quelques pourcents.

Les travaux présentés dans cette thèse ont été menés dans le contexte de la recherche de l'origine de l'homochiralité du vivant, où les interactions LCP – molécules chirales ont joué le rôle central dans la brisure de la symétrie. Dans le cadre de ce projet, les glaces interstellaires simulées au laboratoire ainsi que les échantillons extraterrestres ont été soumis à l'analyse par chromatographie en phase gazeuse bidimensionnelle. La méthode analytique pour la résolution et la quantification d'énantiomères d'acides aminés a été présentée. Les études ont établi un domaine de travail linéaire de la méthode ainsi qu'une limite de détection et de quantification. Finalement, les avantages de la chromatographie bidimensionnelle ont été démontrés sur l'exemple de l'extrait de la météorite de Murchison où les acides aminés extraterrestres ont été séparés et les excès énantiomériques ont été précisément quantifiés. Un excès de molécules gauches dans l'échantillon de météorite Murchison suggère que la brisure de symétrie pourrait s'être produite dans l'espace par interactions avec de la LCP.

Ensuite une série d'analyses a été effectuée pour identifier, des aldéhydes et des sucres dans des analogues de glace cométaire. Une méthode analytique pour cibler les espèces d'aldéhydes a montré la présence de 6 aldéhydes dans la glace interstellaire. Parmi eux, le glycolaldehyde et le glyceraldehyde - deux espèces considérées comme les intermédiaires-clés dans la chimie prébiotiques et plus précisément dans les premières étapes de la synthèse de ribonucléotides. De plus, la présence d'ammoniaque dans des mélanges de glace apparaît essentielle pour la production et/ou récupération de ces aldéhydes. Le mécanisme de ce phénomène n'est pas encore bien compris, mais ce fait est surprenant car les produits finaux sont exempts d'azote.

La détection de glycéraldéhyde dans les analogues de glaces est de toute première importance car on pense que le glycéraldéhyde pourrait dicter la stéréochimie de synthèse des ribonucléotides et donc aurait pu avoir imposé la chiralité spécifique de l'ARN et de l'ADN. La photolyse asymétrique du glycéraldéhyde est peut-être à la base de l'asymétrie du support génétique. Par conséquent, les études en cours se focalisent sur l'enregistrement de spectres de CD et d'anisotropie du glycéraldéhyde à l'état solide. Ces spectres seront par la suite utilisés pour guider le choix de la longueur d'irradiation en lumière polarisée circulairement. Nous anticipons que la photolyse asymétrique du glycéraldéhyde conduira à une plus grande asymétrie que celle obtenue sur les acides aminés. De plus les *ee* attendus devraient avoir un signe inverse pour une hélicité donnée de la lumière à des longueurs d'onde données d'intérêt astrophysique.

L'analyse ultérieure a démontré avec succès qu'une large gamme de sucres peut être formé à partir d'un mélange de gaz H₂O, CH₃OH, et NH₃ dans des conditions simulant la formation de glaces interstellaires. Parmi les sucres détectés on trouve le ribose – un élément important pour comprendre l'origine de l'ARN et donc les origines de la vie et de la transmission de l'information génétique. La présence de divers sucres ainsi que du hydroxyméthylglycérol et du hydroxyméthylthréitol indique un mécanisme de réaction type formose. Dans cette étude, aucune énantioséparation des sucres n'a été effectuée, et du coup il n'y a pas encore eu d'expériences correspondantes de photolyse asymétrique. Dans le prolongement de ce travail, il est envisagé à l'avenir de développer une procédure analytique de séparation d'énantiomère, par chromatographie multidimensionnelle en phase gaz, afin de séparer les isomères optiques d'aldoses. Une telle méthode permettrait de détecter de faibles *ee* dans des analogues de glaces interstellaires et/ou des échantillons à l'état solide irradiés en LPC sur DESIRS. Comprendre la photochimie asymétrique du ribose et d'autres sucres est nécessaire pour expliquer l'asymétrie des molécules portant l'information génétique.

Par conséquent, des expériences de formation/irradiation en LPC de glaces *in situ* ont été programmées. Nous nous attendons à former et détecter une large gamme de molécules chirales prébiotiques dont des sucres, aldéhydes et acides aminés. La formation de glace *in-situ* permet de produire un résidu plus pur que par la méthode de production *ex-situ* (avec une lampe de laboratoire) suivie d'irradiation LPC. Ceci devrait conduire à des mesures fiables d'*ee* pour toutes les molécules chirales détectées dans la glace. Idéalement les acides aminés et les sucres, incluant le glycéraldéhyde, devraient montrer des énantio-enrichissements de signe opposé.

Les résultats obtenus et présentés au travers de cette thèse renforcent le scénario photochimique pour expliquer la brisure de symétrie chirale. Ils montrent que toutes les briques élémentaires constituant les protéines et acides nucléiques peuvent être formées dans l'espace dans des conditions extrêmes, sans doute via une chimie radicalaire. Ceci est en pleine cohérence avec un apport de matière organique sur terre via des météorites, comètes et/ou poussières interstellaires. La découverte du ribose produit probablement via une réaction de type formose, ouvre de nouvelles voies de recherches sur l'asymétrie induite par LPC sur les sucres.

La détection d'aldéhydes dans des analogues de glace interstellaire est bien corrélée avec les résultats de l'instrument COSAC de la mission Rosetta, avec lequel de l'acétaldéhyde, du propionaldéhyde, et du glycolaldéhyde furent aussi détectés. Ces données valident le lien direct entre les résultats des expériences de simulation au laboratoire et la composition "réelle" de la matière cométaire. Les missions spatiales futures pourront aussi bénéficier des procédures analytiques développées pour l'analyse énantiosélective d'échantillons extra-terrestres. De même que les acides amines simples furent d'abord détectés dans des analogues de glaces interstellaires avant d'être probablement identifiés dans l'espace, il est fort possible que de futures missions spatiales parviennent à détecter du glyceraldéhyde.

In fine, les résultats présentés dans ce manuscrit peuvent avoir des applications dans les domaines de l'astrobiologie, de la photochimie et des méthodologies analytiques.

Finalement, les propriétés chiroptiques de molécules chirales comme le camphre et le fenchone, isomères l'un de l'autre, ont été étudiées par double imagerie de coïncidence photoélectron/photoion (i^2 PEPICO). Outre la forte sensibilité à l'isomérisation, nous avons établi que la spectroscopie PECD peut être aussi précise pour les mesures d'excès énantiomériques relatifs que la chromatographie multidimensionnelle en phase gaz.

Une extension possible de ce travail consiste en la détermination multiplexe *d'ee* dans un mélange complexe d'énantiomères par PECD-PICO. Dans ce contexte, la GC \times GC permettrait de comparer et conforter les résultats obtenus par PECD. Comme nous l'avons établi sur les cas du camphre et de la fenchone, la séparation énantiomérique par GC \times GC en phase gaz peut être utilisées non seulement pour l'analyse de glaces ou d'échantillons météoritiques mais aussi pour l'analyse des terpènes, de grande importance dans les domaines de l'agro-alimentaire et des parfums.



CONCLUSIONS (EN)

There exist two main groups of theories explaining the origin of biomolecular homochirality: *deterministic* theories and theories based on *chance* mechanisms. According to the first group the asymmetry of biomolecules is linked to either the internal asymmetry of molecules (i.e. an energetic difference between two enantiomers governed by parity violation in the weak nuclear force) or to the influence of chiral forces like circularly polarized light (CPL) or magnetic fields colinear with the propagating vector of a light beam. Conversely, chance theories explain the origin of homochirality by random spontaneous symmetry breaking, consequently the type of enantiomers that is predominant in all living organisms on Earth was a result of simple chance.

Unlike the chance theories, deterministic theories can be subjected to experimental confirmation, since if there was in fact a chiral influence that imposed its effect this should, in principle, be reproducible. Among them only the influence of chiral forces can be systematically measured by current analytical instruments, while parity violation on the molecular level is too weak to be recorded by existing spectroscopic techniques. Furthermore, if we compare two forces, CPL and a magnetic field with nonpolarized light, we realize that both of them are present in space but only CPL is known to be able to produce enantiomeric excesses of several percent.

The presented work was conducted in the context of investigations on the origin of the homochirality of life, where interactions of CPL with chiral molecules played a central role in absolute symmetry breaking. Within this project, laboratory simulated interstellar ices as well as extraterrestrial samples were subjected to enantioselective analyses by two-dimensional gas chromatography. The analytical method for the resolution and quantification of amino acids enantiomers was presented. The studies determined the linear working range of the method along with detection and quantification limits. Finally, the advantages of two-dimensional gas chromatography were demonstrated on examples of extracts of the Murchison meteorite, where extraterrestrial amino acids were separated and enantiomeric excesses were precisely quantified. An excess of left-handed amino acids in the investigated samples of the Murchison meteorite suggests, that molecular symmetry breaking may have originated in interstellar space due to interaction with CPL.

A series of analyses has been performed to identify aldehydes and sugars in cometary ice analogues. An analytical method developed for aldehyde detection enabled the identification of 6 aldehydes in interstellar ices. Among them glycolaldehyde and glyceraldehyde – two species proposed as key prebiotic intermediates towards ribonucleotide syntheses. Moreover, the presence of ammonia appeared to be crucial for the recovery and production of those aldehydes. The mechanism of this phenomenon is not yet well understood and is quite surprising since the final products do not carry any nitrogen atoms.

The detection of glyceraldehyde within the simulated interstellar ice is of particular interest since glyceraldehyde was proposed to stereodictate the synthesis

of ribonucleotides, and therefore it may have imposed the distinct chirality of RNA and DNA. The asymmetric photolysis of glyceraldehyde may be key to the asymmetry of genetic material. Therefore ongoing studies are focused on recording CD and anisotropy spectra of glyceraldehyde in the solid state. Those spectra will be further used in irradiation experiments with circularly polarized light as a guide for a wavelength selection. We anticipate that the enantioselective photolysis of glyceraldehyde will result in higher asymmetry than what was previously obtained for amino acids. Furthermore, the opposite sign of enantioenrichment is expected for a given light helicity and at relevant astrophysical wavelengths.

The following analyses successfully demonstrated that a wide molecular diversity of sugars can be formed from a gas mixture made of H₂O, CH₃OH, and NH₃ in the conditions simulating the formation of interstellar ices. Among the detected sugars we identified ribose – an important element for understanding the origins of RNA and thus the molecular origin of life itself. The presence of diverse sugars as well as hydroxymethylglycerol and hydroxymethylthreitol indicates a formose type reaction mechanism. In the conducted study no sugar enantioseparation has been achieved, therefore the effect of asymmetric photolysis has not yet been investigated in this particular case. As a perspective of this study we envisage the development of an enantioselective analytical procedure employing multidimensional gas chromatography to separate optical isomers of aldoses. Such method would enable the detection of small *ee*'s within the simulated interstellar ices and/or solid states samples irradiated with the DESIRS-CPL. Understanding the asymmetric photochemistry of ribose as well as other sugars is crucial to explain the asymmetry we find nowadays within the genetic material.

As a consequence, experiments on in-situ ice formation and simultaneous CPL irradiation have been scheduled. We expect to form and detect a wide range of chiral prebiotic molecules including sugars, aldehydes, and amino acids. The in-situ ice simulation allows for a more pure organic residue to be recovered as compared to the ex-situ (with a laboratory lamp) ice production followed by the CPL-irradiation step. This should provide reliable *ee* values for all chiral molecules detected within the ice. Ideally, amino acids and sugars including glyceraldehyde will show opposite sign of enantioenrichment.

The results obtained and presented throughout this thesis, strengthen the photochemical scenario for the absolute symmetry breaking. They indicate that all building blocks required for the generation of proteins and nucleic acids could be formed in space in very extreme conditions, probably initiated by radical chemistry. This is fully coherent with the fact that organic material could have been delivered on Earth by meteorites, comets, and/or interstellar dust particles. The detection of ribose and the indication of formose-type reactions open a window to new research perspectives, such as the investigation of asymmetry induced in sugars by CPL.

The detection of aldehydes in simulated interstellar ices correlate well with the results provided by the COSAC experiment on the Rosetta mission, where acetaldehyde, propionaldehyde, and glycolaldehyde were detected as well. These data provide a direct link between laboratory simulation experiments and a 'real' cometary composition. Upcoming space missions may also benefit from the

developed analytical procedures for enantioselective analyses of extraterrestrial samples. Eventually, as the simplest amino acids were first detected within the simulated interstellar ice and then only may have been identified in space, similarly we expect that in the near future space scientists will report on the detection of glyceraldehyde.

All in all, the results presented herein could find applications in the domains of astrobiology, photochemistry, and analytical method development.

Finally, chiroptical properties of the chiral molecules camphor and fenchone were studied by double imaging photoelectron/photoion coincidence (i^2 PEPICO). Besides a strong sensitivity to isomerism, we found that PECD spectroscopy is as precise as multidimensional gas chromatography in measurements of relative enantiomeric excesses.

A further prospective of this work would be the multiplex determination of *ee* values in a complex sample including a mixture of optical isomers by PECD-PICO. In this context GC \times GC would support and benchmark the results obtained from PECD spectroscopy. As we can see from the fenchone and camphor enantioseparation the two-dimensional gas chromatography can be used not only for the analysis of complex ice and meteorite samples but also for terpenes analysis, which is particularly useful in food and fragrance chemistry.



INDEX

- absolute asymmetric synthesis 12,
16, 28
- aldehydes
glyceraldehyde 38, 39, 75, 79, 80,
81, 82, 83, 84, 85, 86, 95, 100,
101, 109, 116, 117
glycolaldehyde 38, 39, 77, 79, 82,
83, 84, 85, 86, 100, 105, 109,
116
lactaldehyde 79, 82, 83, 85
- aldopentoses 27, 35, 39, 95, 99
- amino acids
alanine 8, 9, 11, 13, 15, 41, 66
anisotropy spectra 34
circular dichroism 32
cometary ice 11
deracemization 8
ee 8, 9, 35, 36
extraction 68
glycine 8, 10, 11, 39, 86, 106
isoleucine 8, 37, 60
isovaline .. 8, 9, 10, 39, 53, 58, 59,
65, 66, 67
leucine 8, 15, 53, 60
mass spectra 54, 69
Murchison meteorite .8, 9, 51, 59,
61
N-ethylglycine 8, 53
N-methylalanine 8, 53, 58
proline 8, 16, 58
proteinogenic 9, 11, 14, 15, 51,
52, 53, 58, 60, 61, 66
racemization 9, 15, 52, 58
tert-leucine 8, 53
tyrosine 15
valine 8, 16
 α -aminobutyric acid 8
 α -methylvaline 8
 β -alanine 8, 53, 66
- anisotropy
amines 40
amino acids 34
carboxylic acids 41
factor 32, 33, 35
parameter 128, 134, 137
spectroscopy 13, 29, 30, 32, 42
- astrophysical scenario 25, 29, 31, 35,
79, 98, 119
- autocatalysis 16
- Barron L. 14
- Blackmond D. 16
- bremsstrahlung 15
- Buhse T. 16
- camphor
chiral parameter 127, 128, 134,
135
comparison 132, 134
ee 128
isosurface plot 145
optical rotation 123
PECD 121, 122, 123, 125, 126,
133
structure 133
VMI difference 125
- circular dichroism .. 4, 13, 15, 25, 29,
30, 31, 121, 122
- column
Chirasil-L-Val 54, 58, 59
Chirasil-Val 58
Chirasil- β -Dex 58, 59
DB Wax 54, 123
- comet
19P/Borrelly 6
1P/Halley 6
67P/C-G 6, 17, 27, 39
81P/Wild 2 6, 10, 39
9P/Tempel 1 6
Lovejoy 100
- Cooper C. 41, 84
- COSAC 6, 17, 18, 27, 39, 63, 87
- derivatization
BSTFA 109
ECHFBF 53, 54, 72
OPA/NAC 58

- PFBO-TMS 79, 80, 81, 93
 DESIRS 108, 124, 128
 Dworkin J.P. 10
 ESA 5, 6, 17
 Faraday effect 14
 Faraday rotation 14
 fenchone
 chiral parameter 131, 134, 135
 comparison 132, 134
 ee 130
 isosurface plot 145
 optical rotation 123
 PECD 121, 122, 123, 129, 130,
 133
 structure 133
 formose reaction 75, 84, 95, 104,
 105, 111, 116
 Frank F.C. 16
 Garay A. 15
 GC × GC . 10, 51, 53, 54, 58, 59, 62,
 87, 93, 98, 109, 111, 112, 123,
 125, 126, 128, 130, 131, 133,
 134, 135
 Glavin D.P. 10
 Greenberg J.M. 10, 35, 36
 i²PEPICO... 2, 4, 121, 123, 124, 148,
 150
 interstellar ice
 aldehydes 27, 77, 85
 aldoses 99
 amines 39
 amino acids 11, 39
 ee 12
 glyceraldehyde 39, 77, 85
 glycolaldehyde 77, 85
 ketoses 99
 ribose 27, 39, 97
 saccharinic acids 99
 simulation.... 6, 10, 11, 12, 39, 41,
 42, 61, 84
 sugar alcohols 99
 sugars 97
 magnetochiral dichroism 14, 29
 mass spectra
 aldehydes 80
 amino acids 69
 arabitol 115
 glyceraldehyde 81
 ribonic acid 116
 ribose 115
 Meierhenrich U.J. 53
 Meinert C. 11, 40, 41
 meteorite
 amines 39
 amino acids 52
 carbonaceous chondrites . 7, 8, 41,
 52, 86
 carboxylic acids 7
 diamino acids 7
 ee 52
 hydroxycarboxylic acids 7, 41
 insoluble organic matter 7, 41
 monocarboxylic acids 41
 Murchison . 7, 8, 9, 10, 37, 41, 51,
 52, 53, 60, 61, 62, 68, 73, 84,
 100
 Murray 7, 9, 84
 N-alkylated amino acids 7
 nucleobases 7, 52
 Orgueil 9
 soluble organic matter 7, 86
 sugar acids 7, 52
 method validation
 calibration curves ... 53, 57, 66, 67
 limit of detection ... 55, 56, 57, 58,
 61, 67
 limit of quantification.. 55, 56, 57,
 58, 61, 67, 117
 regression line 57
 working range 57
 Miller S.L. 7
 mission
 Deep Impact 6
 Deep-Space 1 6
 Giotto 6
 Rosetta 5, 6, 17, 87, 106
 Stardust 6, 39
 Vega 6
 Monod J. 12
 parity violation 5, 15, 18, 28, 149
 Pasteur L. 6

- PECD
analytical aspect 119
asymmetry 129
camphor . 122, 123, 125, 126, 133
comparison 132, 134
ee 127
fenchone . 122, 123, 129, 130, 133
measurments 124
REMPI 122, 130, 133
sensitivity 136
time resolved 122
Philae 6, 17, 27, 36, 39, 106
photochirogenesis 5, 27
Pizzarello S. 37, 41, 60
Quack M. 15
ribose
formose rection 105
interstellar ice 27, 39, 97
mass spectra 115
yield 105
- RNA 16, 36, 85, 97, 98, 106
Rosetta
chirality module 5, 6, 17, 18
lander 6, 17, 27, 39
mission 5, 6, 17, 36, 87, 106
spacecraft 5, 17
Soai K. 16
SOLEIL 108, 124
spontaneous symmetry breaking... 14
Sutherland J.D. 38
symmetry breaking 5, 13, 14, 15, 18,
25, 27, 42, 52, 119
true chirality 13
Urey H.C. 7
Vester-Ulbricht 15
Viedma C. 15, 16
Viedma ripening 14
 β -decay 15
 β -electrons 15